Determination of Trace Elemental Species in Periostracum of Cypraea Shells

Dissertation

zur Erlangung des Grades

“Doktor der Naturwissenschaften”

am Fachbereich Chemie

der Johannes Gutenberg-Universität Mainz

Analía Leticia Soldati

geb. in Buenos Aires, Argentinien.

Mainz, 2005

Dekan:

1. Berichterstatter:

2. Berichterstatter:

Tag der mündlichen Prüfung:

Dedicada
a mis padres Viviana Valente y Luis Soldati,
a la Virgen de San Nicolás
a Michael Zöller

Index of Contents

SECTION III: RESULTS

Index of Figures

Index of Tables

Abbreviations

AcH-buffer	Acetic Acid - Ammonium Acetate Buffer
AM	Average Material (relative to the shell powder)
C	Colored (relative to the layer)
C.	Cypraea
CLSM	Confocal Laser Scanning Microscope
DTNB	5,5´-dithio-bis-(2-nitrobenzoic acid)
EDTA	Ethylene-diamine-tetraacetic acid
ESI	Electro Spray Ionization
EXAFS	Extended X-Ray Absorption Fine Structure
FE-SEM	Field Emission Scanning Electron Microscope
GE	Gel Electrophoresis
HPLC	High presition Liquid Cromatography
I	Current
ICP	Inductively Coupled Plasma
INAA	Instrumental Neutron Activation Analysis
IOM	InsolubleOrganic Matrix
LA	Laser Ablation
LD	Limit of Detection
M	Magenta (relative to the layer)

Mag.	Magnification
MS	Mass Spectrometry
MWCO	Mass Weight Cut Off
Ø	Diameter
OM	Organic matrix
P	Periostracum (relative to the layer)
RP	Reverse Phase
rpm	revolutions per minute
RS	Raman Spectroscopy
S	Striped (relative to the layer)
SDS	Sodium Dodecyl Sulfate
SE	Size Exclusion
SEC	Size Exclusion Chromatography
SEM	Scanning Electron Microscope
SOM	Soluble Organic Matrix
UCT	Ultracentrifugation-filtration
UV	Ultra violet
V	Voltage
Vis	Visible
W	White (relative to the layer)
XAS	X- Ray Absoption Spectrometry
XRD	X- Ray Diffractometry
µ-RS	Micro Raman Spectrometry

Determination of Trace Elemental Species in Periostracum of Cypraea Shells

Doctoral Thesis

Dipl. Eng. Analía Leticia Soldati

Abstract

In this work, three *Cypraea* species (*C. talpa*, C. *tigris* and C. *zebra*) were exhaustively studied. The shells have been separated in the structural layers. The mineralogy, ultra- and micro-structure of each layer were analyzed by Confocal Laser Scanning Microscopy (CLSM), Scanning Electron Microscopy (SEM), X-Ray Diffractometry (XRD) and Raman Spectroscopy (RS). The presence of biologically relevant trace metals (Mn, Co, Fe, Zn, Cr, etc.) has been investigated using Instrumental Neutron Activation Analysis (INAA) and Inductively Coupled Plasma – Mass Spectrometry (ICP-MS) as detection tool. A new method has been developed and optimized to extract and analyze the soluble organic matrix (SOM) of the shell. Although the molecular nature of the SOM is not really known, it contains at least large protein fraction, if not only consists of proteins. The extracted matrices were compared between layers and species using Size Exclusion High Performance Liquid Chromatography coupled with Ultra Violet Spectrometry (SE-HPLC-UV), Gel electrophoresis (GE) and protein quantification tests.

For the first time to our knowledge the association of trace elements to the protein in the SOM of the shell was studied using hyphenated on line as well as combined off line techniques and validated through inter-comparison tests between the different methods applied. Interesting correlations between the trace element concentration, the microstructure and the protein content were directly and indirectly detected. The metals Cu, Ni, Co and Zn have shown to bind to the SOM extracted from *C. talpa*, *C. tigris* and *C. zebra* shells. Within the conclusions of this work it was demonstrated that these protein-metal-complexes (or metal containing proteins) change from one layer to the other and are different between the three snails analyzed. In addition, the complexes are clearly related only to certain protein fractions of the SOM, and not to the whole SOM observed. These fractions and show not to be very metal-specific (i.e. some of these fractions bind two or three different metals).

Bestimmung von Spurenelementspezies im Periostracum von Schnecken der Gattung Cypraea

Dissertation

Dipl. Ing. Analía Leticia Soldati

Zusammenfassung

In dieser Arbeit wurden drei Cypraea-Arten (*C. talpa*, *C. tigris* und *C.zebra*) ausführlich studiert. Die Schalen jeder Art wurden gemäss ihrer verschiedenen strukturellen Schichten getrennt. Mineralogie, Ultra- und Mikrostruktur jeder einzelnen Schicht wurden mit Hilfe von CLSM, REM, Röntgenbeugung und Raman Spektroskopie analysiert. Die Anwesenheit von biologisch relevanten Spurenmetallen wie z.B. Mn, Co, Fe, Zn, Cr, etc. konnten unter Verwendung von INAA und ICP-MS nachgewiesen werden. Dabei wurde eine neue Methode für die Extraktion und die Analyse von löslichen organischen Anteilen in Schneckenschalen entwickelt und optimiert. Obwohl die Molekülnatur der SOM nicht bekannt ist, enthält diese mindestens eine grosse Proteinfraktion, wenn sie nicht überhaupt nur aus Proteinen besteht. Alle extrahierten Matrizes der verschiedenen Schichten der einzelnen Spezies wurden miteinander über Grössenausschlusschromatographie (SE-HPLC-UV), Gelelektrophorese und einem Proteinquantifizierungstest (Bradford-Test) verglichen.

Soweit bekannt, wurden zum ersten Mal Bindungen zwischen Spurelementen und den Proteinen in der SOM von Schneckenschalen mit gekoppelten Analysemethoden vergleichend untersucht. Interessante Korrelationen zwischen der Spurenelementkonzentration, der Mikrostruktur und dem Proteingehalt konnten direkt und indirekt gemessen werden. Auch zeigte es sich, dass die Metalle Cu, Ni, Co und Zn an die lösliche organische Matrix der Schalen von *C. talpa*, *C. tigris* und *C. zebra* gebunden sind und mit dieser extrahiert werden können. In dieser Arbeit wurde gezeigt, dass Protein-Metall-Komplexe (oder metallhaltige Proteine) von Schicht zu Schicht und auch zwischen den drei Arten verschieden sind. Deutlich wird, dass die Metalle an bestimmte Proteinfraktionen nicht pauschal an die SOM gebunden sind. Diese Fraktionen sind allerdings nicht sehr spezifisch bzgl. eines Metalls (z.B. bindet ein und dieselbe Fraktion zwei oder drei verschiedene Metalle).

Summary of this Thesis

Two years ago, when I was looking for a PhD theme, I asked Prof. Dr Baumann for an analytical work related to the environment, where I could extend as much as possible my knowledge in different analytical areas, including trace elements, microanalysis micro imaging and of course not to forget the further development of my nuclear origins at the nuclear activation laboratories. Some days later, he came with two bugs of marine beautiful shells in his hands. He told me: “nobody knows why this shell from the same family as the other one, has a better response against the bio-fouling attack of algae and fungi. Nobody knows anything about which species are found in the surface of the shell. And nobody knows how could be these species be implicated with the physical observations. I think it is a good theme for a PhD. thesis…”.

The Chapters Distribution

This thesis was organized in four sections. The ***first section*** contains a brief introduction to the cowries shell biology and construction. The aim of this section is to specify the type of material in which the investigations will be done and which kind of results can be expected. The ***second section*** resumes all methodologies used in this work for the investigation of the C*ypraea* shells, presenting a short theoretical introduction to the methodology and the experimental set up. This section is subdivided in methods for trace analysis, methods for separation, methods for protein quantification and other methods. The ***third section*** contains the results obtained in this work. The first chapter here is dedicated to the results of the mineralogical and microscopic analyses. In the second chapter all results related to the trace elemental analysis and their correlation with the microstructure of the three *Cypraea* species are found. The third chapter resumes the characteristics of the organic matrix extracted from the different *Cypraea* shell samples. The fourth chapter is dedicated to the results obtained when organic matrices and trace elements are analyzed together. Results of indirect observed correlations are here validated with coupled techniques. The ***fourth section*** is dedicated to discussion and conclusions. Here are commented a summary of all results, the comparison with literature observations and further possible developments.

A set of information considered very important for someone who continues this research, but not relevant for the understanding of this thesis, was attached as ***appendix***. Regarding to the

shell organic matrix extraction it could be found an exhaustively analysis of the state of the art, description and comparison of different extraction methodologies obtained from literature. Two extraction systems and the different methodologies selected for the *Cypraea* shell samples preparation, powdering, decalcification, purification, concentration and conservation are tested and compared. All sample treatments and pretreatments, extractions and quantifications were analyzed for possible interferences, organic and inorganic contaminations or sample destruction. The optimized methodology for the organic matrix extraction, analysis and characterization is in these appends elucidated and tested in *Cypraea tigris* shells.

SECTION I.
INTRODUCTION

1. Introduction

An exhaustive analysis of the literature from different biological, mineralogical and chemical sources was done with the aim of understanding the bio-construction, functions, characteristics and composition of the bio-mineralized shells of cowry snails. These investigations were summarized in this chapter to give an introduction on the material on the basis of which this thesis was developed.

1.1 Motivation

The properties attributed to cowry shells are deep growing in the folk's belief. In some countries, cowries are believed to represent fertility, and are given to brides to guarantee offspring and provide a safe delivery. In other countries, it was believed that the shell protects against the evil eye. They were also attached to fishing nets to promise a good day. The golden cowries from the Fiji and Solomon Islands are a symbol of power and rank for chieftains. They have also been used in art, as money, jewelry and as religious symbols since the beginning of mankind. Nevertheless these transparent, brilliant and smooth shells are not only interesting because their beautiful aspect and "unconventional" properties, but also since some of these shells have a protective role against epibiotic agents. Prof. Dr. Raimundo Damaceno of the Universidade Federal Fluminense of Niterói, Brazil, has observed that *Cypraea zebra* snails, abundant in the costs of this country, have shown interesting properties of antifouling activity in their shells. This phenomenon was not observed for example in *Cypraea talpa* or *Cypraea tigris* exemplars.

The shells of the marine Gastropods *Cypraea* are composed of different layers of bio-mineralized calcium carbonate (as aragonite and calcite) organized in distinctly layered, prismatic and crossed lamellar structures (Bøggild, 1930). The most superficial layer is an organically highly enriched layer called periostracum. The periostracum function is to protect the shell from abrasive erosion and water corrosion. It serves also as initial substrate for mineral deposition to build the underlying shell layers (Almeida et al., 1998). In the case of *Cypraea* shells the periostracum is a transparent, varnish-like, 40 to 100μm thick layer. This brilliant smooth coverage gives them not only their common names of „cowries" or „porcelain

snails“, but also is believed to act as a protection shield against epibiotic agents, acting as an anti-fouling trick (Wahl et al., 1998). Of course, *Cypraea* shells have a natural antifouling adaptation. The mantle (soft body) itself cleans the surface thanks to its continuous movements around the shell. But this simple hypothesis does explain neither why different *Cypraea* species have different responses to fouling organisms, nor why this phenomenon is observed when the shells are unoccupied.

Antifouling activity (Thakur, 2001) is not rare in nature. The effect can be achieved through very different mechanisms. Different animals have developed different methods to fight against epibiotic agents, employing either one or a combination of ecological, physical and chemical defense mechanisms. Some snails introduced mechanical, pH dependent or surface tension dependent protections (Wahl et al., 1998). A wide range of marine organisms such as bacteria, sponges and algae are found to be a potential source of antifouling metabolites. This effect observed in nature was also repeated in technological applications. Actually, metals (and especially organically complexed metals) are usually used as paints and toxics to fight against the fouling organisms for example on ships and heat exchangers. One clear example is the environmentally very toxic TBT. Natural products are explored now as an environment friendly alternative.

It is very well known that metal-organic species in nature have different functions, such as pigments, structural hardening and stabilization (Smith et al., 1999; Raz et al., 2003; Wang et al., 2003), physiological functions (Gribble et al., 1999), protection against fouling agents (Foster et al., 1994), adhesion improvement (Lowenstan et al., 1981) or control of bio-mineralization (Swann et al., 1998; Vasin et al., 1998). Whether metal-organic species are responsible of the antifouling activities observed in some *Cypraea* shells, is a question that remains open. No works directed to explain the speciation of trace elements in shells are found in literature.

Because *Cypraea* snails do not have important economic or environmental implications, very little was studied about the composition and speciation of elements in their shells, and only few references are given as comparison between other species (Dauphin et al., 2000) or as data for bio-monitoring studies (Hung et al., 2001). The aim of this work was to investigate trace elemental species in *Cypraea zebra* and *Cypraea talpa* shells, compare them, and elucidate which kind of role they may play in the protective adaptation defense or in other characteristics like the bio-mineralization process or the structural hardening, with special attention to the outmost layer, the periostracum. To our knowledge it is the first time that an approach of this kind was done for *Cypraea* samples.

To develop this research, it was necessary to review information about how *Cypraea* shells are built up, which kind of inorganic and organic materials are involved in the building and repair processes, which kind of elemental bindings can be expected, which elements and trace elements are found in the shells, where and in which concentrations they appear, how the elements can be introduced into the shell or how the shell reacts under a contaminated environment. A brief introduction to the most important aspects of these informations is found in the sections below. More detailed discussions are found in the cited literature.

1.2 Cowry Shells

There are about 50.000 species of mollusks described and therefore the *Mollusks* belong to the top three animal phyla together with the *Mandibulata* and *Chelicerata*. From the seven classes of existent molluscs, *Gastropoda* is the largest class, including abundant mollusks and all marine and terrestrial snails, with *Cypraedae* snails between them. These gastropods[1], of the Ctenobranchina suborder, like to live in tropical and subtropical waters, in shallow to relatively deep water (3m to 14m deep), of about 24ºC to 27ºC and pH around 8, with night predator habits (feed on algae and sponges) and are very appreciated by collectionists because of their very beautiful aspect.

Cyprea Snails

Phylum: Mollusk
Class: Gastropoda
Order: Prosobranchia
Suborder: Ctenobranchina
Family: Cypraedae
Species*:* zebra, talpa, tigris.

Figure 1: *Cypraea tigris* schematic representation. Picture and data from Bøgglid, O.B. The shell structure of the molluscs. From Videnskabernes selskabs skrifter. Coppenhagen 1930. Page 231-326.

Cypraea animals have a covering mantle, which wraps around the entire shell (See Figure 1), sparcing extrapallial fluid over the entire surface. Thanks to that, the exterior of the shell is a transparent, brilliant, smooth and highly polished layer ranging from 20 to 100μm thickness. This special coverage gives them their common name of “cowry snails”. During the Roman period,

[1] From web pages 1 to 4, on-line literature.

C*ypraea* snails were known as Porculi, meaning little pigs. The name was later lengthened to Porceletta. When fine pottery was introduced to European society from the Far East, the shape of these new items reminded people of the Porceletta shells. Thus, the term porcelain was given to the pottery[2].

1.3 Shell Ultra Structure

Basically the snail shell consists mostly of calcium carbonate, as well as various organic compounds, in several different layers, divided in three classes (See Figure 2). The hypostracum as innermost layer; followed by the multilayered ostracum, as the basic shell-building unit and the outermost layer: the periostracum (Manigault et al., 1930; Franc et al., 1978; Ziegler et al., 1991).

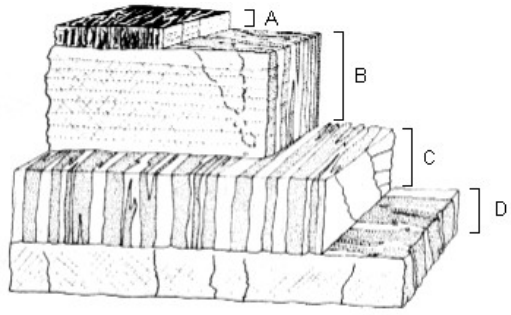

Snail Shell Structure

A: Periostracum, most superficial layer with a high organic content.

B+C: Ostracum, layered arrangement of aragonite or calcite prisms.

D: Hypostracum, nacred layer of hexagonal aragonite columns.

Figure 2: Schematic representation of a snail shell. Picture from „Fauna von Deutschland“, Brohmer. Quelle & Meyer Verlag, Wiebelsheim. 2000: i-xiv, 1-791.

The *ostracum (*ostracukon = shell), is the thickest of the three shell parts, secreted by the outer fold of the mantle margin. It is build by several layers of prism shaped calcium carbonate crystals, in aragonite or calcite form, embedded into a protein matrix. By oblique laying of the calcium carbonate prisms, a higher hardness is achieved. Among some snail species, the shell bio-mineral can be much harder than the mineral itself.

The *hypostracum* (hypo = under), secreted by the outer mantle epithelium, is made of thin hexagonal sheets of aragonite crystals (a mineral form of calcium carbonate) oriented parallel to the surface. This layer is also called mother-of-pearl or *nacre*, and is the one that is in contact with the soft body of the animal.

[2] From web page 5, on-line literature.

The *periostracum* (peri = around) is the thin outer layer and consists mostly of an organic proteinaceous substance known as conchyolin. The periostracum is also known as *outer skin*, *horny covering* or *cuticle* of the shells. Sometimes the periostracum can be removed by bleach to get a clean specimen for display. Its function is to protect shells from corrosion and erosion. The thicker it is, the darker the color and the more the shell is protected underneath from sand grains and other abrasive elements of the animal's environment and from acidic water, which some of the harder gastropods and bivalves can survive in.

In cowries the mantle covers the entire shell, when the creature is extended, protecting and maintaining the gloss, which is why their shells are so smooth and shiny. The color and pattern of the periostracum can be very variable and is taxonomically important for the identification. The basic color and the design are determined genetically, although variations may develop due to factors like temperature and environmental conditions.

1.4 Shell Microstructure

Shells consist basically in four types of micro structured calcium carbonate forms. Generally, the first microstructures observed consist of spherulitic prisms. These include sub-units radiating in three dimensions from a single nucleation site, or spherule, towards the depositional surface. This first microstructure consists of aragonite and calcite. The second microstructure group consists of laminar, columnar nacreous structures. These structures are deposited near the shell margin, forming the nacre. The tablets are stacked in columns with coinciding centers, an arrangement only found in some gastropods and cephalopods. The mineralogy of this group is always aragonite. The third microstructure group is a fibrous, prismatic structure. The prisms are simple crystals with large length/width ratios. The mineralogy of this group is aragonite and calcite and the prism boundaries are well defined. The fourth microstructure group is an irregular complex, cross-foliated structure. This group commonly appears in the inner shell layers, and is a distinct type of shell structure at the point of pallial muscle attachment. This group is adjacent to aggregations of numerous parallel, elongate sub-units that showed three or more predominant directions.

1.5 Shell Construction

The shell is secreted by the mantle, a considerably specialized structure that covers the dorsal or upper part of the animal soft body. Shells vary in composition throughout the various mollusk groups, but they typically contain a mixture matrix of protein and calcareous components. Calcite and aragonite are common mineralogical forms of the calcium carbonate ($CaCO_3$), both often found in the same shell. The first layer formed, the periostracum, is often a wholly proteinaceous covering. The protein continues throughout the shell as the fiber matrix that the calcareous mineral is deposited upon. The organic content accounts for about 0.01% to 15% of the whole shell weight, varying between species. The snail extracts the calcium of the surrounding environment and stores it in certain cells for further shell growth, repair or enlarging. Initial shell secretion occurs at the outer or growing edge of the animal's shell. Subsequent deposition by the underlying mantle thickens the shell. In large benthic mollusks, mostly clams and some snails, the shell may get quite thick and heavy. Those mollusks found in the depth abysms, where calcium carbonate is very soluble, often have shells made totally of protein.

1.6 Shell Growth

The growth of a snail shell is influenced by a variety of factors, including growth hormones, food and temperature. For many species it is a continuous growth, and it could be observed shell rings parallel to the shell rim due to changes in the growth rates. In the stage of growth, the periostracum is secreted by the secretory cells of the periostracal groove in a soluble protein form and tanned on the surface. The new periostracum seals the extrapallial space creating a regulated compartment, were soluble calcium carbonate together with a proteinaceous matrix are secreted into the extrapallial spaces by the mantle epithelium. In the case of cowries, there is a continuous juvenile shell growing, and maturity produces the adult shell that does not grow any more but becomes heavier with age.

1.7 Shell Organic Matrix

Generally for all snails and molluscs, the shell bio-construction is promoted by an organic matrix, composed mainly of glycoproteins, acidic proteins, mucopolysacharides and β-chitin

(Marxen et al., 1997; Marin et al., 2001; Dauphin et al., 2003; Wang et al., 2003) secreted by the periostracal groove in the mantle border (Meenakshi et al., 1969). The organic matrix was investigated by many authors, and aspartic acid, serine and glycine are found as the main amino acid components (Almeida et al., 1998). The organic matrix (around 0.01 to 10% of the whole shell mass) is generally extracted with an acidic buffer and divided into a water soluble and a water insoluble fraction (Balmain et al., 1999; Bédouet et al., 2001; Marxen et al., 2003). The water soluble organic fraction was extensively studied since the ´70s (Grégoire et al., 1972), but not all components and their biochemical implications are yet understood.

1.8 Shell Major and Trace Elements

Previous elemental studies in marine Gastropoda and Bivalvia shells were done by many authors (Masuda et al., 1980; Dauphin et al., 2000 and 2003; Choi et al., 2000; Hung et al., 2001; Lazareth et al., 2003;). Although no one has measured *Cypraea talpa*, *zebra* or *tigris* before, the results averaged for different *Cypraea´s* shells by Dauphin et al. (2003) are presented in Figure 3. In this case, the used technique was microprobe analysis.

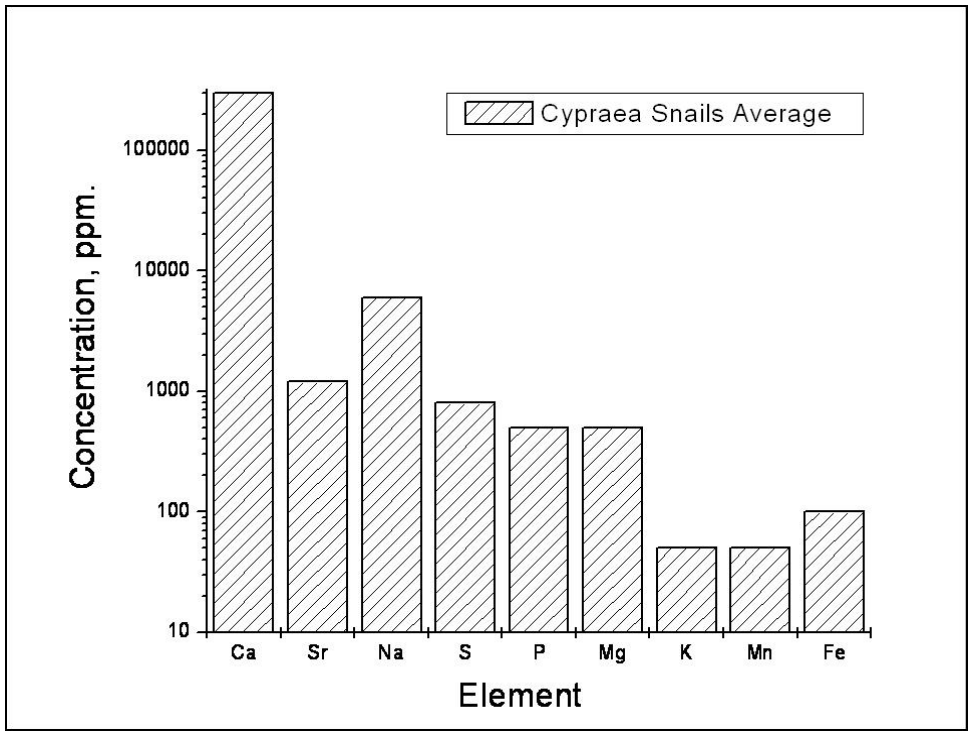

Figure 3: Concentration of some elements commonly found in *Cypraea* shells. Graphic made with data taken from Dauphin 2003.

This summary gives an idea which elements and in which concentrations may be expected in this kind of samples. Clearly, calcium is found in the highest concentration as structural element, followed by sodium and strontium. Under concentrations of 1000 ppm appear sulphur and phosphor. These elements are related to the organic matrix of the shells.

Major and trace elements are incorporated to the shell by absorption from the ocean water and suspended material or by uptake in the diet, for example demonstrated in the work of Mai for the element Zn (Mai et al., 2002). The trace element content levels of the whole shell are very variable depending on the environment, the kind of suspended material, type of sediment, particle size, seasonal variability, and other factors like pH, temperature, etc.

The distribution of the elements in the shell can be separated into three types of incorporation. Elements with ionic radius and charge similar to Ca^{2+} can be built in the inorganic structure replacing the calcium ion. A good example of this kind of incorporation is for example known for the element Sr^{2+}. The second type is generally observed for little species like Na^{+} and K^{+}, which can be found as inorganic species occupying interstitial places of the carbonate mineral structure. The third type corresponds to a not yet well understood incorporation and is observed especially for some metals found in the organic matrix of the shell.

Trace elements like As, Ba, Bi, Cd, Cu, Co, Cr, Mo, Ni, Pb, Sc, Sb, V and Zn where measured in mussels and bivalves samples at ppm and ppb concentrations (Ravera et al., 2003; Lazareth et al., 2003). As it can be concluded from Figure 3 the principal challenge with *Cypraeidae* shell samples is that the trace elemental concentrations are four or five orders of magnitude lower compared to the major elements. All processes applicable to lower the Ca, Sr, and Na content, as EDTA or Ca precipitation for example, can result in the trace elemental leakage by co-precipitation and in the loss of element speciation.

Many authors have measured with success trace elements in shell samples by microprobe and LA-ICP-MS (Lazareth et al., 2003; Putten et al., 2000; Siegele et al., 2001). In both cases the shells need very low or almost now chemical treatment. The decisive parameter for the detection and quantification is in all cases the ratio between the detection limit of the trace element and interfering background created by the major elements.

1.9 Speciation in Shells

Although trace elemental analysis in shell samples is very common, especially for bio-monitoring and bioaccumulation studies, speciation analysis is a rare topic. Only few examples are found in the works of Dauphin (2003) and Cuif (2003), handling with the speciation of sulphur in oysters and corals, or in the work of Yasoshima (2000), who worked on copper speciation in oyster of contaminated basins In both cases, EXAFS was used as instrumental analytical technique.

Elemental mapping and microscopy studies demonstrated that the trace element distribution in the shell is highly dependent on the shell structure itself, as shown by Masuda (1980). The relation between element concentration and microstructure in the shell is still unclear (Carriker, 1996), but interesting correlations between different elements were found in some cases, as for example those observed within Sr, Mg and Ba in bivalve shells by Lazareth (2003) and Putten (2000).

On the other hand, not only strong evidences of correlations between trace elements and structures, but also between different elements and the organic matrix present in the shell were reported. For example, Mn correlations with organic material-rich regions in freshwater mussel shells have been observed by Siegele (2001) and Nyström (1995). Higher amounts of manganese and iron were found by Swinehart (1979) in bivalve periostracum. Carriker (1996) found slightly higher concentrations of most trace elements in the pigmented sectors of oyster *Crassostrea virginica* shells and Almeida (1998) reported Fe, Mn and Zn associated to the organic matrix in the prismatic layer in *crassostrea gigas* oyster shells. Although these associations between the elements and organic-rich sectors are clearly interesting, no one of these authors has studied the speciation state of the elements, nor the binding form.

1.10 Open Questions

The literature analysis of the bio-construction, characteristics and elemental composition of the shells has let many open questions. Are the trace elements present in the shell found as inorganic substituents in the $CaCO_3$ matrix? Are they occupying interstitial places? Are they bound to the organic matrix of the shell? Then: are metal-organic species existing? And if not, why are there evidences of metal accumulation in the organic rich regions (especially in the periostracum) of the shells? And in this case, and remembering the special properties observed in the *C. zebra* specimens, could metal-organic species be the responsible factor of the antifouling activity?...

It is the motivation of this work to bring hints that help to find the answers to these questions from the point of view of the trace elemental and the speciation analysis.

SECTION II.

MATERIALS AND METHODS

2. Material

In this research, different treatments as powdering, fracturing and cutting were applied to prepare the shell samples for trace analysis determination, microscopy, spectroscopy and organic characterization. In this chapter are described the different types of samples and reference materials used.

2.1. Shell Acquisitions

C. talpa and *C. zebra* shells were obtained through collaboration with Prof. Dr. Damaceno from the Universidade Federal Fluminense of Niteroi (Brazil). The origin of the first ones is the Philippines Islands and the second were collected in the coasts of Brazil. The shells of *C. tigris* were bought in a shell shop of Mainz, Germany. These shells came also from the Philippines. *C.tigris* shells allowed us to prove all experiments and optimize the methods and parameters. There is no information about the the previous treatment of these shells, but the periostracum was well conserved in all of the specimens elected. Only adult shells were examined, omitting all evolutionary stages, and confine the study to the main upper part of the shell, omitting all special features at the margin edge where the structure is more complicated.

2.2. Shell Preparation

C. tigris, talpa and *zebra* adult shells were washed with MilliQ water and air dried. All shells were examined, photographed and indexed. With special attention the conservation state of the periostracum was observed. Shells where the periostracum was seriously damaged were excluded from the research.

.

2.3. Samples for Microscopy

Polished Cross Sections

Adult shell samples were cut in cross sections with a diamond saw in transversal ring sections of 5 mm thickness, at the centre of the shell. Only the upper part of the shells was investigated, avoiding the margins and ventral edges where the microstructure is more complicated (See Figure 4).

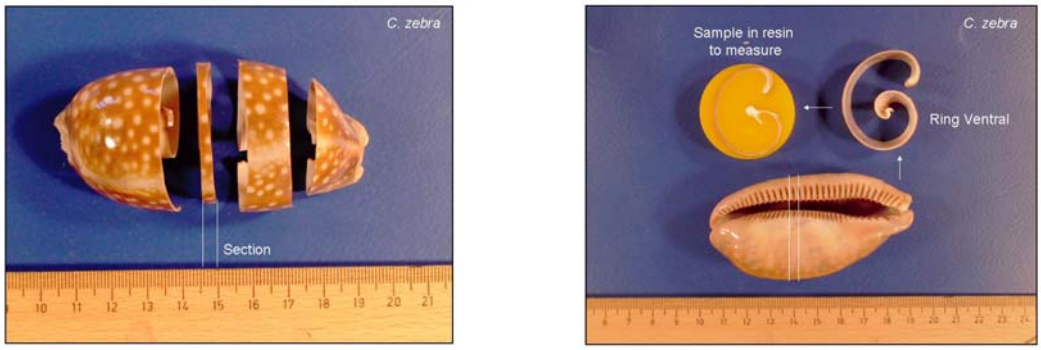

Figure 4: (left) Cross section cuts of a *C. zebra* specimen. (right) Intermediate and final sample for CLSM measurement**.**

Single sections were embedded in a resin, air dried and polished with a diamond paste paper series from to obtain a mirror-like reflective surface (Figure 4, right).

Structure Samples

Three different treatments where applied to 1 cm^2 samples of shell to reveal the 3D structure: fractured, cut with a diamond saw, and etched. Thick cross section rings, of about 2 cm, were cut with a diamond saw (See second ring on Figure 4, left). They were hand fractured in pieces of about 1 cm^2 to study the fracture edges. For the etching, different pieces were submersed in MilliQ water 24 h, NaOCl 3 % 1h, HNO_3 10 % for 10 s, acetic acid buffer 15 % for 5 s, 10 s and 20 s , and protease 24 h to reveal the different structures.The samples were paste in the microscope support and covered by graphite.

Multilayer Samples

Different shell layers were revealed mechanically by the aid of a diamond milling cutter from an about 2 cm^2 piece of shell from the upper part of a ventral ring (See Figure 4, left). Figure 5 represents the five layers found in a transversal cut: a 40 to 120 μm transparent layer correspondent to the periostracum (1), a coloured layer (2), of about 100 μm, where the shell pigments are bound, a striped layer (3) of 400 μm with two different colours, the thickest layer of the shell with about 2 mm in a magenta or dark brown colour (4) and finally a talcously white layer (5). The internal nacreous layer (not shown) was not studied.

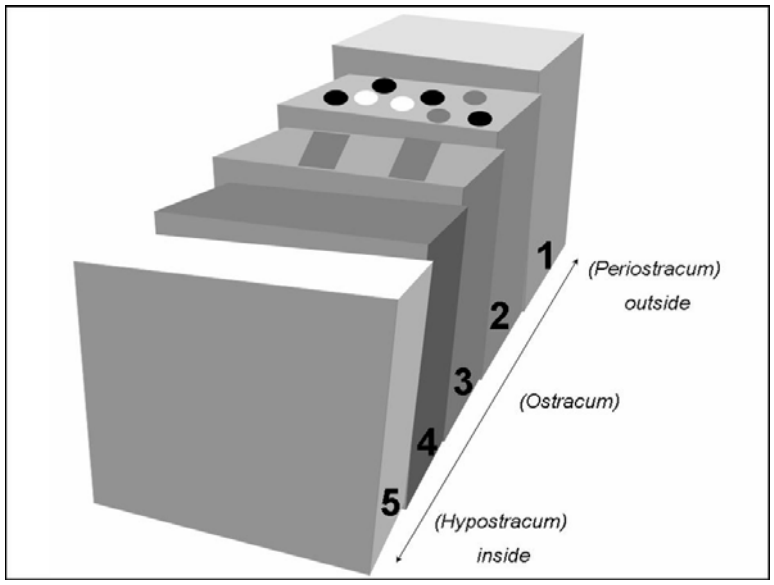

Figure 5: Schema showing the different layers. For description of the layers 1 to 5 see text.

To get homogeneity for the detection using microscopic and spectroscopic methods, all layers must be present in the same sample. For that purpose a *"multilayered sample"* was done. Using the milling diamond cutter, the shell was eroded at different depths, revealing the different observable layers (See Figure 6).

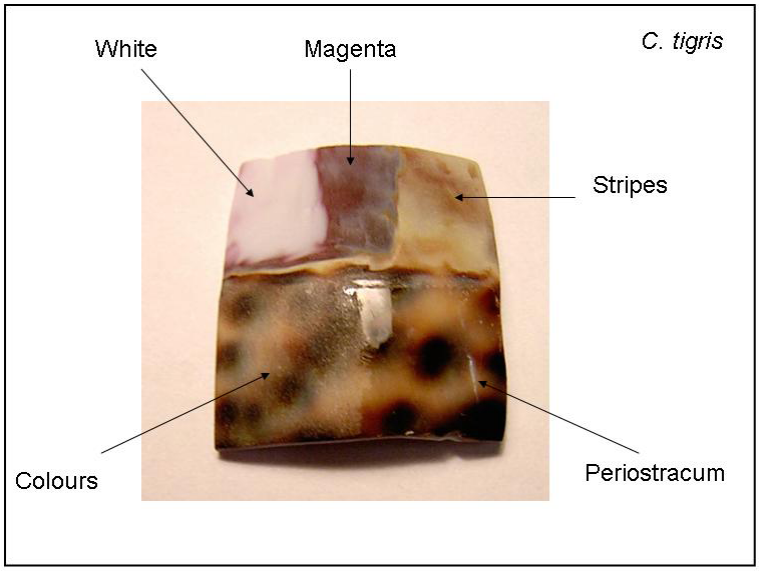

Figure 6: Photography of a multilayered sample obtained from *C. tigris* shells.

2.4. Powdered Samples

Cypraea adult shells between 7 and 10 cm were washed with Milli-Q water and submersed 1 h in NaOCl 3 %, to remove organic contaminants and soft tissue rests of the shell interior. They were then washed with Milli-Q water and air dried. Two types of powder material were prepared, an average powder material as well as a layer separated material. Each sample was an average from ten to twelve shells of the same species. Both were powdered by different methods, obtaining comparable independent results.

Whole Shell Average Material

In this case each shell was put in a plastic coverage (five bags one inside the other, for stability) and broken down to pieces of about 1 cm^2 with the aid of a tungsten carbide press. About 50 g fractured pieces were put in a rotating agate mill and shaked at 3000 rpm for 1 h. In this case the obtained powder is an average of the whole shell or shells milled. The method does not give layer separated samples but has the advantage of easily getting larger average samples (Compare the amounts obtained with both methods in Figure 7).

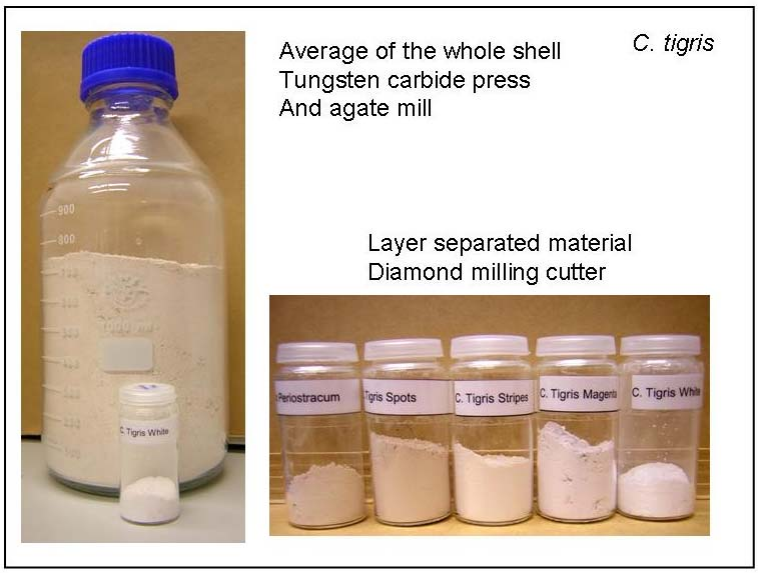

Figure 7: Whole shell average material (left) and layer separated material (right) obtained from *C. tigris* shells.

Specific Layer Material

With help of a cylindrical diamond micro milling cutter of 1 mm diameter, commonly used by dentists, thin layers, optically distinguished thanks to their different colours and textures, were carefully powdered off. Only the upper part of the shell was used to get the layer specific material. All margin borders, where the structure is more complicated, were not studied. For each layer ten to twelve shells of the same species were averaged. Compared to the fracturing and milling method, this last allows for preparation of samples according to specific properties like per colours or layers, etc. On the other hand, this method is very time consuming and requires technical experience.

2.5. Standard Samples

Certified Standard Material (CSM)

Absorption Spectroscopy Standard Solutions from Merck of a certified concentration of (1000 ± 5) ppm in HNO_3 1 M were used as standards for the INAA. Elements analyzed were: Na, Mg, K, Ni, Ba, Ca, Sr, Br, Fe, Co, Cr, Zn, Au, Ag, Cd, Se and Hg. In each case, the standard was diluted to achieve a maximal activity at the irradiation end of 20kBq and a final standard

sample volume of 2 ml. Blanks of HNO_3 1 M were always irradiated and measured under the same conditions as the samples and the standards. The specific activity obtained was then subtracted from the respective sample activity.

Multielemental standards CERIPUR® for ICP-MS from Merck, of a certified concentration of (1000 ± 5) ppm in HNO_3 1M, were used as standards for the ICP-MS analysis. Elements certificated were: Na, Mg, K, Ni, Ba, Ca, Sr, Br, Mn, Fe, Co, Cr, Zn, Au, Ag, Cd, Cu, Ni, Sn, Se and Hg. The standard was diluted 1:1000 to achieve a concentration of 1ppm and called "standard solution" and kept at room temperature; this solution was then if necessary diluted to make the calibration curves from the measurement in the same day.

Certified Reference Material (CRM)

Due to the fact that there are no mussel shell materials available in the CRM market, other biological matrices were chosen. Five certificated reference materials[3] of dry biological samples and sediments were used. For a list of the elements certified in each one, see Appendix XIV ("Data of Some Standards Used").The advantage of using CRM in comparison to the CSM is that the sample original state is also a powdered matrix, more similar to that of the solid shell samples.

2.6. INAA Samples

Solid Samples for INAA

The mass of powdered shell to be analysed was chosen as 100-150mg, because the activated sample should not have an activity higher than 20kBq. Taking into account only the elements Ca, Sr and Na, the main components, this activity is achieved with 150mg per sample. The samples were filled in 5 ml PEEK tubes. To avoid possible metal contaminations, the tubes were previously immersed in p.a. HNO_3 1 M for 8 h, rinsed three times with MilliQ water and dried. After the irradiation and prior to the measurement, the capsules were changed for new ones (none irradiated) and the transferred mass weighted again.

[3] Commission of the European Communities- Community Bureau of Reference- Report EUR10997, EUR11850 and EUR8119.

Liquid Samples for INAA

Shell samples were also dissolved in p.a HNO_3 1 M. This procedure has two advantages, on one hand that a liquid sample is more homogeneous, and on the other hand that the difference between samples and standards in geometry, density and absorption are minimized. For this treatment 100-150 mg shell powder were directly dissolved with 2 ml HNO_3 1 M in the 5 ml pre-washed PEEK capsules then used for the irradiation. In this case the capsule was also changed for the measurement step after the irradiation step.

Blank Samples for INAA

The blank for the liquid samples for INAA were 2 ml HNO_3 1 M. Solid samples did not need blanks.

2.7. ICP-MS Samples

Liquid Samples for ICP-MS

The solid shell samples were dissolved in a mixture of HNO_3 and HCl at proportion 3:1. The mass m_P of powder (generally, 1 g) was dissolved in the volume V_1 (5 ml) of acid. An aliquot m_A (500 μg) of this latter solution was then diluted to a volume V_2 of MilliQ water. Finally, to maintain all metal species in ionic form, HNO_3 2 % and ^{103}Rh in 0.01 % as internal standard were added.

Blank Samples for ICP-MS

The blanks of the ICP-MS analysis were MilliQ water samples, in a volume equal to the final volume (V_2) of the samples, with the addition of ^{103}Rh 0.01% and HNO_3 2 %.

2.8. HPLC Materials

The Solvents

The solvents chosen for the chromatographic separation (See Appendix XV) were ultra sounded with an ultrasound finger during 20 min or degassed with the DEGASYS® DG 1310 device. The solvents were mixed to the required concentration automatically in the auto-sampler unit. The pumping system gives also the possibility to make constant concentrations as well as different types of gradients between four solvents.

2.9. GE Materials

The Buffers

The corresponding running and sample buffers were acquired from Anamed, and diluted to the work concentration with MilliQ water. For Mops gels, the running buffer stock solution (20x) consists in a mixture of 600 mM Mops, 1.2 M TRIS and 2 % SDS, at pH 8.4. The sample stock solution buffers (2x) is composed of TRIS-Mops, at a pH 6.9. Bromophenol blue is used in the latter as colorant.

The Staining Solutions

The solutions for *Coomasie Brillant Blue* and Silv*er* staining were obtained from Anamed. In the first case, the product *AzurGel Super*® is ready to use; it does not need sensitizing steps. The advantage is that solvents like acetic acid or methanol are not used and that the gel can be destained with water. The whole process takes about 3 h and the detection limit per band is 7 ng of reduced BSA (Anamed, home page). The silver staining method was done using the kit *ArgentQuick*®, which contains the sensitizer, the staining solutions, the developer and the stopper solutions. The duration of the silver staining is around 2 h, and the detection limit reported for this method is 0.8 ng reduced BSA, one order of magnitude higher than the *Coomasie Blue* method. For both methods, ultra pure MilliQ water was used to clean the gels and to make all staining solutions. For silver staining also p.a. methanol and p.a. acetic acid from Sigma were used.

Non Reduced Samples

The different lyophilized standards and organic matrices extracted from *Cypraea* shells were dissolved in MilliQ water, at a concentration approximately of 10 ppm and mixed with the Mops-TRIS-SDS buffer in a relation 1:1.

Reduced Samples

10 % Mercaptoethanol in ethanol was added 1:5 to the non reduced samples. The probes were mixed well and heated in water bath at 100 ºC for one hour. This process produces a volume reduction of about 50 %.

2.10. Solvents

Acetic Acid Buffer

The acetic acid at a concentration 15 % was prepared adding 75 ml of glacial acetic acid of analytical purity, delivered in plastic bottles, to a 500 ml NALGENE® bottle and diluting with MilliQ water. The acid was buffered by the addition of ammonium acetate from Sigma until pH 4.75 (aprox. 54 g). The solution was stored at room temperature.

HCl 15%

HCl at a concentration 15 % (v/v) was prepared diluting 250ml of HCl 30 % ultrapure with 250 ml MilliQ water in a 500 ml NALGENE® bottle. The solution was stored at room temperature.

2.11. Organic Matrix Materials

Soluble Organic Matrix

The extraction method was studied divided in four steps: demineralization, purification, pre-concentration and conservation. For all of them, two or more methods were tested (See Appendix IX ("Experimental Study of the Different Extraction Steps", for detailed information of each method). The extraction processes were divided by the amount sample dissolved. The optimized final extractions are described briefly below.

Large Amount Samples

Drops of HCl 15 % were added to MilliQ water until a pH 5.5 was reached. An amount of 100 ml of this solvent was added to 50 g of powdered *average material* shell. Under 4 ºC, acid drops were added slowly, under continuously stirring. The pH was not let to diminish below 4, and the temperature was maintained between 4 ºC and 8 ºC during the evolution of the demineralization process.

Each time that a volume of 250 ml was reached, the solution was decanted, the liquid fraction collected and reserved. The process was repeated with the rest of the material until the whole decalcification of the mass. NaN_3 0.01 % was added as antibiotic and the solution was incubated for 8 h at 10 ºC. After that the pH was adjusted to 7 with NaOH 1 M at 4 ºC. The sample was let to incubate for 30minutes and was centrifuged at 4000 rpm for 15 min. The insoluble brown precipitate was collected, washed with MilliQ water and centrifuged at 4000 rpm for 15 min three consecutive times. The washing liquid fractions were added to the soluble fraction, and the insoluble precipitate was lyophilized and called "Insoluble Organic Matrix" (IOM).

The 500 ml soluble fraction was exhaustively dialyzed with Spectrapore® CE7 membranes (3 kDa MWCO, 5 cm width) against MilliQ water for two days, against a volume 10 times bigger than the sample. The precipitated material has been removed by centrifugation at 4000 rpm for 10 min. The liquid sample was then frozen at -10 ºC, lyophylized, rediluted in 10 ml MilliQ water and aliquoted in 1 ml samples. The final sample, called "Soluble Organic Matrix" (SOM), was conserved at -10 ºC.

Also the purification by ultracentrifugation-filtration (UCF) was evaluated with the "big amount" samples. For that, the dialysis step was replaced by UCF purification. The 500ml soluble fraction was divided in Y3000 Amicon® UCF tubes (3kDa MWCO) and centrifuged at 3000 rpm for 1 h. The <3kDa fraction was discarded and the >3kDa was refilled with milliQ water. The process was repeated six times. At the end, the last fractions bigger than 3kDa (around 3 ml) were frozen at -10 ºC and lyophilized.

Small Amount Samples

Drops of HCl 15 % were added to MilliQ water until a pH 5.5 was reached. Five ml of this solution were added to 1 g of powdered shell, at 4 ºC. The sample was titrated using an automatic titrator with 10μl drops of AcH-buffer o HCl under continuous stirring, maintaining pH>4, until the whole decalcification. The solution was incubated 8 h at 4 ºC. After, NaN_3 0.01 % was added to the sample and the pH was changed to 7 with NaOH 1 M. The solution was centrifuged for 15 min at 4000 rpm, the liquid fraction reserved, and the precipitated matrix washed with milliQ water and centrifuged again, for three times. The insoluble fraction was lyophylized and called IOM. The liquid of the washing processes was added to the reserved fraction and the solution was exhaustively dialyzed with Spectrapore® CE7 membranes (3 kDa MWCO, 5 cm width) against MilliQ water for two days. Finally the SOM samples were lyophilized, rediluted in 5 ml MilliQ water, aliquoted in 1 ml Eppendorf vessels, and stored at -10 ºC.

Insoluble Organic Matrix

The insoluble fractions (IOM) extracted from the powdered shell were partially solubilized in 10 ml SDS 10 % at 100 ºC for 1 h. After that treatment the samples were centrifuged at 10000 rpm for 15 min and the soluble fraction recollected. SDS 10 % was then treated as a blank for the IOM.

3. Methods of Trace Element Analysis

Three *Cypraeidae* shells were investigated for their composition by different analytical methods. INAA and ICP-MS were the two chosen for quantification. Powdered shells as well as HNO_3 dissolved samples were studied. Good results were obtained with three irradiations, of 1 h, 6 h and 24 h, and decay times of 30 min, 3 d and 20 d respectively for INAA and with the "S-option" optic for the ICP-MS measuring each mass during 100 ms. In this chapter the two techniques and their experimental methods are described. Accuracy, performance, interferences and limitations for the analysis of *Cypraea* shells are evaluated in the Append V "Analysis and Comparison of INAA and ICP-MS".

3.1 Introduction

Analyzing the actual alternatives for trace elemental analysis, between the techniques capable of measuring the concentrations of determined elements in a complicated matrix, INAA was selected as the tool to define the composition in the shells. The main reason is its precise multi-elemental analysis in a very large concentration range. In addition the advantage that the samples can be measured without any preparation process means the lowest sample contamination or element loss possibility.

On the other hand, INAA requires long times of analysis, and allows only few samples to be handled. That makes the INAA not useful for the optimization of the experiments, when different parameters are changed daily. For that latter purpose, trace element analysis by ICP-MS was used. The advantage of ICP-MS is the speed and simplicity of the analysis. This method is more sensitive than INAA for most elements, but has two big disadvantages: the first one is that it requires sample preparation and dilution. The second one is that it presents isobaric interferences, often very difficult to be detected and treated. In this chapter, both experimental methods are described.

3.2 Instrumental Neutron Activation Analysis

3.2.1 Introduction to INAA

Neutron activation analysis[4] is based on the conversion of a stable nuclide A of the element to be determined into a radionuclide B, using a nuclear reaction induced by collision with neutrons (n). Chemical elemental analysis using INAA is based on the gamma radiation emitted by excited radionuclide in a (n,γ) de-excitation process. The stable mother isotope A (n, Z) is irradiated with neutrons inside a reactor. Usually a capture reaction occurs, and A is converted into a B (n+1, Z) nucleus. If the latter is not a stable nucleus, it emits the excess of energy through a radioactive decay, with a characteristic half life and brings mostly the daughter nucleus to an excited state. In a secondary process gamma radiation is emitted to the ground state. This gamma radiation is characteristic of each nucleus and the number of mother atoms can be calculated through its quantification.

3.2.2 Performance and Limitations in General for INAA

INAA can be applied to determine major and trace elements, in the ppm and sub-ppm concentration range (for environmental samples for example), for a very wide spread type of samples and matrices. The advantages of this technique (Kellner et al., 2004) are a low to very low matrix interference effect, minimizing possible sample contamination thanks to the low or almost no necessary sample preparation, easy detection and calculation of interfering reactions and low necessary sample mass (50 to 250mg). Nevertheless, not all elements can be detected by INAA, the target elements must well fulfil at least some of certain properties. The activation is favoured as for example for good cross sections in comparison with the matrix elements, for big gamma yields in measurable energy ranges, for a measurable half life (not too short or too long), for high isotopic abundance of the mother nucleus, etc. The big disadvantage of the method is the analysis time required the need of a nuclear reactor and the special cares that imply working with irradiated material.

[4] An introduction to nuclear radiations, neutron induced nuclear reactions, relevant parameters determining the neutron activation yields and implications of an INAA measurement are described elsewhere (See for example Beckurz K.H 1964; Cohen B.L., 1971; Knoll F.G., 1989.

3.2.3 Experimental Set Up for INAA Measurements

The TRIGA MARK II Nuclear Reactor[5]

To make the neutron activation analysis the TRIGA Mark II facility of the Institute for Nuclear Chemistry at University Mainz was used for this purpose. This reactor is a 20 % enriched U^{235}, light water moderated reactor. Its maximal thermal power is 100 kW. There are two irradiation positions, one in the central position and the other in the periphery (only thermal flux) with a rotating carrousel that allows the irradiation of 80 samples in 40 places simultaneously. The election of the measurement parameters, the experiments and the calculations were done in collaboration with Dr. N. Trautmann and Dr. S. Zauner from this Institute.

Experimental Set Up

Majority metal elements found in shell samples are Ca, Sr, Na and Mg. This elements cause a big background and interference at low energies by Compton Effect that avoids the detection of other signals. By INAA, it is possible to play with the decay time of Na, Mg and Ca to reduce their relative importance in the spectrums. For that aim, irradiation and measurement parameters were elected to optimise the results on the metal trace elements of interest (observed before in literature K, Mn, Ni, Cu, Fe, Co, Zn, Ba, etc.).

In this case, three consecutive irradiations were planed. Elements with half live shorter as 30 min (for example Mg) could not be observed because the high background. The rest of the elements were divided per half live in short (1 h to 24 h), middle (1 d to 5 d) and long (> 5 d), and the irradiations were performed as shown in the next table.

Irradiation	Irradiation time	Decay time	Detection time	Position	Neutron Flux $n.cm^{-2}.s^{-1}$
Short	60 min	60 min	60 min	Carrusel	$0,7 \times 10^{12}$
Medium	6 h	5 days	3 h	Carrusel	$0,7 \times 10^{12}$
Long	24 h	20 days	6 h	Carrusel	$0,7 \times 10^{12}$

Table 1: INAA parameters used for the analysis of shell samples in the TRIGA MARK II Nuclear Reactor in the Institute for Nuclear Chemistry at the University of Mainz.

[5] Home page Institut für Kernchemie – Uni Mainz.

Irradiations in the central position were also performed, to have a high dose in shorter times. Nevertheless, due to the fact that in this position there is no place for the normal 5ml PEEK irradiation capsules (see sample preparation, Chapter 2.6), the solid samples were irradiated inside plastic envelopes. This procedure brought no good results for two reasons: the main reason because the high doses fragilices the plastic in which the powder samples were enveloped, with the consequence that the powder could not be separated any more from the bug. The second reason is that the standards used for quantification must be irradiated also in a solid form, meaning very small masses that introduce large errors in the quantification.

Energy Calibration

The Ortec HPGe detectors MOPS47, MOPS37 and MOPS35 from the institute for Nuclear Chemistry at the Mainz University were calibrated one time at the beginning of the measurements by measuring a multi-isotopic radioactive source QCY48 from Amersham for one hour. The calibration fit for the channel vs. energy curve was done automatically by the acquisition program (Intergamma Version 5.1 from Intertechnique).

Efficiency Calibration

Because the method used for concentration calculation is a “relative method” (see next section) the concentration is independent of the absolute efficiency (in the case that samples and standards are measured in the same configuration). Therefore for this work, the absolute efficiency of the detector was not measured.

3.2.4 Trace Element Quantification by INAA

Calculation of the Concentration by INAA

The activation equation (See Soldati, 2002 Eq 2.8), taking the concrete case of the reaction $^{23}Na(n,\gamma)^{24}Na$ gives for the concentration of sodium C^{X}_{Na} in a sample X (in g of Na per g of sample), using for the detection the gamma emission of the gamma line 1368 keV:

$$C^{X}_{Na} = \frac{\Sigma^{X}_{\substack{^{24}Na \\ 1368keV}} \cdot \lambda_{^{24}Na} \cdot M_{Na}}{m^{X} \cdot \eta_{^{23}Na} \cdot \varepsilon_{1368keV} \cdot \left(\frac{Y^{^{24}Na}_{1368keV}}{100} \right) \cdot \left(\left\langle \sigma_0 \cdot \phi_{Th} + I_0 \cdot \phi_e \right\rangle \right) \cdot F^{X}_{^{24}Na}(t_i, t_d, t_m) \cdot \mu^{X}_{1368keV}} \quad \text{Eq. 1}$$

Where,

Σ is the number of counts (net area) of the peak

λ is the decay constant for the excited isotope (in seconds)

M is the molecular weight of the element

m the mass of the measured sample

η the isotopic abundance of the mother nuclei

ε the efficiency of the detector system for the γ energy

Y the yield of the γ emission of the excited isotope (in percent)

σ_0 the neutron cross section for the reaction (n,γ)

I_0 the epithermal resonance integral for the reaction (n, γ)

ϕ_{Th} the thermal flux in the reactor irradiation position

ϕ_e the epithermal flux in the reactor irradiation position

μ the absorption coefficient of the material at a γ energy

And F the time factor:

$$F^{X}_{^{24}Na}(t_i, t_d, t_m) = \left(1 - e^{-\lambda_x \cdot ti}\right) \cdot \left(e^{-\lambda_x \cdot td}\right) \cdot \left(1 - e^{-\lambda_x \cdot tm}\right) \qquad \text{Eq. 2}$$

Assuming that the neutron flux is the same for all irradiated samples (this is a correct hypothesis, because the samples are irradiated in a rotating carrousel), that the samples are measured in the same geometry (same efficiency), and arranging the constant terms (these which only depend of the isotope and its gamma line in concrete, not on the sample) in Eq 1,

$$C^{X}_{Na} = \frac{\Sigma^{X}_{^{24}Na\ 1368keV}}{m^{X} \cdot F^{X}_{^{24}Na}(t_i, t_d, t_m) \cdot \mu^{X}_{1368keV}} \cdot k \qquad \text{Eq. 3}$$

where k,

$$k = \frac{\lambda_{^{24}Na} \cdot M_{Na}}{\eta_{^{23}Na} \cdot \varepsilon_{1368keV} \cdot \left(\frac{Y^{^{24}Na}_{1368keV}}{100}\right) \cdot \left(\left\langle \sigma_0 \cdot \phi_{Th} + I_0 \cdot \phi_e \right\rangle\right)} \qquad \text{Eq. 4}$$

is a constant which does not depend on the sample X, but on the irradiation and measurement parameters and the isotope constants. The specific activity (A^*) for the sodium ^{24}Na in an X sample as can be then defined as the X dependent term in Eq. 3:

$$A^{*24Na}_{1368keV}\Big|_X = \frac{\Sigma^X_{\substack{24Na \\ 1368keV}}}{m^X \cdot \mu^X_{1368keV} \cdot F^X_{^{24}Na}(t_i, t_d, t_m)} \qquad \text{Eq. 5}$$

The error of which can be propagated and approximated as:

$$\Delta A^{*24Na}_{1368keV}\Big|_X \cong A^{*24Na}_{1368keV}\Big|_X \cdot \sqrt{\left(\frac{\Delta m^X}{m^X}\right)^2 + \left(\frac{\Delta \Sigma^{X\ \ ^{24}Na}_{\ \ 1368keV}}{\Sigma^{X\ \ ^{24}Na}_{\ \ 1368keV}}\right)^2} \qquad \text{Eq. 6}$$

Measuring then the specific activity for a standard (S), a CRM or CSM sample, where the concentration, mass, absorption and times factors are known, an external calibration can be made to obtain the concentration of an (X) of an unknown sample as in Eq. 7.

$$C^X_{Na} = C^S_{Na} \frac{A^{*24Na}_{1368keV}\Big|_X}{A^{*24Na}_{1368keV}\Big|_S} \qquad \text{Eq. 7}$$

In the case that the element has two or more gamma emissions that can be used for the detection, the final concentration for the element can be calculated as an average of both results, due to the fact that the concentration calculated in Eq.1 is already independent of the isotope or gamma line in question.

3.3 Inductive Coupled Plasma-Mass Spectrometry Analysis

3.3.1 Introduction to ICP-MS

A mass spectrometer[6] separates a stream of gaseous ions into their different mass to charge (m/Z) values. In the case of the ICP-MS, a high frequency generator operating at 27 MHz or 40 MHz, is used to produce an electromagnetic field through an induction coil. Generally the gas used to create the plasma is Ar, monoatomic, inert and with a high ionization energy. Consequently almost all the elements of the periodic table can be excited in a secondary step in the plasma, ionized by Ar, and detected in the MS device.

[6] More information about ICP-MS can be found in the book “Analytical Chemistry” Kellner et al. (2004).

3.3.2 Performance and Limitations in General of the ICP-MS

ICP-MS provides an efficient combination between precision (better than a few %), accuracy, number of determinable elements, limits of detection and sample throughput. For most elements, the limits of detection are in the range 0.1-10ppb for the quadrupole filter. The major limitation of the quadrupole ICP-MS is the presence of isobaric interferences such as those arising from molecular species formed with Ar, for example $^{40}Ar^{16}O^{+}$ on $^{56}Fe^{+}$, $^{40}Ar^{35}Cl^{+}$ on $^{75}As^{+}$, $^{40}Ar^{40}Ar^{+}$ on $^{80}Se^{+}$, etc. In addition isobaric interferences are also observed for elements forming refractory oxides (Ca, Ti, Zr, Mo, La, Ta, rare earths, etc.) or elements forming doubly charged ions (Ca, Ba, U, etc.). The isobaric interferences can be partly solved by using a high resolution SF-MS or the addition of a collision cell to a quadrupole system to eliminate the molecular species that cause spectral interferences. In cases where such solutions are not possible, the interferences are calculated theoretically and substracted from the spectra.

3.3.3 Experimental Set Up for ICP-MS Measurements

ICP-MS from the Geochemistry Group at UNI-Mainz

On line and off line measurements were done with the ICP-quadrupole MS *PlasmaQuad 3* device of the Geochemistry division at the Mainz University. Measurements were done in collaboration with Dipl. D. Kremer from the working group of Prof. Kersten.

Experimental Set Up

The tuning was made with the standard calibration solution of CertiPUR® XVI (Merck) diluted to 10ppb, optimizing the torch position as well as lenses and the nebulizer intensity to get a number of counts around 300000 cps for the elements of interest. For the measurement in the range of 1-50 ppb, the “S” optic, much more efficient than the normal optic, was chosen. For each sample, the masses of interest were measured for 100ms, in five sweeps. Five to ten runs were averaged for each sample. The standard deviation of this average was taken as the experimental error of the measurement. The equipment characteristics and settings for the “S optic” are summarized in the next tables.

Parameters	***ICP-MS quadrupole***
Equipment	VG Experimental
Model	PlasmaQuad 3
Frequency	27 MHz
Peristaltic Pump	Perimax 12 Spetec
Nebuliser	Mainhard
Spray Chamber	VG Impact bead water cooled (10ºC)
Auto sampler	ASX - 510 Cetac
Plasma gas	Ar 4.6

Table 2: Instrumental Parameters for trace element determination and quantification in shell samples with the ICP-MS VG PlasmaQuad3 from the Environmental Geochemistry Group at the University of Mainz.

ICP- MS Settings		***Autosampler coupled***	***HPLC coupled***
Power / W		1350	1350
Lenses / V	Extr	486	485
	L1	0	0
	L2	-46.7	-46.7
	L3	-126.3	-126.3
	D1	-38.5	-38.5
	Focus	27.5	26.5
	PB	2.3	2.3
Gas Flows / $L.min^{-1}$	Plasma	14	14
	Auxiliar	0.90	0.88
	Nebulizer	0.85	0.88
Measurement	Adquisition	100ms	100ms
	Sweeps	5	1
	Runs	5 to 10	3

Table 3: Measurement settings for trace element determination and quantification in shell samples with the ICP-MS VG PlasmaQuad3 from the Environmental Geochemistry Group at the University of Mainz.

The liquid samples (Chapter 2), were measure by five consecutively runs, and averaged. The protocol of the measurement was: at the beginning the blanks, followed by the standards for calibration, 5 times each sample. After those, ten samples were measured. At continuation the measurements for the blank, the standard for 10 ppb and the standard for 500 ppb were repeated. If the cps obtained for this measurement did not coincide with the cps obtained at the beginning inside the interval error, the device was again calibrated, for the next 10 samples.

3.4 Summary

The comparison between both analytical techniques used for trace element analysis in this thesis is shown in the next table.

	INAA			***ICP-MS***
	Short	***Medium***	***Large***	
Institute	Kernchemie Uni-Mainz			Geochemie Uni-Mainz
Detection	Gamma Spectrometer			Mass Spectrometer
Type	HPGe			Quadrupole
Concentration range	0.3ppm-500mg/g			1-100 ppb
Calibration	External			External
Standards	CRM			SRM
Internal Standard	no			^{103}Rh
Sample Type	Solid or Liquid			Liquid
Sample pretreatment	Not necessary for powdered samples, dissolution in HNO_3 1M for liquid samples			Dissolved in HNO3 or in HNO_3:HCL
Sample Quantity	100 - 150mg			10mg
Analysis time per sample	Ti= 1h Td= 0.5h Tm=1h	Ti= 6h Td= 2d Tm=6h	Ti= 24h Td=20d Tm=8h	5min
Experience Requirement	High			Middle
Personal Requirement	90%	10%	10%	90%
Use optimized for	Final quantification of unprepared samples			Development Contaminations Blanks Metal-Proteins

Table 4: Comparison of different parameters for the trace analysis detection methods

4. Separation Methods

Different mass separation techniques were applied to the organic matrix extracted from the *Cypraea* shells. In this chapter a brief description of each technique and their experimental methodology is made. More information about the main parameters and characteristics, the optimization for the measurements, the blanks and standards used and the protocols applied in each case are found in the appends.

4.1 Introduction

The separation of a sample means the isolation of individual components or groups of components from the accompanying constituents. In this case separation applied to the organic matrix of *Cypraedae* shells comprises not only the sample preparation and treatment to achieve the individual constituents, but also the analytical characterization of these components. Chromatographic and electrophoretic methods were the two techniques applied to isolate the different proteins present in the shell matrix, based on the charge and the size of the molecules. In the following a description of the methodologies applied in both cases are found[7].

4.2 High Performance Liquid Chromatography

4.2.1 Introduction to Liquid Chromatography

The principle of chromatography is based on the passage of the constituents to be separated between two immiscible phases. For this, the sample is diluted in a mobile phase (a liquid or a gas) and moved through a stationary phase that can either be a solid or a liquid in a column or on a solid surface. Due to the different interactions of the constituents with both

[7] A description of the theoretical principles, parameters involved and instrumental techniques of GE and HPLC are commented for example by Kellner et al., (2004) and Harris et al. (1999).

phases, they appear at different times at the end of the column, where they can be detected externally.

In liquid chromatography, the analytes have interaction both with the stationary phase and with the mobile phase, and the separation mechanisms can be divided into adsorption, distribution, ion exchange or size exclusion. The distribution is based on dispersion forces and occurs between molecules that have no permanent or induced dipoles. Adsorption is based on polar interaction, arising from electrical forces between localized charges such as permanent or induced dipoles. Ionic interactions involve permanent negative or positive charges on the molecule, and the exclusion is base on the molecular sieving effect. In this work, two types of liquid chromatography were used: bonded phase chromatography (particularly reverse phase chromatography) and size exclusion chromatography

4.2.2 Experimental Set Up

The Equipment

A Perking Elmer *Series200* pump was coupled with a Bischoff *Lambda 1000* spectrophotometer detector equipped with a deuterium lamp, allowing absorption detection between 190 nm and 900 nm in mono wavelength mode. The system is provided with a *peltier* cooled Perking Elmer *Series200*auto-sampler that controls the temperature of the sample chamber as well as the injection parameters, resumed in the next table (Table 4):

Sampling parameter	***RP***	***SEC***
Washing Volume	100 μl	100 μl
Injection Volume	20-100 μl	20-100 μl
Temperature of the Samples	10 ºC	10 ºC
Equilibration time	1 min	1 min
Running time	11 min	35 min

Table 5: Characteristics of the sampling methods used for RP and SE chromatography.

The acquisition and control were made with the program Analyst™ Version 1.2 (Applied Biosystems). After the UV detector, the system can be coupled on line to an ESI-MS instrument. This coupling has not been done for SEC, because Cl^- ions (from the TRIS buffer) affect the half life of the electron-multiplier from the MS detector.

The Columns

For the separation of the organic matrix of *Cypraedae* shell, a reverse phase *300 ProntoSil C18* column (from Bischoff) and a size exclusion *Biosep S 2000* column *(*Phenomenex) were used. The *Biosep S 2000* is a hydrophilic bonded silica column with the advantage of low adsorption and high sample recovery, with stability under high salt concentrations. The characteristics and dimensions of these columns are found in the next table:

Column	***Prontosil 300 C18***	***Biosep S 2000***
Type	RPLC	SEC
Fabricant	Bischoff	Phenomenex
Length	150mm	300mm
ID	4mm	7.8mm
Particle size	5μm	5μm

Table 6: Characteristics of the RP and SE columns used

The mobile phases elected for the C18 column were isocratic mixtures of water, water-methanol and water-acetonitrile, or linear gradients between them. The mobile phase for the SEC column was a 20 mM TRIS-HCL solution, at pH 7.4. Information and protocols regarding the cleaning and equilibration of the columns are found in the Appendix III.1 (HPLC Columns Treatments, Equilibration Procedure).

Sampling Procedure

For size exclusion chromatography, a flux between 0.8 and 1 ml/min was used. For the reversed phase case the flux elected was between 0.3 and 0.5 ml/min. The sampling was made automatically using the auto-sampler. The sample volume was 100 μl. The injection volume was 50 μl (50 μl used for pre-washing of the needle). The samples were maintained in at 15 ºC. For all measurements, the column was equilibrated one minute with the mobile phase solvent. At least three measurements were averaged for each sample. At least one washing run with MilliQ water samples was performed before sample change. Information regarding the cleaning between samples and washing procedures to remove attached ions or proteins is written in Appendix III.2 (HPLC Columns Treatments, Washing Procedure).

Calibration

The mass calibration for the proteins eluted with the SE column *Biosep S2000* was done using an external calibration with proteins standards. More information about this topic is listed in the Appendix IV “SE-HPLC Column Characterization”.

4.3 Gel Electrophoresis

4.3.1 Introduction to Gel Electrophoresis

The separation by gel electrophoresis (GE), widely used in biology and biochemistry for separation, isolation and analysis of proteins, polynucleotides and other biopolymers, was introduced here as an alternative to check the chromatographic separations. This technique is based on the migration of ions in a supported electrolyte under the influence of an electric field; it differs from chromatography because the analyte does not equilibrate between a stationary and a mobile phase. The rate of migration of the specific compounds of the sample makes the separations of the particles possible. In GE the ions migrate on a support gel such as agar or polymers, saturated with the electrolyte. The two opposite sides of the gel plate are submersed in buffer solutions containing the electrodes. The samples are applied in a line at one run of the gel and migrating lines are formed. The electropherogram can be then evaluated by dye-staining or spectroscopic methods[8].

4.3.2 Experimental Setup

The Gels

Precasted VarioGels® from Anamed were used for the PAGE SDS separation. A pH-neutral polyacrylamid gel, *Mops-TRIS-SDS 9%* (Mops), was chosen for its longer conservation time (6 months), short running times (30-40 min), and good performance for protein separation between 220 and 2kDa. The characteristics of this gel are listed in the next table (Table 7).

[8] Detailed information about the GE theory, techniques and relevant parameters can be found for example in Stryer et. al, 2003.

Parameter	
Gel	VarioGel® Polyacrylamide
Manufacturer	Anamed
Type	Mops-TRIS-SDS 9%
pH	neutral
Chambers	10
Chamber Volume	25μl
Layer Thickness	1 mm
Store Life	6 months
Separation	2-220kDa

Table 7: Characteristics of the Mops gels.

The gel cassettes were put into the electrophoresis chamber, adjusted, and the inner and outer pool filled with the running buffer. Then the plastic cams were separated from the cassette gel and the sample chambers washed with running buffer to remove the rests of NaN_3 in which the gels had been conserved. 25 μl of sample, reduced or not (see Chapter 2.9), were injected with a capillary pipette tip, directly into the gel. The running conditions are resumed in Table 8. After the running time, the cassettes were opened and the gels carefully extracted. They were washed three times with MilliQ water to remove the rest of the buffer solution, and two types of staining were done independently.

Running Parameter	
Buffer	MOPS-Tris-SDS
Sample	25 μl
Voltage	200 V
Current	90 mA
Preparation Time	60 min
Run Time	Aprox 35 min

Table 8: Parameters for GE runs with MOPS gels

Calibration

The calibration of the gels was done using a standard protein mixture of known masses DALTON® from Sigma. The lyophilized standards were prepared as indicated for the reducing and non reducing conditions, in the section 2.9 Chapter 2 (GE Materials). In each run at least one standard was also measured. The calibration of the gel was made directly comparing the spot positions of the known standards with those of the unknown samples.

5 Protein Quantification Methods

The Ellman´s and the Bradford test, two methods used to quantify the protein concentration in water solutions, were checked and optimized to determine the best methodology applicable to detect and quantify shell proteins. Possible interferences were, in case of the Bradford test, study in Appendix VII.

5.1 The Bradford Test

One of the most frequently used tests for protein quantification is the Bradford test, which uses *Coomasie blue* as dye to complex the amino group of the proteins (Bradford, 1976). The complexed dye changes its colour from red to blue. A linear relationship between absorption with the protein content exists at 595 nm.

5.2 Procedure

5.2.1 Procedure for Standard Micro - Measurements

For that experiment, a Perkin Elmer *Lambda 2* UV/Vis spectrometer was used. The dye was bought ready for use (Sigma). To measure protein contents at concentrations of ppm, 1 ml of Bradford reagent, and 1 ml of a sample, must be mixed and incubated for 30 to 45 minutes in the dark. The reaction was made directly in 1.5 ml plastic UV / semi-micro cuvettes (Plastibrand). After the incubation time, the samples were measured at 595 nm and are stable for one hour. Batch samples must be measured within 15 minutes.

5.2.2 Modification of the Micro Procedure for Low Quantities

The Bradford test was modified for little amounts of sample in the ng range. For this method 100 µl protein solution are mixed with 100 µl Bradford reagent in a micro cuvette of 250 µl (Plastibrand). Standards of 0 to 10 ppm BSA and blanks samples were also prepared in the

same way. The cuvette was shaken for 5 minutes and the mixture was incubated for 30 min at room temperature in dark. The absorption at 595 nm was measured with the Perkin Elmer *Lambda 2* UV/Vis spectrometer, using a window of 4 mm diameter in the centre of the cuvette. A linear dependence with the protein content is in this case also obtained. The great advantage of using lower samples quantity (100 μl) makes this procedure excellent for the shell protein analysis.

Calibration

For quantification, an external calibration with a protein standard (BSA) was done. BSA solutions, in the range 1 to 10 ppm, were freshly prepared all days. For each measure batch, three to five standards of each concentration were prepared, measured and averaged. The calibration was accepted, when the standard deviation between samples of the same concentration was lower to 1 % and the linear regression coefficient was found between 0,98 and 1.

5.3 The Ellman´s Test

The Ellman´s Test is based on the reaction introduced by Ellman in 1959, using 5,5´-dithio-bis-(2-nitrobenzoic acid), known as DTNB. This reagent is a water soluble compound used to quantify free sulfhydryl groups ($R\text{-}S^-$). The complexation of DTNB with the free sulfhydryl group produces a yellow product that can be detected at 412 nm. To estimate the quantity of sulfhydryl groups in the sample, cysteine standards were prepared between 300 and 0 ppm; 10 ppm was the observable minimum concentration.

5.3.1 Procedure for the Ellman´s Test

A reaction buffer of 0.1 M sodium phosphate (Roth) containing 1mM EDTA (Roth) is prepared and brought to pH 8.0 with Na(OH) 1 M. 4 mg of the Ellman´s reagent (Roth) are added to 1 ml reaction buffer. 100µl sample or standard are added to 20 µl prepared reagent plus 1.5 ml reaction buffer, mixed directly in 1.5 ml plastic semi-micro cuvettes (Plastribrand). After 15 min incubation, the absorption is read at 412 nm in the *Lambda 2 Perkin Elmer* Spectrometer. Because the test applied to the shell samples and blanks was always negative, no further studies were done about this method.

6 Other Methods

Microscopy and Spectroscopy studies were done in *Cypraea talpa*, *tigris* and *zebra* shells, in collaboration with the different groups of the University of Mainz and the Max Planck Institute. A brief description of the instruments used and the methodologies applied is described in this chapter.

6.1 Confocal Laser Scanning Microscopy (CLSM)

The shell layer microstructure was studied with a TCS SP2 X1 Confocal Laser Scanning Microscope of Leica® Microsystems in collaboration with the group of Prof. Dr. H. Duschner, "Angewandte Struktur- und Mirkroanalytik" from the Uni-Klinik Mainz[9]. The advantage of this type of microscopy is that the confocal plane can be put inside the sample, revealing its 3D structure, without any special treatment (commonly etching) on the surfaces. Crop measurements were made in air with a red laser He-Ne 10 mW at 632 nm. To achieve a better resolution, more energetic lasers (Ar-Ion Laser 100 mW at 514 nm, and He-Ne 1.2 mW at 543 nm) were also used under oil immersion. The oil has shown to attack after some days the resin in which the samples are embedded, but not the sample itself. To avoid possible oil effects on the shell, the samples where polished some µm again for each measurement. Imaging in fluorescence mode was taken using the blue laser, and oil immersion.

6.2 Micro Raman Spectroscopy (µ-RS)

Raman spectra were recorded using a Jovin Yvon Induram µ-Raman Spectrometer, coupled with the latter described CLSM, working in close collaboration with Dipl. Biol. B. Schwartz and Dipl. Phys. H. Götz from the group "Angewandte Struktur- und Mirkroanalytik". For better resolutions, oil immersion was always used. The confocal plane was elected 10 µm inside the surface. The pinhole used was 20 µm. The scattered light was collected at an angle of 180° (back-scattering). The signal original from the oil and of the resin in which the samples are embedded was also scanned to compare it with the sample signal. There were studied

[9] Home page Angewandte Struktur- und Mirkroanalytik.

spectra of especially interesting structures (as for example periostracum or prisms border edges) and lines crossing the complete sample in 20 μm steps.

6.3 Field Emission - Scanning Electron Microscopy (FESEM) - Energy Dispersive X-Ray Analysis (EDX)

A FESEM Leo® 1530 built on a GEMINI field emission column, coupled with an EDX system of Oxford® from the Cosmochemistry Research Group of the Max Planck Institute in Mainz was used, in close collaboration with J. Huth, for detailed surface imaging and X-ray analysis at the nano-scale. The observations were made under carbon coverage and detected with a secondary electron detector (SED) or a backscattered detector (BSD). The magnification, resolution and accelerating voltage are written in the caption of each micrograph.

6.4 X-Ray Diffractometry (XRD)

To investigate the mineralogy of the different layers and shells, 200 mg of powdered layer of C*ypraea* shells were measured in a 2θ diffractometry analysis with a XRD 3000 TT from Seifert, using Cu Kα radiation (40kV and 30mA) with a Ni filter. The scanning speed was set in 0,005º 2θ s^{-1}. The time constant was elected as 2 s. The measurements were done in the Geochemistry group of Mainz University.

6.5 Microprobe Analysis (MP)

The mapping and quantification for trace and main elements of *Cypraea tigris* shell samples by X-ray microprobe was done at the Institute of Geosciences of the Mainz University. This technique permits high resolution at low acceleration voltages, allowing detailed surface imaging and X-ray analysis at the micro scale. Thin polished shell samples were analysed in the Jeol JXL 8900RL electron microprobe. The operating conditions were 15kV and 8mA, and the calibration was made with mineral samples. Twenty point measurements were averaged following a line from the outside to the inside of the shell, each 20μm.

SECTION III.
RESULTS

7. Micro and Nanostructure of *Cypraeidae* Shells

In this chapter, three *Cypraeidae* shells were investigated for the mineralogical structure. Many different image methods were used and the micro and nanostructure was photographed and explained. Optically distinguishable layers, for its colours and textures, were manually extracted and analysed. The results were compared between layers and between shells. Our contribution in this topic focuses on the differences of composition trace elements and organic content related to the micro and nanostructure observed in these *Cypraea* exemplars.

7.1 Optical Observations

As it was already said, *Cypraea* snails present a transparent, brilliant and smooth periostracum. During the entire live of the animal the periostracum is enlarged with the continuous addition of substance, thanks to the mantle wrap around the surface. Under this surface is found a coloured layer. The pigments (different tones of yellow, brown, white and black) are visible through the first transparent layer and give the snails its beautiful and very different species dependent pattern. From the outside, only these two layers are observable in *C. tigris* and *C. talpa*. In *C. zebra* specimens a third striped dark-light layer can be easily observed trough the spots. The optical observation of adult *Cypraea tigris, talpa* and *zebra* shells are compared in Table 9.

To investigate the shells, the periostracum and the pigmented layer were carefully removed using a dentist diamond milling cutter. Under these both observable layers, there were found four other layers of different microstructure, colour, and composition (See Chapter 2, Figure 5). In total were found six optical observable different layers, and the first 5 were studied in this work.

Characteristic	*C. tigris*	*C. talpa*	*C. zebra*
Periostracum	Varnish like, transparent	Varnish like, transparent	Varnish like, transparent
Pattern	spotted surface	striped surface	spotted surface
Pigmentation upper surface	black, brown, yellow, white	brown, yellow	light-brown, white
Pigmentation ventral zone	white	dark brown	light-brown
Ventral length	9 to 15 cm	7 to 10 cm	7 to 11 cm
Studied layers	P, C, S, M, W	P, C, S, W	P, C, S, M, W

Table 9: Optical comparison between three different *Cypreadae* species.

7.2 Microstructure

The terminology of shell microstructures is usually based on the morphology of sub-units as observed in thin-sections with a petrographic microscope or with an SEM (Chateigner et al., 2000). In the present work it was described the shell microstructures of *C. tigris*, *zebra* and *talpa* using the terminology of Carter and Clark (Carter et al., 1985). The terms “first” and “second order” are used to characterize increasingly fine micro and nano structural elements (Dauphin et al., 2000).

7.1 Results of CLSM

The microstructure observable from CLSM measurements shows three structural different layers (Figure 8). The coloured and white layers correspond to a prismatic structure, the magenta and the striped layers to a cross lamellar and the structure of the periostracum and the nacre is not clear in these pictures.

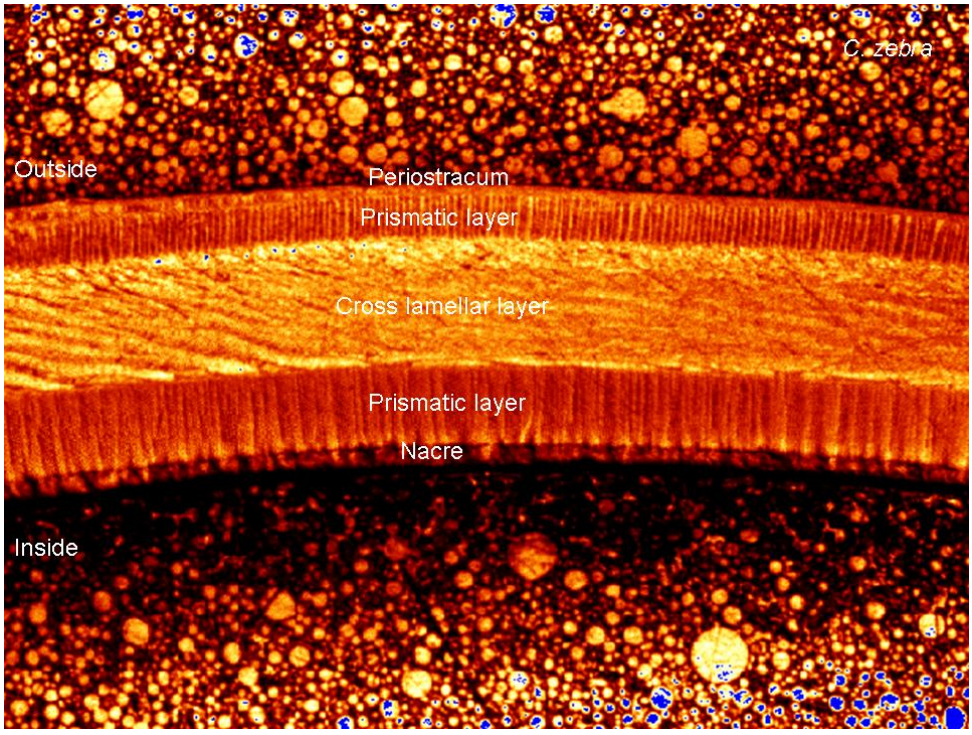

Figure 8: CLSM micrograph showing the different layers of a *Cypraea zebra* shell cross section.

CLSM: The sample was prepared by polishing a cross section ring. The picture was obtained by CLSM-Normal mode; the confocal plane was chosen 10 μm under the surface. Energy of excitation= 632 nm. Pinhole= 20 μm.

A higher magnification (Figure 9) shows the structure of the periostracum to be a homogeneously layered surface, without observable presence of prisms or crossed lamellar structures. Figure 9 shows for example a cross section of a *C. talpa* exemplar, where the homogeneous layered conformation of the periostracum, the simple prismatic structure of the coloured layer and the first crossed lamellar layer corresponding to the striped layer are clearly represented.

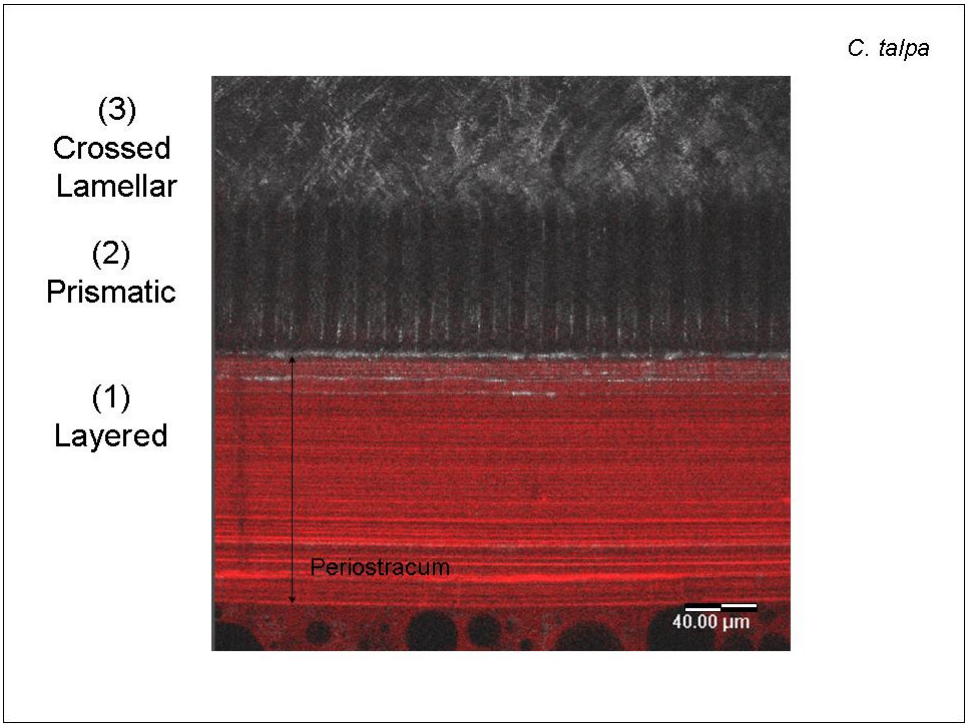

Figure 9: CLSM micrograph showing the periostracum, prismatic and crossed lamellar structures in a *C. talpa* shell.

CLSM: The sample was prepared by polishing a cross section ring. The picture is a sum of CLSM-Normal mode (gray tones) and CLSM-Fluorescence mode (red tones); the confocal plane was chosen 10 μm under the surface. Energy of excitation= 514 nm. Pinhole= 20 μm.

Working with the CLSM in fluorescence mode a surprising fluorescence of the periostracum, the nacre and the prisms borders were observed. The fluorescence (red) shows the layered periostracum structure commented in the previous paragraph. This micrograph was obtained averaging a normal CLSM mode image with the image obtained by fluorescence mode (Figure 10) from a *C. talpa* polished sample. The same behaviour was observed in *C. tigris* and *C. zebra* (data not shown).

Of course the pattern observed can be a growth signal. In addition, the resin where the samples were embedded showed also a fluorescence (porous structure at the left of the picture), and it was not possible to polish the samples without resin. Nevertheless, the regions that show a high signal by fluorescence are these expected to have high organic matrix content and it is known that proteins and organic material have this kind of fluorescence (the same is for example observed for in teeth material).

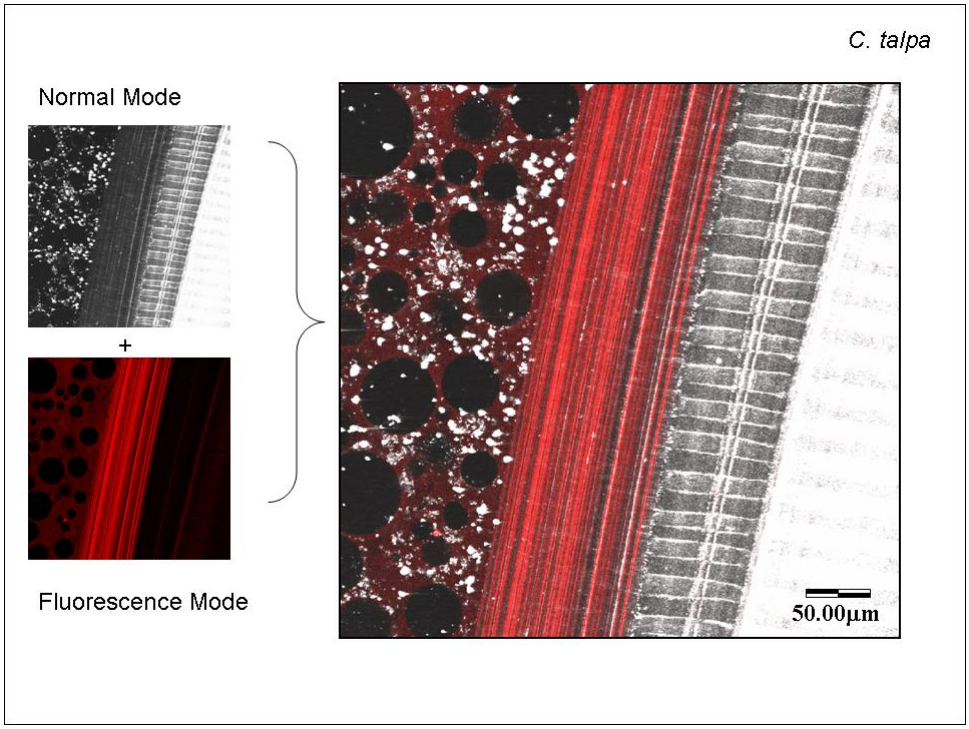

Figure 10: Fluorescence image (in red colour) added to the normal CLSM view (grey tones) of a *C.talpa* exemplar.

CLSM: The sample was prepared by polishing a cross section ring. The picture was obtained by CLSM-Fluorescence mode; the confocal plane was elected 20 µm under the surface. Energy of excitation= 512 nm. Pinhole= 20 µm.

7.2 Results of FE-SEM

The scanning electron microscopy allows the imaging of the structure at the µm and nm scale. In a fracture piece of *C.tigris* three characteristic structures can be recognised (Figure 11). Interestingly three composing parts of the periostracum are recognizable in this picture: the outer (1a), the middle (1b) and the inner (1c) periostracum. In the same picture the prismatic structure of the coloured layer (2) and the crossed lamellar (3) structure corresponding to the striped layer are also well represented.

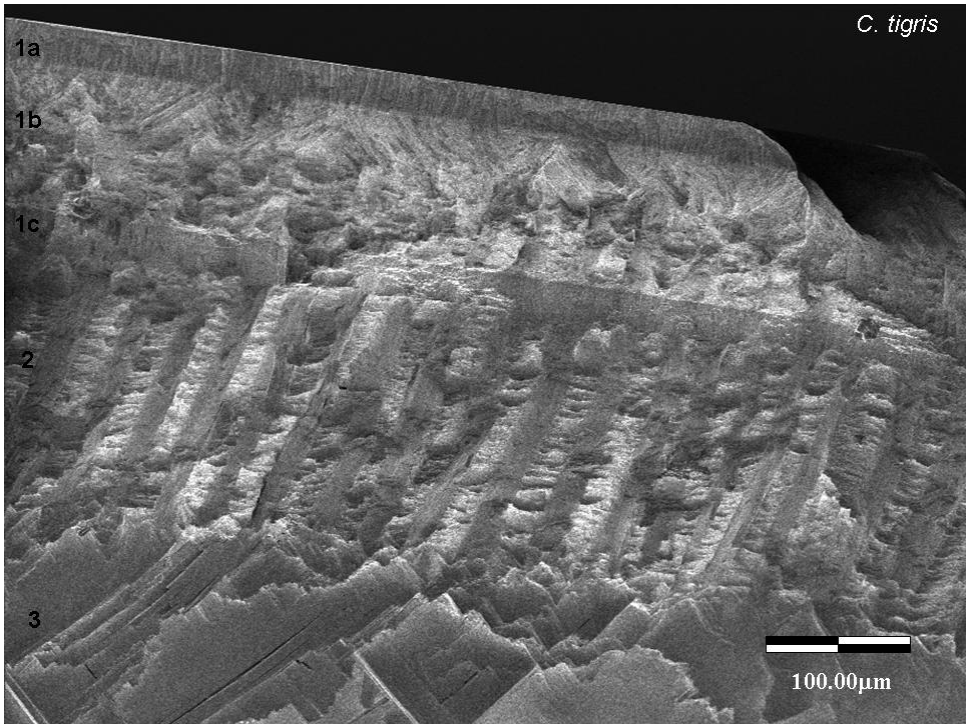

Figure 11: FESEM micrograph of a fractured piece of *C.tigris* shell.

FESEM: Magnification: 519X. ETH= 2.5 kV. I= 178 µA. The sample was fractured normal to the surface.

The different etching treatments over polished or fractured samples revealed not only the different layer structures but their fine structure. Etching with acids and EDTA provokes the complexation of the Ca ions and consequent demineralization of the shell. In some cases the organic matrix was also destroyed. Attack with protease destroys partially the organic matrix but does not affect the mineral part. For this work, only micrographs of *C. tigris* are shown. The same structures and behaviour were found for *C. talpa* and *C. zebra*.

Periostracum Layer Observed by FE-SEM

The different treated samples of the periostracum layer have shown under SEM that this coverage, brilliant to the eyes, corresponds to a very smooth surface (Figure 12A). Magnification of a fracture normal to the shell surface shows a homogeneously layered surface, possibly indicating the growing pattern. These layers, of about 100 nm thickness, are coincident with those observed in CLSM imaging for the same region (Figure 9 and Figure 10). Magnification of this picture at the fracture edge (Figure 12B) has shown that these layers are not simple structures. The secondary structures of the layers are micro-spheres of about 50 nm (Figure 12C). Further magnification, ranging to the resolution limits of the equipment, shows that these micro-spheres are also composed of a third order

nanostructure: agglomeration of spheres ranging 5 to 10 nm (Figure 12D). The structure has shown to be homogeneous trough the whole periostracum.

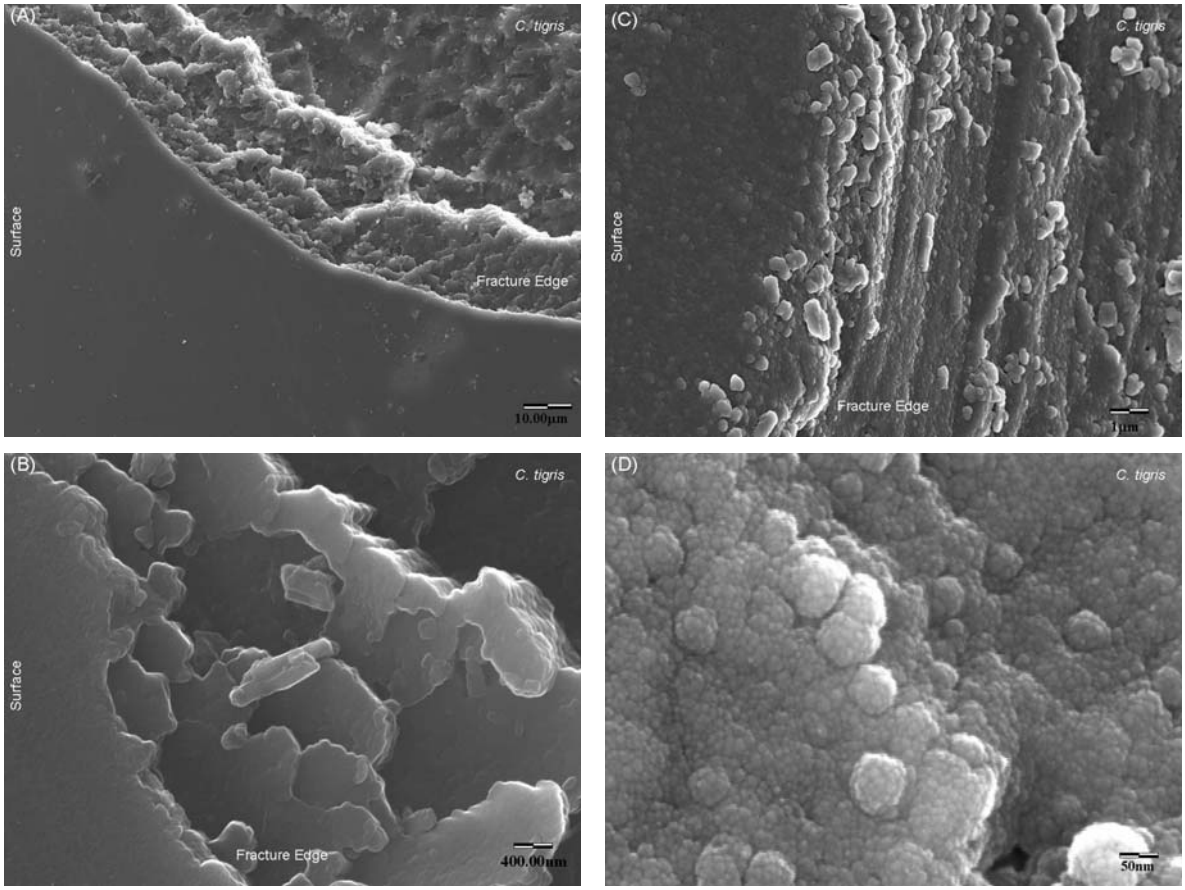

Figure 12: FESEM micrographs showing the periostracum of fractured section from a *C. tigris* shell.

FESEM: imaging under carbon coverage. ETH= 20 kV. I= 160 µA. (A) Periostracum at the margin of fracture showing the smooth coverage and layer microstructure. Mag= 3 kX. (B) Layered first order microstructure of periostracum at the fracture edge. Mag= 26 kX. (C) Amplification showing the spheres second order microstructure of each layer. Mag= 66 kX. (D) Third order microstructure revelled after NaClO etching. Some spheres have been lost and the nano-spheres can be better observed. Mag= 500 kX.

The periostracum has been moderately affected by the NaClO etching with loss of the firsts spherulitic layers. Nevertheless, the glomerular structure is recognisable as well as the nanostructure of the spheres (See Figure 12D). Under acid and EDTA etching, the destruction of the periostracum was complete (Data not shown). Protease treatment has shown to affect the inter-glomerular surface, (Figure 13 A-B). The arrows show the regions where the matrix was attacked by protease.

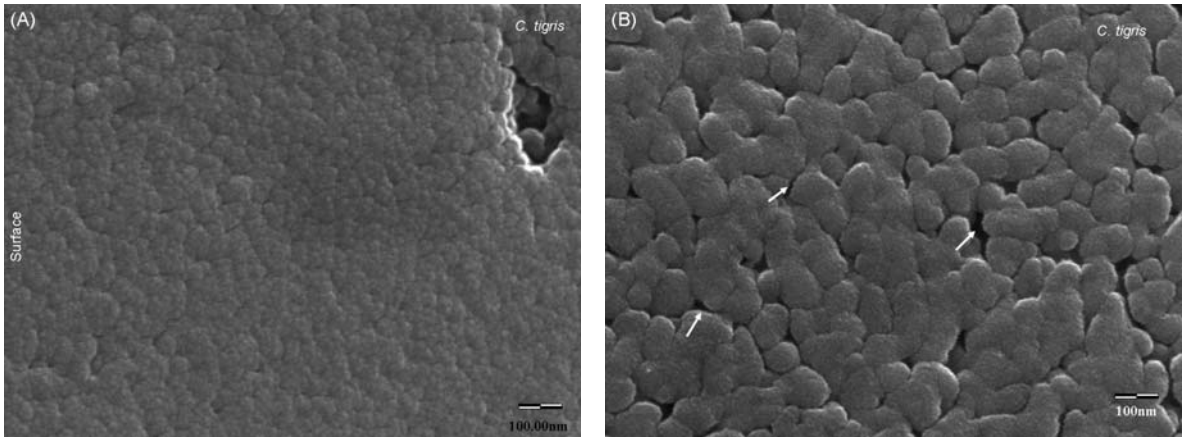

Figure 13: FESEM micrographs showing the periostracum of *C. tigris* before and after protease etching.

FESEM: imaging under carbon coverage. *C. tigris* periostracum without treatment (A) ETH=20 kV. I=160 μA. Mag= 285 kX. (B) *C. tigris* periostracum after protease etching; ETH=15 kV. I=190 μA. Mag= 265 kX.

Prismatic Layers Observed by FE-SEM

In this case, the fractured pieces observed with the FE-SEM have shown a first order prismatic microstructure (Figure 14A). The prisms are about 120 μm long per 15 to 20 μm width. Longitudinal axes are oblique or perpendicular to the shell surface. These structures show regular polygonal sections as well as homogeneous dimensions. Adjacent prisms have are shown in (Figure 14B). Prisms are not mono-crystals, since they are composed of a second order prismatic structure. The dimensions of this fine prisms structure are around 10μm large and 2μm diameter, perpendicular to the growth lines. The third order fine structure is composed again of prismatic units, in this case in the range of 4μm large per 100nm width (Figure 14C). The fourth order structure observed is an about 50nm glomerular conformation, similar to that found in the periostracum (Figure 14D). Neighbour prisms present a different orientation in an angle 60º. A perpendicular to the normal surface view shows that the prisms in this surface form semi-round figures, with well defined borders. Also to note in this last micrograph: the presence of columns that bound the prisms together.

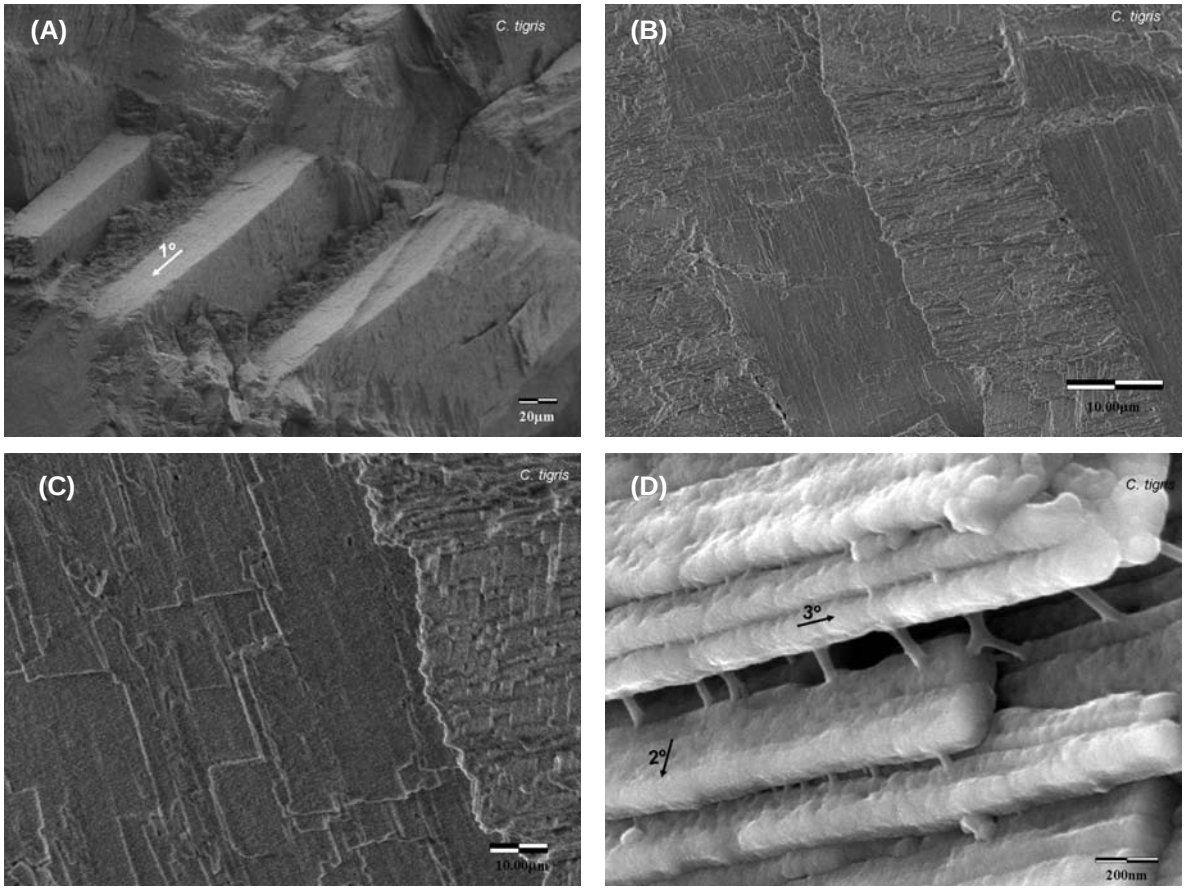

Figure 14: FESEM micrographs of the prismatic layer of C. tigris shells.

FE-SEM: imaging under carbon coverage of a prismatic layer; (A) Fracture edge ETH=2.5 kV. I=180 µA. Mag= 1 kX. (B) Adjacent prisms have perpendicular orientations; Fractured piece; ETH=2.5 kV. I=180 µA. Mag= 5 kX. (C) Amplification showing the second order prisms. ETH=2.5 kV. I=180 µA. Mag= 34 kX. (D) Second and third order prisms, after protease etching; ETH=5 kV. I=190 µA. Mag= 188 kX.

Cross lamellar Layer Observed by FE-SEM

No information was found about the crossed lamellar (CL) layers of *Cypraea* shells. Dauphin et al. (2003) has fully described the CL structure of *Concholepas concholepas*. She identifies five orders of crystallites (Figure 15) composing the CL structure. In our investigations, four orders were detected; the last one, a spherulitc material, at a resolution of about 5 nm to 10 nm.

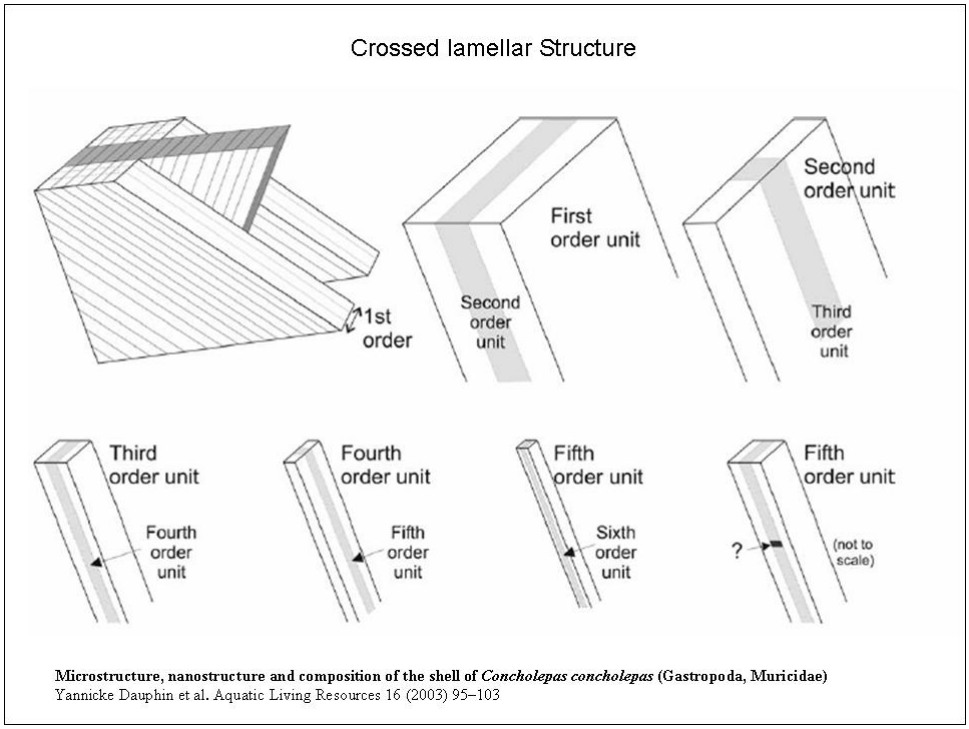

Figure 15: Schematic representation of the different orders composing a crossed lamellar structure.

A normal SEM view of the CL layer of a *C. tigris* specimen, etched with acetic acid 15 % for 1 h or HNO_3 for 10 s shows a composed structure in lamellae form (Figure 16A-B). In these pictures, longitudinal adjacent lamellae of the first order and perpendicular structures (second order) could be observed. The angle between adjacent lamellae is 60º between. HNO_3 treatment attacked more intensively the shell in one of the growth directions, revealing clearly the longitudinal first order structure.

The first and second order lamellae do not have equal dimensions (from 10 μm to 30 μm). Surrounding each "block" there is a dark region, where no material is observed. It is suggested by these photographs, in comparison with the work of Dauphin et al. that this region corresponded to an organic reach material.

The third order observed is a perpendicular crystallite of about 200 nm diameter (Figure 16C). As in the periostracum, these units are composed of spheres of about 50 nm with a fine structure of 5 to 10 nm (Figure 16D).

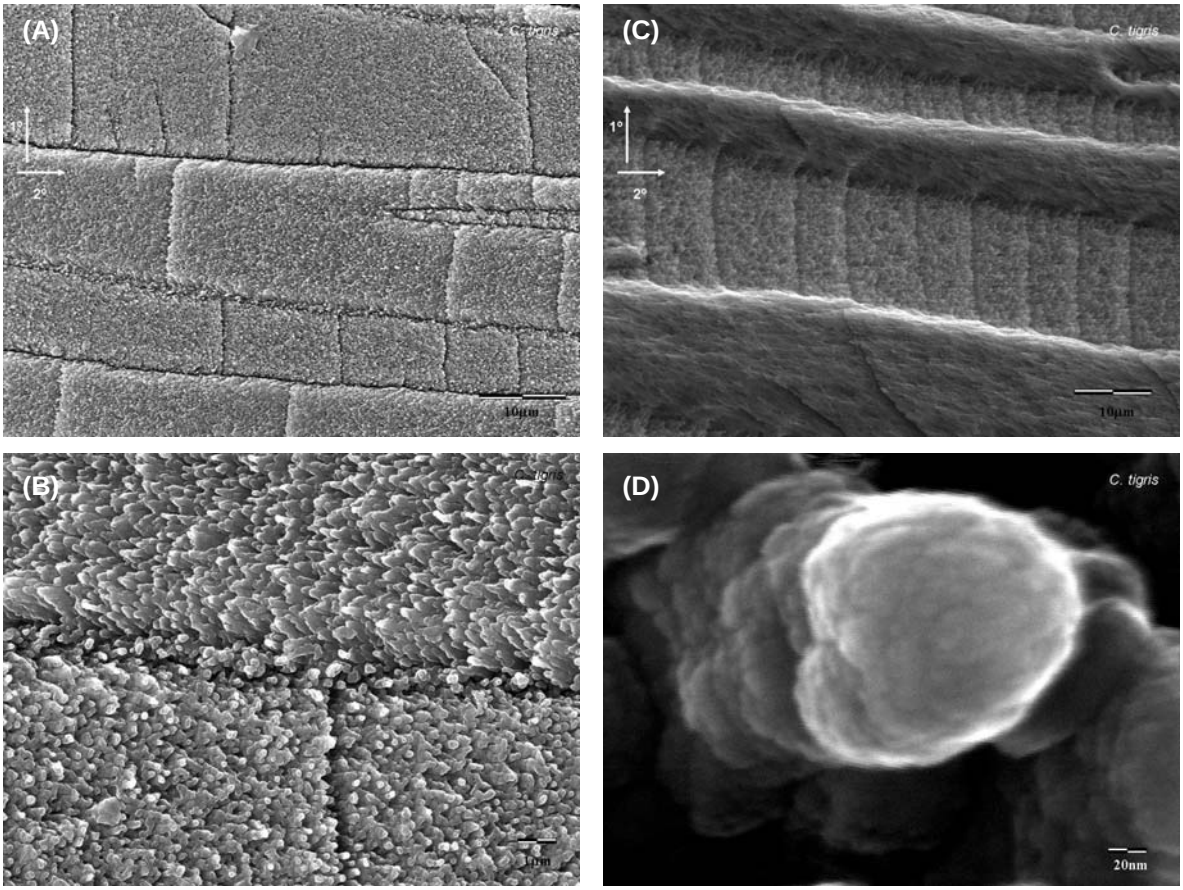

Figure 16: FESEM micrographs showing the crossed lamellar layer of *C. tigris* shells.

FESEM: imaging under carbon coverage. (A) normal view (polished section etched with acetic Acid 15 % for 1 h, Mag= 5kX, ETH= 20 kV). (B) Mag= 20 kX, ETH= 20 kV. (C) Normal view (polished section etched with HNO_3 1 M 10 s, Mag= 5 kX, ETH= 20 kV). (D) One of the third order lammelar units showing the glomerular fourth order nanostructure (Acetic Acid 15 % for 1 h, Mag 1000 kX, ETH= 20 kV).

7.3 Mineralogy

7.3.1 Results of X-ray Diffraction Analysis

The XRD results (See Figure 17) of the layer separated powder material of *C. tigris* shells show that all layers have a similar mineralogical structure. The sharp peaks mean a well crystallized mineral phase, in this case aragonite. The mineral was identified using the diffraction angles 26.18, 33.15, 38.10, 45.79 and 52.55 of the reflections (111), (021), (010) and (010) of the aragonite mineral. In all samples, a peak of the (012) diffraction is observed too. Standard spectra of calcite, aragonite and other minerals commonly found in shells were obtained from the data base of the equipment. Comparing with the standards (Figure 18) the

diffraction peak (012) corresponds to the most significant peak of calcite. Other peaks from calcite are also present, but in very little amounts in comparison to the aragonite ones.

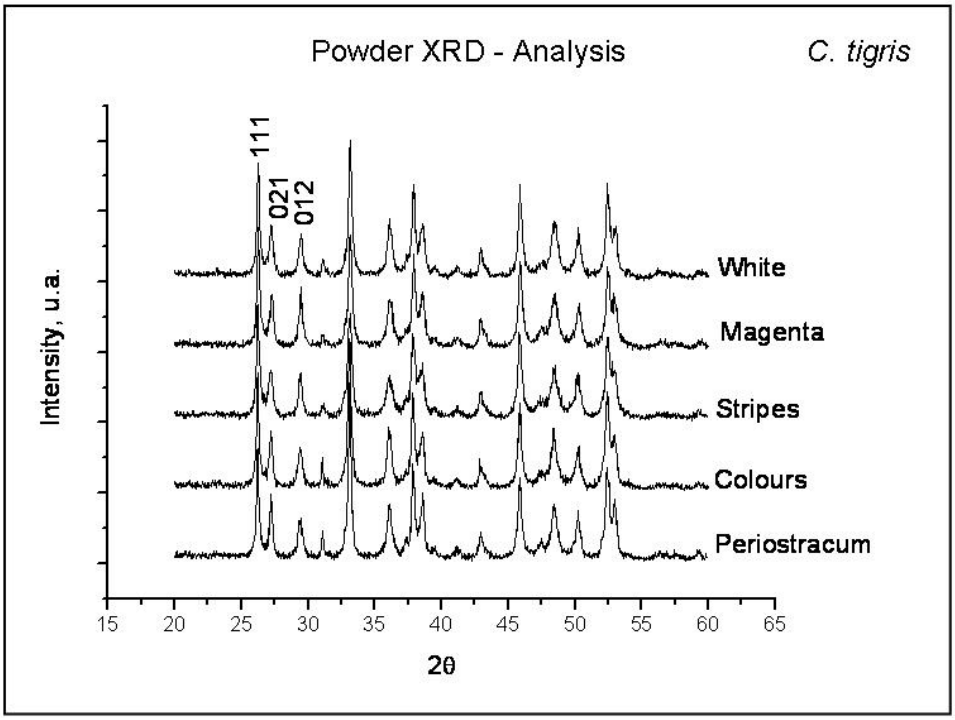

Figure 17: X-ray diffraction spectra of five different layers of *C. tigris* shells, powdered as "layer separated material"

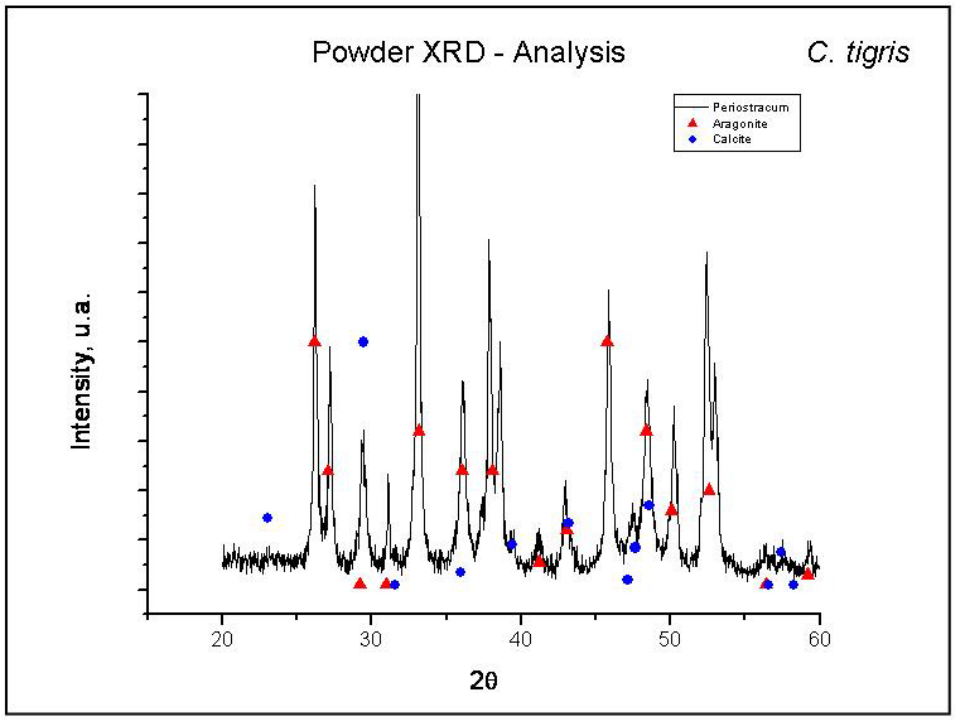

Figure 18: X-ray diffraction pattern of *C. tigris* periostracum in comparison with the most important peaks of aragonite and calcite obtained from a data base bibliography.

The first implication of these results means that the powder is not only composed of aragonite, but aragonite and traces of calcite. The presence of calcite could also be the result of an increased temperature by the powdering process, where a fraction of the original aragonite could have been transformed into calcite. This effect was already well studied, also heating mother pearl of oyster shells, were the complete transition from aragonite to calcite occurs at 300-400ºC (Bailman et al., 1999).

7.3.2 Results of Raman Spectroscopy coupled with CLSM

About the Mineral Structure

The symmetric stretching vibration of the carbonate anion in $CaCO_3$ produces in Raman spectra at 1085 cm^{-1} a strong band, observable in all spectra. This peak is present in aragonite as well as in calcite structures. To distinguish between both forms, a double peak at 701-705 cm^{-1} in aragonite and 711-716 cm^{-1} in calcite can be used. This doublet is assigned to the n4 vibration of the carbonate anion and was also found in all periostracum, prismatic and crossed lamellar studied, in perfect agreement with the XRD results. No doublets in 711-716 cm^{-1} from calcite bio-mineral were observed. The other bands of aragonite (143, 153, 180, 190, 206 and 282 cm^{-1}) are difficult to recognize because of the high background of the equipment at low wavelengths.

Six Layers by Micro-Raman Spectroscopy

Samples of *C.tigris* shells developed layer by layer (see Chapter 2, multilayer samples) have shown by Raman spectroscopy the peaks corresponding to the bio-mineral aragonite. In the layers periostracum, “colours” and “magenta” also other peaks of higher wave numbers were observed (See Figure 19 and Figure 20). The layers “stripes” and “white” and nacre have a spectrum closer to that of pure aragonite.

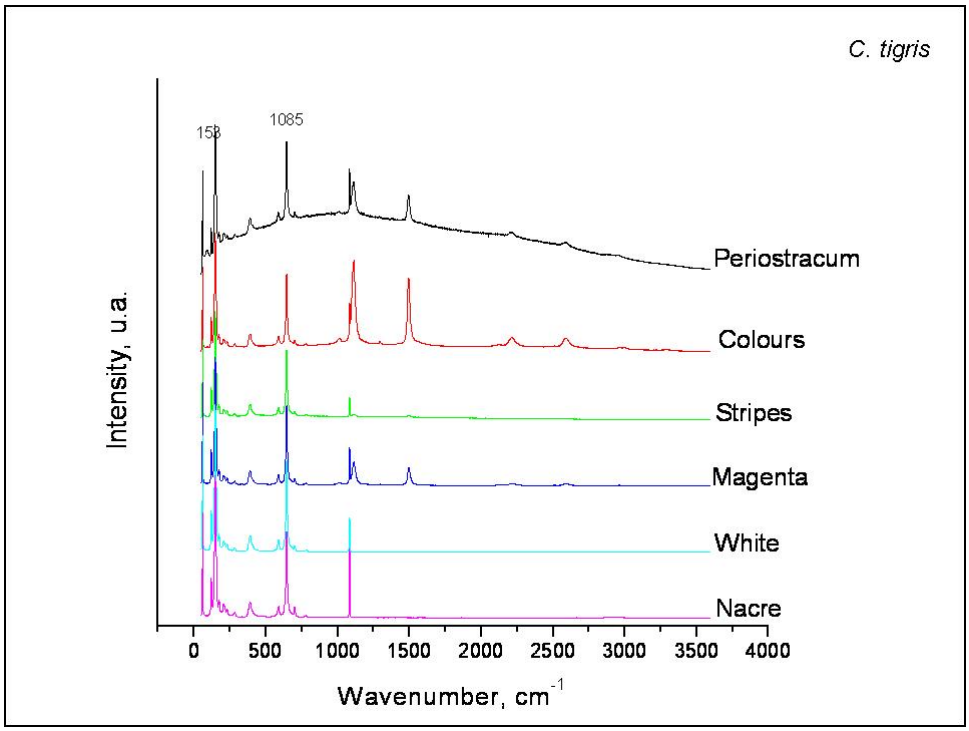

Figure 19: Micro-Raman Spectra of *C. tigris* layers.

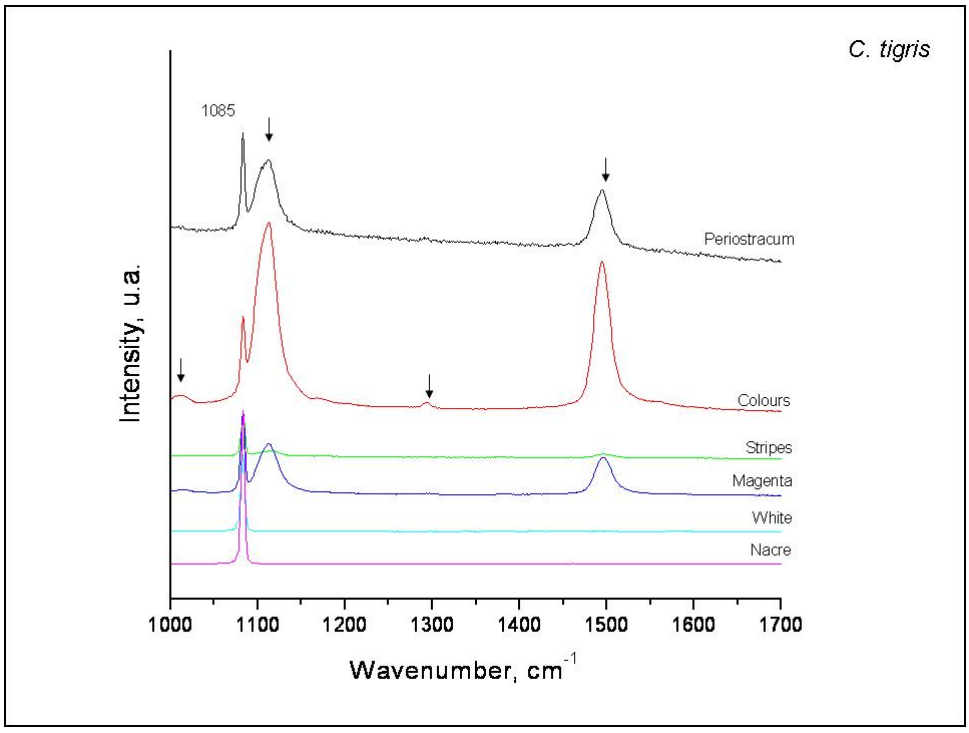

Figure 20: Micro-Raman Spectra of *C. tigris layers,* zoom of a region of interest.

To investigate the behaviour of these peaks in relation to the structure, polished cross sections were made. Periostracum and prismatic and crossed lamellar layers were analyzed by Raman in the three shells. The spectra were taken in a 2μm x 2μm spot, normal to the surface, each 10μm (white points in the next figures). The regions of interest were previously chosen by an on line coupled CLSM (See Figure 21).

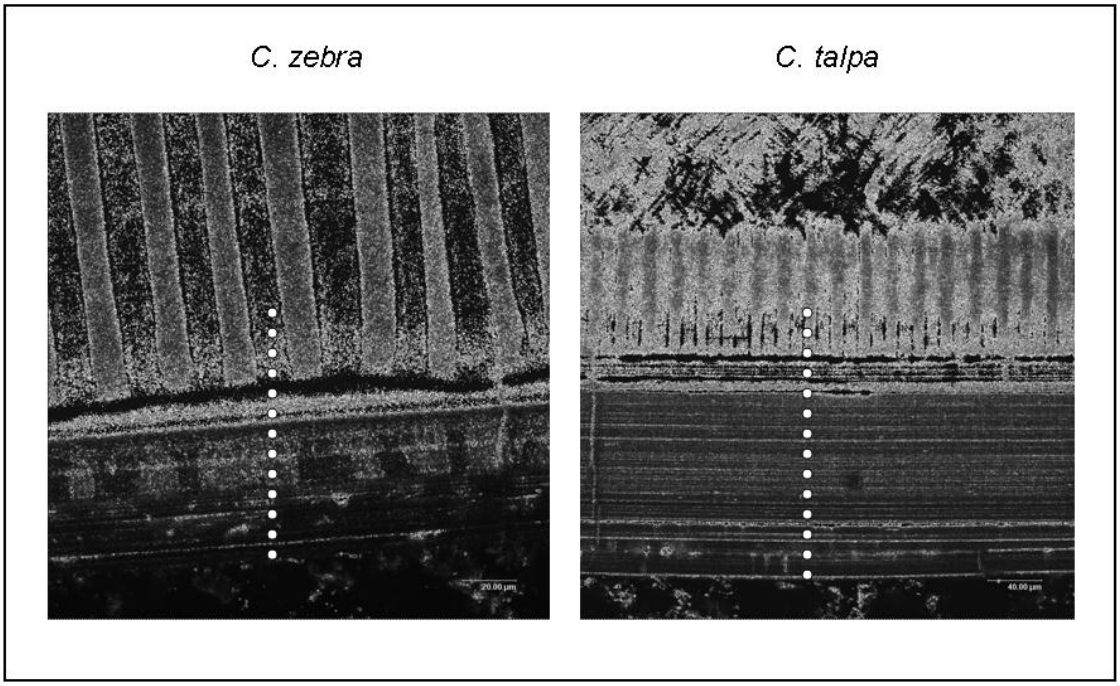

Figure 21: CLSM micrograph. White points show the region of interest for the micro-Raman analysis in C.zebra (A) *C. talpa* (B) shells.

Periostracum by Micro-Raman Spectroscopy

The periostracum layers show under Raman spectroscopy a huge hill over the whole spectra (Figure 22 and Figure 23) compared with the background spectrum. This effect is explained by fluorescence of the sample, in agreement with the observations of CLSM in fluorescence mode. Comparing both figures it can be seen that the fluorescence of *talpa* shells is much more intense than for *zebra* shells. The maximum of the fluorescence hill shows a complicated dependence with the depth of the layer investigated and is shell and species dependent (See Figure 25 and Figure 24). In this two specimens analyzed, *talpa* has shown to have a 120 μm thick periostracum, since the *zebra* only 30 μm. The first one presents fluorescence much more deviated from the average than the second, indicating that the agent that fluoresce is more heterogeneously located. In general, it was found that *C.talpa* has shown more fluorescence than *C. zebra*.

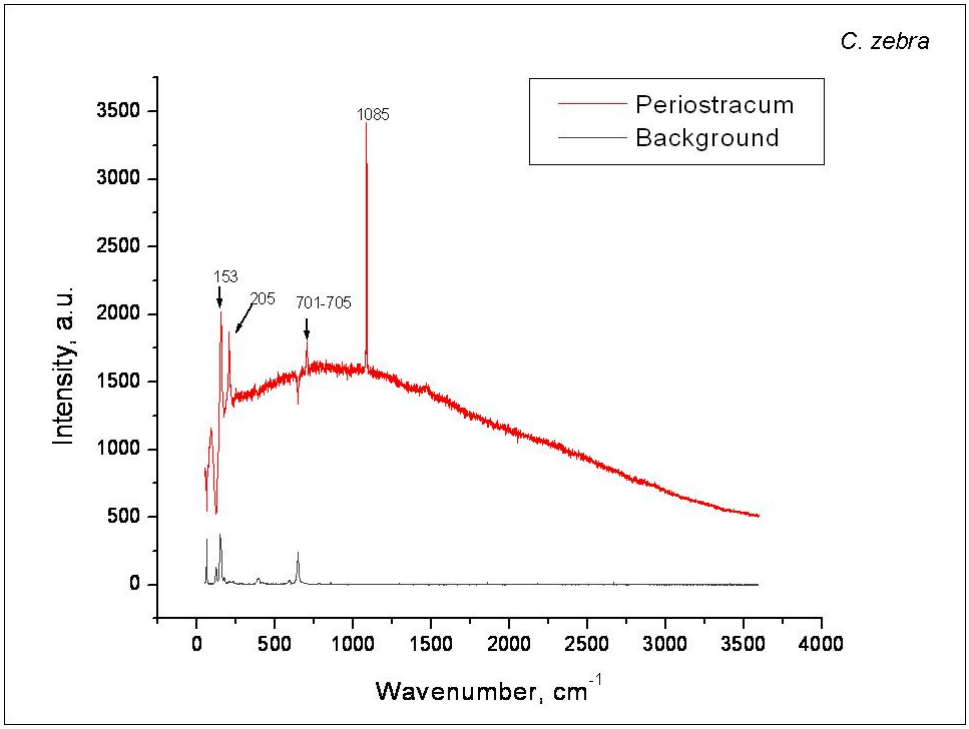

Figure 22: Micro-Raman spectra of *C.zebra* periostracum showing four peaks corresponding to aragonite bio-mineral.

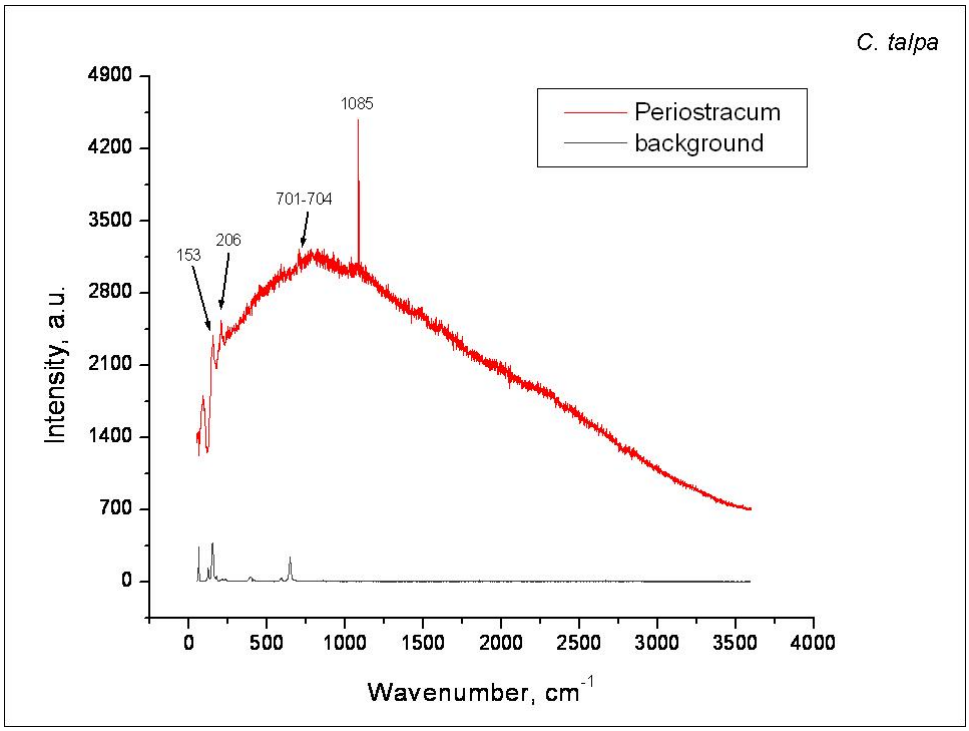

Figure 23: Micro-Raman spectra of *C. talpa* periostracum showing four peaks corresponding to aragonite bio-mineral.

SAMPLE: periostracum layer of a *C. zebra* and *C.talpa* exemplars. Raman spectra from one of the white points shown in Figure 21.

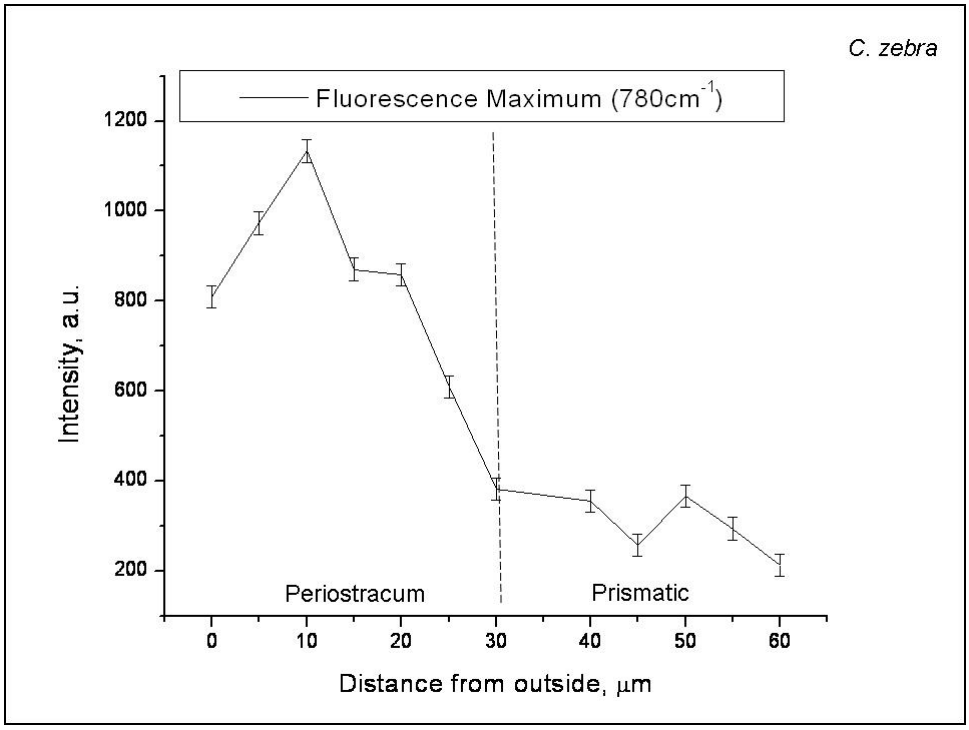

Figure 24: Fluorescence maximum at 780 cm^{-1} of the μ-Raman spectra of *C.zebra*.

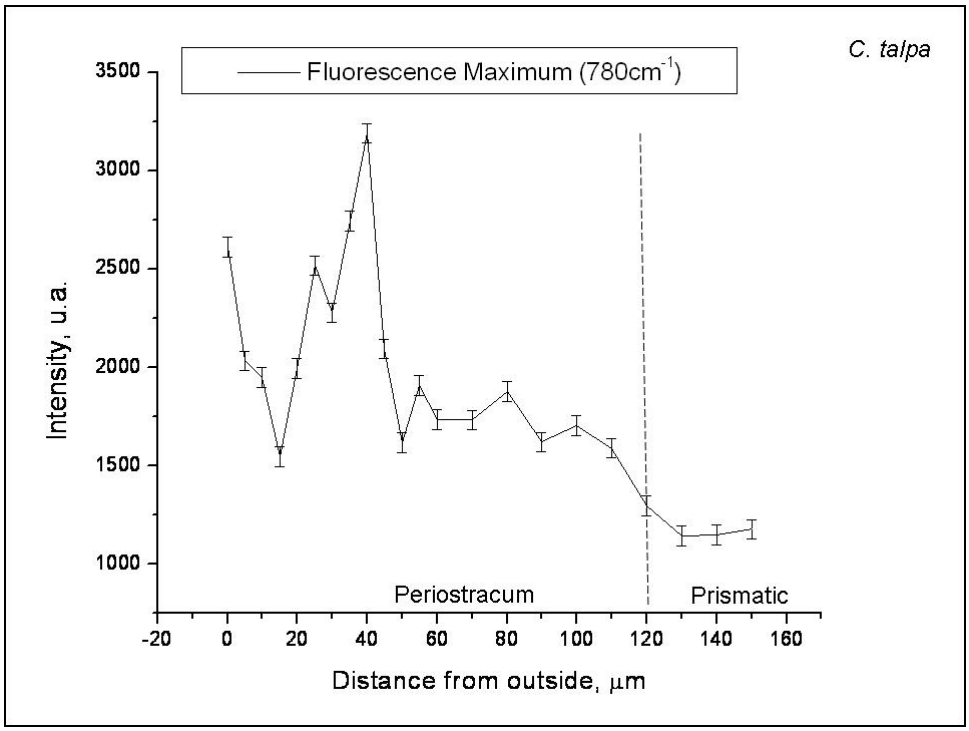

Figure 25: Fluorescence maximum at 780 cm^{-1} of the μ-Raman spectra of *C. talpa.*

SAMPLE: periostracum and start of the prismatic layer of a *C. zebra* and *C.talpa* exemplars. Raman spectra analyzed from each of the white points shown in the micrograph of Figure 21 for both shells. The dashed line shows the interface between both layers.

Prismatic layer by Micro-Raman Spectroscopy

The prismatic structure identified as the coloured layer (about 70 μm large) by the microscopic methods, present a Raman spectrum without the typical fluorescence observed in the periostracum. In this case also the doublet 702 cm^{-1} indicates the mineralization as aragonite. There are also other observable interesting peaks at 1007-1114 cm^{-1}, 2112-2122 cm^{-1}, 2210-2222 cm^{-1} and 2584-2595 cm^{-1} and also two sharp peaks at 1115 cm^{-1} and 1495 cm^{-1}, (See arrows in Figure 26 and Figure 27). These peaks disappear gradually from the beginning to the end of the prismatic layer. The last measurements show very clean spectra in these ranges, where only the mineral peaks corresponding to aragonite are detectable. The observation is present in *C.talpa* as well as *C.zebra* shells.

Comparing our results with the work of Withnall et al. (Figure 28 and Figure 29) the two sharp peaks in question can be identified as carotenoids, with high similitude to the *periwinkle* shell sample. The other peaks present in the spectra were recognised as overtone and combination progressions in the n1, n2 and n3 vibrational modes by analogy with that observed in other carotenoids.

Using Whitnall´s correlation between the wave number location and the conjugated carbon-carbon double bounds in the main carotenoid chain, it can be concluded that the carotenoids observed in *Cypraea* shells have an 11 conjugated double bond chain. Very interesting is the fact that three different shells, from very different origins, built their completely different shell using similar type of pigments, as it was demonstrated by their Raman spectrum.

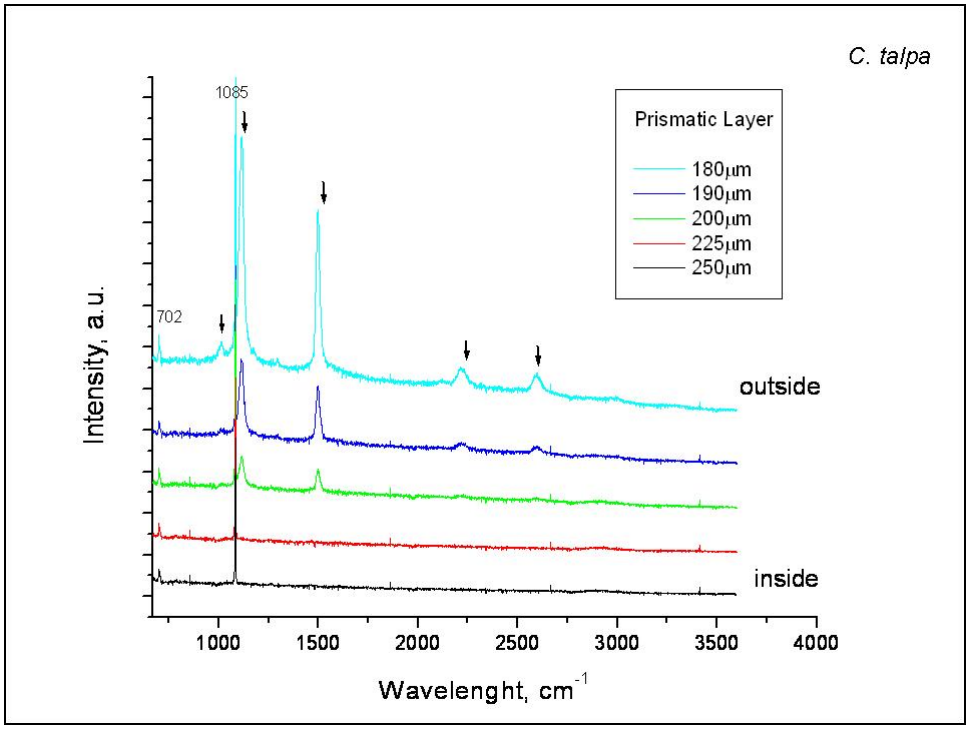

Figure 26: Micro-Raman spectra of *C. talpa* prismatic layer showing peaks corresponding to aragonite bio-mineral at 1085 and 702cm^{-1}. The arrows show peaks of organic origin. Polished shell sample. CLSM under Oil immersion.

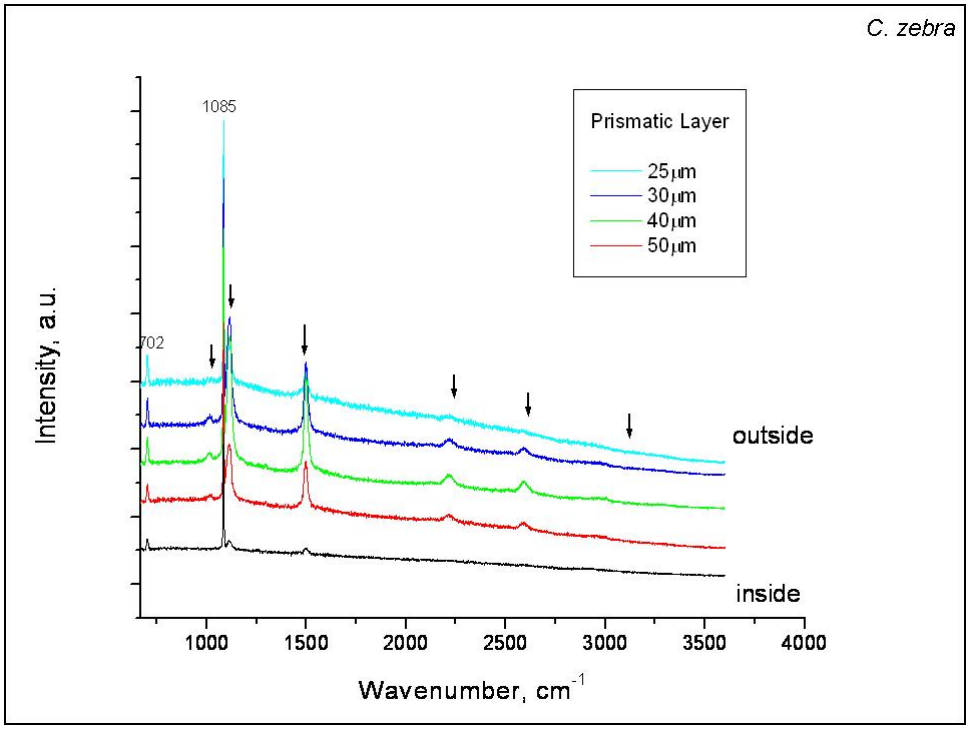

Figure 27: Micro-Raman spectra of *C.zebra* prismatic layer showing peaks corresponding to aragonite bio-mineral at 1085 and 702cm^{-1}. The arrows show peaks of organic origin. Polished shell sample. CLSM under Oil immersion.

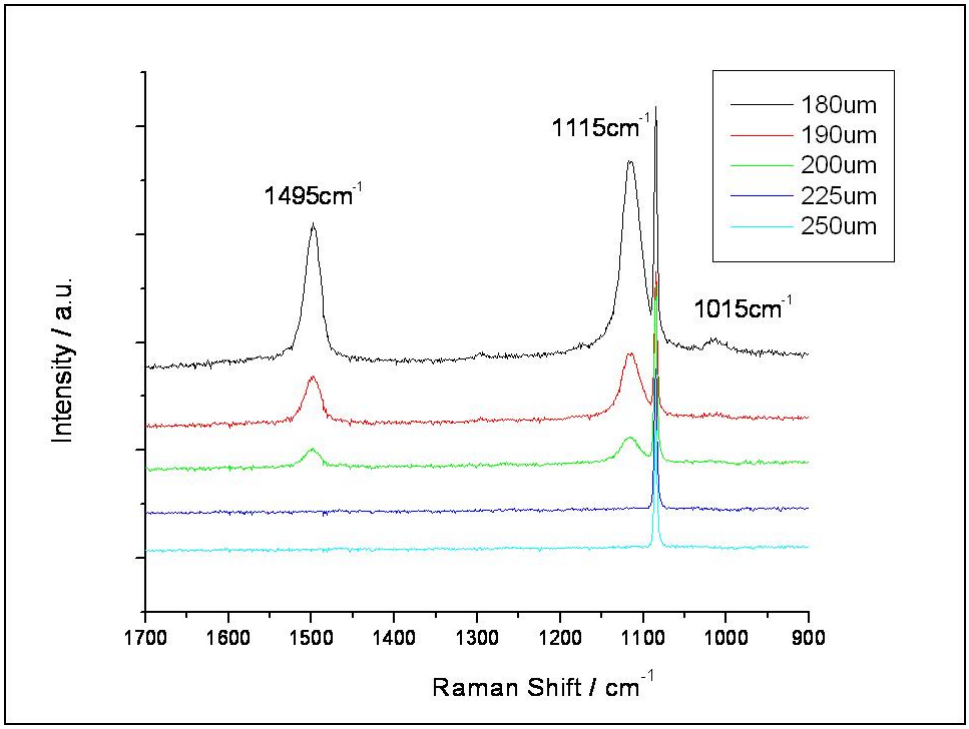

Figure 28: Micro-Raman spectra of *C. talpa* prismatic layer showing peaks corresponding to aragonite bio-mineral and to carotenoids. Polished shell sample. CLSM under Oil immersion.

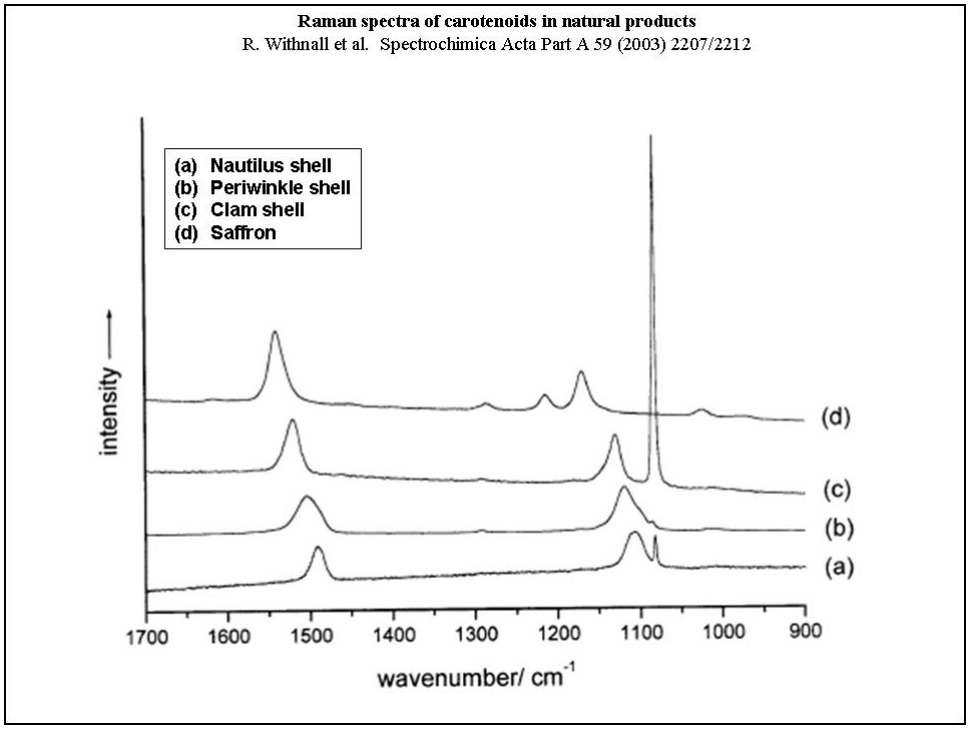

Figure 29: Micro-Raman spectra of different marine shells and saffron samples showing the carotenoids peaks at 1110-1120 cm^{-1} and 1495-1520 cm^{-1}. From Withnall et al.

Crossed Lamellar Layer by Micro-Raman Spectroscopy

The crossed lamellar layer does not present any fluorescence, as it was demonstrated already by the simple CLSM imaging. Low traces of the peaks identified in the last section as carotenoids are also observed (See arrows Figure 30). Carotenoid presence could be the reason of the magenta and brown colours observed in crossed lamellar layers.

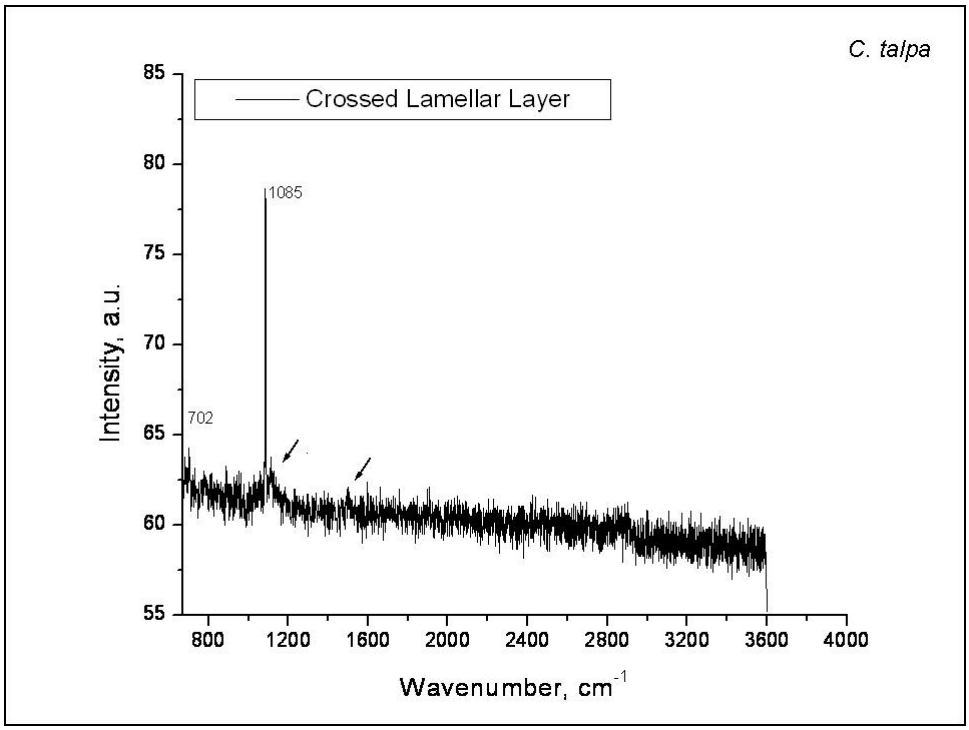

Figure 30: Micro-Raman spectrum of *C. talpa* crossed lamellar layer showing peaks corresponding to aragonite bio-mineral and to carotenoids (arrows). Polished shell sample. CLSM under Oil immersion

7. 4 Summary of Results

The results obtained from the micro and nanostructure analysis are listed in Table 10.

	Perios-tracum	***Colours***	***Stripes***	***Magenta***	***White***
Colour	Transparent, brilliant	Black, yellow, white	White, Brown	Magenta, Brown	Talk white
Pattern	no	Spots stripes	Stripes, zig-zag	no	no
Thickness SEM and CLSM	30-120μm	50-70μm	50-70μm	50-70μm	50-70μm
Mineralogy XRD and RS	aragonite	aragonite	aragonite	aragonite	aragonite
Fluorescence CLSM	Layers	Border prisms	no	no	no
Microstructure SEM and CLSM	Layered	Prismatic	Crossed lamellar	Crossed lamellar	Prismatic
First order	Layers	Prisms	Lamellae	Lamellae	Prisms
Second order	Spheres 50-80nm	Sheets	Sheets	Sheets	Sheets
Third order	-	Prisms 4μm×200nm	Prisms 4μm×200nm	Prisms 4μm×200nm	Prisms 4μm×200nm
Nanostructure	Spheres 5-10nm	Spheres 5-10nm	Spheres 5-10nm	Spheres 5-10nm	Spheres 5-10nm
Carotenoids μ-RS	Not observable	Yes	Not observable	Yes	Not observable

Table 10: Summary of the micro and nanostructure results on *Cypraea* shells.

8. Organic Matrix Analysis in *Cypreadae* Shells

Optically differentiable specific shell layer material was obtained from *Cypraea tigris*, *talpa* and *zebra* shells. The powder was demineralized with HCl 15 %, purified by dialysis (MWCO 3 kDa) and concentrated by lyophylization. The resultant soluble organic matrices are analyzed and compared in this chapter.

The components of the organic matrix extracted from the different layers of *Cypraea tigris* , *talpa* and *zebra* shells and rediluted in MilliQ water were separated using GE and SE-HPLC, and analyzed for the protein content, the UV absorption and the molecular mass using diverse methods. The detailed explanation of these topics is described in the Chapter 3 “Methods of Separation” and Chapter 4 “Methods of Protein Quantification”.

8.1 UV Spectroscopy

The UV absorption spectrum was measured from 190 nm to 300 nm, in QS quartz cuvettes. The reference used was MilliQ water and the running speed was 120 nm/min. The results obtained for this measurement are shown in Figure 31 for *C. tigris* shells, in Figure 32 for *C. zebra* shells and in Figure 33 for *C. talpa* shells.

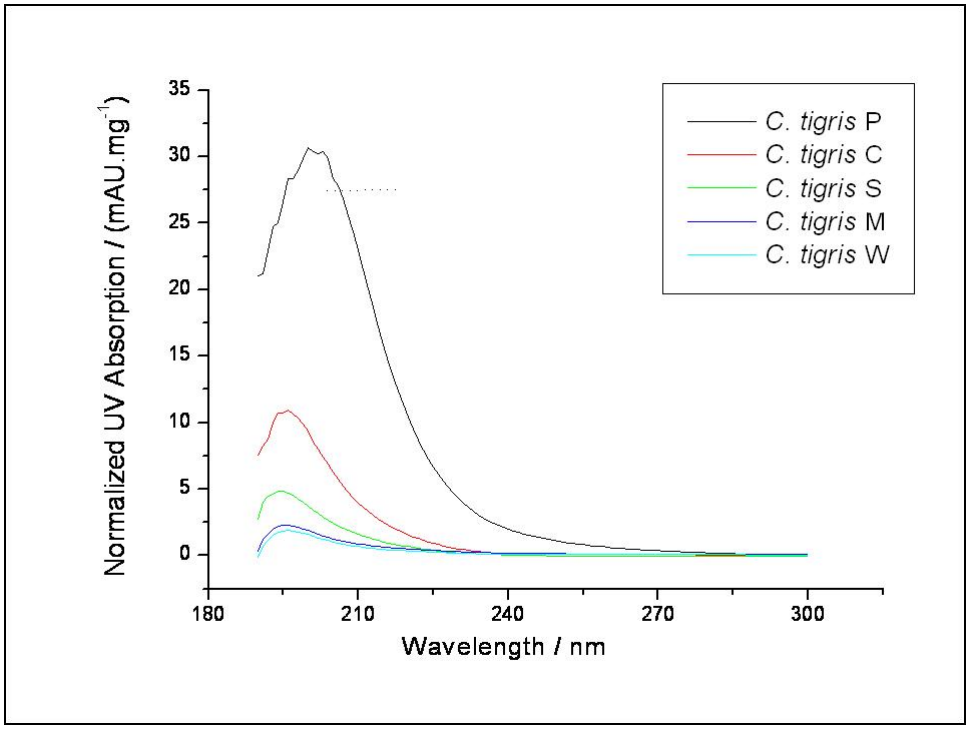

Figure 31: UV absorption spectrum of the SOM extracted from the different observable layers of *C. tigris* shells. Normalization Factor: the dry layer mass. In dashed line: the saturation limit of the equipment.

MATERIAL: Material: SOM extracted from 1g specific layer powdered shell, with HCl 15 %. Solvent: MilliQ water, centrifuged 10 min at 10000 rpm. Blank: 1g $CaCO_3$ treated sample.
UV PARAMETERS: Range: 190-300 nm. Scanning speed: 120 nm/min. Cuvette: QS quartz 3 ml. Ø Window: 3 mm. Reference: MilliQ water.

The UV spectrum of the different layers of *C. tigris* shells show to be similar for all layers, affected only for a concentration factor. The absorption is higher at smaller wavelengths, with a principal peak around 200 nm. It is to note that peak is observable at 280nm as it could be observed for other proteins such as BSA (data not shown).

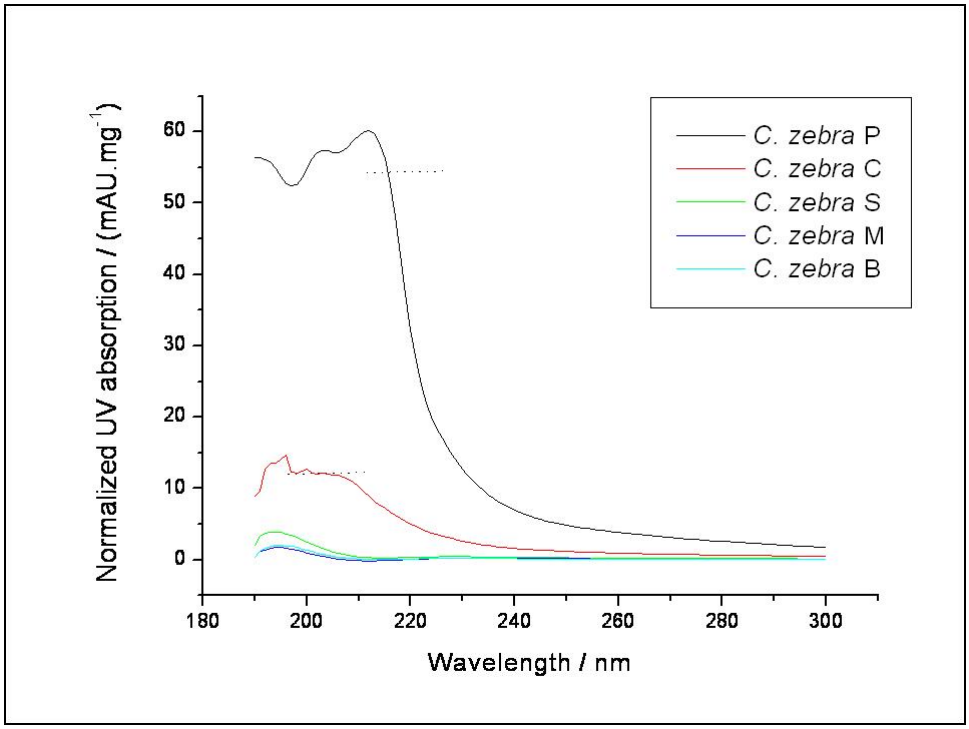

Figure 32: UV absorption spectrum of the SOM extracted from the different observable layers of *C. zebra* shells. Normalization Factor: the dry layer mass. In dashed line: the saturation limit of the equipment.

MATERIAL: Material: SOM extracted from 1 g specific layer powdered shell, with HCl 15 %. Solvent: MilliQ water, centrifuged 10 min at 10000 rpm. Blank: 1 g $CaCO_3$ treated sample.
UV PARAMETERS: Range: 190-300 nm. Scanning speed: 120 nm/min. Cuvette: QS quartz 3 ml. Ø Window: 3 mm. Reference: MilliQ water.

For the case of *C. zebra* snails (Figure 32), the spectrum is different to that observed for the *C. tigris* species, but here is observed too, a concentration relationship between the five spectra.

For *C. talpa* layers (Figure 33), the case is similar as that observed for C. *tigris* and C. *zebra* snails: the different layers produce different absorptions. The form of the spectra differs from that of Figure 31 and Figure 32, but the periostracum is the layer which presents more absorption at small wavelength and the signal decreases with the layer depth, as in the other both cases.

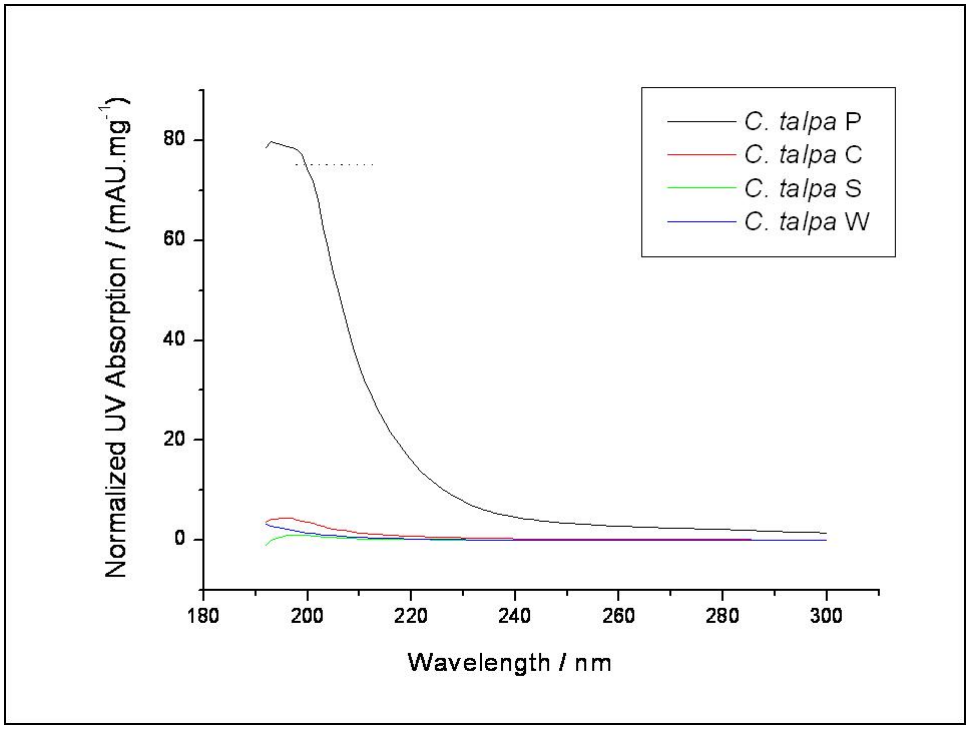

Figure 33: UV absorption spectrum of the SOM extracted from the different observable layers of *C. talpa* shells. Normalization Factor: the dry layer mass. In dashed line: the saturation limit of the equipment.

MATERIAL: Material: SOM extracted from 1 g specific layer powdered shell, with HCl 15 %. Solvent: MilliQ water, centrifuged 10 min at 10000 rpm. Blank: 1g $CaCO_3$ treated sample.
UV PARAMETERS: Range: 190-300 nm. Scanning speed: 120 nm/min. Cuvette: QS quartz 3 ml. Ø Window: 3 mm. Reference: MilliQ water.

8.2 Bradford Tests

The total protein content was quantified by the Bradford Test, using the modified micro test. Averaging three measurements, the protein content for the SOM extracted from 1 g of specific layer material for *C. tigris*, *C. talpa* and *C. zebra* shells are shown in Figure 34. The periostracum samples were diluted to a concentration of 75 %, 50 % and 25 % with milliQ water and the protein content for the 100 % (when out of range) was recalculated.

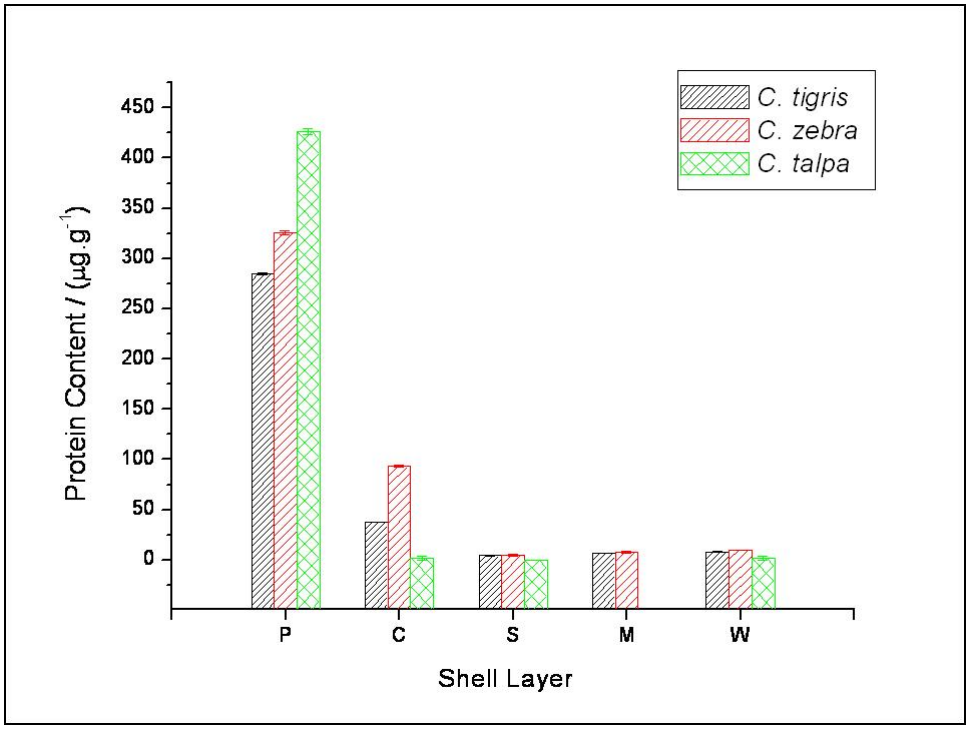

Figure 34: Protein content per gram shell powder, measured with the Bradford Test.

MATERIAL: Material: SOM extracted from 1 g specific layer powdered shell, with HCL 15 % (P= Periostracum, C= Colored layer, S= Striped layer, M= Magenta, W= White layer). Solvent: MilliQ water, centrifuged 10 min at 10000 rpm. Blank: 1 g $CaCO_3$ treated sample. Standard: BSA 0 to 10 ppm.
BRADFORD PARAMETERS: Test: modified micro-test. Repetitions per sample: 3. Samples Averaged: 3.

The results of the Bradford test show a similar decreasing profile from the outside to the inside of the shells for the three species. In accordance with the UV measurements (Figure 31 to Figure 33) the periostracum shows to be the layer with the highest organic content, followed by the colored layer. In the inner parts of the shell, the layers present about the same concentration. The striped, magenta and white layers present about the same concentration, although the striped layer shows to be slightly less concentrated than the white and the magenta layers (absolute values and uncertainties are given in the Appendix XIII ("Tables of Results").

8.3 Ellman´s Tests

The presence of free sulfhydryl groups in the SOM extracted from the different shell layers was investigated using the colorimetric *Ellman´s* tests. The presence of sulphur in the shells was demonstrated by microprobe (See Figure 49, Chapter 9). Nevertheless, the test was

negative for all samples, independent of the layer or the shell measured. The fact that no sulfhydryl groups are observed, may mean for example that the sulphur species present, could be more closed to a sulphated or sugar species, as for example that found by Dauphin (2003).

8.4 Gel Electrophoresis

Gel Electrophoresis was used to separate the SOM per mass, using MOPS tris-glycin gels, running with tris-glycin buffer, at 200 V and 100 mA for half an hour approximately. The standardization was made with the Dalton® cocktail mixture of proteins. More details about the GE methodology are found in chapter "Separation Methods". The results are shown below:

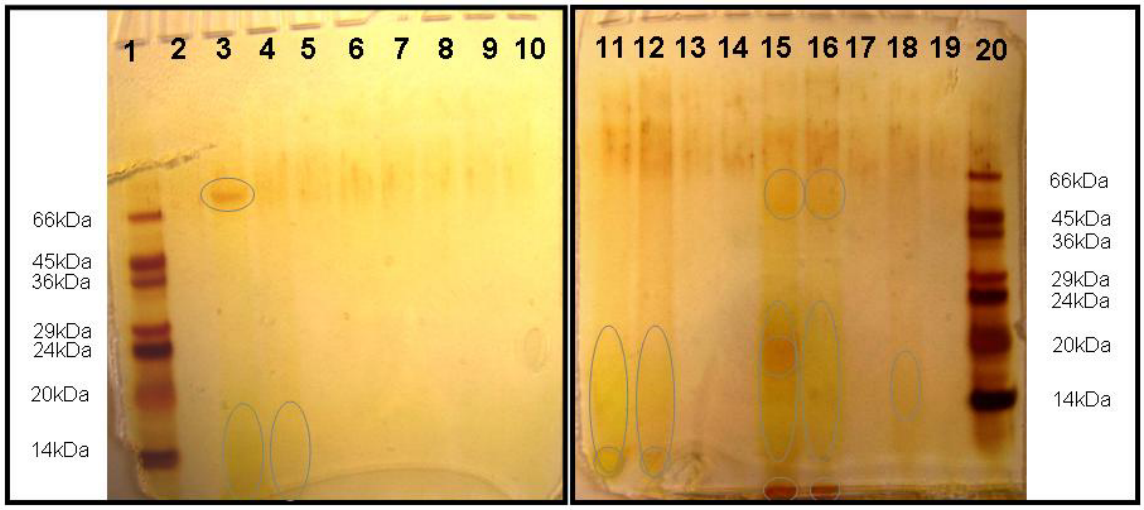

Figure 35: GE of the SOM extracted from the different layers of *C. tigris, C. talpa* and *C. zebra* shells.

MATERIAL: Material: SOM extracted from 1g powdered shell, with HCl 15%. Solvent: MilliQ Water, centrifuged 10 min at 10000 rpm. Sample Buffer: Tris-glycin-SDS. Reducing agent: Mercaptoethanol at 70 ºC, heating during 1 h.
GEL PARAMETERS: Gel: MOPS tris-glycin 9 %, Buffer: Mops-Tris-glycin, Voltage: 200 mV, Current: 100 mA, Time: aprox. 40 min., Revealing: Silver staining.
GEL DESCRIPTION: Line 1 and 20: Dalton mixture. Line 2: Blank MilliQ water. Lines 8 and 14 Blank $CaCO_3$. Tigris: Periostracum (3) Colors (4) Stripes (5) Magenta (6) White (7).; Talpa: Peristracum (12) Colors (11) Stripes (10) White (9); Zebra: Periostracum (15) Colors (16) Stripes (17) Magenta (18) White (19)

As it can be observed from Figure 35, the analysis of the MilliQ blank sample shows that the method does not introduce any signal (See line 2). Nevertheless the bands for the $CaCO_3$ blank (lines 8 and 14) show a very diffuse signal at masses bigger than 66 kDa, present in all cases. The SOM extracted from the different layers of the three shells are similar in behavior,

although not the same. The periostracum and the colored layer present in all three cases a particular “band” staining (See lines 3, 4, 11, 12, 15 and 16). This type of staining can be recognized as organic matrix of continuous mass distribution. Inside these bands, some spots or dark zones can be recognized. For the three shell species, a yellow zone between 20 kDa and 3 kDa is present on the bottom of the gels. The SOM from the periostracum of the *tigris* shells present in addition a clear spot corresponding to masses around 70 kDa. The SOM extracted from the periostracum of *zebra* presents two dark spots around 45 kDa and 20 kDa and an orange stain at very low masses (on the bottom of the gel). The periostracum SOM of *talpa* shows a dark yellow zone at masses smaller than 14 kDa. The striped and white layers of the three shells are poorly stained and only the blank signal (also observed in the $CaCO_3$ blanks) is visible. The magenta SOM differs from *tigris* to *zebra* species. In the first one no particular staining is observed, while in the second one a continuous band is clearly formed, with a dark zone between 20 kDa and 14 kDa.

8.5 SE-HPLC-UV

Size exclusion chromatography coupled with a Bischoff UV detector was used to separate and detect the components of the SOM extracted from 1 g specific layer material of *Cypraea tigris*, *talpa* and *zebra* shells. SEC column used was *Biosep S2000* from Phenomenex. The absorption was detected at 220 nm. The achieved results are plotted in Figure 36, Figure 37 and Figure 38. As it can be observed comparing these figures, there are two main peaks. The first of them is a broad peak that elutes between 7.5 min and 12.5 min; it is present in all colored and periostracum layers. The second one is a sharp peak that elutes in all samples, around 13 min. Because this second peaks is observable even in the $CaCO_3$ blanks, it is concluded that it is an interference signal probably originated from the extraction processes (similar peaks were obtained for example for MilliQ water treated with membrane filters, dialysis or UCF, see for example A-Figure 21 in the Appendix IX).

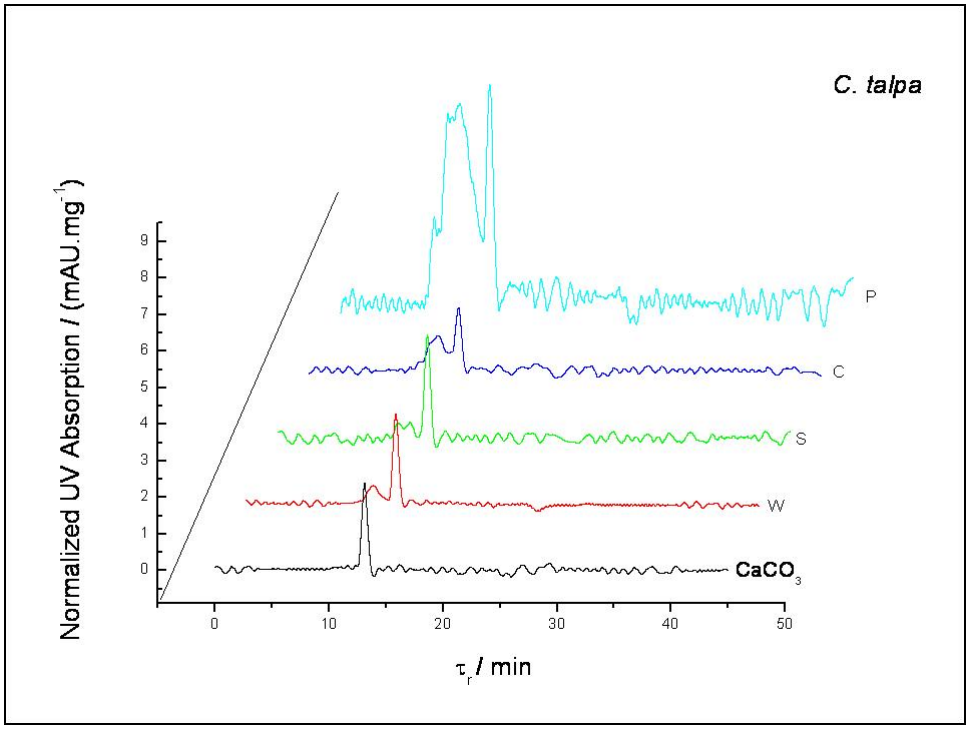

Figure 36: Chromatogram of the SOM extracted from different layers of *C. talpa* shells. For more details see caption Figure 38.

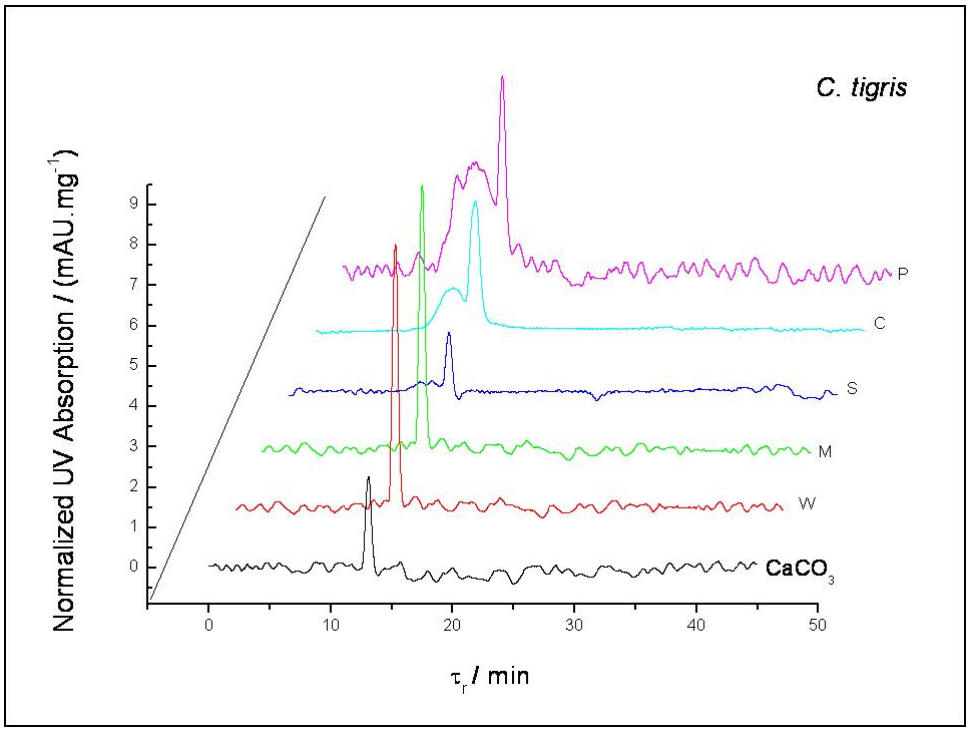

Figure 37: Chromatogram of the SOM extracted from different layers of *C. tigris* shells. For more details see caption Figure 38.

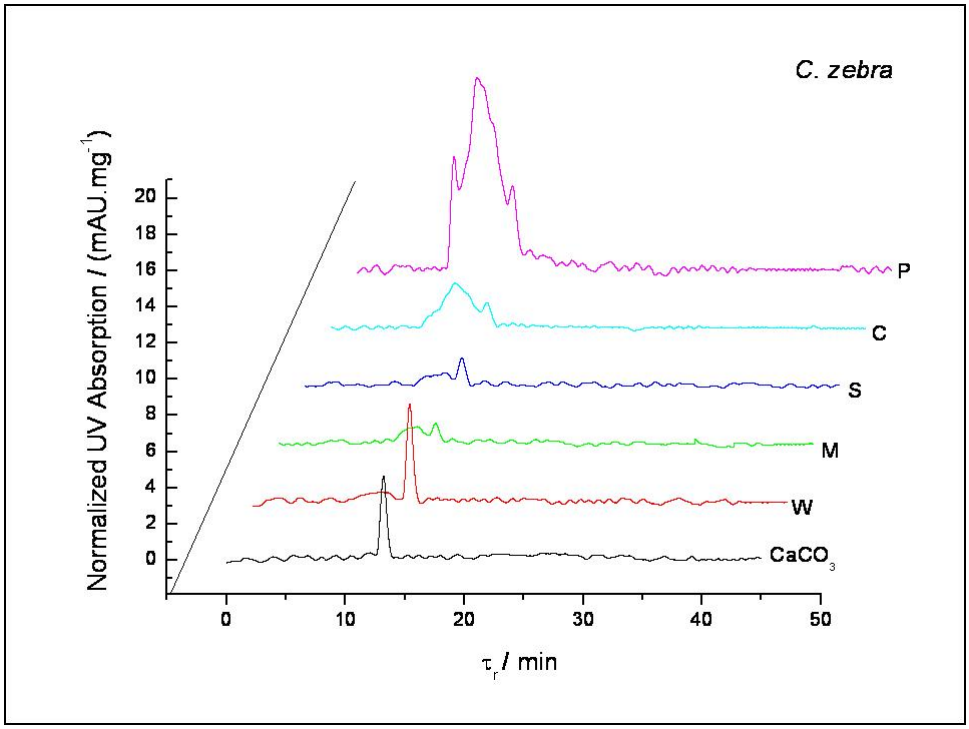

Figure 38: Chromatogram of the SOM extracted from different layers of *C. zebra* shells. Technique: SE-HPLC-UV. Wavelength: 220nm. Normalization Factor: dry mass of shell layer.

MATERIAL: SOM extracted from 1g specific layer material of *C. talpa, C. tigris and C. zebra* shells with the HCl 15% "small amount samples" methodology. The lyophilized final SOM was re-suspended in MilliQ water. Blank sample: $CaCO_3$.
SEC: Column: *Biosep S 2000*. Mobile Phase: 20mM Tris-HCL pH 7.4. Flux: 0.8ml/min. Wavelength: 220nm.

The chromatograms of the different layers of the same shell species were compared with each other. The periostracum SOM (Figure 39) is the layer most rich in peaks. At least 6 peaks are detectable (peaks a to f in Figure 39, including the inorganic one, f). For the three shells, the periostracum organic matrix shows small differences and is affected by a concentration factor. The colored layer (Figure 40) presents also a couple of peaks similar to those observed in the periostracum. For the striped layer (Figure 41), the presence of the first peak is highly reduced in all three shell species, although remains well observable for the zebra specie. For the striped layer, the fine structure of this peak can not be differentiable from the background structure. Here the signal to noise ratio is this time about 50%. The magenta layer SOM (Figure 42), present only in *tigris* and *zebra* specimens, differs between both matrices. The SOM extracted of the *zebra* layer presents a small recognizable signal for the first peak while the SOM extracted from *tigris* does not. The white layer SOM in the inside of the shells (Figure 43) shows no first peak for *tigris* snails, but a small yet observable first peak for the *talpa* and *zebra* species.

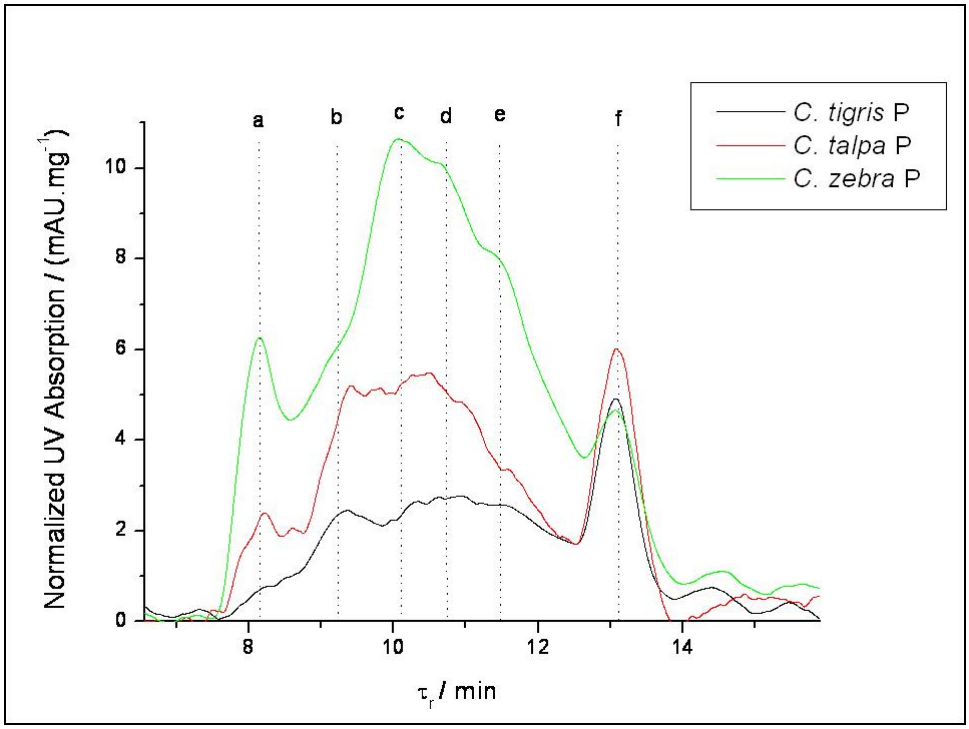

Figure 39: Chromatogram of the SOM extracted from the periostracum of *C. tigris, C. talpa* and *C. zebra* shells. Technique: SE-HPLC-UV. Wavelength: 220nm. Normalization Factor: dry mass of shell layer. For more details see caption Figure 38.

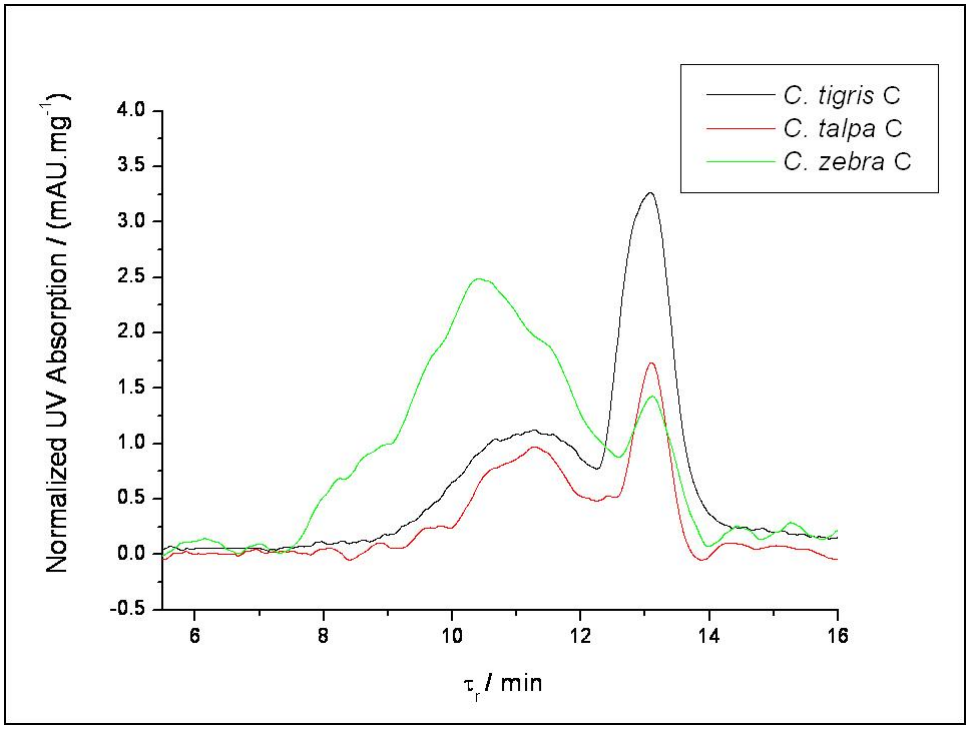

Figure 40: Chromatogram of the SOM extracted from the colored layer of *C. tigris, C. talpa* and *C. zebra* shells. Technique: SE-HPLC-UV. Wavelength: 220nm. Normalization Factor: dry mass of shell layer. For more details see caption Figure 38.

.

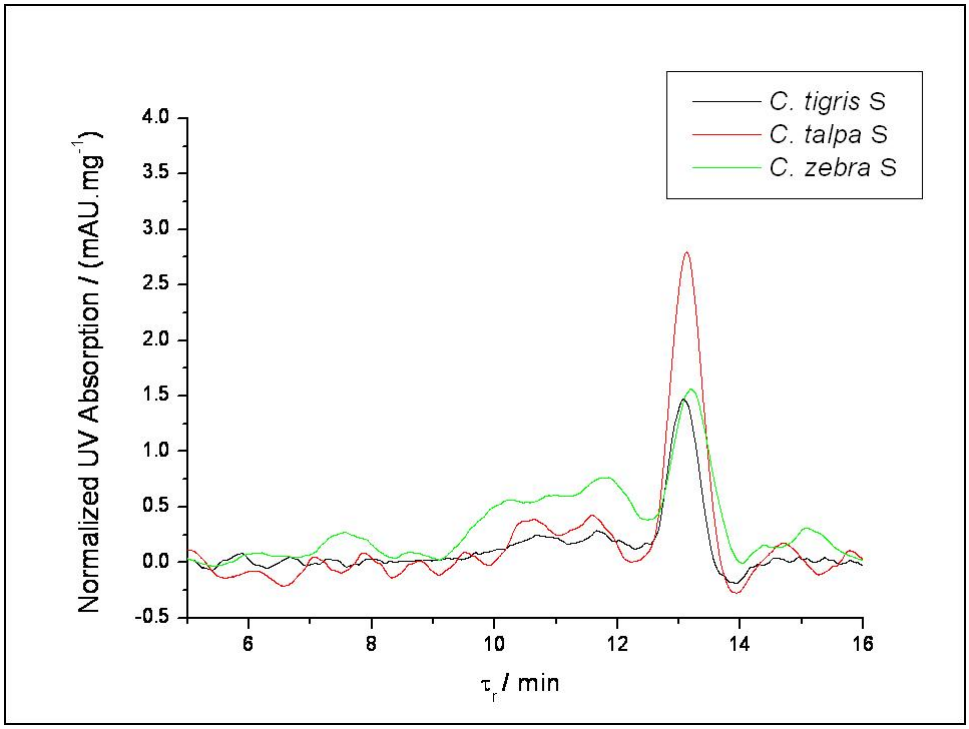

Figure 41: Chromatogram of the SOM extracted from the striped layer of *C. tigris, C. talpa* and *C. zebra* shells. Technique: SE-HPLC-UV. Wavelength: 220nm. Normalization Factor: dry mass of shell layer. For more details see caption Figure 38.

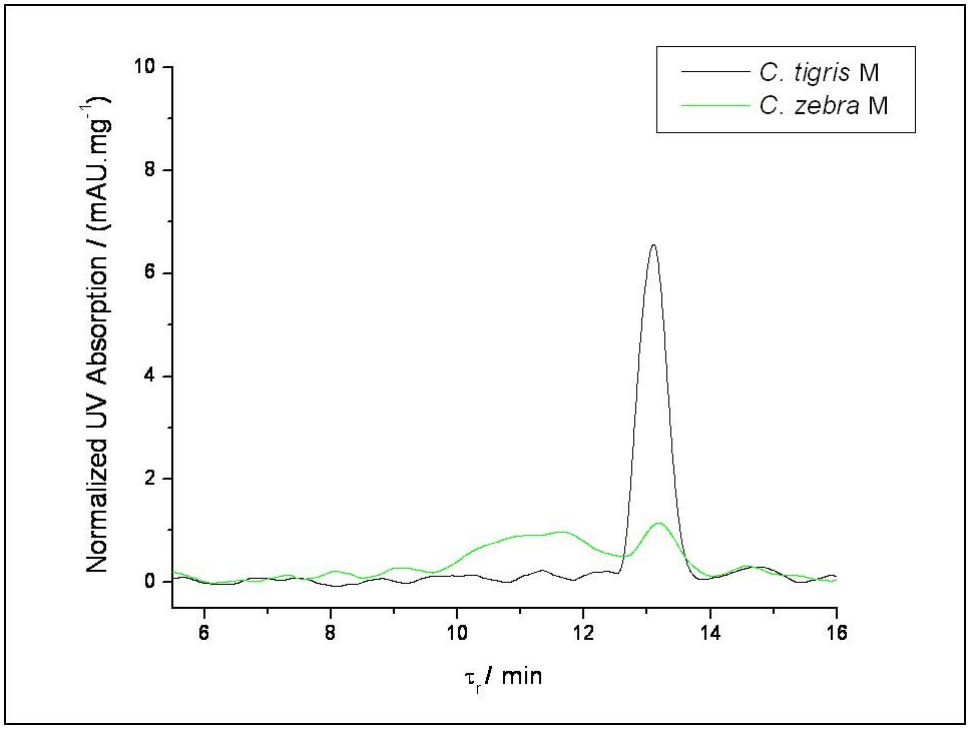

Figure 42: Chromatogram of the SOM extracted from the magenta layer of *C. tigris* and *C. zebra* shells. Technique: SE-HPLC-UV. Wavelength: 220nm. Normalization Factor: dry mass of shell layer. For more details see caption Figure 38.

.

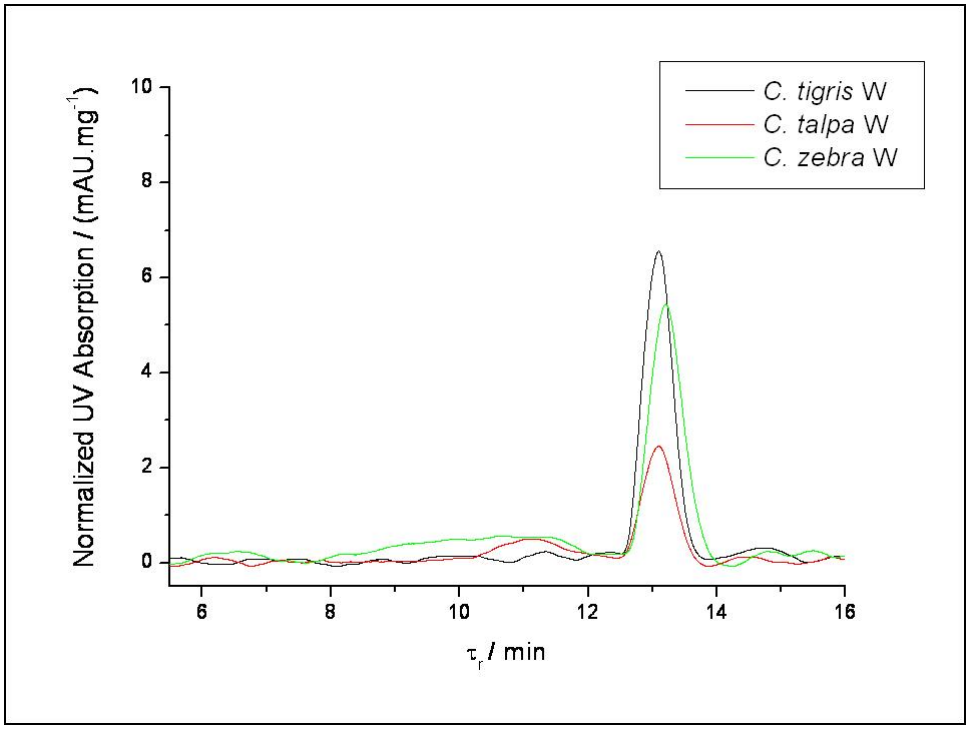

Figure 43: Chromatogram of the SOM extracted from the white layer of *C. tigris, C. talpa* and *C. zebra* shells. Technique: SE-HPLC-UV. Wavelength: 220nm. Normalization Factor: dry mass of shell layer. For more details see caption Figure 38.

8.6 Validation Between Different Techniques

8.6.1 The SOM Protein Content

The proteins were quantified directly by comparison with BSA standards with the Bradford test. With these measurements, a decreasing concentration profile of the protein quantity per layer was found. The main peaks of UV and SE-HPLC-UV analyse show also a similar relation with the protein content per layer. Normalizing all intensities to the value found in the periostracum layer for each technique, a very good correlation is found between the three techniques, for the three shells analyzed (See Figure 44 to Figure 46).

The correlations observed between the data, validate the conclusions obtained with each test separately. First, the proteins present in the soluble organic matrix extracted from the *Cypraea* shell layers have a decreasing profile from the outside to the inside of the layers. Second, the relation between the protein content found in a layer relative to the content in the periostracum is in the quantitative test in agreement with the other two tests. The points obtained from the three measurements differ lower than a 10 %. Third, the organic material

that is separated in the HPLC experiments is directly correlated with the brilliant blue positive organic material from the Bradford test, it means: directly correlated to the protein fraction.

8.6.2 The SOM Protein Size

HPLC and Gel Electrophoresis were two independent techniques used to quantify the size, i.e. mass, of the organic matrix extracted from the different shell species. GE has shown that the main components of the SOM cannot be separated in discrete masses. In contrary continuous mass bands were observed. The comparison between the position of these bands and the peaks obtained with the SEC separation are shown in Figure 47 for the periostracum of the three species. As it could be observed, the presence of dark yellow tones coincides with the maximum of the peaks observed in SEC.

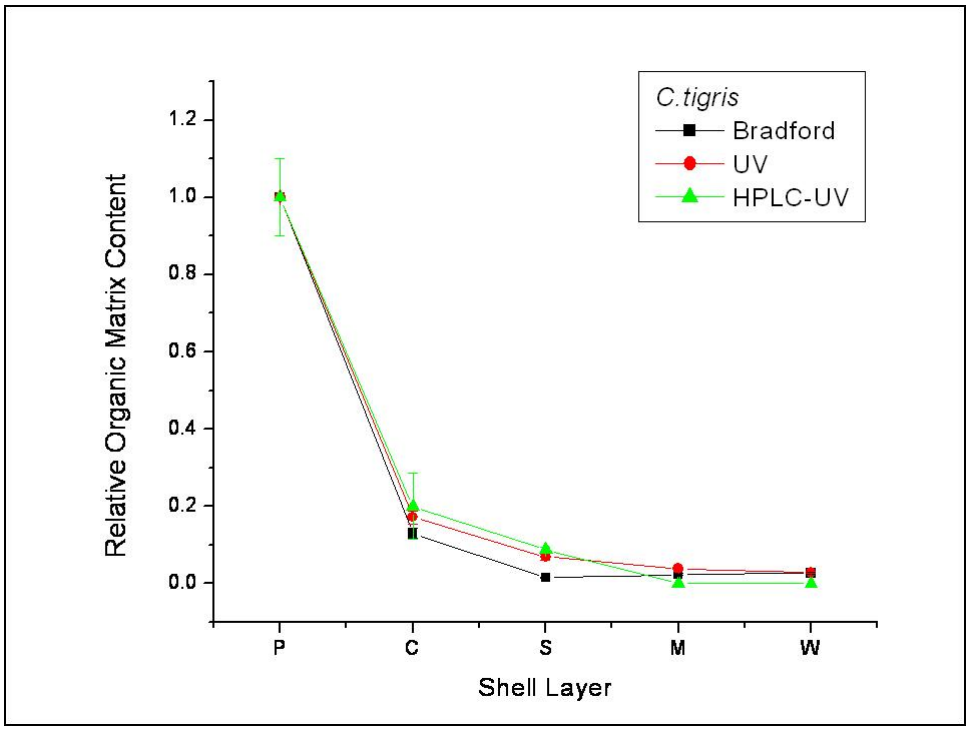

Figure 44: Organic matrix content found with three different techniques in *C. tigris* SOM. Techniques: (square) protein content found with the Bradford test, (circle) UV signal at 220nm, (triangle) Maximum of the UV peak signal after HPLC separation. Normalization Factor: Value on the periostracum layer.

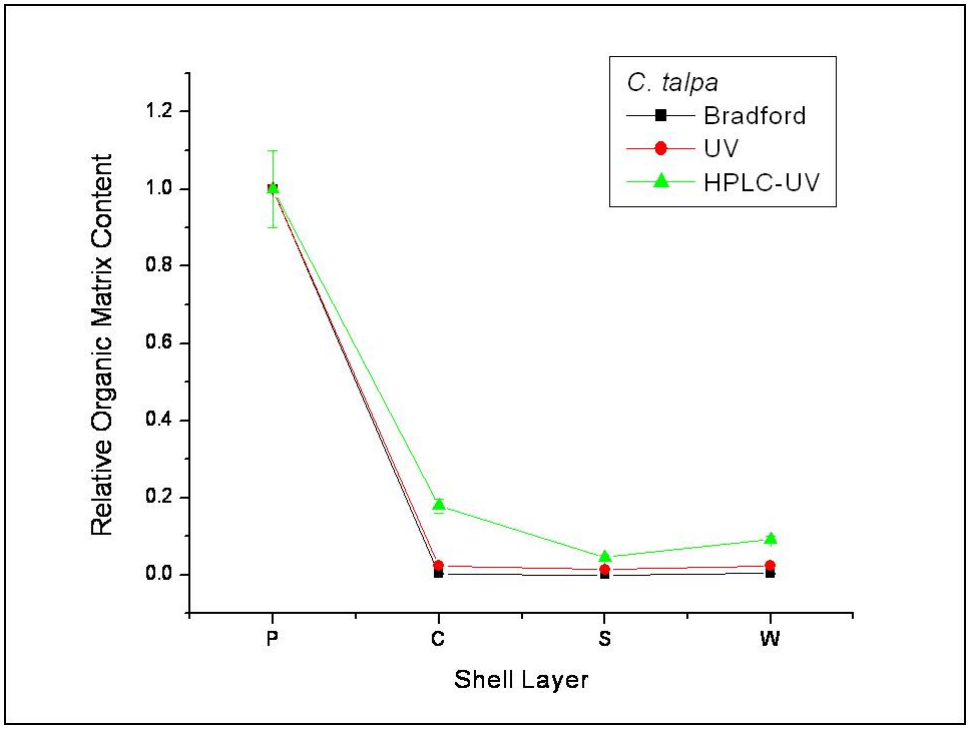

Figure 45: Organic matrix content found with three different techniques in *C. talpa* SOM. Techniques: (square) protein content found with the Bradford test, (circle) UV signal at 220nm, (triangle) Maximum of the UV peak signal after HPLC separation. Normalization Factor: Value on the periostracum layer.

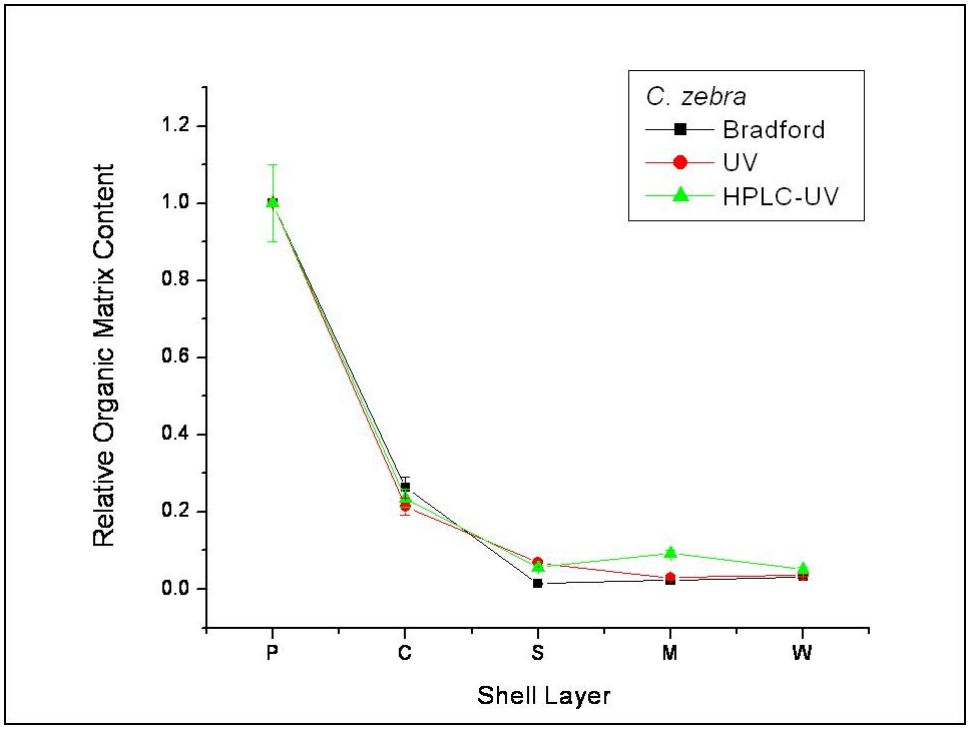

Figure 46: Organic matrix content found with three different techniques in *C. zebra* SOM. Techniques: (square) protein content found with the Bradford test, (circle) UV signal at 220nm, (triangle) Maximum of the UV peak signal after HPLC separation. Normalization Factor: Value on the periostracum layer.

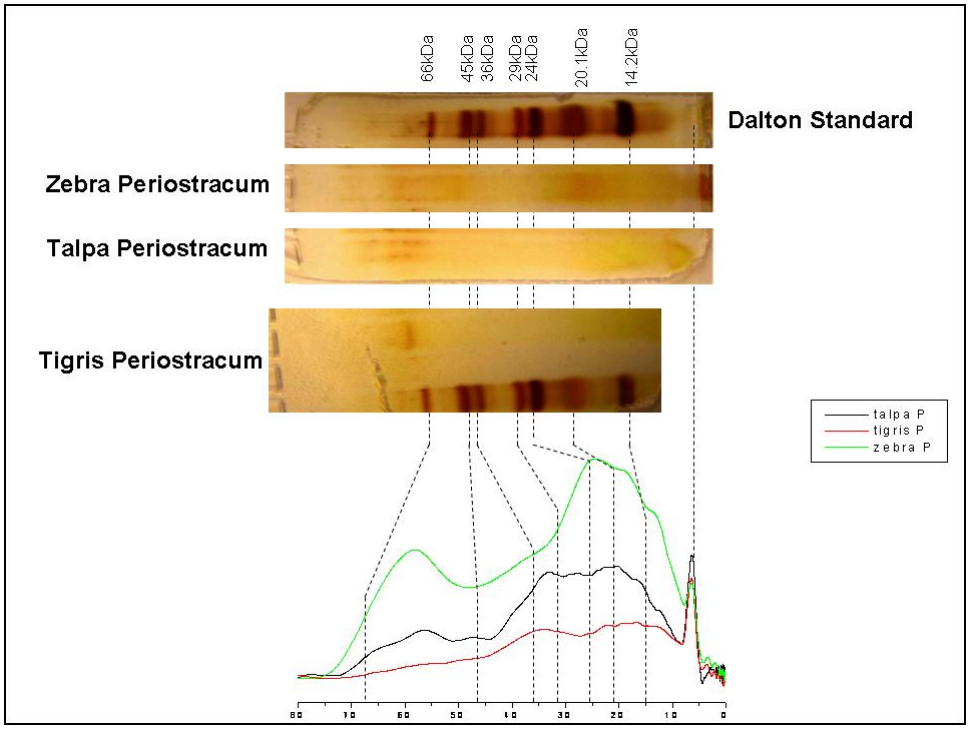

Figure 47: Correlation between the GE and the HPLC-UV measurements, for the SOM extracted from the periostracum of *C. tigris, C. talpa* and *C.zebra* shells.

8.7 Summary of Results

The organic matrix present in the different shell layers of *C. tigris*, *C. talpa* and *C. zebra* was separated from the mineralized structure applying an optimized method using HCl 15 % as demineralization agent. The proteins present in the soluble matrices were studied for protein content and characterized by size using diverse methods. The three species have shown to be more organic in the outside of the shell, presenting a decreasing organic profile to the inside.

The SOM has shown to present small differences between the shells. Between layers of the same shell, deduced through the observation of the SEC and GE results, not only the quantity of the proteins, but also the structure of the SOM changes from one layer to the next. These results are in agreement with the hypothesis that the SOM helps in the bio-construction of the shell and therefore must change to produce the different types of structures and interfaces between them.

The results obtained from protein quantification and mass characterization tests are presented in Table 11, Table 12 and Table 13, for *C. tigris*, *C. zebra* and *C. talpa* respectively.

Cypraea tigris	**P**	**C**	**S**	**M**	**W**
Protein Quantity / ppm	285 ± 2	37 ± 2	5 ± 2	8 ± 2	7 ± 2
S-H Proteins / ppm	<LD	<LD	<LD	<LD	<LD
UV signal / nm	190 - 280	190 - 250	190 - 220	190 - 250	190 - 220
Size of Proteins by GE / kDa	70 20-7	20-7	<LD	<LD	<LD
Range Size of Proteins by SE-HPLC-UV / kDa	88-32 28-16 15-7	35-16 15-7	<LD	<LD	<LD
Maximum Size of Proteins by SE-HPLC-UV / kDa	72, 38, 28, 25, 24, 22, 20, 17, 15	22, 19, 17, 15	<LD	<LD	<LD

Table 11: Summary of results obtained for *C. tigris* shells.

Cypraea zebra	**P**	**C**	**S**	**M**	**W**
Protein Quantity / ppm	342 ± 2	90 ± 2	5 ± 2	8 ± 2	11 ± 2
S-H Proteins / ppm	<LD	<LD	<LD	<LD	<LD
UV signal / nm	190 - 280	190 - 250	190 - 220	190 - 250	190 - 220
Size of Proteins by GE / kDa	70 25-16 14-7	30-16 14-7	<LD	<LD	<LD
Range Size of Proteins by SE-HPLC-UV / kDa	87-56 39-16, 15-7	90-43 36-17 16-7	<LD	20-14	<LD
Maximum Size of Proteins by SE-HPLC-UV / kDa	75 36, 26, 22, 17, 15	71, 49, 33, 24, 18, 15	<LD	19, 15	<LD

Table 12: Summary of results obtained for *C. zebra* shells.

Cypraea talpa	**P**	**C**	**S**	**W**
Protein Quantity / ppm	426 ± 2	1 ± 2	1 ± 2	2 ± 2
S-H Proteins / ppm	<LD	<LD	<LD	<LD
UV signal / nm	190 - 280	190 - 250	190 - 220	190 - 220
Size of Proteins by GE / kDa	20-7	20-7	<LD	<LD
Range Size of Proteins by SE-HPLC-UV / kDa	87-61, 43-18 15-7	87-56 39-16 15-7	<LD	<LD
Maximum Size of Proteins by SE-HPLC-UV / kDa	71 36, 30, 23, 20, 17, 15	75, 36, 26, 22, 17, 15	<LD	<LD

Table 13: Summary of results obtained for *C. talpa* shells.

9. Trace Elemental Analysis of *Cypraea* Shells

In this chapter the results of main and trace elemental analysis done on the shell *of C. talpa*, *C.* zebra and *C. tigris* snails are presented. Trace elements at ppb and ppm concentration levels were detected by INAA in the powder of the differentiable shell layers. Biologically relevant elements like Cr, Zn, Co, Fe, Mn, and the rare earths Eu, Ta, and La were found at concentrations between 50 ppb and 1000 ppm. Mn, Br and Zn concentrations show strong layer dependence for the three animals. Interesting similarities of the elemental mapping between the snail species were found.

9.1 Analysis of Major Elements

To obtain a tentative element map on the shells, samples of *C. tigris*, *C. talpa* and *C. zebra* were prepared for electron microscopy in fractured and polished sections (See Chapter 2). The samples were photographed and then analyzed using SEM-EDX and microprobe. The results obtained for example for a *C. tigris* sample can be observed in Figure 48:

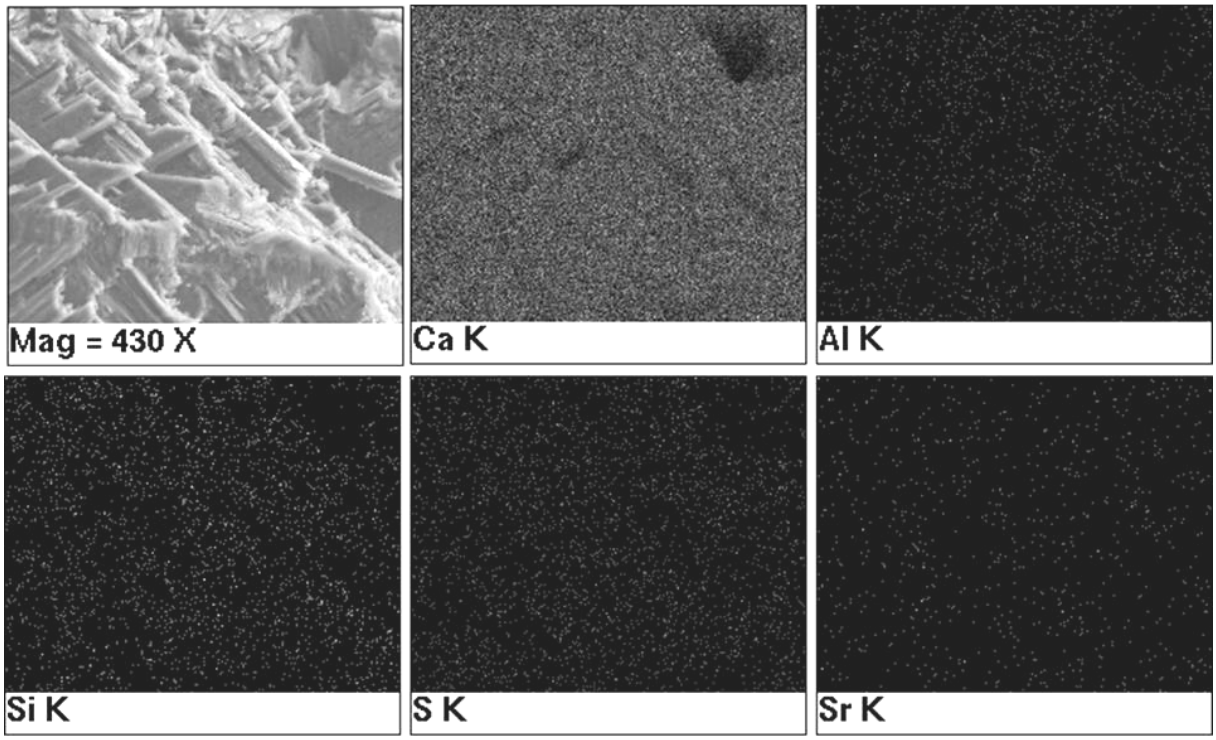

Figure 48: SEM micrograph and EDX analysis of the K shell emission for main elements present in the crossed lamellar layer of a *C. tigris* exemplar, prepared by fracturing a crossed section. The magnification used was 430X.

As it can be observed from the previous mapping, only a homogeneous distribution of major elements is detected. In the case of the microprobe analysis, the elements found (coincident with those found by EDX) could also be quantified (See Figure 49). The elements detected others than Cl, are all known structural elements (Ca, Sr, Na, S, and Si). The elements P, Ba, Mg and Al were under the detection limit of the microprobe analysis (LD = 80, 350, 90 and 60 ppm respectively).

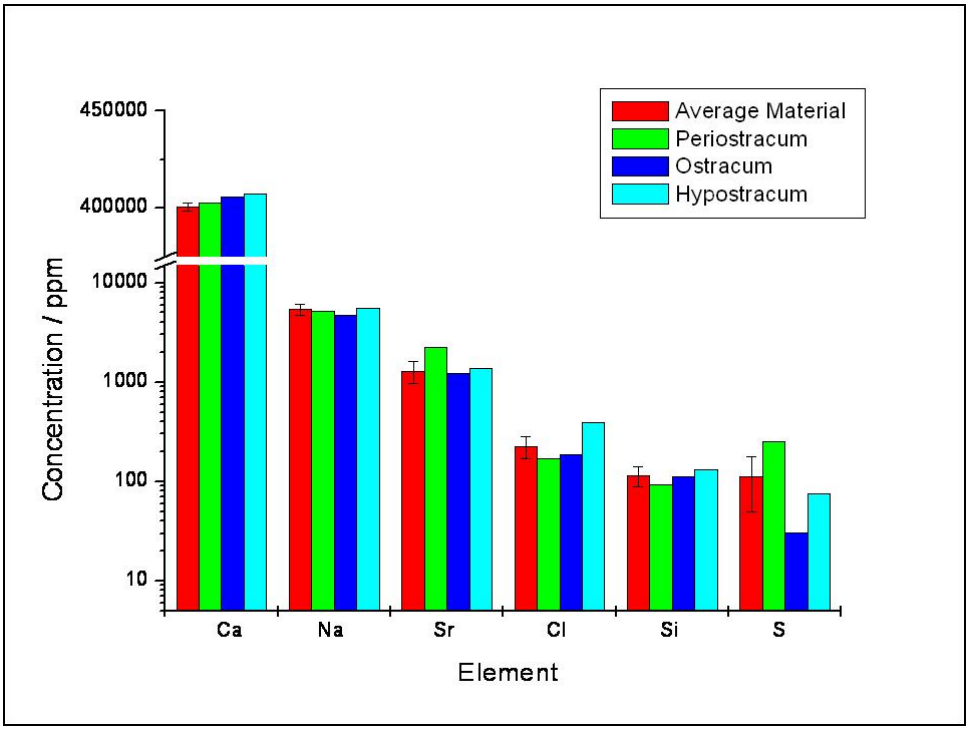

Figure 49: Microprobe analysis of an exemplar of *C. tigris* shell (cross section, parallel to the surface, on the top of the shell). The error bars are for all measurements similar to those shown for the average material.

In agreement with the SEM-EDX observations, no spatially resolved concentration differences between layers or structures, inside the uncertainty of the method, were observed. It means that the main elements are related to the mineral structure, the aragonite, and it does not change substantially from one layer to the other. These values are therefore well represented by the average measure.

The composition analysis for major elements by INAA made on powdered average and specific layer material has shown (in accordance to the microprobe analysis) that the main structural elements Ca, Na and Sr are found at almost in the same concentration in all layers. Ca is found in these shells at around 450000 ppm, Na at about 5000 ppm and Sr between 1500 and 4500 ppm. These data are in good agreement with other marine gastropod shells analysed by different authors (Dauphin, 2000; Almeida, 1998;).

Other structural elements such as Mg, that belong to the short half life elements with its 9.45 minutes, could not be determined by short irradiation, because of the high background activity of other elements present in the sample. Sulphur as well as Phosphor, known structural elements of the proteins present in the shell, are not appropriate elements to be determined by INAA because they do not emit gamma rays (^{35}S, ^{32}P) or belong to the short half life elements (^{37}S) and therefore could not be detected or quantified in *Cypraea* samples.

9.1.1 Layer Dependence of the Major Elements

To compare the concentration of major elements between the five layers, for the three species, the concentration found in each layer of a particular shell was normalized as a percentage of the highest concentration found in the shell. The layers are indicated with the initial letters of the words: periostracum (P), coloured layer (C), striped layer (S), magenta layer (M) and white layer (W). The results for Ca, Na and Sr are shown in Figure 50, Figure 51 and Figure 52 respectively.

As it can be observed from Figure 50 and Figure 51, the major elements Ca and Na, measured by medium and short irradiations respectively, are found in each layer at about the same concentration. The variation found per layer is about 5% for Ca and 15% for Na. No decreasing or increasing pattern is observed with the depth of the layer. This behavior is representative for all three shells analyzed. For the element Sr (Figure 52) the behavior is completely different. Decreasing concentrations with the layer depth is observed for *tigris* and *zebra* species, while the pigmented layer of *C. talpa* shows a 60% Sr increment in respect to its concentrations in the other layers.

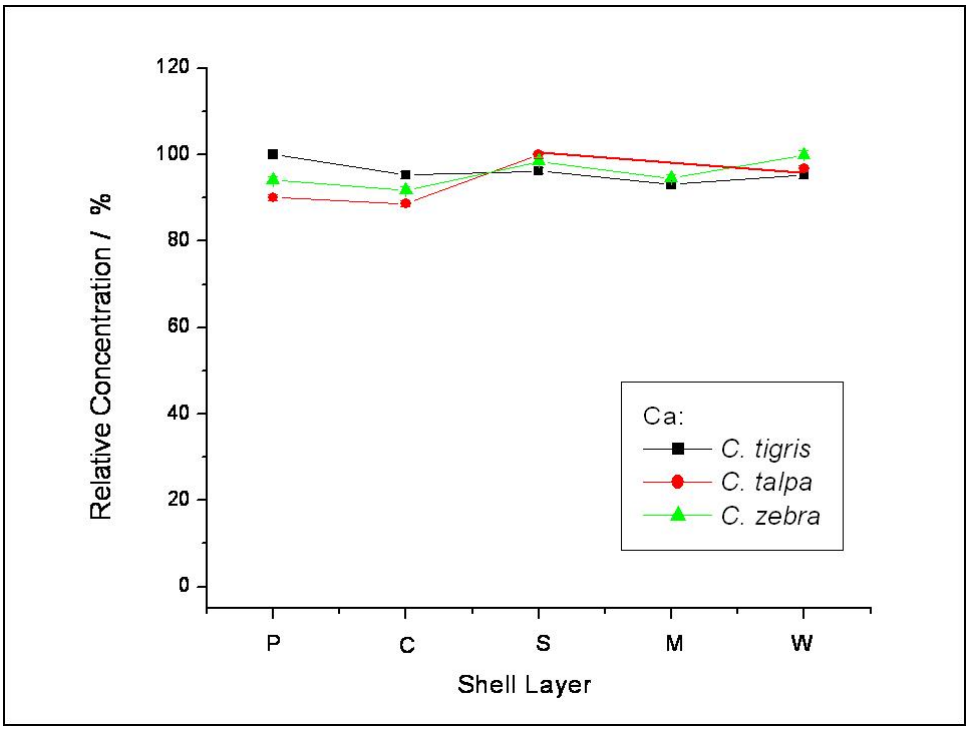

Figure 50: Relative concentration of calcium found in *Cypraea* shells by INAA, in relation to the shell layer. Error bars not observed are smaller than the point.

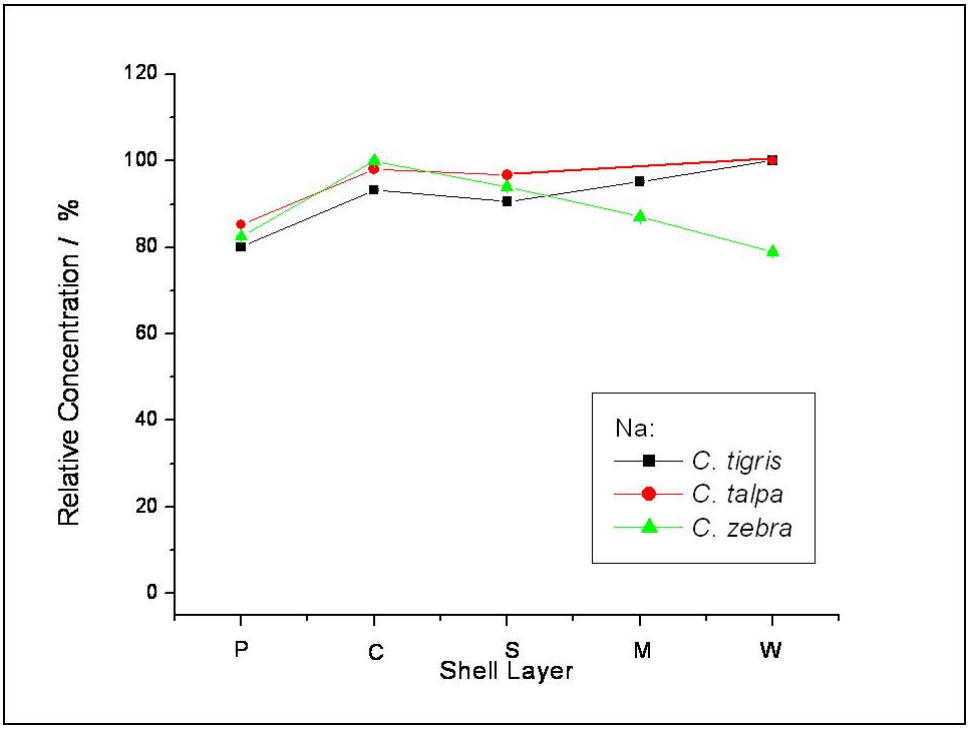

Figure 51: Relative concentration of sodium found in *Cypraea* shells by INAA, in relation to the shell layer. Error bars not observed are smaller than the point.

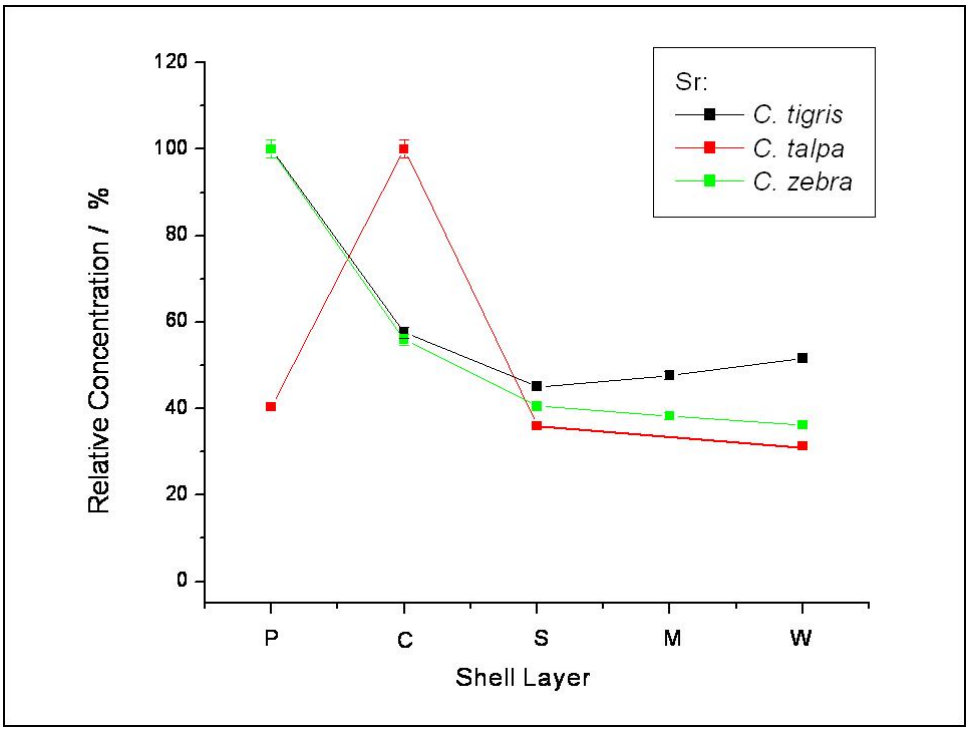

Figure 52: Relative concentration of strontium found in *Cypraea* shells by INAA, in relation to the shell layer. Error bars not observed are smaller than the point.

9.2 Trace Elements Analysis

Minor elements found by INAA in the *Cypraea* shell samples were Mn, Br, Cr, Co, Fe and Zn, (See Figure 53) in concentrations between 0.05 and 1000 ppm, element and sample dependent. The detection limit was improved by the long irradiation method for the elements Cr, Co, Fe and Zn. Rare earths Eu, Ta and La were identified (data not shown) in the three snails. These latter elements were not quantified.

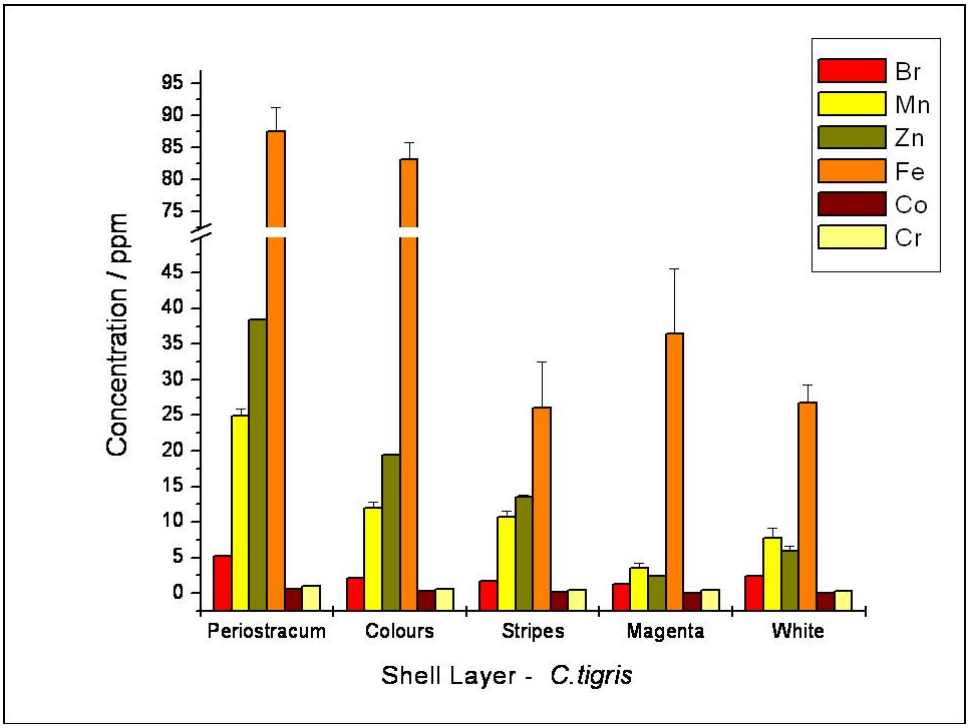

Figure 53: Concentration found by INAA for different minor elements in five optically differentiable shell layers of *C. tigris* snail.

It is not rare to find these elements in the shells; they are commonly found in the aquatic environment on sea and could be incorporated to animals through the diet. Mn and Fe were already measured in *Cypraea leviathan* specimens at concentrations around 50 and 100ppm respectively (Dauphin 2003). Data of Co, Cr and Zn are not found in *Cypraea* species but in other mussels and bivalves, where also As, Ba, Bi, Cd, Cu, Mo, Ni, Pb, Sc, Sb, Sn and V presence were reported (Ravera, 2003; Lazareth, 2003). The elements Ni, Ba, Cu (short irradiations), As, Mo, Ag, Au, Sb, Sc, Rb, V, Ce, Cs, and Tb (middle irradiations) and Sn, Cd and Se (long irradiations) were in all powdered samples under the detection limit of the INAA measurements. Short life time elements as Al, Si and Mg, could not be measured because of

the high activity achieved for the highly abundant matrix elements Ca, Na and Cl. Other elements which have no gamma lines like Pb could regrettably not be determined by this technique.

9.2.1 Layer Dependence of the Trace Elements

As for the mayor elements (See for example Figure 50) the trace elements Co, Cr, Zn, Fe, Br and Mn were normalized to the biggest concentration found in each shell and plotted against the shell layer. The layers are indicated with the initial letters of the words: periostracum (P), coloured layer (C), striped layer (S), magenta layer (M) and white layer (W) Each element was compared between the three species. The results are found in Figure 54, Figure 55, Figure 56, Figure 57, Figure 58 and Figure 59 respectively.

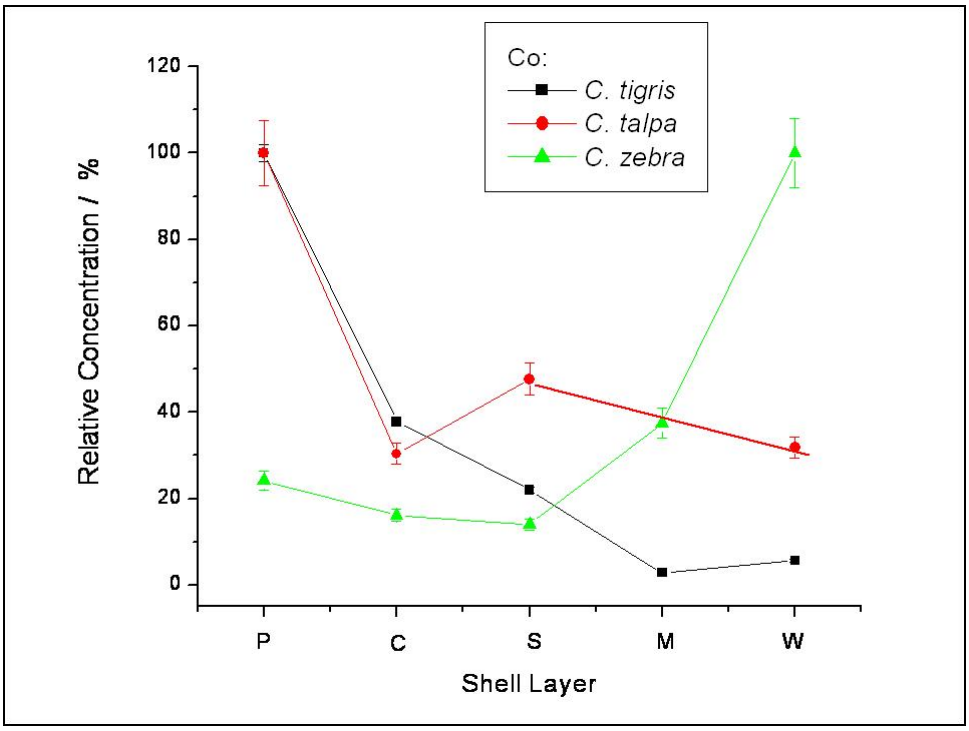

Figure 54: Relative concentration of cobalt found in *Cypraea* shells by INAA, in relation to the shell layer. Error bars not observed are smaller than the point.

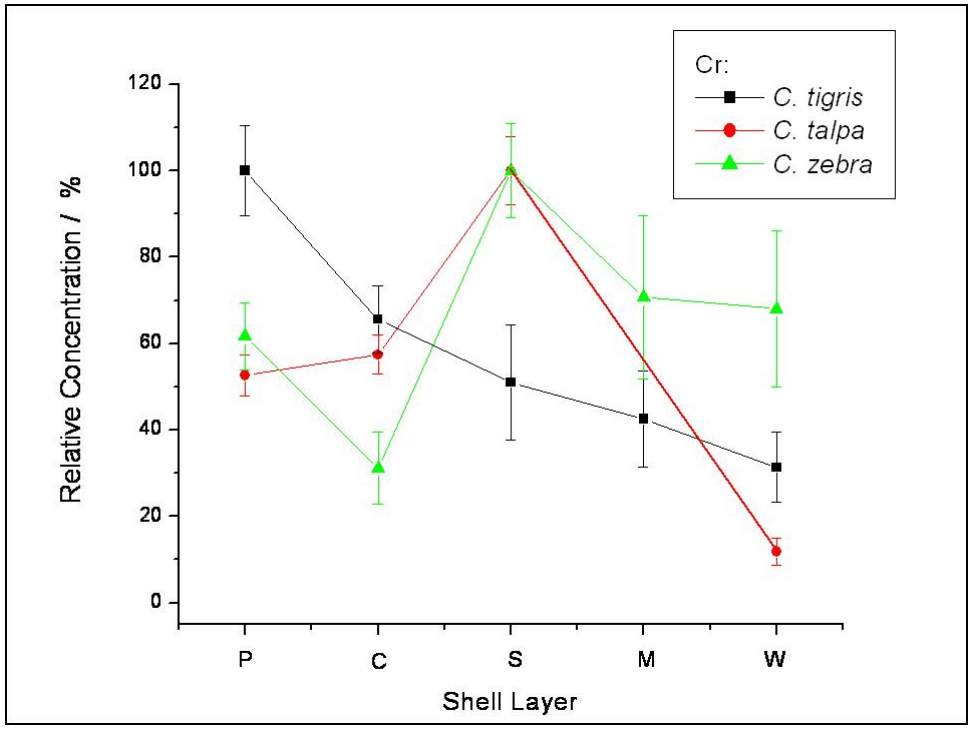

Figure 55: Relative concentration of chromium found in *Cypraea* shells by INAA, in relation to the shell layer. Error bars not observed are smaller than the point.

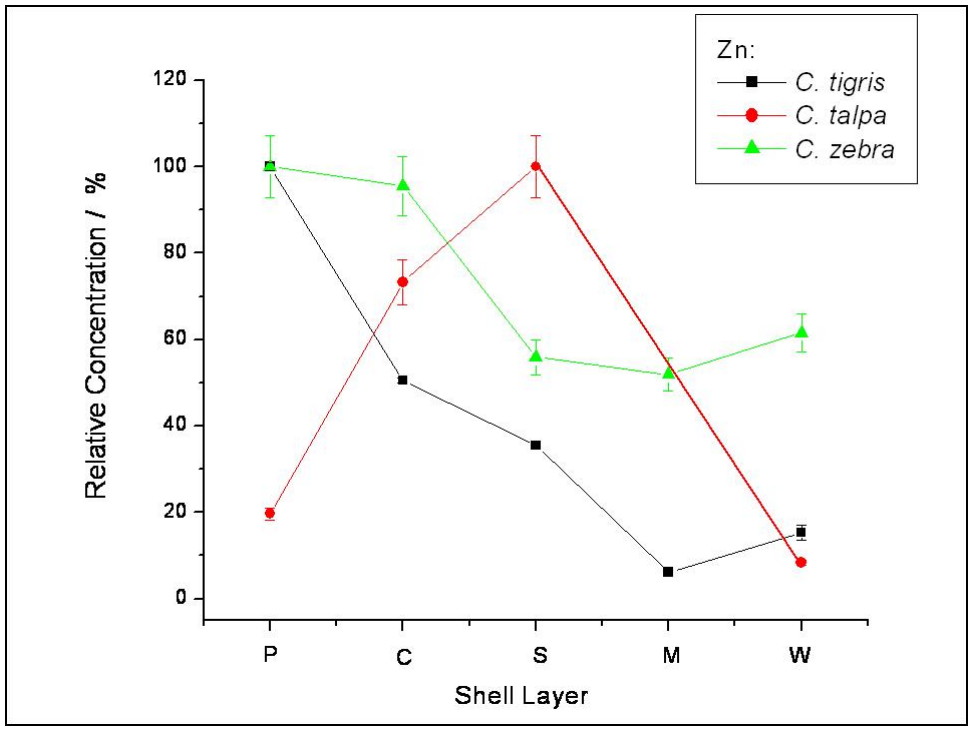

Figure 56: Relative concentration of zinc found in *Cypraea* shells by INAA, in relation to the shell layer. Error bars not observed are smaller than the point.

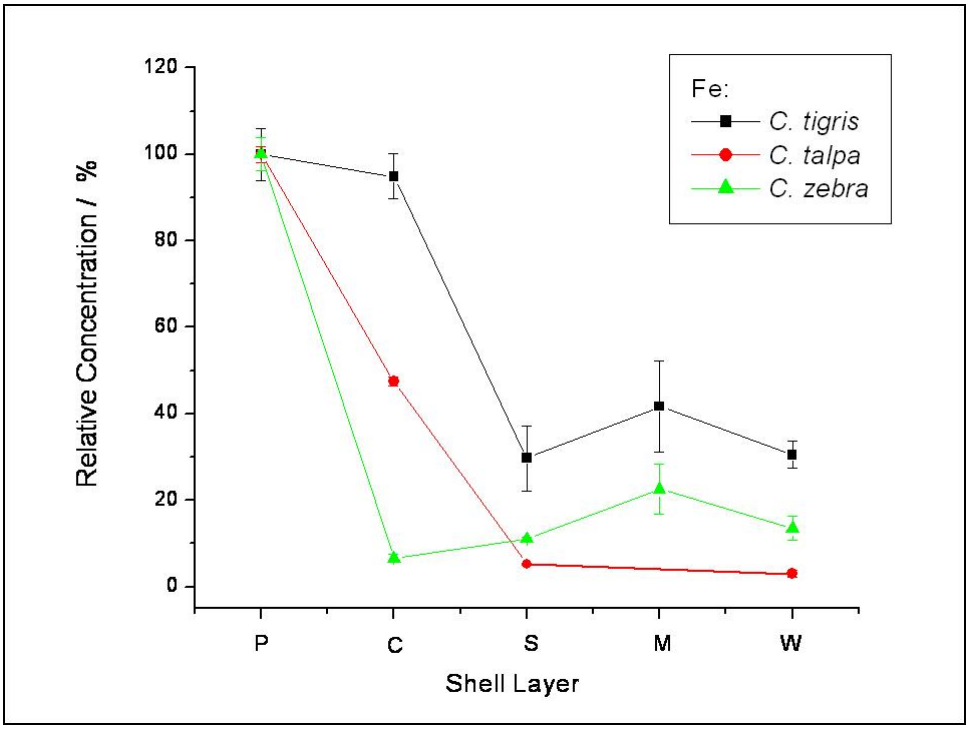

Figure 57: Relative concentration of iron found in *Cypraea* shells by INAA, in relation to the shell layer. Error bars not observed are smaller than the point.

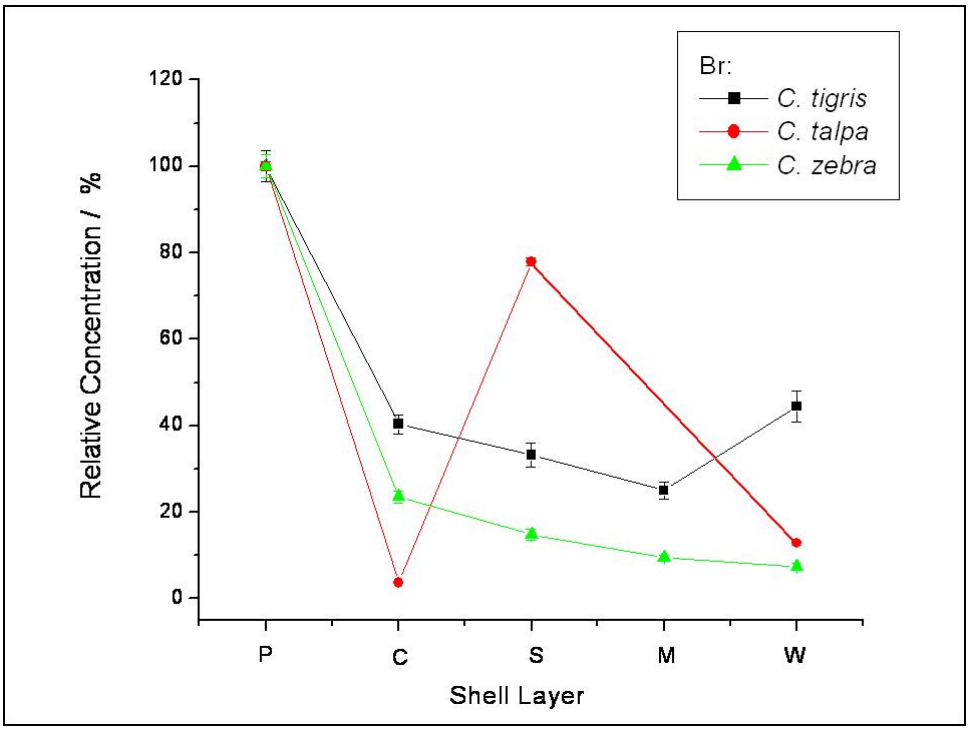

Figure 58: Relative concentration of bromine found in *Cypraea* shells by INAA, in relation to the shell layer. Error bars not observed are smaller than the point..

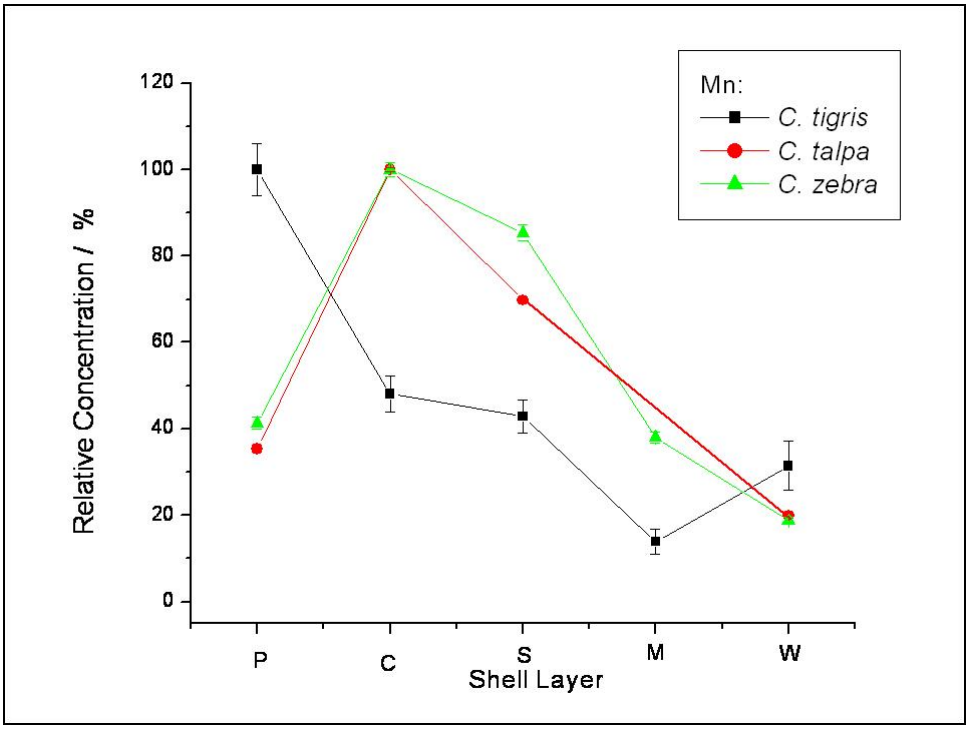

Figure 59: Relative concentration of manganese found in *Cypraea* shells by INAA, in relation to the shell layer. Error bars not observed are smaller than the point.

For the element Cobalt (Figure 54), a clear decreasing profile from the outside (P) to the inside (W) is observed for *tigris* shells. For the *talpa* species, the dependence is also decreasing, but the striped layer presents a Co enrichment with respect to the neighbor layers. For *zebra* snails, the situation is inverse to that found for *tigris*, and the profile is ascendant to the interior of the shell (W). For the element Chromium (Figure 55), again a clear decreasing profile form the outside (P) to the inside (W) is observed for *tigris* shells. For the *talpa* and *zebra* species, this time is the striped layer which presents more Cr, diminishing to both borders. The elements Zinc (Figure 56), and Bromine (Figure 58) show a decreasing profile from the periostracum to the white layer for *tigris* and *zebra*, and a peak for the *talpa* snails in the striped layer respectively. The element Iron (Figure 57) presents a decreasing profile for the three shells. Manganese concentration (Figure 59) present a minimum in magenta layer of the *tigris* shells, being more abundant in the periostracum. For the *zebra* and *talpa* snails it is also a decreasing profile to the inside of the shell, with a peak in the pigmented layer.

9.2.2 Comparison of the Absolute Concentration

The absolute value of the concentration found by INAA on powdered shell samples is shown in the Appendix XIII ("Trace Analysis Results") for *C. tigris*, *C. talpa* and *C. zebra*. The absolute concentrations were analyzed between the three different snail species. For that, the concentrations found for *C. talpa* and *C. zebra* snails were plotted against the concentration found for *C. tigris* shells in each layer. *C. tigris* data were elected for the longitudinal axis, because it was the shell used as test sample during the whole development of this research. The layers are indicated with the initial letters of the words: periostracum (P), coloured layer (C), striped layer (S), magenta layer (M) and white layer (W). X-error bars are the same for *C. talpa* and *C. zebra* snails (only showed for *C. talpa*). The Y-error bars that are not observed are smaller than the point size.

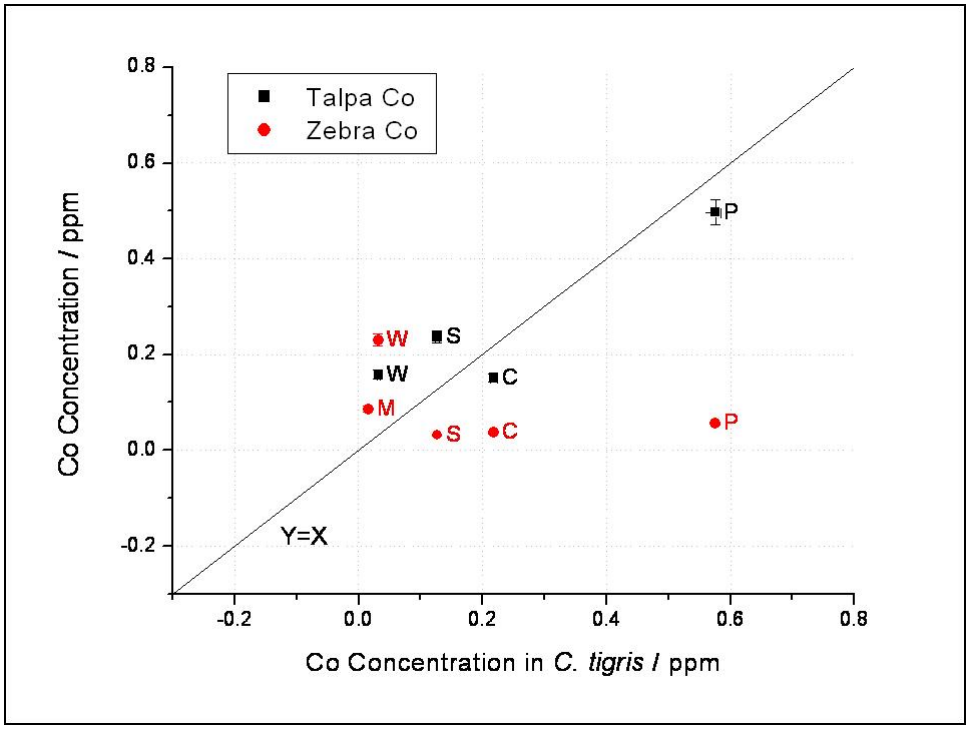

Figure 60: Concentration of Cobalt for *C. talpa* and *C. zebra* shells in relation to the concentration found for *C. tigris* shells, by INAA. Results calculated with the emissions 1332 keV and 1173 keV of the isotope ^{60}Co.

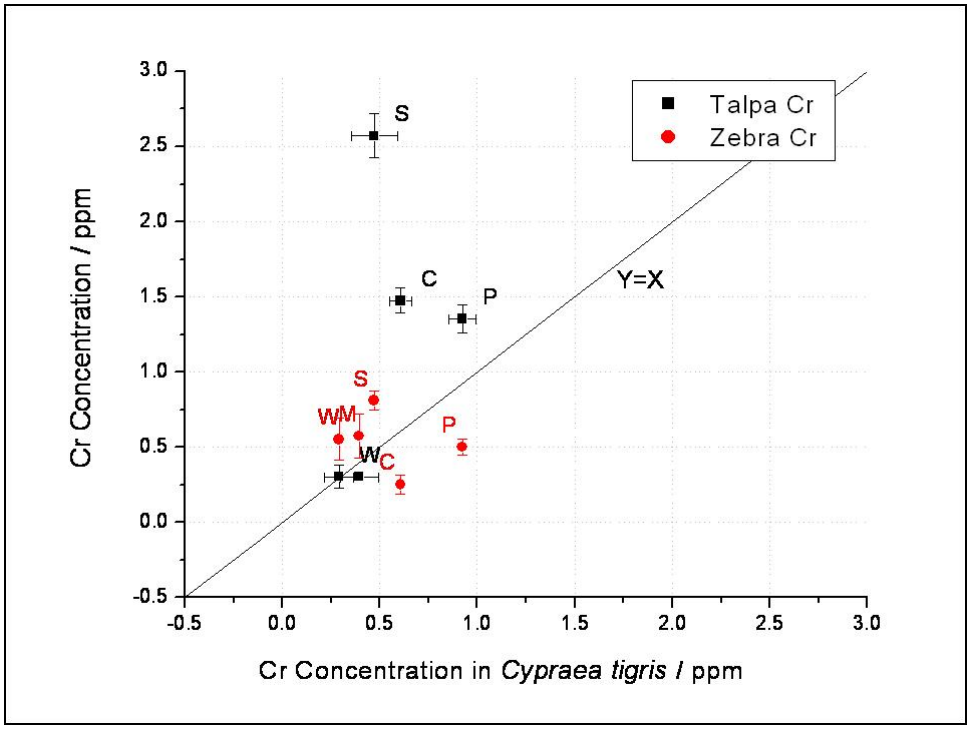

Figure 61: Concentration of Chromium for *C. talpa* and *C. zebra* shells in relation to the concentration found for *C. tigris* shells, by INAA. Results calculated with the emission of 320 keV of the isotope ^{51}Cr.

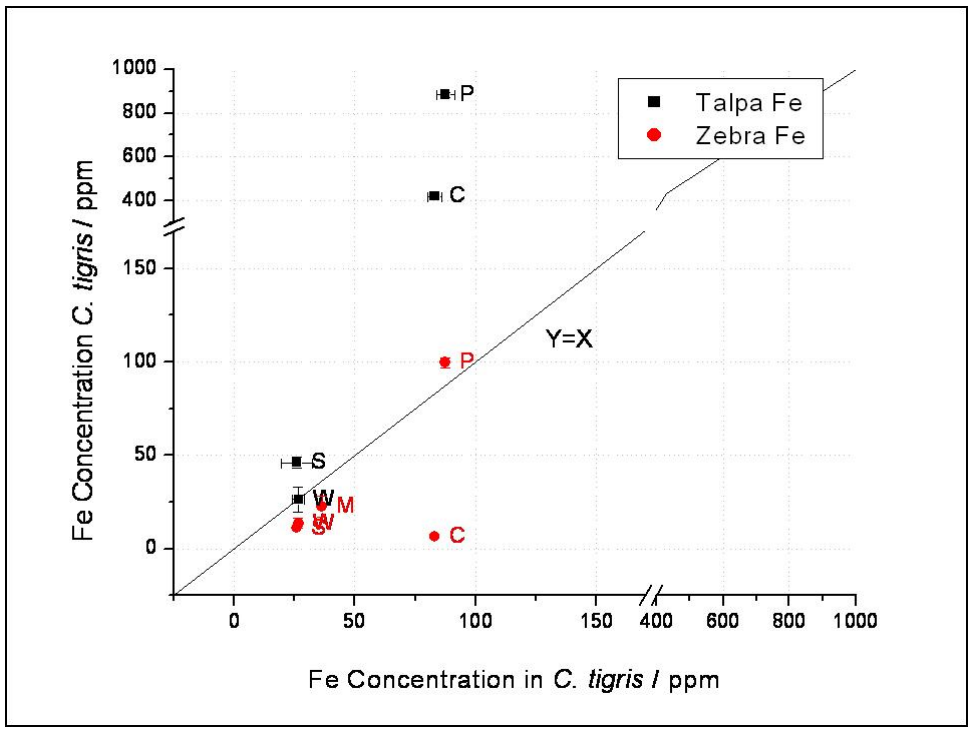

Figure 62: Concentration of Iron for *C. talpa* and *C. zebra* shells in relation to the concentration found for *C. tigris* shells. Results calculated with the emissions1099 keV and 1291 keV of the isotope ^{59}Fe.

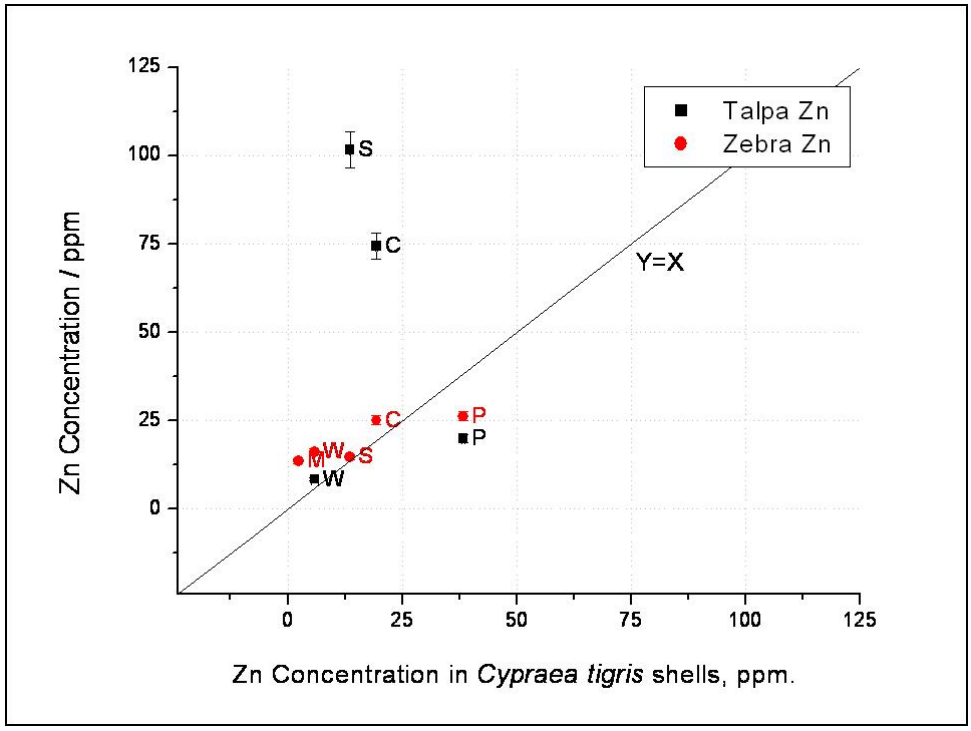

Figure 63: Concentration of Zinc for *C. talpa* and *C. zebra* shells in relation to the concentration found for *C. tigris* shells. Results calculated with the emission 1115keV of the isotope ^{65}Zn.

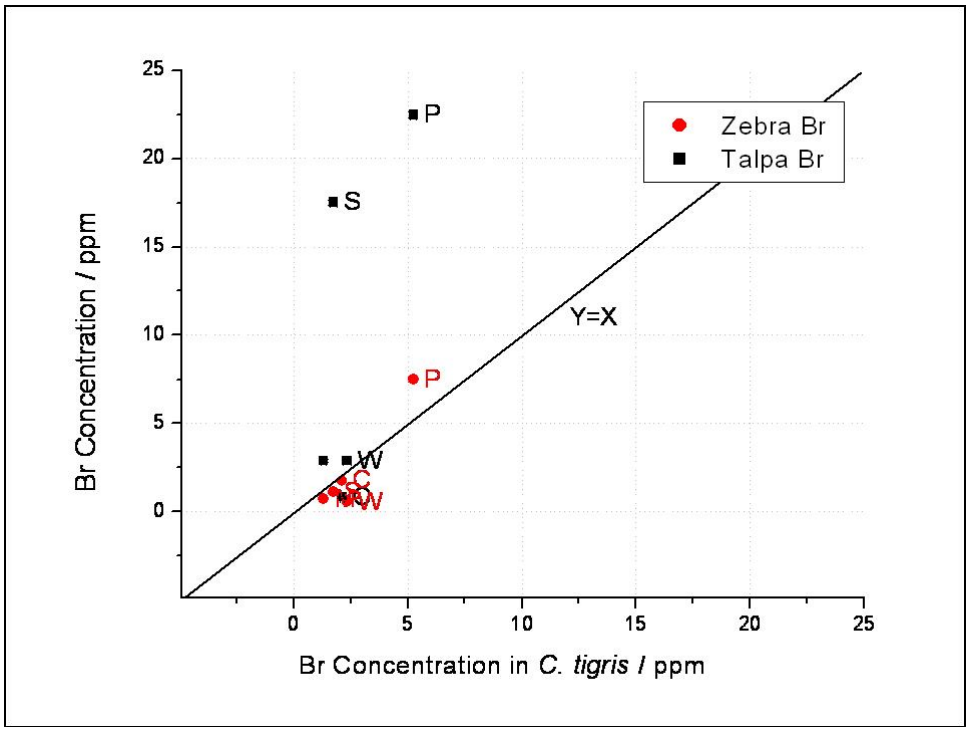

Figure 64: Concentration of Bromine for *C. talpa* and *C. zebra* shells in relation to the concentration found for *C. tigris* shells, by INAA through "medium" irradiations. Results calculated with the emissions 554 keV and 776 keV of the isotope ^{82}Br.

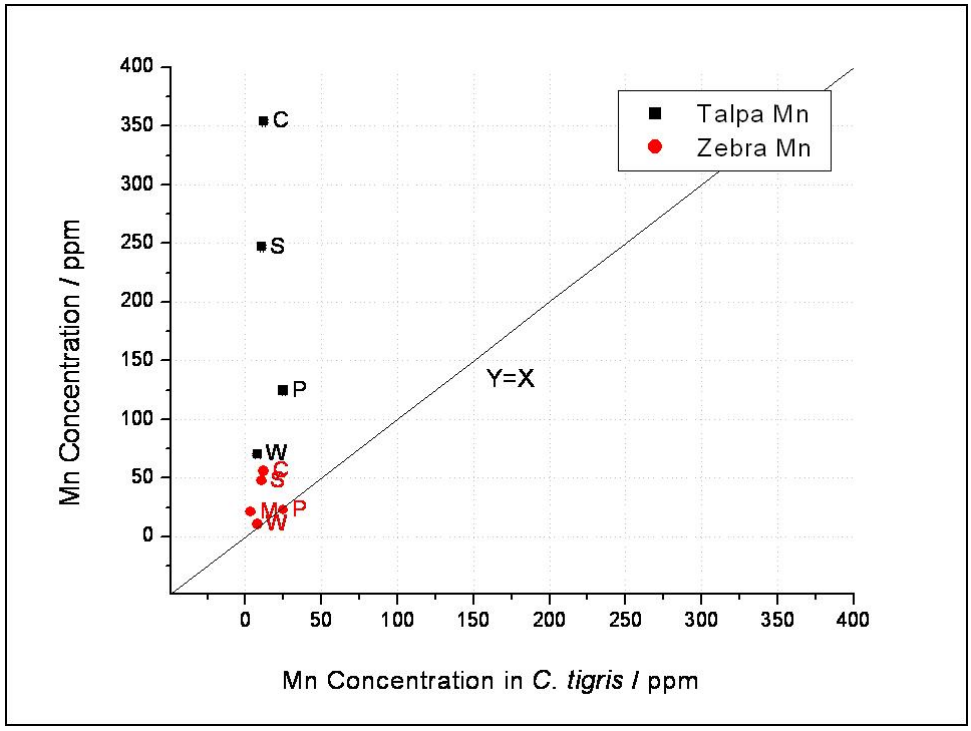

Figure 65: Concentration of Manganese for *C. talpa* and *C. zebra* shells in relation to the concentration found for *C. tigris* shells. Results calculated with the emissions 1846 keV and 776 keV of the isotope ^{56}Mn.

One fact that is very visible from the latter figures is that the periostracum, the coloured and the striped layers of the snail *C. talpa* present higher concentrations of Br, Cr, Fe, Mn and Zn, than its partner *C. zebra* or *C. tigris*. In the case of the element Bromine, the concentration for all three shells remains near, between 1 and 10 ppm for all layers others than *talpa* P and S, where the concentration has reached higher values. For Cobalt the values found are between 0.05 and 0.6 ppm, and in this case the *C. tigris* periostracum presents higher values than with the other two shells. The presence of Chromium is homogeneous for *zebra* and *C. tigris*, and presents again the difference in *C. talpa* S, C and P layers, where the values are higher. For Iron the case is similar but the concentrations achieved in C and P layers are remarkably higher than for the other layers. In the case of Manganese, the values found in *C. tigris* are very low, followed by the values of *zebra*. For *C. talpa* the concentrations are very disperse and reach the highest values. The element Zinc is found in about the same concentrations for all species, but again this time the C and S layer from the *C. talpa* snail show higher values.

The fact that for some elements, the concentration found in internal layers are higher than the concentrations in the external layer agrees with the hypothesis that the elements are not simply present due to a diffusion process from the environment, but are related to the structure, the layer characteristics, and the presence of organic material and pigments. For

all three snails, the concentration of trace elements in the white internal layer is generally lower than for all other layers. Periostracum and coloured layers have generally shown higher concentrations than the rest of the layers in the shells. Most often the concentration in periostracum was higher than in the coloured or the striped layers, but the reverse was observed too, as for example in the Zn for *C. talpa* snails (Figure 63).

9.3 The Same Depth Profile as Observed in the Organic Content?

The powdering of C*ypraea* shells has shown the presence of different layers of different colors, hardness and thickness (see results in Chapter 7). The organic matrix extracted from these layers was studied and described in Chapter 8. The Bradford test, as well as the information recovered by UV Spectroscopy and SE Chromatography has shown a decreasing depth profile for the protein content per layer, from the outside to the inside of the shells. In agreement with the literature, the periostracum is found to be the most organic layer, followed by the colored layer. It was also already demonstrated (by Micro-Raman Spectrometry studies in Chapter 7) that a portion of the organic material observed corresponds to pigments (caroteinoids).

In addition, the trace analysis done by INNA on the different layers in this chapter demonstrated that some major elements, like Na, show a homogeneous distribution in the shell, while other minor elements like Mn, Br, Co, Fe and Zn present an interesting increasing or decreasing profile when passing from the outside to the inside of the shell layers, being more accumulated in one or other layer. Probably, the first kind of ions may occupy interstitial sites of the structure; while the second group indicates a more complicated interaction with the shell matrix.

Regrouping the information of this chapter (Trace Elemental Analysis) with those of Chapters 7 (Micro and Nanostructure), Chapter 8 (Organic Matrix), new information is won. For some elements is true that the quantity of the element and the quantity of the organic material are correlated in the layers. The elements are more concentrated where the layers are more organic, and vice versa. Illustrative examples for that are the element manganese in the *C. tigris* samples (Figure 65) and the element zinc in *C. zebra* shells (Figure 66).

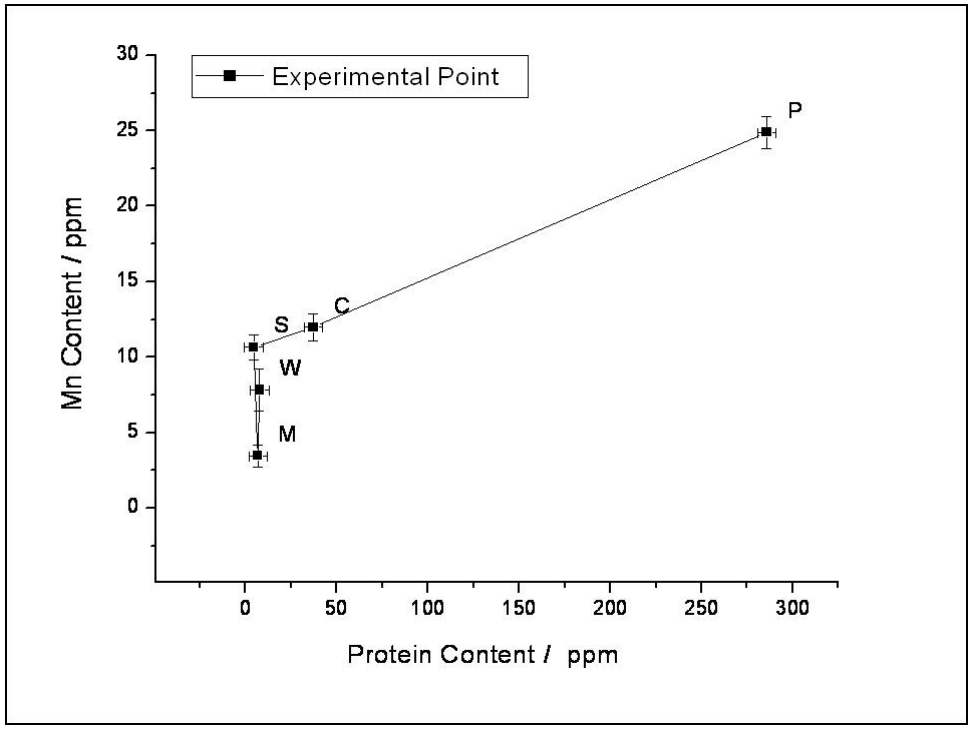

Figure 66: Concentration of Manganese found by INAA in relation to the concentration of proteins found by Bradford Test, for *C. tigris* shells.

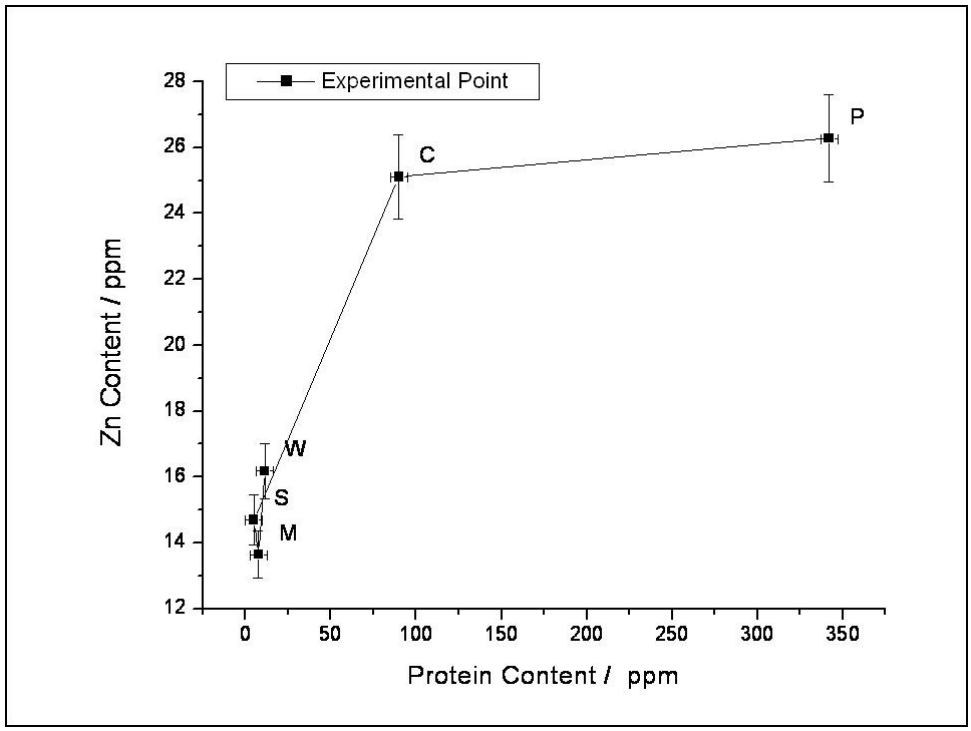

Figure 67: Concentration of Zinc found by INAA in relation to the concentration of proteins found by Bradford Test, for *C. zebra* shells.

Of course, if these correlations are true and the organo-metalic complexes are enough strong, that the complexes survive the OM extraction, there is a possibility to find them in the

SOM matrix. This hypothesis will be checked by on-line HPLC-ICP-MS measurements in the next chapter.

9.4 Summary of Results

In the present chapter, optically differentiable shell layers of *Cypraea tigris*, *talpa* and *zebra* snails were carefully separated using a diamond micro milling cutter. The presence of biologically relevant trace metals (Mn, Co, Fe, Zn, Cr, etc) and main structural elements (Ca, Na, Sr, etc) has been investigated by INAA and Microprobe as detection tool. These data were related to the microstructure of the shell. The element content per layer was compared between the three species analyzed. Structural elements Ca and Na are distributed homogeneously and about the same elemental concentrations were found for the three species. Higher quantities of the elements studied were found in the periostracum and in those layers where pigments are observable. A summary of all conclusions obtained from the latter analysis is listed in the next table.

Element	***C. tigris***	***C. talpa***	***C. zebra***
Ca	Structural	Structural	Structural
Na	Structural	Structural	Structural
Sr	Decreasing Max: P	Decreasing Max: C	Decreasing Max: P
Co	Decreasing Max: P	Decreasing Max: P	Increasing Max: W
Cr	Decreasing Max: P	Maximum Max: S	Maximum Max: S
Zn	Decreasing Max: P	Maximum Max: S	Maximum Max: P
Fe	Decreasing Max: P	Maximum Max: P	Decreasing Max: P
Br	Decreasing Max: P	Decreasing Max: P	Decreasing Max: P
Mn	Decreasing Max: P	Maximum Max: C	Maximum Max: C

Table 14: Summary of the major and trace elements results obtained by INAA on *Cypraea* shells. Max = layer with the higher concentration.

10. Results of Coupled Analysis

The Soluble Organic Matrix (SOM) of *Cypraea tigris, talpa* and *zebra* snails was analyzed by HPLC-ICP-MS. Metallic species have shown to be associated to the organic shell matrices, in agreement with correlations done with off line measurements. The results were compared between layers of the same shell and between the three different snail species.

The SOM extracted from the different layers from *tigris*, *talpa* and *zebra* snails where injected in a SE *Biosep S2000* column, which was coupled on line to an ICP-MS detector. This hyphenated technique permits to record on line the metals that elute from the column, at the elution time. Correlating the ICP-MS spectra for each metal observed with those of simple HPLC-UV experiments (Chapter 8), a possible correlation between the metal and the protein content could be achieved.

10.1 Characterization of the SEC Column

The behavior of the SE column with free metals was studied injecting a CERTIPUR® XVI multi-elemental standard solution (Merck) diluted at a concentration of 10 ppb. This solution is made of salts of the metals, and therefore they should not be retained in the column.

As it can be observed in Figure 68, all free ions elute as a sharp peak at 13.63min. Surprisingly, this time does not correspond to the dead volume of the column (around 22min, see Appendix IV). This result shows that the *Biosep* bed material does not work as a normal "pure SEC" column (small proteins are more retarded that free ions. Nevertheless, the use of this column to observe correlations between organic and metal species is valid. The interesting region to study (5 to 12 minutes), where the SOM proteins have shown appear in this column (see Chapter 8, section 8.5) is free of interferences from inorganic ions.

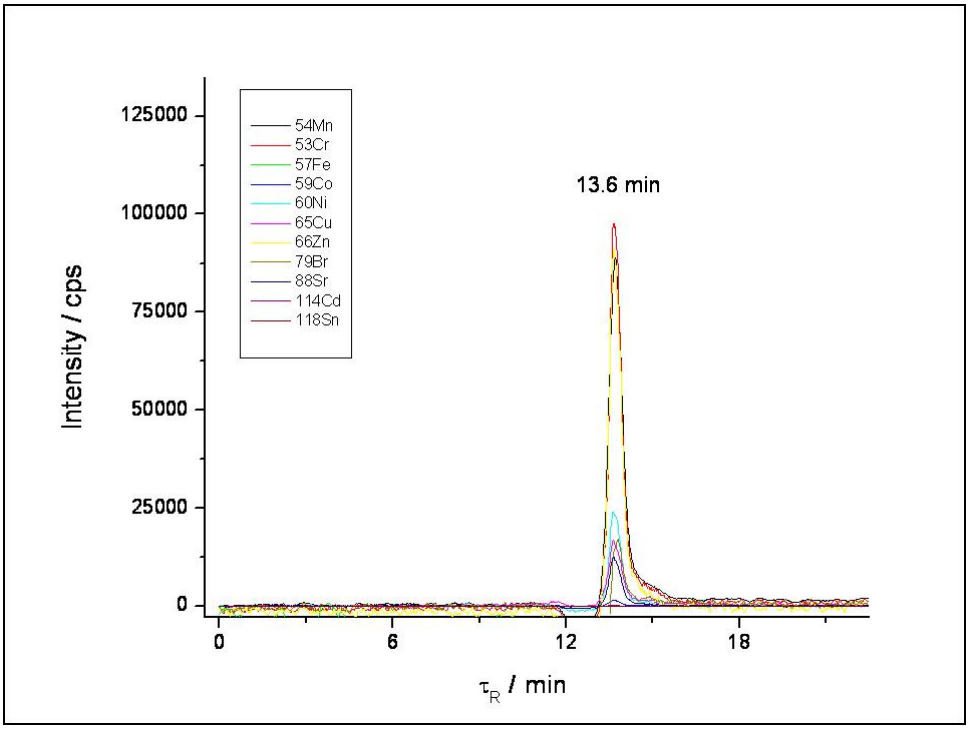

Figure 68: HPLC-ICP-MS chromatogram of an inorganic multi-elemental certified solution, eluting through a SE column.

SE-HPLC: column: *Biosep S2000*, mobile phase: Tris-HCl pH 7.4, flux: 0.8 ml/min, Injection loop: 20 µl.
ICP-MS: sweeps: 5, acquisition time: 100 ms each mass.

10.2 The Elements Observed by HPLC-ICP-MS

The elements studied by HPLC-ICP-MS in *Cypraea* shell samples were Mn, Cr, Fe, Co, Ni, Cu, Zn, Br, Sr, Cd and Sn. In accordance with the results obtained in Chapter 8 and Chapter 9, the periostracum is generally the layer that contains more traces of elements. The chromatograms obtained for the different layers of *C. tigris*, *talpa* and *zebra* samples show elements like Cu, Ni and Sn, that even if they were expected from literature data, were not observed under the detection limits of the INAA analysis of the shell powders. These results are not surprising if the elements are associated to the organic matrix, because the SOM extraction procedure concentrates the proteins (i.e. the metals associated to the proteins) by a factor 10^6 of the concentration in the shell powder.

Two interesting elements in the measurement were Mn and Sr. For both cases, in the three snail species analyzed, a particular behavior was observed. On one hand, no inorganic or organic peaks were eluted in the normal times, as for the other elements studied. On the other hand, after about 50min of measurement, a drift of the base line, with the form of a big bright peak was detected. Because these times were out of the calibrated range of the

column, it could not be distinguished whether they were really retarded peaks or an overcharge effect of the ions on the column.

The Relation between HPLC-UV and HPLC-ICP-MS

In the next three figures the chromatograms obtained from HPLC-UV and HPLC-ICP-MS are represented, measured under the same HPLC conditions and parameters, for the periostracum layer of each shell. For the three graphics, the position where inorganic elements elute is marked with a dashed line.

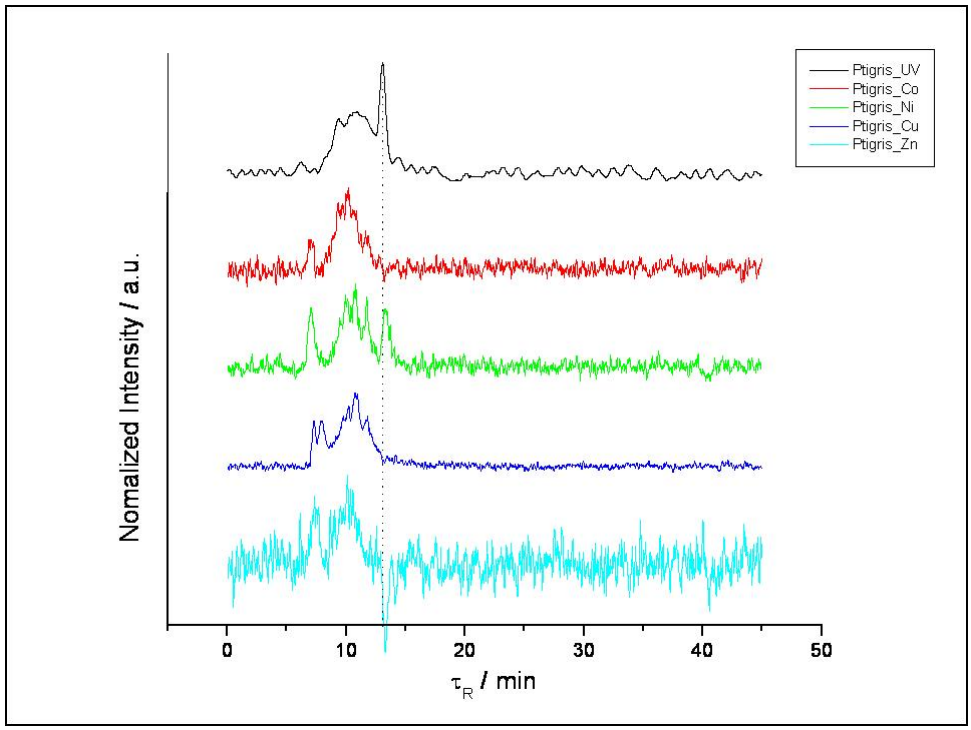

Figure 69: Correlation between HPLC-UV and HPLC-ICP-MS measurements for the periostracum of *C. tigris* shells.

As it can be seen from Figure 69 to Figure 71, the UV signal at 220 nm from the UV measurement coincides with the presence of certain metals detected by ICP-MS. The correlation between the data observed by HPLC-UV and HPLC-ICP-MS are in accordance with the hypothesis that some metals are not simply bound as inorganic Ca^{2+} substituents or occupying interstitial places in the shell bio-mineral. Moreover these results show a metal-organic bond to the proteins present in the soluble organic matrix.

For this study, the correlations are shown for the periostracum layer only, because it is the richest layer in proteins as well as in metals, although for each shell, all layers were studied. In the following the correlations for *C. talpa* (Figure 70) and *C. zebra* (Figure 71) are shown.

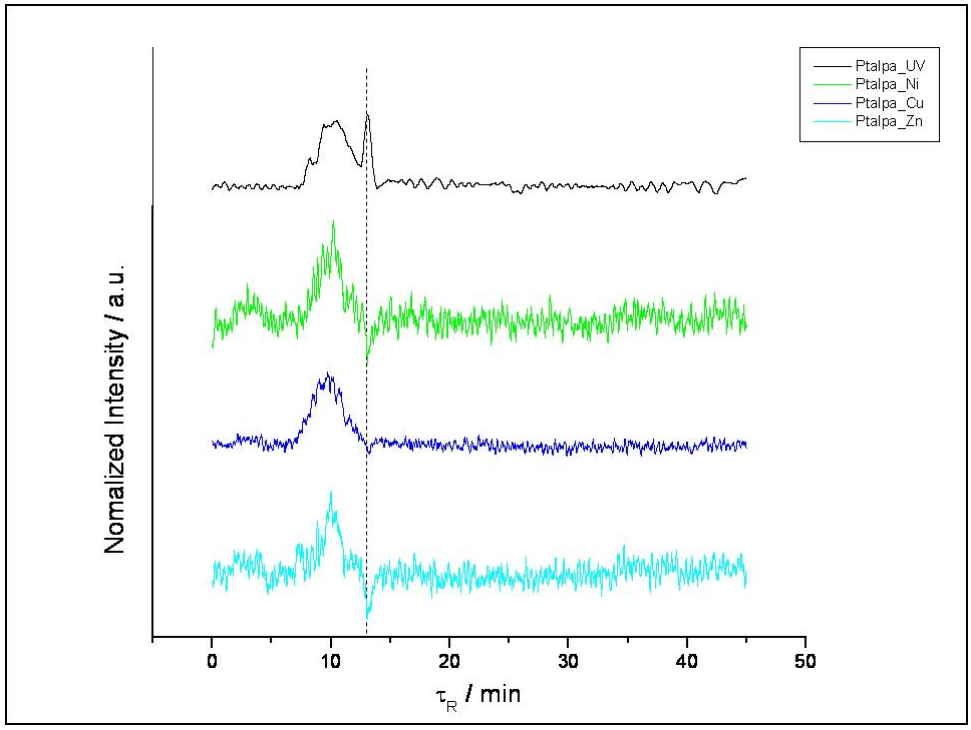

Figure 70: Correlation between HPLC-UV and HPLC-ICP-MS measurements for the periostracum of *C. talpa* shells.

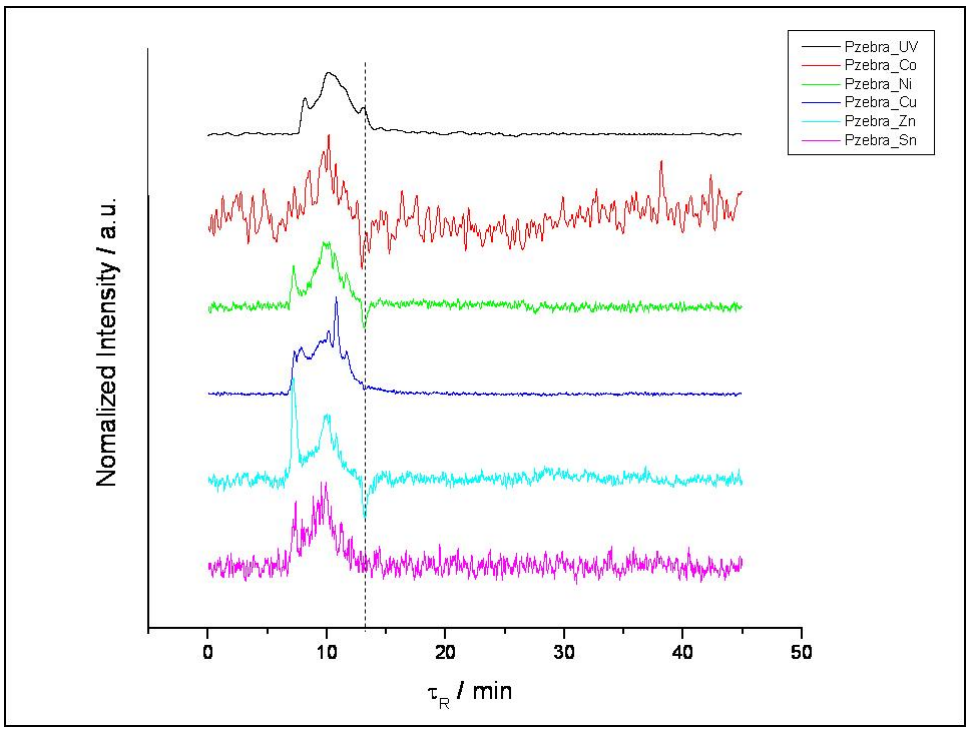

Figure 71: Correlation between HPLC-UV and HPLC-ICP-MS measurements for the periostracum of *C. zebra* shells.

On-line Measurements for C. tigris Layers

In the case of Cu (Figure 72), no inorganic material (13.6min) is observable. In contrast, the ^{65}Cu ions may be associated to different fractions of the organic matrix, because there are many peaks recognizable between 8 and 12min. In addition these peaks change in form and intensity from one layer to the next, indicating a possible transformation of the metal-organic complexes and in accordance with the conclusion that the protein presence in the SOM decreases and changes when passing from the outside to the inside of the shell.

For the element Ni (Figure 73), measured through the isotope ^{60}Ni, the effect observed for ^{65}Cu is again repeated. In this case too, no inorganic peak is observed but at least five peaks present in the periostracum are nicely separated. For the rest of the layers only the colored layer shows Ni presence.

The elements Zn (Figure 74) and Co (Figure 75) could be detected previously by INAA in the shells. The correlation between the contents in the shell powder and the protein content per layer has indicated indirectly a possible metal-organic union, or at least that both values were much higher in the periostracum. With the on-line measurements, this hypothesis could be validated. No Zn or Co is observed as an inorganic peak. In contrary, even in very low quantities, Zn and Co eluted together with to fractions of the periostracum organic matrix. For the other layers, the element Zn remains always around the noise signal. The observations were corroborated for the isotopes ^{66}Zn and ^{68}Zn (Data not shown) in good agreement. For the element Co, another peak is only observable in the striped layer, at about one third of the intensity observed in the periostracum.

The element Sn (Figure 76), detected through the isotope ^{118}Sn has shown to be associated only to the SOM of the colored layer in *C. tigris* shells. Different from the other elements, Sn does not appear in the periostracum. This fact could indicate that is not a simple absorption of the element from the environment. If this would be the case, the element must also be observed in the outside layers of the shell.

The concentration of Br in the shell powder found by INAA has shown to have a relation to the protein content. Nevertheless, the on-line measurements of Br, as well as Cd and Fe did not show organic or inorganic peaks, for the five layers. This result could mean that the association found before for Br was not really an organic complex, or that it was a complex to the IOM and not to the SOM, or that it was a complex to the SOM<3kDa and therefore got lost in the process, or finally that the extraction or the measurement method have destroyed the complex.

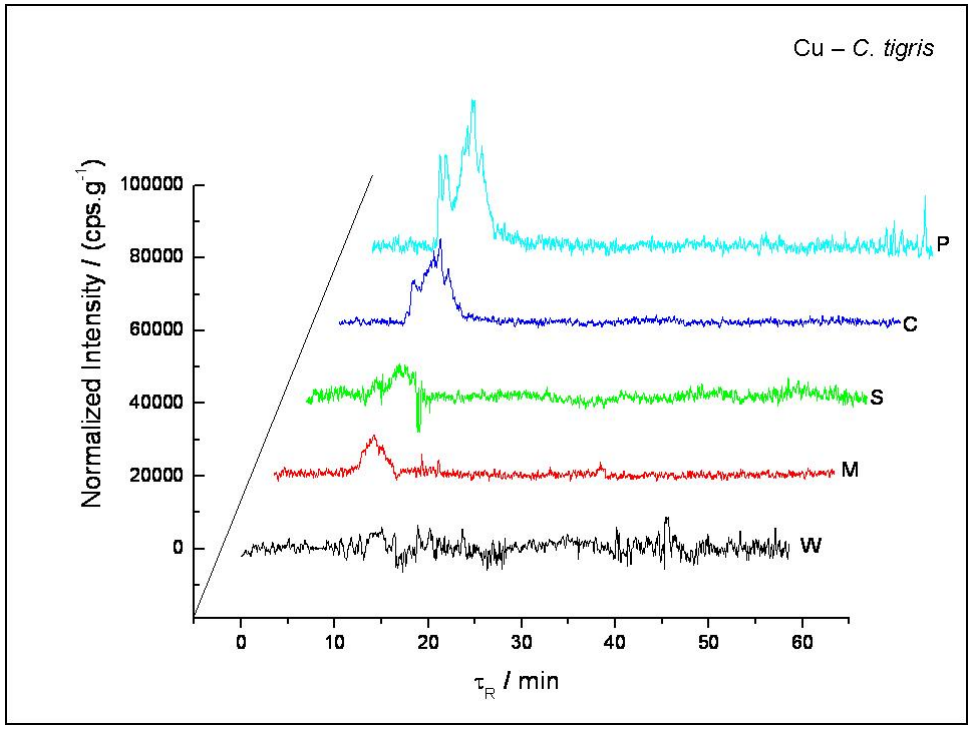

Figure 72: SE-HPLC-ICP-MS chromatogram of the SOM extracted from the five structural layers of *C. tigris* shells, showing ^{65}Cu.

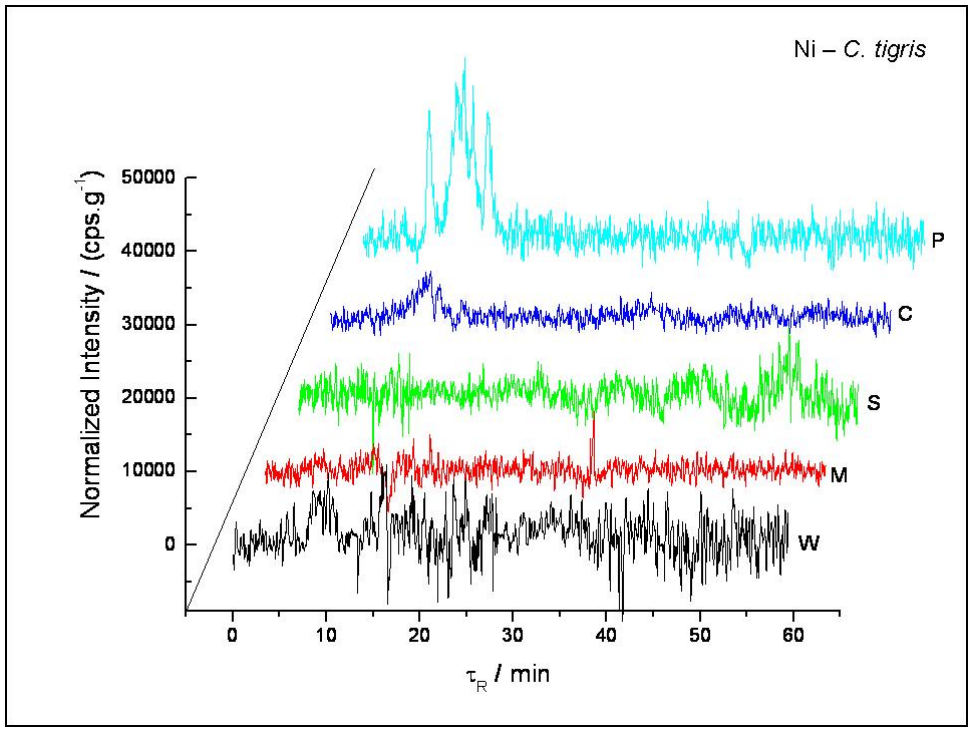

Figure 73: SE-HPLC-ICP-MS chromatogram of the SOM extracted from the five structural layers of *C. tigris* shells, showing ^{60}Ni.

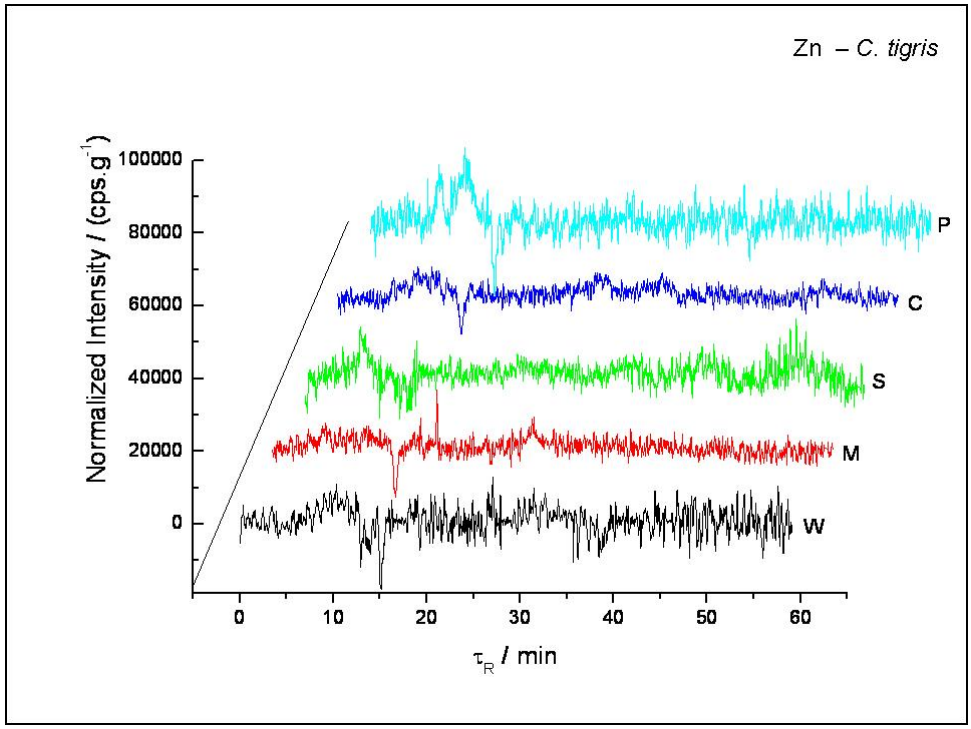

Figure 74: SE-HPLC-ICP-MS chromatogram of the SOM extracted from the five structural layers of *C. tigris* shells, showing ^{66}Zn.

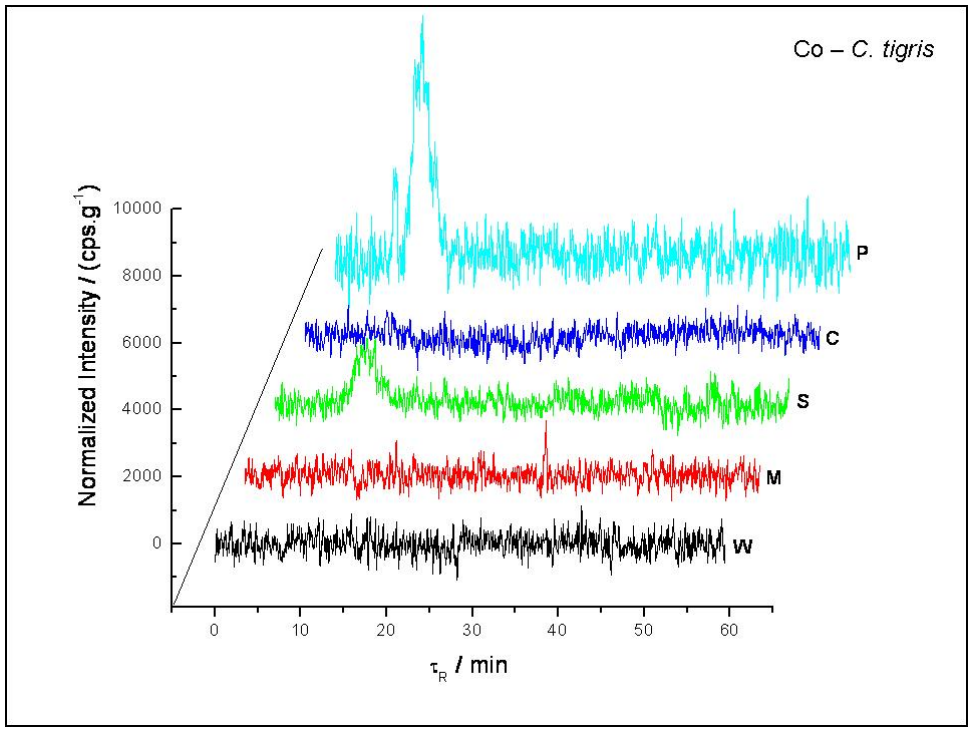

Figure 75: SE-HPLC-ICP-MS chromatogram of the SOM extracted from the five structural layers of *C. tigris* shells, showing ^{59}Co.

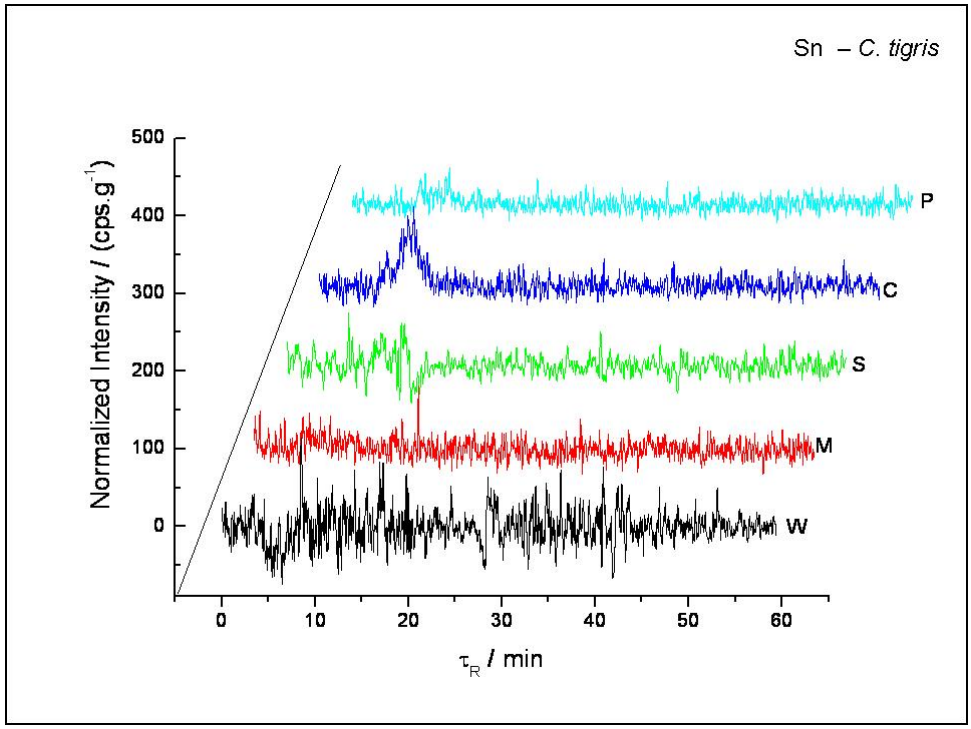

Figure 76: SE-HPLC-ICP-MS chromatogram of the SOM extracted from the five structural layers of *C. tigris* shells, showing ^{118}Sn.

On-line Measurements for C. talpa Layers

As in the case of C. tigris, Cu (Figure 77), Ni (Figure 78) and Zn (Figure 79) were also present in *talpa* shells, eluting with the organic fraction, between 8 and 12 min. At difference from *tigris* shells, only one main peak was observed, even for the last layer. Co, Cr, Fe, Br, Cd and Sn remain in the background level during the whole acquisition (data not shown). For Mn and Sr the same behavior as in *C. tigris* were observed: no inorganic signal was eluted as in the Mn^{2+} or Sr^{2+} inorganic standard, but a retardation of the peaks, with a column overcharge was detected.

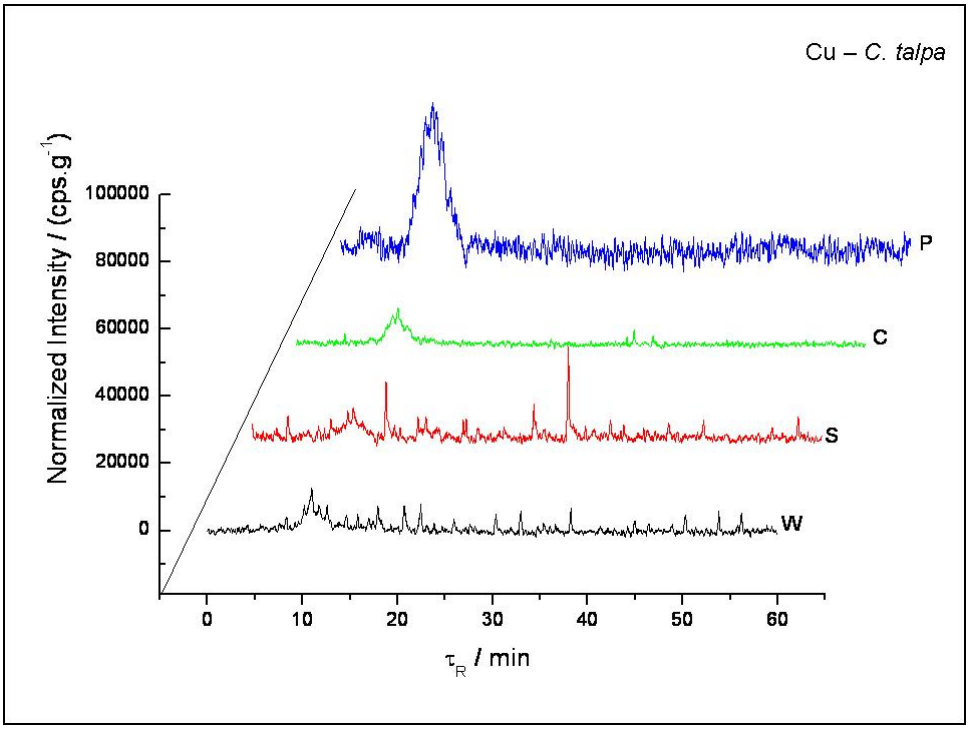

Figure 77: SE-HPLC-ICP-MS chromatogram of the SOM extracted from the five structural layers of *C. talpa* shells, showing ^{65}Cu.

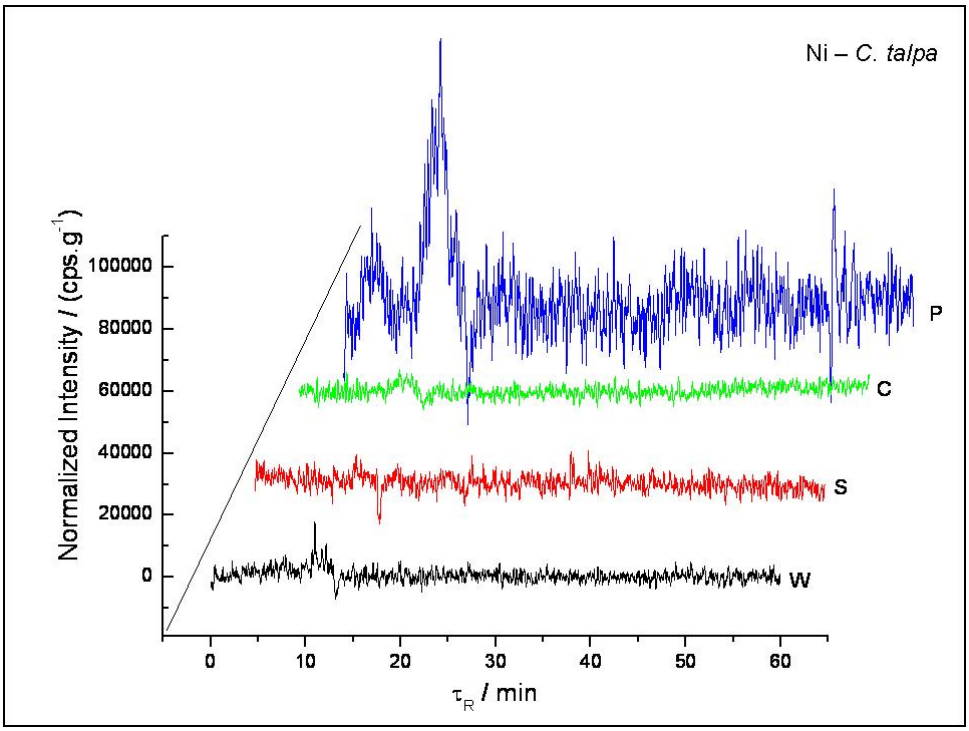

Figure 78: SE-HPLC-ICP-MS chromatogram of the SOM extracted from the five structural layers of *C. talpa* shells, showing ^{60}Ni.

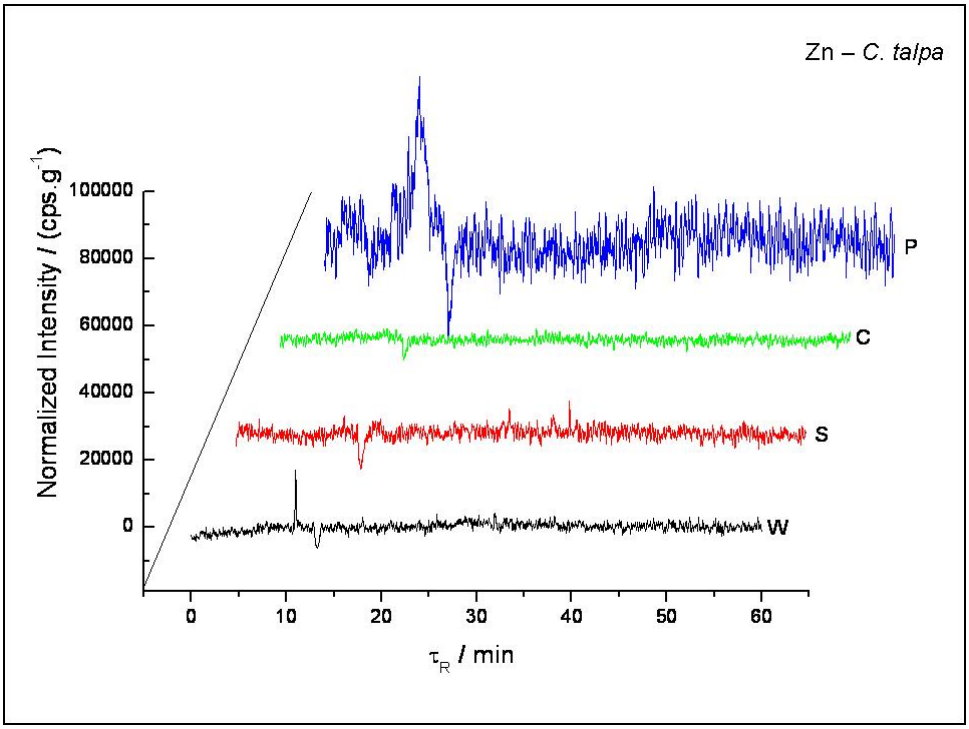

Figure 79: SE-HPLC-ICP-MS chromatogram of the SOM extracted from the five structural layers of *C. talpa* shells, showing ^{66}Zn.

On-line Measurements for C. zebra Layers

The element Cu (Figure 80) shows for the *zebra* species, to be more similar to that of *tigris* than to *talpa*. In this case, also a structure can be detected in the main organic peak, and no traces of inorganic Cu is present in the sample. Going to the inside of the shells, the peaks separate, and their intensities vary. It could mean that the complexation of the Cu ions with the matrix change, in agreement again with the observations for the *tigris* SOM. Ni (Figure 81), Sn (Figure 83) and Zn (Figure 82) are also observed coincident with two of the main peaks of Cu, in the periostracum and the colored layer. This fact shows that the organic matrix bounding these ions may be not very selective. Co (Figure 84) is observed only for the periostracum.

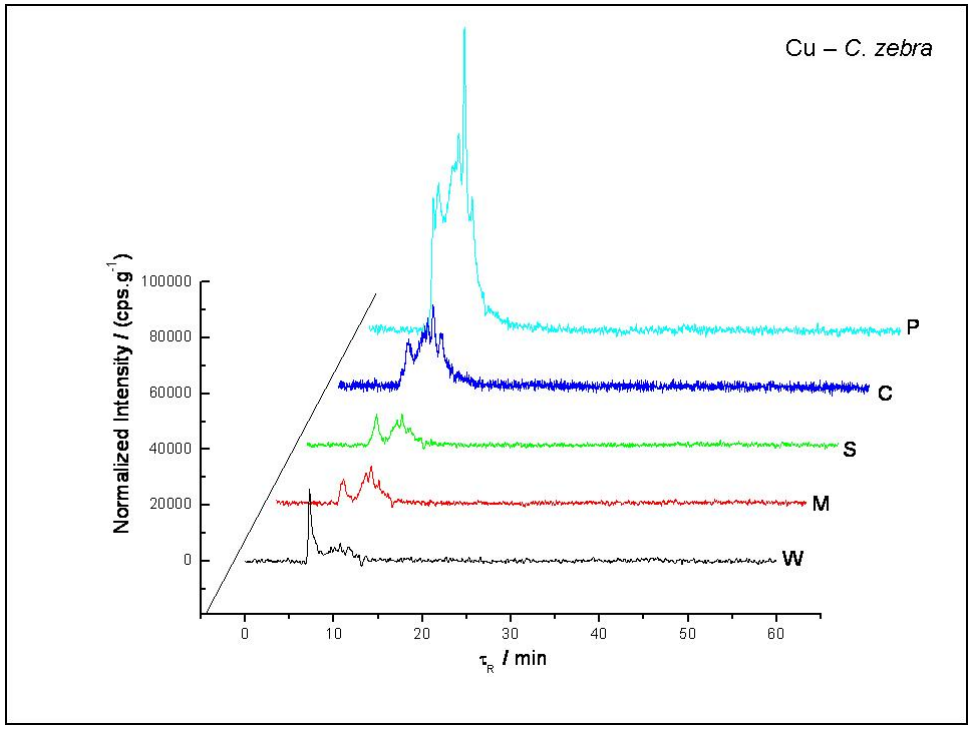

Figure 80: SE-HPLC-ICP-MS chromatogram of the SOM extracted from the five structural layers of *C. zebra* shells, showing ^{65}Cu.

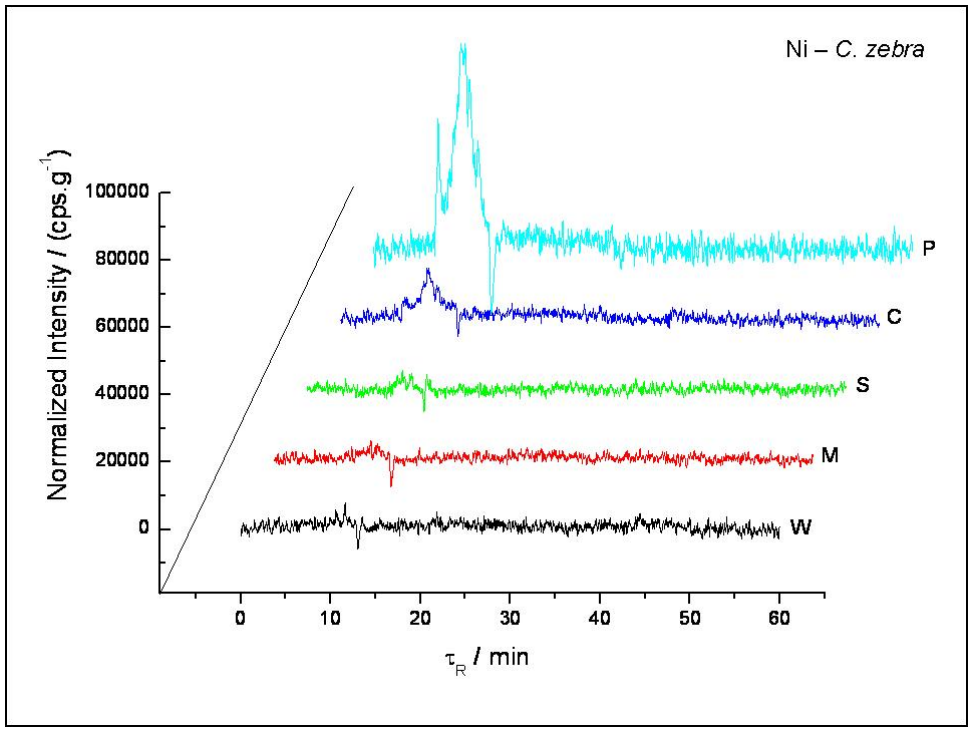

Figure 81: SE-HPLC-ICP-MS chromatogram of the SOM extracted from the five structural layers of *C. zebra* shells, showing ^{60}Ni.

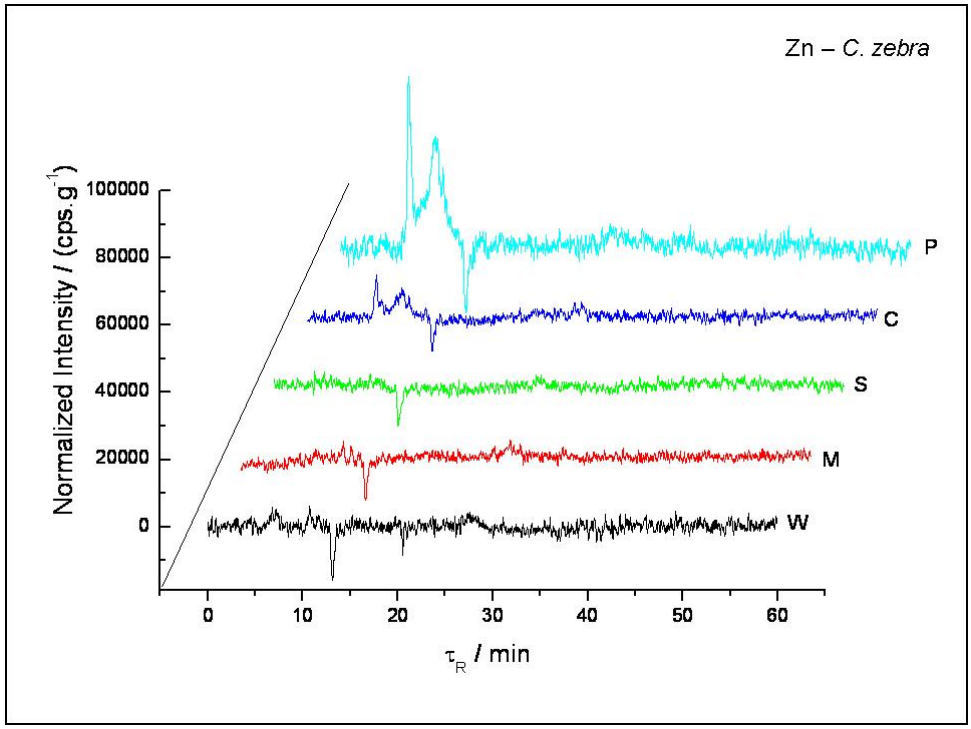

Figure 82: SE-HPLC-ICP-MS chromatogram of the SOM extracted from the five structural layers of *C. zebra* shells, showing ^{66}Zn.

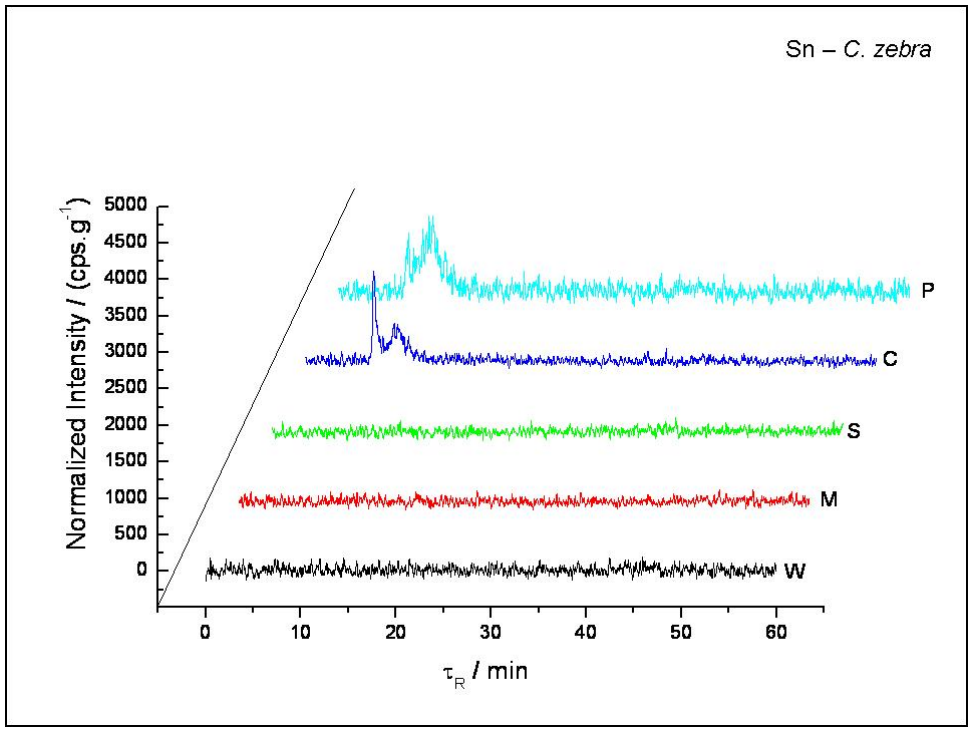

Figure 83: SE-HPLC-ICP-MS chromatogram of the SOM extracted from the five structural layers of *C. zebra* shells, showing ^{118}Sn.

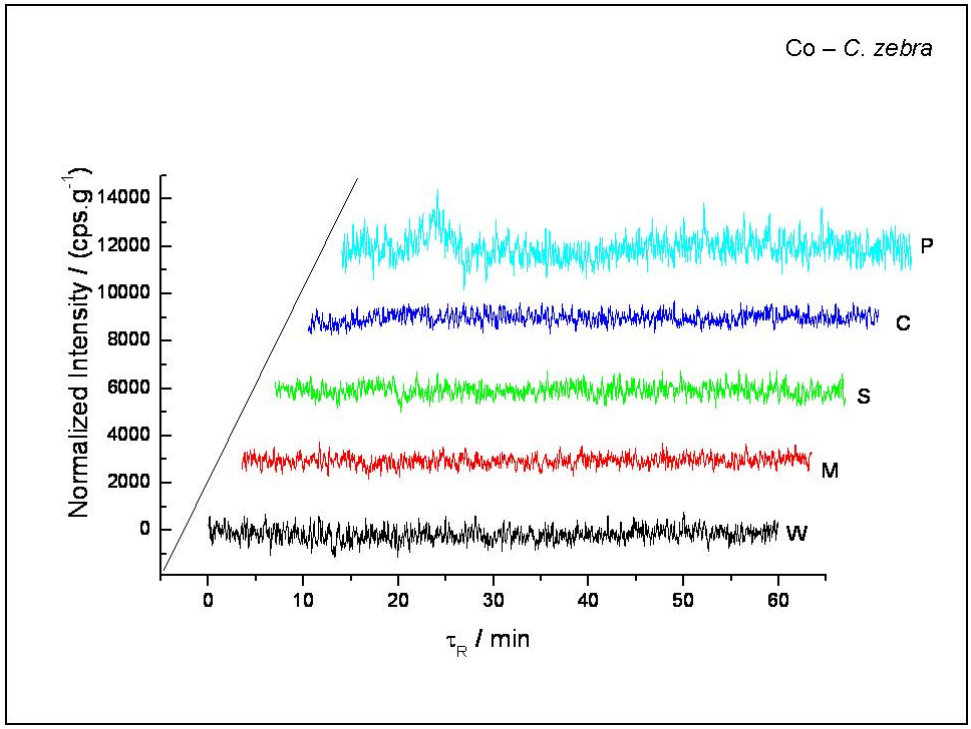

Figure 84: SE-HPLC-ICP-MS chromatogram of the SOM extracted from the five structural layers of *C. zebra* shells, showing ^{59}Co.

10.3 Summary of Results

A hyphenated on line technique, HPLC-ICP-MS, was used to investigate the presence of real complexes between the elements and the soluble organic matrix extracted from the three shells. The results show that not only Zn is bound to the organic phase of the shell, but also that this is the same case for the elements Cu, Ni, Co, Sr and Sn. These elements, which were not observed off line in the shell powder, could be yet observed thanks to the about one million concentration achieved through the SOM extraction. The organo-metallic complexes found between layers and shells (see Table 15), even if not substantial differences could be observed, are not equal, in good agreement with the concept of a complicated incorporation of the metals to the shell and the biological roll they may play.

Elements	***C. tigris***	***C. talpa***	***C. zebra***
Which present a correlation between INAA and Bradford Test	Co, Cr, Mn, Zn, Br, Sr	Co, Fe, Mn, Br	Co, Cr, Mn, Zn, Br, Sr
Which do not present a correlation between INAA and Bradford Test	Ca, Na, Fe	Ca, Na, Cr	Ca, Na, Fe
Which present a correlation between HPLC-UV and HPLC-ICP-MS	Co, Ni, Cu, Zn	Ni, Cu, Zn	Co, Ni, Cu, Zn, Sn

Table 15: Summary of the results obtained by coupled methodologies in *Cypraea* shells.

SECTION IV.
DISCUSSIONS AND CONLCUSIONS

11 Discussion and Conclusions

11.1. Micro and Nanostructure

Cypraea tigris, talpa and zebra shells were analysed for mineralogy and microstructure using spectroscopic as well as microscopic methods. Raman and XRD spectroscopy showed that aragonite is the mineral form of the biogenic calcium carbonate found in all three species. The shells were mechanically eroded and optically differentiable layers were obtained. In case of *C. tigris* and *zebra*, the shell is composed of six layers. In this work, they were named as:

1-“Periostracum”: the most outer layer.
2- “Colours”: the one where the pigments are deposited homogeneously or in spots
3- “Stripes”: where not more as two colours are found (generally white and brown), deposited as stripes or zig-zag.
4- “Magenta”: a thick magenta or dark brown layer.
5- “’White”: a white talk layer.
6-“Nacre” or “Mother Pearl”: the innermost layer.
In the case of *C. talpa* shells the magenta layer was not present.

The different layers have shown under FESEM and CLSM different structures. The periostracum, a transparent smooth surface of 30 to 120μm thickness, presents a layered microstructure, of approximately 1μm thickness. Under higher magnifications and different etching treatments, these layers have been identified as about 50-nm conjuncts of spheres. These latter are of about 5-10nm size. The etching with protease during 24 h has shown to attack the inter-spheres walls but not the spheres self.

The coloured and white layers have a prismatic structure, of about 20 μm × 120 μm. A crossed lamellar structure was found in stripes and magenta layers. The lamellae of the first order have variable length and thickness, this last ranging between 10 μm and 30 μm. Adjacent lamellae have an angle of 60º in between. Each prism and lamella is composed of a fine structure revelled after fracture, polishing or etching treatments. The second order structure may be called sheets in the micrometer range, composed of third order prisms of

about 4 μm × 200 nm. These prisms may be bound together with organic material and organic bridges, indicated after protease and etching treatments. The nanostructure of the third order units was this time also spherical agglomerations of about 5-10nm, similar to that observed for the periostracum.

Raman spectroscopy has shown to be a useful tool to identify mineral as well as organic components present in the shell. Eleven conjugated double bound carotenoid chains are present in the firsts 40 μm of the pigmented layer prisms. All three shell families have shown the same peaks, may be the same pigment organic material. Magenta layer and in some cases the lasts μm of the periostracum have also shown carotenoid characteristic peaks, at much more lower intensities in comparison to the coloured layer.

Under CLSM in fluorescence imaging the periostracum presents a fluorescence signal. This fluorescence is also observed as a maximum in the periostracum Raman spectrum. The same occurs only in nacre and in border prisms, but there at very low intensities and is not observed with Raman spectroscopy. This effect may highlight the organic material presents in periostracum, nacre and interprismatic walls. Nevertheless, no hints to this matrix were found in the spectroscopic methods used. Because the organic matrix is found at very low concentrations, an extraction and purification process, and other methodologies are needed for further analysis.

11.2. Organic Matrix

An organic matrix extraction process was developed and optimized for *Cypraea* shells. Two different processes were evaluated: a soft demineralization using a buffered system and a mild acid attack. Different purification, concentration and conservation methods were compared and tested for the treatment of big and small amounts of sample, and the whole process was optimized to extract the soluble organic matrix of 1 g of powdered shell. Soluble and insoluble organic matrices could be obtained. Both processes have finally shown to separate the organic matrix of the mineral phase with approximately the same recovery. The system HCl has been chosen for further analysis because it presents lower interferences with the used spectroscopic methods.

The organic matrix present in the different shell layers of *Cypraea tigris*, *talpa* and *zebra* shells was separated successfully from the mineralized structure using HCl 15 % as

demineralization agent. The proteins present in the soluble matrices were studied for their protein concentration and characterized by size using diverse methods. The SOM accounts in average for the 0.05% of the shell weight. The three species have shown to be more organic in the outside of the shell, presenting a decreasing profile to the inside. The SEC shows that the SOM extracted from the periostracum is the most organic abundant layer, in agreement with the results of the UV measurements and the Bradford tests. In second place stays the colored layer, and the organic peaks observed for the rest of the layers disappears to the inside of the shell. The striped layer has shown to be the most inorganic one. In average for the three shells, about 300ppm, 40ppm, and 10ppm are the concentration of the material *Coomasie brilliant blue* positive in the periostracum, the colored and the rest of the layers respectively.

The matrices could be analyzed with UV, SEC and GE. Even they have not shown to be the same, they did not differ substantially. The separation by GE and SE-HPLC has shown that the main organic material has a continuum mass between 80kDa and 10kDa, present as a positive silver stained band in the GE and as a broad peak in the SEC. Other spots could be detected by GE as dark zones in the bands, in good agreement with the structure observed for the SEC peak (well observable only in the periostracum and the colored layers). Between layers of the same shell, not only the quantity of the proteins, but also the structure of the SOM has shown to change from one layer to the next. These results are in agreement with the hypothesis that the SOM helps in the bio-construction of the shell and therefore must show different constitution in order to produce the different types of structures and interfaces between the layers.

The techniques used were validated comparing the results obtained by one technique to the results from another technique. The size determination, comparing SE-HPLC-UV with GE has shown excellent accordance between both techniques. For the protein quantity, Bradford Tests, UV analysis and HPLC-UV spectra, normalized to the intensities found in the periostracum layer, have shown to differ no more than 10%. These comparisons between the results obtained with different measurements proved indirectly that the methodologies and techniques used were correctly applied, and that the conclusions are therefore reliable.

11.3. Elemental Analysis

The optically differentiable shell layers of *Cypraea tigris*, *talpa* and *zebra* snails were carefully powdered using a diamond micro milling cutter and analyzed for their elemental contents. The presence of biologically relevant trace metals (e.g. Mn, Co, Fe, Zn, Cr) and main structural elements (e.g. Ca, Na, Sr) has been investigated by INAA and Microprobe as detection tool. These data were related to the microstructure of the shell. The element content per layer was compared between the three specimens analyzed. Structural elements are distributed homogeneously and about the same absolute elemental concentrations were found for the three species. In agreement with the observations of other authors, higher quantities of the elements studied were found in the periostracum and in those layers where pigments are observable.

About the techniques used, INAA seemed to be more favorable than Microprobe analysis for detecting trace elements in the high Ca content environment of *Cypraea* shells. Nevertheless some elements can not be optimized for INAA. For example, if the half life time is shorter than 15 minutes, the big background of the main elements Ca, Sr, Na, Cl, Mn and Br make it impossible to detect such elements at the low given concentrations, as is the case for Mg and Al. Elements like sulfur or phosphor that have only activable isotopes without gamma emission (^{35}S, ^{32}P) or with a very short half life (^{37}S) can not be detected by INAA in *Cypraea* shell samples.

The concentrations found in *Cypraea tigris* shells for the structural elements Ca, Sr, Na, Cl and Si, are in accordance between both methods used (INAA and Microprobe), and also between the concentrations observed for other gastropods by different authors. The elements Ca and Na have demonstrated to be homogeneously distributed in the shells, not depending on the structure or characteristics of the layers. The concentrations found by INAA between the three species studied coincide in the interval of uncertainty.

For the element Sr, *zebra*, *talpa* and *tigris* shells have shown higher concentrations in the periostracum and the colored layers, than in the rest of the shell, may be indicating an incorporation by diffusion in the most external layers or another type of association of this element, than the simple Ca replacing in the aragonite structure. About Sr other authors have observed correlations between Sr, Mg and Ba in bivalve shells. This behaviour could not be explained in their works by seasonal variation of the elements in see water, and they concluded that their results hint to a complex incorporation of Sr to the shell, perhaps

indicating association to the organic matrix (Lazareth et al., 2003; Putten et al., 2000). Nevertheless no correlations are found to our knowledge even in the periostracum or the pigmented layer. Our results are in agreement not only to the hypothesis of a complex incorporation of Sr to the shells but also hint to a layer dependent incorporation.

Trace elements found in *Cypraea* shells were Br, Mn, Co, Cr, Fe and Zn, in concentrations from 0.05 ppm to 1000 ppm, element, layer and shell species dependent. Also rare earths Eu, Ta and La were identified, but not quantified. Mn and Fe were already reported in other *Cypraea* specimens at concentrations around 50 and 100 ppm respectively (Dauphin et al., 2003). It is in agreement with the results obtained for *zebra* and *tigris* shells, although for *talpa* higher concentrations were found. In the case of bromine, no observations were found in literature with respect to its presence in relation to the ultrastructure of the shells. Nevertheless, ocean water has around 65 mg/l bromide concentration and it is concentrated in bromine species in marine animals and algae, which can be incorporated to the shell by the diet (Gribble, 1999).

The presence of Co, Cr and Zn is not reported in *Cypraea* species in literature but in other mussels and bivalves, where also As, Ba, Bi, Cd, Cu, Mo, Ni, Pb, Sc, Sb, and V were identified (Ravera et al., 2003; Lazareth et al., 2003). The elements Ni, Ba, Cu (1 h irradiations), As, Mo, Ag, Au, Sb, Sc, Rb, V, Ce, Cs, and Tb (6 h irradiations) and Sn, Cd, Hg and Se (24 h irradiations) were in all samples investigated and found under the detection limit of the INAA for these measurements.

Regarding the elemental mapping of the trace elements found in the three C*ypraea* species, the pigmented layers and the periostracum have shown higher presence of metals than the more internal layers or the white last layer, showing that these elements are not homogeneously distributed through the shell, intercalated in the aragonite structure, contrary for example to the case of Na, where no difference in the concentration with the depth profile was found. These data indicate a clear relationship between the element presence and the layer structure of the shell, indicating some kind of a probably more complicated interaction with the bioorganic matrix of the shell.

11.1 Elemental Environment

To elucidate the possible relation of the elements found in *Cypraea* shells to the bio-organic matrix, it was necessary to know to which environment belongs each element. For that, the results of the elemental analysis and the results of the organic matrix characterization were re-examined together. Interesting correlations were found between Co, Mn, Zn, Br and Sr determined traces and the protein content per layer, for the different animals. In contrast, the case of known structural elements as Ca and Na did not present any specific functionality with the organic material, in agreement with the hypothesis that those elements belong to the inorganic mineral phase.

A hyphenated on line technique, HPLC-ICP-MS, was use to investigate the metal-organic correlations observed before. These results have shown not only that a fraction of the Co, Mn, Zn and Sr found in the shells is really bound to the organic phase, but also that this is the same case for the elements Cu, Ni, and Sn. These elements, which were not observed by INAA in the shell powder, could now be observed thanks to the about one million concentration achieved through the SOM extraction.

Regarding manganese and zinc organic bound in the shells, correlation with organic material rich regions were observed for manganese in freshwater mussel shells by Siegele et al. (2001) and Nyström et al. (1995). Almeida et al. (1998) has found about 20% to 25% of Mn and Zn, in the prismatic layer in *Crassostrea gigas* shells, to be associated to the organic matrix. Higher amounts of manganese and iron were found by Swinehart et al. (1979) in bivalve periostracum, creating a defensive buffer against acid attack. The off line correlations between the element and the protein presence found for *Cypraea* snails are in accordance with these authors, indicating that manganese and zinc may bind to the organic material present in the biological shell matrix. On line measurements, in agreement with the off line data and the literature cited, show that Zn elutes together with an organic matrix environment and that Mn does not elute as an inorganic ion. For manganese it was no possible to determine on line the elemental environment, because Mn appears as a retarded broad peak in not calibrated ranges of the HPLC column.

The off line coupling between elemental composition and organic material data indicate a possible relationship between the Br, Cr and Sr and the protein depth profile. For Sr, on line correlations did show that no inorganic species were present in the eluting matrix, but could also not prove that Sr is bound to the proteins (because of the same reason as for Mn).

Elements Br and Cr, were under the detection limit of the HPLC-ICP-MS technique for the samples analyzed. This fact could mean on one hand that the elements did never belong to an organic environment or on the other hand that the complexes were destroyed in the organic matrix extraction process.

Comparing the organo-metallic interactions between layers of the same shell, an evolution and a change of the complexes have been observed. When passing from the outside to the inside of the shells, the metals complexed fractions of different masses. This observation, in addition to the fact already commented that the SOM changes between layers, are in agreement with the hypothesis that the SOM produces the different types of structures and interfaces of the shell. The different metal-organic species observed could be a simple effect of the matrix self development or may agree with the concept of a complicated incorporation of the metals to the shell and the biological and mineralogical role they may play in the specially properties observed in bio-minerals like their hardness, toughness, pigmentation or antifouling properties.

11.2 Antifouling

About the different antifouling properties observed between *talpa* and *zebra* snails, it was not found any clear response. Nevertheless, the fact that the *zebra* shell may present elements like Sn and Zn (known antibactericides) organically bound to the shell matrix, and *talpa* shells do not, could be in principle a difference. This is nothing but a hypothesis, because the organic matrix has shown to be not very ion selective (Cu, Ni, Zn, Co were sometimes together observed correlating with the same mass peaks) and if the elements are not bio-available for *talpa* snails in the sea environment, than could be a simple reason to explain why organo-tin or organo-zinc species could not be found in *talpa* shells.

11.3 The End and the Future

In this work new information was collected about three different shells of the family *Cypraedae*. The shells *C. tigris*, *talpa* and *zebra* were analyzed for elemental and organic composition, from the point of view of the interaction between elements and proteins. These data were in addition related to the mineral structure of the shell, treating the problem as a complete unit.

For the first time to our knowledge, the correlations observed before only from mapping studies, were observed directly by on line and off line techniques, and validated through inter-comparison tests between the different applied methods. The metals Cu, Ni, Co and Zn have shown to bind the soluble organic matrix extracted from *C. talpa*, *C. tigris* and *C. zebra* shells. The complexes are clearly related only to certain fractions of the organic matrix, and not to the whole soluble organic matrix observed. Some of these fractions bound two or three different metals. Within the conclusions of this work it was also demonstrated that these metal-organic complexes have a dynamic interaction with the layer microstructure: they change from a layer to the other, and are also not equal for the different species. In addition it was demonstrated that they are enough stable to survive the extraction process.

With these investigations and the conclusions achieved, the question for the speciation of metals in shells is open. Further studies could be directed in one hand to determine which metal species are present in the organo-metallic complexes observed. For example, continuing developing and optimizing coupled techniques as HPLC-ICP-MS, testing independent methodologies as LA-GE and also applying different techniques, where the shell samples could be measured without previous extraction of the OM, such as MALDI-TOF-MS-MS or μ-EXAFS. On the other hand, the further development of this research could be achieved through an interdisciplinary work, where the valuable collaboration of biologists, bio-geologists and biochemists could enrich the processes, methodologies and of course the conclusions and their implications.

Acknowledgments

The realization of this work was possible thanks to a fellowship of the ***Deutsche Forschungsgemeinschaft*** between October 2003 and 2005 as participant of the Graduated College for Elemental Speciation, and a fellowship of the ***BAföG*** between November 2005 and March 2006.

I want to thank the ***Interdisciplinary Research Training Group Program for Elemental Speciation***, for the possibility that give me to develop my work inside a multidisciplinary net of excellent groups, using the most novel techniques and instrumentations. I am also very grateful to all professors and colleagues of the GK for the many interesting and well organized ring courses, talks, seminars and workshops.

I want to thank the group of **"*Angewandte Struktur- und Mikroanalytik*"** from the Uni-Klinik Mainz, for their collaboration in the microscopy measurements. I want to thank the group of **"*Umweltgeochemie*"** from the research group of Prof. Dr. Kersten at Uni Mainz, for the collaboration with the ICP-MS measurements. I want to thank the people of the **"*Institut für Kernchemie"*** at Uni Mainz, especially to Dr. Trautmann for the many enriching theoretical discussions and Dr. Zauner and the people who work in the reactor, for the help with the irradiations and measurements. Many Thanks also to the group of **"*Cosmochemistry*"** from the research group of Prof. Dr. Hoppe at the Max Planck Institute, and especially to J. Huth, for his invaluable collaboration with the SEM measurements.

I want to thank Samara N. Jähnke, Victor V. Vilas, Daniel Kremer, Utta Limper, Valeria Loretti and Natalia Poperechna, for their help with instrumentation, materials and methods…even in the weekends! Many thanks to Dr. Sound and Dr. Pfeiffer for the correction and to the professors that read and evaluated this work.

Finally,

Muchas gracias al Profesor Baumann por su invaluable ayuda como docente y ser humano, por haberme ayudado a crecer professional y personalmente, y por haber creido en mi desde el comienzo.

Muchas gracias a mis nuevos amigos de Mainz: Samara y Bernd, Victor y Lidia, Andrea y Kai, Marta, Noelia, Helga y Axel, Valeria y Angelo, Maria…y si me olvido de alguno sepan disculpar…por haber por acercarme alegría, paciencia, diversión y felicicidad. Muchas gracias también a mis amigos de siempre, por estar siempre ahi!

Muchas gracias a mi familia y a mi novio, por su apoyo y amor incondicionados.

12 Bibliography

1. Almeida M.J. L-3,4-Dihydroxiphenylalanine (L-DOPA) secreted by oyster (Crassostrea gigas) mantle cells: functional aspects. Comparative Biochemistry and Physiology Part B 120 (1998) 769-713.

2. Almeida M.J., Temporal and local variations in biochemical composition of *Crassostrea gigas* shells. Journal of Sea Research 40 (1998) 233-249.

3. Azouzi H. Multielemental analysis of mussel samples by atomic absorptions spectrometry after room temperature sonication. J. Anal. Atom. Spec. Vol. 13 (1998) 533-538.

4. Balmain J. FTIR and XRD Analyses of Mineral and Organic Matrix during heating of mother of pearl (Nacre) from the shell of the mollusc *Pinctada maxima*. J. Biomed Mater Rs 48 (1999) 749-754.

5. Beckurz K.H., Neutron Physics, Springer Verlag, Berlin (1964).

6. Bédouet L., Soluble proteins of the nacre of giant oyster *Pinctada maxima* and of the abalone *Haliotis tuberculata*: extraction and partial analysis of nacre proteins. Comp. Biochem. Physiol. Part B 128 (2001) 389-400.

7. Belcher A.M. Control of crystal phase switching and orientation by soluble mollusc-shell proteins. Nature 381 (1996) 56-58.

8. Berman A. Intercalation of sea urchin proteins in calcite: study of a crystalline composite material. Science (1990)250-664.

9. Bøggild O.B. The shell structure of molluscs. D.Kgl Danske Vidensk. Selsk. Skrifter, Naturevidensk. Og Math. 9, (1930) 230-236.

10. Bollag D. M et al. Protein Methods. Ed Wyley-Liss. 1991.

11. Bowen C.E. Conchiline Protein in aragonite shells of mollusks. Comp Biochem Physiol. Vol115A Nº4 (1996) 269-275.

12. Bowerbank, J. S. On the structure of shells of molluscous and conchiferous animals, Trans. Microsc. Soc. London 1 (1844) 123-152.

13. Bradford, M., A rapid and sensitive method for the quantification of microgram quantities of protein utilizing the principle of dye-binding. Anal. Biochem. 72, (1976) 248-254

14. Blumer M. Organic Pigments: their long-term fate. Science 149 (1965) 722-726.

15. Carriker M. Ontogenic trends of elelments (Na to Sr) in prismatic shell of living *Cassostrea virginica* (Gmelin) grown in three ecologically dissimilar habitats for 28 weeks: a proton probe study. J. Exp. Marine Biol. and Ecol. 201 (1996) 87-135.

16. Cobabe E. Molecular and isotopic composition of lipids in bivalve shells: a new prospect of molecular palaeontology. Geochim. et Cosmochim. Acta Vol 59 Nº1 (1995) 87-95.

17. Cohen B.L. Concepts of Nuclear Physics, Mc Graw-Hill Book Company 1971.

18. Choi C.S A study of the correlation between organic matrices and nanocomposite materials in oyster shell formation. Biomaterials 21 (2000) 213-222.

19. Clark G.R. Organic matrix taxonomy in some molluscan shell microstructures. Palaeogeography, Palaeoclimatology, Palaeoecology 149 (1999) 305–312.

20. Cotton F.A. Advanced Inorganic Chemistry. Johnson Whyley and Sons. Fifth ed. 1988.

21. Cuif J.P. XANES mapping of organic sulphate in three scleractinian coral skeletons. Geochimica et Cosmochimica Acta, Vol. 67, No. 1 (2003) 75–83.

22. Das A. Metal speciation in solid matrices. Talanta 42 (1995) 1007-1030.

23. Drago R.S. Physical Methods in Chemistry. Ed W.B. Saunders Company.1977.

24. Dauphin Y. Structure and composition of the aragonitic crossed lamellar layers in six species of Bivalvia and Gastropoda. Copm Biochem and Phys. Part A 126 (2000) 367-377.

25. Dauphin Y. In situ chemical speciation of sulphur in calcitic biominerals and the simple prism concept. J. Structural Biology 142 (2003)272-280.

26. Dauphin Y. Comparison of the Soluble Organic Matrices of Healthy and Diseased Shells of *Pinctada margaritifera* (L.)and *Pecten maximus* L. (Mollusca, Bivalvia). Journal of Invertebrate Pathology 76 (2000) 49–55.

27. Dauphin Y. Comparison of the soluble matrices of the calcitic prismatic layer of *Pinna nobilis* (Mollusca, Bivalvia, Pteriomorpha). Comparative Biochemistry and Physiology Part A 132 (2002) 577–590.

28. Dauphin Y. Structures, organo-mineral compositions and diagenetic changes in biominerals. Current Opinion in Colloid & Interface Science 7 (2002) 133_138.

29. Dauphin Y. Microstructure, nanostructure and composition of *Concholepas concholepas*. Aquatic living resources 16 (2003) 95-103.

30. Dauphin Y. Soluble Organic Matrices of the Calcitic Prismatic Shell Layers of Two Pteriomorphid Bivalves (*Pinna Nobilis* and *Pinctada Margaritifera*) J. Biol. Chem. Vol. 278, No. 17, Issue of April 25, (2003) 15168–15177.

31. Ellman, G.L. (1959) Tissue sulfhydryl groups. Arch. Biochem. Biophys. 82, 70-7.

32. Foster A C (1994) Current antifouling technologies. Biofouling: Problems and Solutions. UNSW, Sydney, pp 44–48.

33. Franc A. Classe des Gastéropodes (Gastropoda Cuvier 1798) Généralités et définition. Zoologie V. Fasc. 3. Lehrbuch der Zoologie für Studierende von J. E. V. Boas. - 9. Aufl. - Jena : Fischer, 1922.

34. Gao H. Materials become insensitive to flaws at nanoscale: Lessons from nature. PNAS Vol. 100 Nº 10 (2003) 5597–56.

35. Gergerly A. Coordination chemistry of L-DOPA and related ligands. Met. Ions. Biol. Syst 9 (1979) 143-172.

36. Grégoire C. Structure of molluscan shell. Chemical Zoology Vol 7. Academic Press, New York, 45-102.

37. Gribble G.W. The diversity of naturally occurring organo-bromine compounds. Chem Soc. Rev. Vol 28 (1999) 335-346.

38. Harris D.C., Quantitative Chemical Analysis. Fifth Edition. W.H. Freeman and Company. New York. 1999.

39. Hollas J.M. Modern Spectroscopy. Second Edition. Ed JohnsonWiley and Sons, 1992.

40. Hung T.C. Trace elements in different species of mollusca, water and sediments from Taiwan coastal area. Chemosphere 44 (2001) 833-841.

41. Karlsruhe Nuklidkarte – 6 Auflage 1996. Institut für Radiochemie. FZK.

42. Kellner R. Analytical Chemistry, A modern Approach to Analytical Science. Second Edition. Ed Wiley VCH. 2004.

43. Knoll G.F. Methods in Nuclear Science, Springer Verlag. 1972.

44. Knoll G.F. "Radiation detection and measurement", J. Wiley, 1989.

45. Kono M. Molecular Mechanism of the Nacreous Layer Formation in *Pinctada maxima.* Biochemical and Biophysical Research Communications 269 (2000) 213–218

46. Kohlthoff J. Textbook of quantitative inorganic analysis. Ed Milland. 1990.

47. Krampitz, G. Biochemical studies on water-soluble proteins and related components of gastropod shells. In N. Watabe & K.M. Wilbur, Eds., The mechanism of mineralization in the invertebrates and plants, pp. 155-173, Univ. South Carolina Press, Columbia, USA (1976)

48. Lazareth C.E. High resolution trace element profiles in shells of the mangrove bivalve *Isognomon ephippium*: a record of environmental spatio-temporal variations?. (2003) Estuarine, Coastal and Shelf Science 57, 1103-1114.

49. Lowenstam H. Minerals formed by organisms. Sience (1981) 211 1126-1131.

50. Manigault P. Coquille des mollusques: structure et formation. Lehrbuch der Zoologie für Studierende von J. E. V. Boas. - 9. Aufl. - Jena : Fischer, 1823-1843.

51. Masuda F. Chemical composition of some modern marine plecypod shells. Sci. Rep. Inst. Geoscie. Univ. Tsukuba Sec B1 (1980) 163-177.

52. Marxen J. The organic shell matrix of the Fresh water snail *Biomphalaria glabrata*. Comp. Biochem. Physiol. 118B (1997) 23-33.

53. Marxen J. Calcium binding constituents of the organic shell matrix from the freshwater snail *Biomphalaria glabrata* Comparative Biochemistry and Physiology Part B 127 (2000) 235–242.

54. Marxen J. Early mineralization in Biomphalaria glabrata: Microscopic and Structural resuts. J. Moll. Stud. 69 (2003) 113–121.

55. Marxen J. The major soluble 19.6 kDa protein of the organic shell matrix of the freshwater snail Biomphalaria glabrata is an N-glycosylated dermatopontin. Biochimica et Biophysica Acta 1650 (2003) 92– 98.

56. Marin F. Large Scale Fractionation of molluscan shell matrix: Protein Expression and Purification 23 (2001)175-179.

57. Mai K. Effects of dietary zinc on the shell biomineralization in abalone Haliotis discus hannai Ino. J Experimental marine biology and ecology. 283 (2003) 51-62.

58. Masuda F. Masuda, Chemical composition of some modern marine pelecypod shells. Sci. Rept. Inst. Geosc. Univ. Tsukuba B 1 (1980) 163–177.

59. Meenakshi V. R. The chemical compistion of the periostracum of the molluscan shell. Comp. biochem. Pysiol 1969, 29, 611-20.

60. Nakahara, H. An electron microscope study of the growing surface of nacre in two gastropod species, *Turbo cornutus* and *Tegula pfeifferi*.. Venus, Jap. J. Malac. 38 (1979) 205-211.

61. Nakahara, H. Fine structure and amino acid composition of the organic 'envelope' in the prismatic layer of some bivalve shells. Venus Jpn. J. Malacol. 39, (1980) 167–177.

62. Narasimhulu K.V. EPR and IR spectral studies of sea water mussel Mytilus conradinus shells. Spectrochimica Acta Part A 56 2000, 1345-1353.

63. Nyström U., Nuclear Instr. and Meth. B 104 (1995) 612.

64. Putten E.V. High resolution distribution of trace elements in the calcite shell layer of modern Mytilus edulis: Environmental and biological controls. (2000) Geochimica et Cosmochimica Acta, Vol 64, Nº 67, 997-1011.

65. Raz S., The transient phase of amourphous calcium carbonate in sea urchin larval spicules: the involvement of proteins and Mg Ions in its formation and stabilization. Advanced Functional Materials Nº13 (2003) 480-486.

66. Samata, T. Ca-binding glycoproteins in molluscan shell with different types of ultrastructure. *The Veliger*, 33 (1990) 191-201.

67. Sewell P.A. et al. Chromatographic Separations. Analytical Chemistry by Open Learning. Ed. Johnson Wiley and Sons. 1987.

68. Siegele R. Manganese profiles in fresh water mussel shells. Nuclear Instruments and Methods in Physics Research B 181 (2001) 593-597.

69. Smith B.L. Molecular mechanistic origin of the toughness of natural adhesives, fibers and composites. Nature 399 (1999) 761-763.

70. Swann C.P. Preferential manganese accumulation in dreissenid byssal threads. Comparative Biochemistry and Physiology Part B (1998) N119 755-759

71. Swinehart J.H. Iron and Manganese deposition in the periostraca of several bivalve molluscs. Biol. Bull (1979) 156 369-381.

72. Soldati A.L. Determinación de trazas de meltilmercurio en matriz biológica: Extracción Química y Cuantificación mediante INAA. Tesis de Ingenieria. INIS 2002 Vol 33 Nº35.

73. Thakur N.L. Studies on some bioactivity aspects of selected marine organisms. Doctoral Thesis. National Institute of Oceanography. June 2001.

74. Vasin S.L. The role of proteins in the nucleation and formation of Ca-containing deposits on biomaterial surfaces. J Biomed Mater Res, 39 (1998) 491–497.

75. Wada, K. Studies on the mineralization of calcified tissue in molluscs VII. Histological and histochemical studies of organic matrices in shells. Bull. Natl. Pearl Res. Lab., 9 (1964) 1078-1086.

76. Wada, K. Initiation of mineralization in bivalve molluscs. In: Omori, M., Watabe, N. (Eds.), The Mechanisms of Biomineralization in Animals and Plants. Tokai Univ. Press, Tokyo, (1980) 79–92.

77. Wahl M. Non toxic protection against epibiosis. Biofouling (1998) Vol 12 (1-3) 205-226.

78. Wang J. Morphology and crystalline characterization of abalone shell and mimetic mineralization. Journal of crystal growth 252 (2003) 367-371.

79. Weiner S. Organization of extracellularly mineralized tissues: a comparative study of biological crystal growth. CRC Crit. Rev. Biochem. 20 4 (1986) 365-408.

80. Weiner S. Soluble protein of the organic matrix of mollusc shells: Potential template for shell formation. Science 190, (1975) 987–989

81. Weiner S. Aspartic acid-rich proteins: Major components of the soluble organic matrix mollusk shells. *Calcif. Tissue Int.*, 29 (1979) 163-167

82. Weiner S. Macromolecules in mollusk shell and their functions in biomineralization. Phil. Trans R. Soc. London B, 304 (1984) 425-434.

83. Weiner S. Acidic macromolecules of mineralized tissues: The controllers of crystal formation. Trends Biochem. Sci. 16 (1991) 252-256.

84. Weiss I.M. Purification and characterization of perlucin and perlustrin, two new proteins from the shell of the mollusc *Haliotis lae*m*igata*. Biochem. Biophys. Res. Commun. 267 (2000) 17-21.

85. Withnall R. Raman spectra of carotenoids in natural products. Spectrochimica Acta Part A 59 (2003) 2207-2212.

86. Yasoshima M. *Bradybaena similaris* (Ferrusac) Shell as a Biomonitor of Copper, Cadmium, and Zinc. Bull. Environ. Contam. Toxicol. Vol 66 (2001) 239–248

87. Yasoshima M. Speciation of heavy metals accumulated into land snails by XANES spectroscopy. Photon Factory Activity Report 2000 9A/1999G070.

88. Zhaolun Fang. Flow Injection Separation and Pre-concentration. VCH. Germany 1993.

89. Ziegler B. Einführung in die Paläontologie. Teil 2. Gastropoden. E Schweiterbartsche Verlagsbuchhandlung. Stuttgart 1991. 192-208.

Bibliography on line

1. Hawaiian Shells News. Home Page http://www.cowrys.org/

2. The apple snail website. Home page http://www.applesnail.net

3. Man and Mollusc website. Home page http://www.manandmollusc.net

4. Encyclopaedia Britannica On line. http://www.britannica.com

5. The Free Dictionary by Farlex. http://encyclopedia.thefreedictionary.com

6. Home Page Prof. Richard Palmer. Dept. of Biological Sciences University of Alberta Edmonton, Canada. http://www2.biology.ualberta.ca/palmer/palmer.html

7. Die lebende Welt der Weichtiere website. Home page http://www.weichtiere.at.

8. Mother Natures Beads. Beads and Shells written by Peter Francis, Jr. Home page http://www.nfobase.com/html/beads___sea_shells.html

9. Home Page Prof. Richard Fox. Biodiversity Lecture Outlines. Environmental Science 300. Department of Biology Lander University. http://www.lander.edu/rsfox/index.html

10. Home Page Dr. Felix Lorenz. Information on Cowries and other Seashells. www.cowries.info.

11. PIERCE Instructions Ellman´s Reagents. www.pierce.com

12. ANAMED Home Page. www.anamed-gele.com

13. SPEX Certiprep® LRT Home page. http://www.spexcertiprep.co.uk/

14. Uni Mainz - Angewandte Struktur- und Mikroanalytik Home Page. http://www.uni-mainz.de/FB/Medizin/ASMA/

15. Uni Mainz - Cosmochemistry Home page. http://www.mpch-mainz.mpg.de/~kosmo/index.html

16. Uni Mainz - Umweltgeochemie Home page. http://www.uni-mainz.de/FB/Geo/Geologie/Geochem/index.html

17. Uni Mainz - Kernchemie Home page. http://www.kernchemie.uni-mainz.de

APPENDIX

Appendix Contents

Index of Appendix Figures

Index of Appendix Tables

Appendix I: Calibrations

AII.1. External Calibration

Concentration Calculation

The external calibration is done by the measurement of a known quantity of a standard, as for example the certificate standard material. For that, the unknown sample (X) and standard (S) must be measured under the same conditions, and the concentration C_X can be calculated as:

$$C^X = C^S \frac{I^X}{I^S} \qquad \text{A-Eq. 1}$$

For INAA measurements, I represents the specific activity of the samples, for ICP-MS quantifications the intensity in cps. Finally, for Bradford and Ellmans tests, I is the UV intensity measured at the correspondents wavelengths.

Plotting the intensity I obtained for a certain standard set vs. the declared concentration of the element X in the standard, a linear function is obtained, whose experimental points can be fitted with a linear quadratic regression,

$$Y = a + bX \ . \qquad \text{A-Eq. 2}$$

Where a and b are the linear parameters adjusted. Using this curve, the intensity measured for unknown samples can be traduced to concentration, in the range calibrated, using

$$C^X = \frac{\left(I^X - a\right)}{b} \qquad \text{A-Eq. 3}$$

Reconstruction of the concentration for dissolved samples

When samples must be dissolved to be measured, the reconstruction of the concentration for the dry sample is done by

$$C^X\Big|_{sdry} = C^X\Big|_{diluted} \cdot \frac{m_{dry}}{m_{diluted}} \qquad \text{A-Eq. 4}$$

With a propagated error:

$$\Delta C^X\Big|_{dry} = C^X\Big|_{diluted} \cdot \sqrt{\left(\frac{\Delta C^X\Big|_{diluted}}{C^X\Big|_{diluted}}\right)^2 + \left(\frac{\Delta m_{dry}}{m_{dry}}\right)^2 + \left(\frac{\Delta m_{diluted}}{m_{diluted}}\right)^2} \qquad \text{A-Eq. 5}$$

AII.2. Internal Standard

Internal standard calibration was done in ICP-MS measurements. The addition of a known quantity of ^{103}Rh to each sample serves the purpose of controlling the stability and reproducibility of the measurements during the whole measuremet. Then, the intentisity used in Eq 1 can be given as the ratio between the measured intensity I in cps for determinate isotope of the unknown sample and the intensity found for the ^{103}Rh in the same sample:

$$I_x = \frac{I}{I_{^{103}Rh}} \qquad \text{A-Eq. 6}$$

In this way the measurements between samples and samples and standards are comparable, even if there were parameter shifts. The uncertainty propagated for the I_x is then,

$$\Delta I_x = I_x \cdot \sqrt{\left(\frac{\Delta I}{I}\right)^2 + \left(\frac{\Delta I_{103Rh}}{I_{103Rh}}\right)^2} \qquad \text{A-Eq. 7}$$

Appendix II: INAA Spectra Treatment

AII.1. Treatment of the Background

For the isotope *X*, which following its de-excitation emits gamma rays at energy *i*, the number of counts (gamma rays detected) Σ_i^X, plotted versus the energy, gives the characteristic spectra (A-Figure 1) used for INAA.

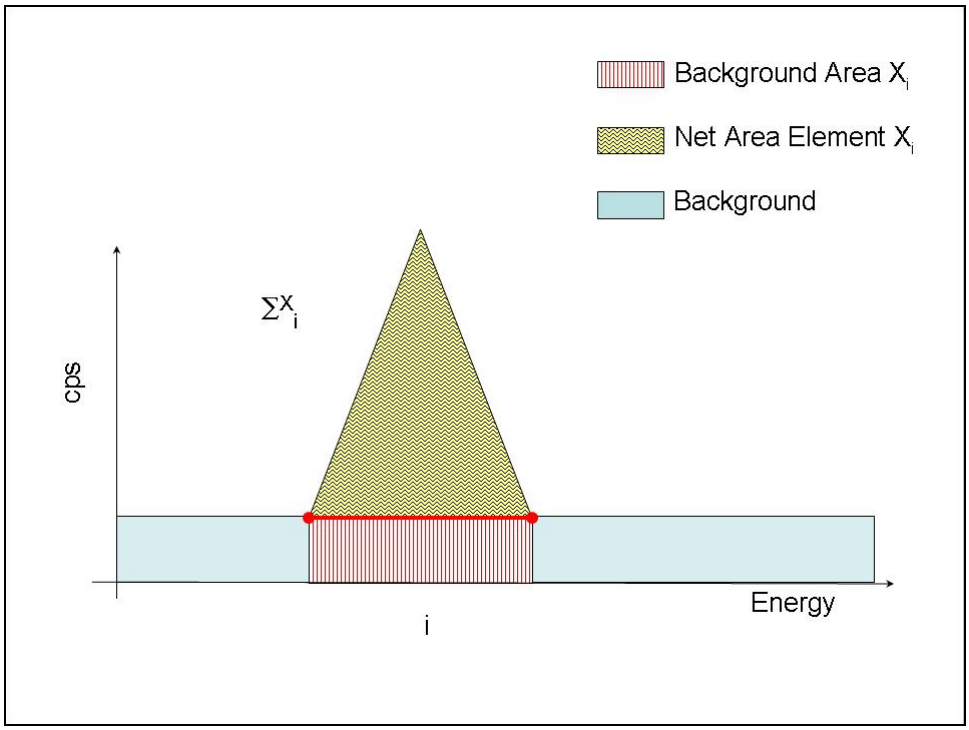

A-Figure 1: Schema of a photo-peak, showing the background treatment.

From the probability stand point of view, ratioactive decay corresponds to a Poision distribution. For a large number of events, the Poison distribution tends to a Normal distribution. The standard deviation SD corresponds then to:

$$SD \cong \sqrt{\Sigma_i^X} \qquad \text{A-Eq. 8}$$

If the background in the region of the peak is important, the dispersion of background counts must be taken into account like:

$$\Sigma_i^X = Area_{Total} - Area_{background}$$
$$SD^2_{\Sigma_i^X} = SD^2_{Area_{Total}} + SD^2_{Area_{background}}$$

A-Eq. 9

AII.2. Treatment of the Interferences

Some of the analysed peaks γ_i of an isotope *Y* could be coincident with peaks of other isotopes also present in the sample. In this case, the measured area Σ_i^Y must be corrected.

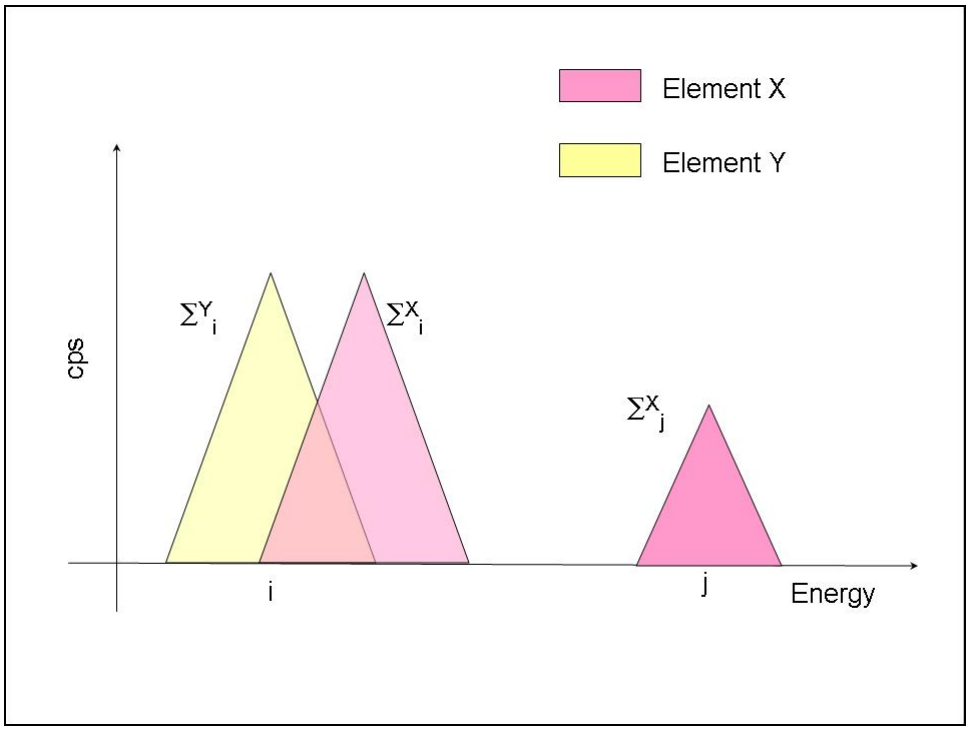

A-Figure 2: Schema of the correction for an interfered peak.

This operation is done in this way: If one isotope *X* has two emissions γ_{Xi} and γ_{Xj}, and γ_{Xi} interferes with a peak of interest γ_{Yi}, in a way that both peaks can not be resolved by the electronic, the corrected area of the incognita peak Σ_i^Y is calculated as:

$$\Sigma_i^X = \frac{\Sigma_j^X \cdot y_i^X \cdot \varepsilon_i^X}{y_j^X \cdot \varepsilon_j^X} \Rightarrow \Sigma_i^Y = \Sigma^X - \Sigma_i^X = \frac{\Sigma_j^X \cdot y_i^X \cdot \varepsilon_i^X}{y_j^X \cdot \varepsilon_j^X}$$

A-Eq. 10

Using A-Eq. 13 were corrected the interferences for all the elements studied.

Appendix III: HPLC Columns Treatment

AIII.1 Equilibration Procedure

The columns were equilibrated before the first use, following manufacturer instructions, by different washing steps of 20 times the volume of the column, eluting by acetonitrile, methanol and MilliQ water successively. The procedure for both types of columns is described in A-Table 1.

Column	*Solvent*	*Quantity*	*Flux*
RP	Acetonitrile 100%	200ml	0.5ml/min
	Methanol 100%		
	Isopropanol 100%		
	Heptane 100%		
	Water		
SEC	Acetonitrile 50%	200ml	1ml/min
	Methanol 50%		
	Water		

A-Table 1: Procedure for cleaning and equilibration of RPLC and SEC columns.

AIII.2 Washing Procedure

The columns were washed between different samples with one or two runs of MilliQ water as sample, eluted under the same condition as the samples; between batches the washing was done eluting a sample of 0.5 % SDS (SEC) or 100% acetonitrile (RP), followed by two MilliQ water samples, as washing runs to clean the column and the injection loop, before the next batch of samples. After use, the SEC column was washed eluting 0.5 % SDS for 10 min, followed by two to three hours of the mobile phase at a flux 1ml/min. For the RP column, acetonitrile 100 % was eluted for 30 minutes at 0.5 ml/min, followed by a run of methanol and a run of MilliQ water.

The columns were stored overnight in running buffer at a flux 0.3 ml/min and for longer periods in 0.5 % NaN_3 or 10 % methanol in water in the case of SEC columns and in 100 % acetonitrile in the case of RP columns.

To clean of proteins attached to the SEC column, SDS 0.5 % was eluted during one and a half hour and then the column was exhaustively cleaned with MilliQ water overnight. To clean attached ions, a sample of mercaptoethanol 1 % in water was run, followed by one or two runs of MilliQ water. A list of these washing processes is found in the A-Table 2.

Process	***RP Solvent /Sample***	***Volume / runs***	***SEC Solvent /Sample***	***Volume / runs***
Washing between samples	Acetonitrile 100%	15ml	MilliQ water sample	1 run
Washing between batches	Acetonitrile 100%	1run	SDS 0.5% sample	1 run
	Methanol 100%		MilliQ water sample	2 runs
	MilliQ water			
Washing of Proteins	Acetonitrile 100%	50ml	SDS 0.5%	100ml
			Mobile Phase	500ml
Washing of ions	Mercaptoethanol 1% sample	1 run	Mercaptoethanol 1% sample	1 run
	MilliQ water sample	2 run	MilliQ water sample	2 run
Long Storage	Acetonitrile 100%	50ml	NaN3 0.5%	100ml

A-Table 2: Procedure for washing columns

Appendix IV: SE-HPLC Column Characterization

As usual, the retention volume, as the product of the retention time of a peak in the chromatogram and the flow of the mobile phase, is used to characterize the separated peaks. This value can be also used for the RP columns. The dead volume V_o is the sum of the interstitial volume V_i and the pore volume V_p. The first represents the elution time of molecules that do not enter the pores (in the case of the SEC columns) or do not have any type of interaction with the material of the columns (in the case of the RP chromatography). The name V_p is given to the maximal retention time of the column, calculated for the minimal molecule size for molecules that enter in all pores.

The Interstitial Volume (V_i)

The SEC column was characterized for V_i with a 1 mg/ml Dextran® standard Merck (molecular mass: 1.750 kDa), using 20mM TRIS-HCl pH 7.4 as mobile phase, for a flux of 0.8ml/min, detecting the UV absorption at 205nm. Five measurements were averaged. The resulting V_i was (6.30 ± 0.04) ml. The same V_i was achieved using a Dextran® standard of 750 kDa.

The Dead Volume (V_0)

The SEC column was characterized for V_0 using a 1 mg/ml solution of thiourea (molecular mass: 77 Da), using 20mM TRIS-HCl pH 7.4 as mobile phase, for a flux of 0.8 ml/min. The absorption was detected at 270nm. Five measurements were averaged. The resulting V_0 was (13.40 ± 0.08) ml.

Mass Calibration of the SEC column

The retention time was correlated with the size of the eluting molecules using different proteins and amino acids at a concentration of 1 mg/ml in MilliQ water (See A-Table 3). For each calibration three measurements were averaged with a standard deviation <1 % for the retention time of the maximum of the peak.

Standard	*Mass*
IgG	150 kDa
Albumin, Bovine	66 kDa
Albumin, egg	45 kDa
Glyceraldehyde	36 kDa
C. Anhydrase	29 kDa
Trypsinogen	24 kDa
Trypsin Inhibitor	20.1 kDa
α-Lactalbumin	14.2 kDa
Citochrome C	12.3 kDa
Cobalamine	1.3 kDa
Triptophan	201 Da
L-Phenylalanine	165 Da
D-Alanine	120 Da
Thiourea	77 Da

A-Table 3: standards used for the column calibrations.

The detection was done simultaneously using an ESI-MS and UV detector. The UV absorption was detected at wavelengths 220nm and 254nm (protein dependent) to improve the detection. As it can be seen from A-Figure 3, there is a linear relation between the retention time and the logarithm of the molecular mass, i.e. size, of the proteins. The equation of the linear regression line can be used to determine the molecular mass of an unknown protein, measuring the retention time of the unknown peak, and applying an external calibration (See Appendix 1).

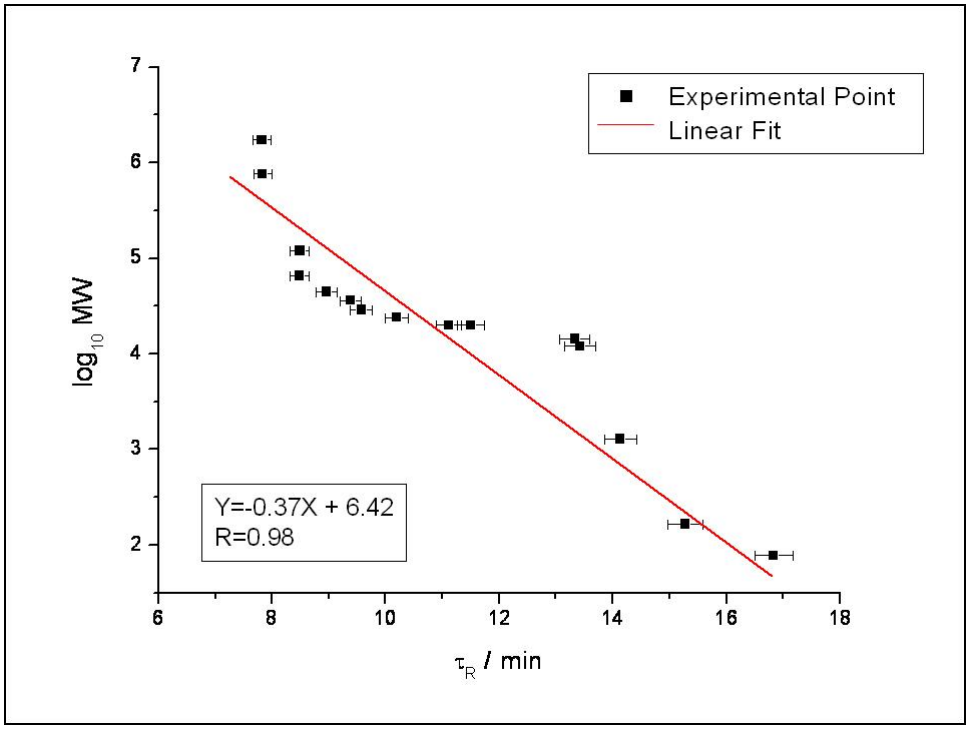

A-Figure 3: Calibration curve of the SEC column *BIOSEP S 2000*.Molecular mass vs. retention time for different proteins and amino acids.

SEC: Column: *BIOSEP S 2000*, Flux: 0.8 ml/min, Wavelength: 220 nm / 254 nm, Mobile Phase: Tris-HCl 20 mM pH 7.4, Injection loop: 100 µl.
SAMPLE: Different proteins in a concentration of 1mg/ml, with molar masses between 120 kDa and 77 Da.

Appendix V: Analysis and Comparison of INAA and ICP-MS

AV.1 Analysis of the INNA Technique

Uncertainty and Accuracy

The uncertainty of each concentration measured by INAA under the conditions specified in the experimental set up is isotope, gamma line, sample and concentration dependent. Nevertheless in average (See A-Figure 4) the relative error of each measurement could be approximated to be 10 % for concentrations bigger than 1 ppm, and around 15 % for lower concentrations (as for example the standard of brown bread).

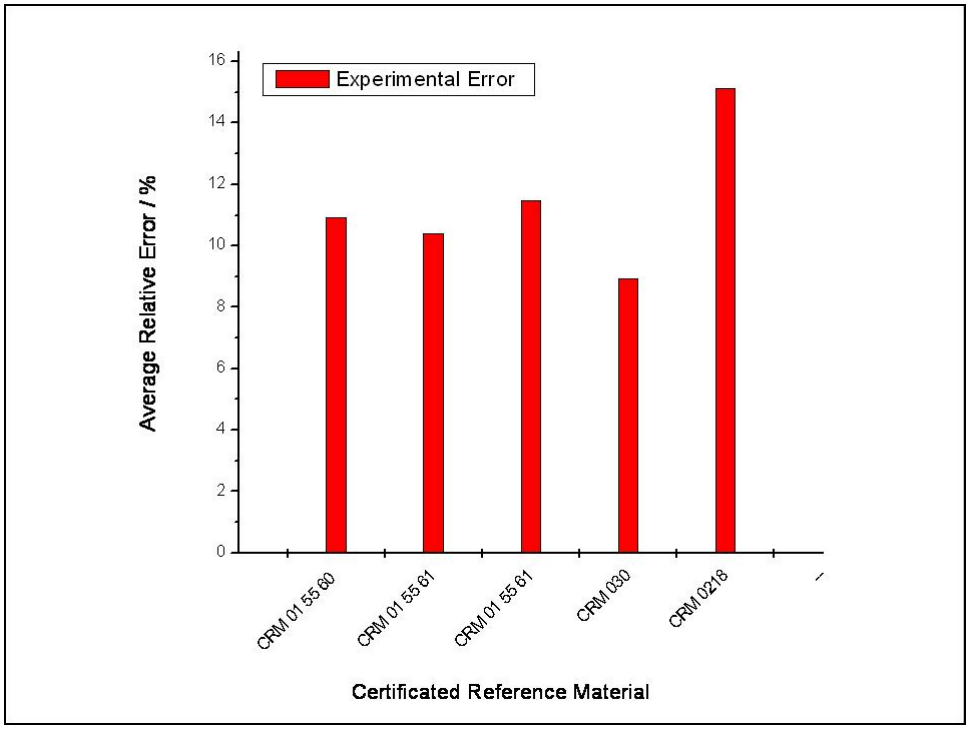

A-Figure 4: Average value, found for 5 different samples, of the relative error for the concentration found in long INAA measurements.

MATERIAL: 100 mg of different CRM. ISOTOPES: ^{60}Co, ^{56}Fe, ^{52}Cr.
INAA: Irradiation Time= 24 h; Decay Time= 20 d; Measurement Time= 8 h.

These values were calculated measuring the concentration of CRM standards for different elements, in a long irradiation. The relative error was averaged over all elements, isotopes and gamma emissions analyzed.

Accuracy for the multi-isotopic determination of an element

The accuracy of the determination of one element using two gamma emissions of the same isotope was evaluated by measuring the activity of ^{60}Co in the same batch of measurements with the gamma emissions at 1132keV and 1173keV. Both isotopes are free of interferences, and the correlation between the calculated concentrations is 1, as shown in A-Figure 5.

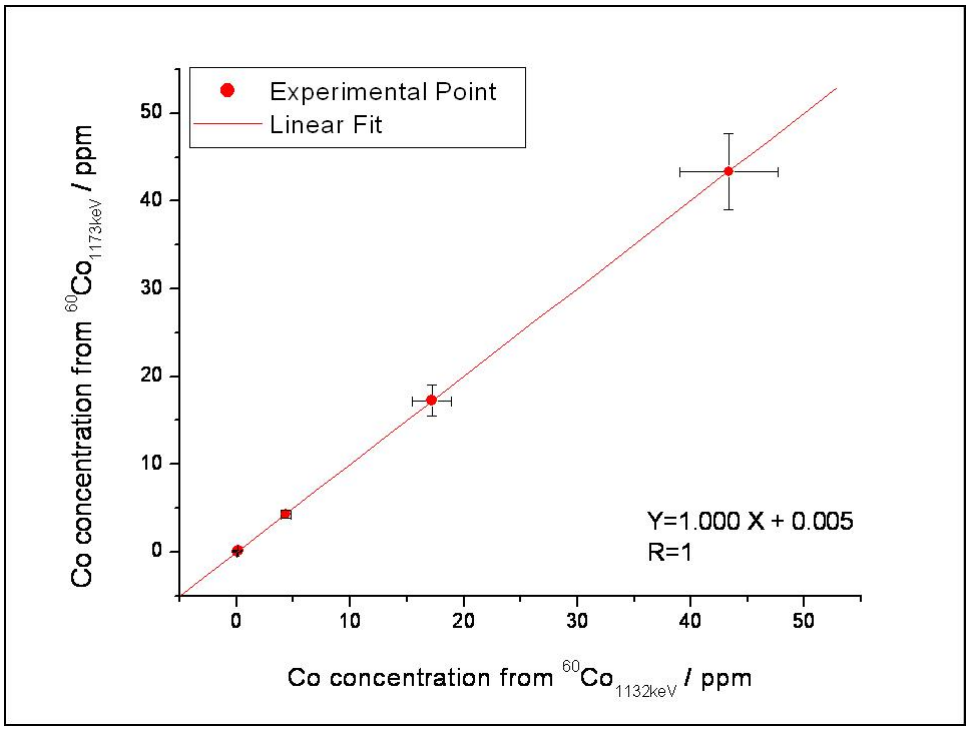

A-Figure 5: Correlation of the concentration of Co in CRM samples using two different gamma emissions from ^{60}Co for the calculation. The error bars that are not observed are smaller than the point size.

MATERIAL: 100 mg of different CRM. ISOTOPE: ^{60}C0, Gamma Line= 1332keV and 1173keV. INAA: Irradiation Time= 24 h; Decay Time=20 d; Measurement Time= 8 h.

Recovery of Certified Reference Material

To evaluate how distant is the measurement of the real value, five certificated reference materials were measured in the same conditions as the samples using a CSM external calibration. From each material only one sample was prepared and measured for some elements certified or indicated. The recovery as percent of the certificated value was calculated for the different elements, and is shown in A-Figure 6 and A-Figure 7 for a short and a long irradiation respectively.

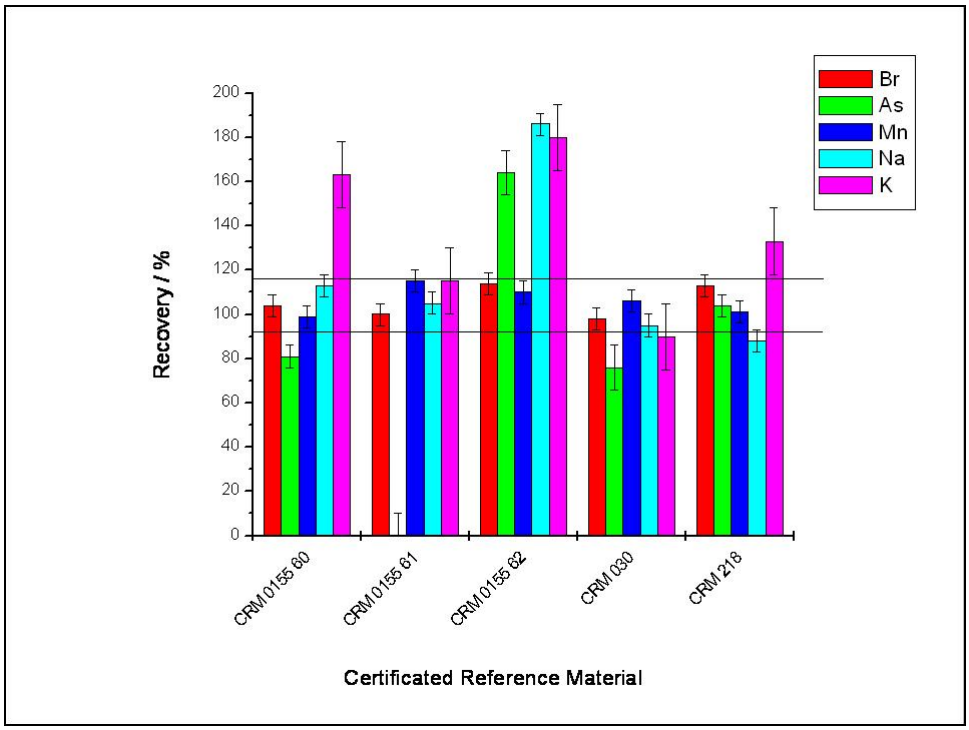

A-Figure 6: Recovery for different elements obtained for CRM by a short irradiation.

MATERIAL: 100 mg of different CRM. ISOTOPES: ^{82}Br, ^{59}As, ^{56}Mn, ^{24}Na, ^{42}K.
INAA: Irradiation Time= 1 h; Decay Time=1 h; Measurement Time= 1 h.

As it could be observed from these graphics, the concentration found for most elements analyzed is around the (100 ± 15) %. The variability of the INAA results is made up of factors, some of which can be estimated (for example counting and weighting errors, and others like geometrical variations due to sedimentation or thickness and packing density differences of the vials, which can not be quantified. Only few elements, as for example K, were not well recovered for all reference materials under the conditions chosen for the analysis. For the trace elements of major interest: Br, Mn, Co, Cr and Zn the resultant value was in good agreement with the certificated or indicated value.

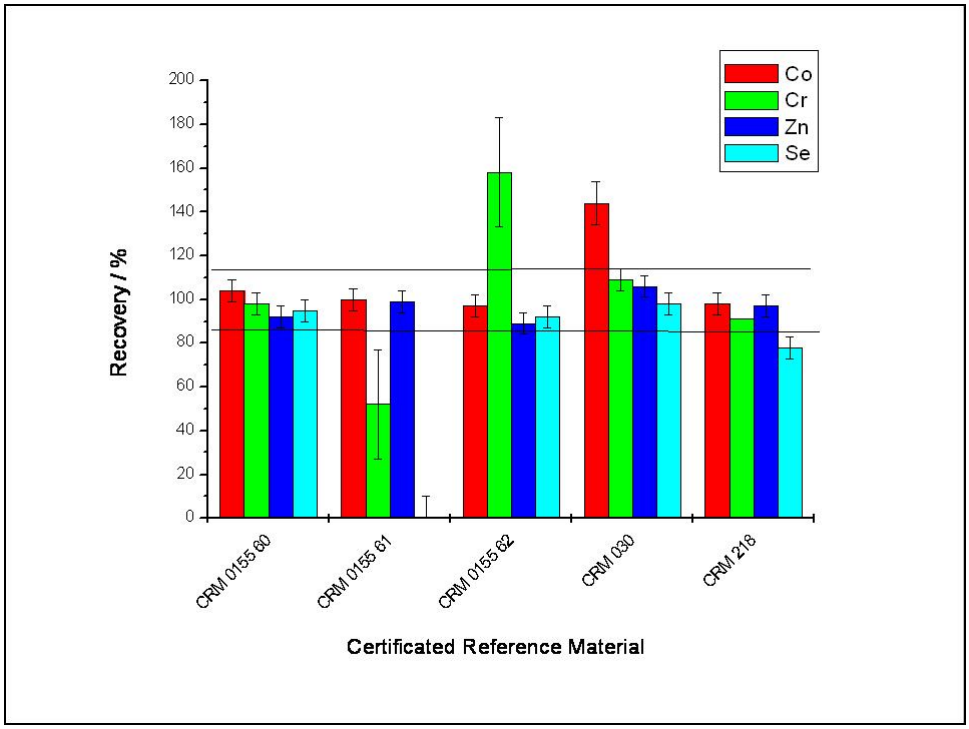

A-Figure 7: Recovery for different elements obtained for CRM by a long irradiation.

MATERIAL: 100 mg of different CRM. ISOTOPE: ^{60}C0, ^{52}Cr, ^{65}Zn, ^{75}Se.
INAA: Irradiation Time= 24 h; Decay Time=20 d; Measurement Time= 8 h.

AV.2 Analysis of the ICP-MS Technique

Uncertainty and Accuracy of the ICP-MS Analysis

The uncertainty of each concentration measured by ICP-MS is isotope, sample and concentration dependent, but in average takes a maximal value of 5 % for concentrations between 0 and 100 ppb and to of about ± 10 % for bigger concentrations. These values were calculated measuring the concentration of SRM standards between 0 and 250 ppb, five times for each isotope. The SD of the concentration value was calculated for the 5 measurements, and averaged over all isotopes measured (see A-Figure 8).

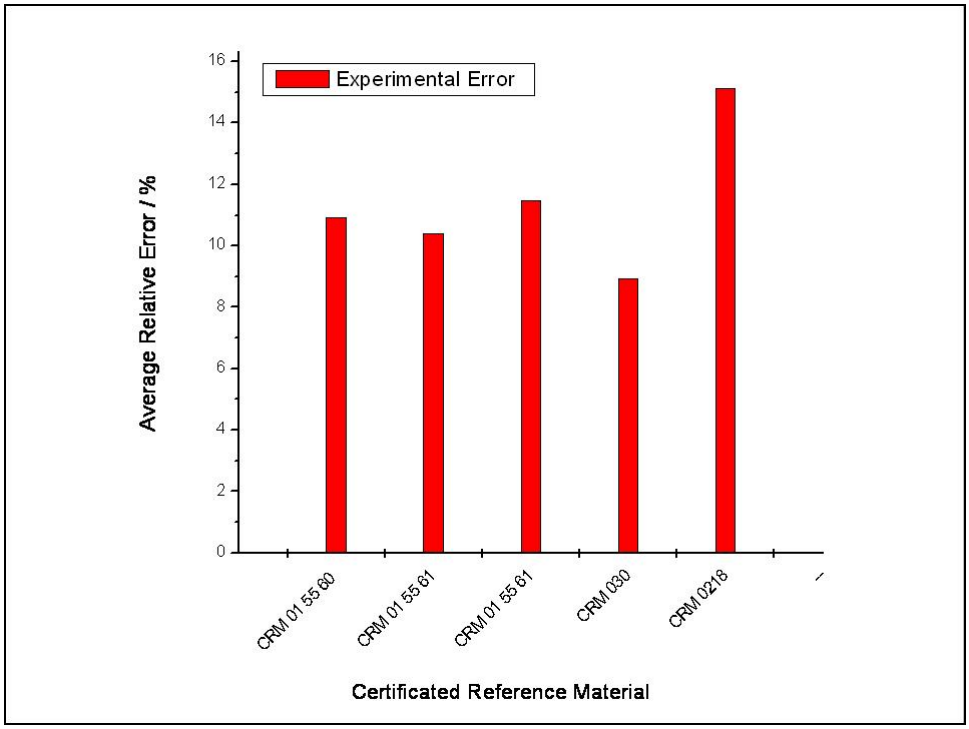

A-Figure 8: Average value, found for 15 different isotopes, of the Standard Deviation for the concentration found in 5 different measurements of each isotope.

MATERIAL: CERTIPURE® Standard calibration solution (Merck) at concentrations between 0 and 500 ppb, in HNO_3 2 %; internal standard ^{103}Rh 100 ppb.
ICP-MS:. 5 main runs averaged, 100 ms acquisition time for each element, with 5 sweeps per run.

Accuracy for the multi-isotopic determination of an element

The accuracy of the multi-isotopic determination of one element was evaluated by measuring Zn in the same batch of measurements with the isotopes ^{64}Zn and ^{65}Zn. Both isotopes are free of isobaric interferences, and the correlation between them is found very close to 1 (See A-Figure 9).

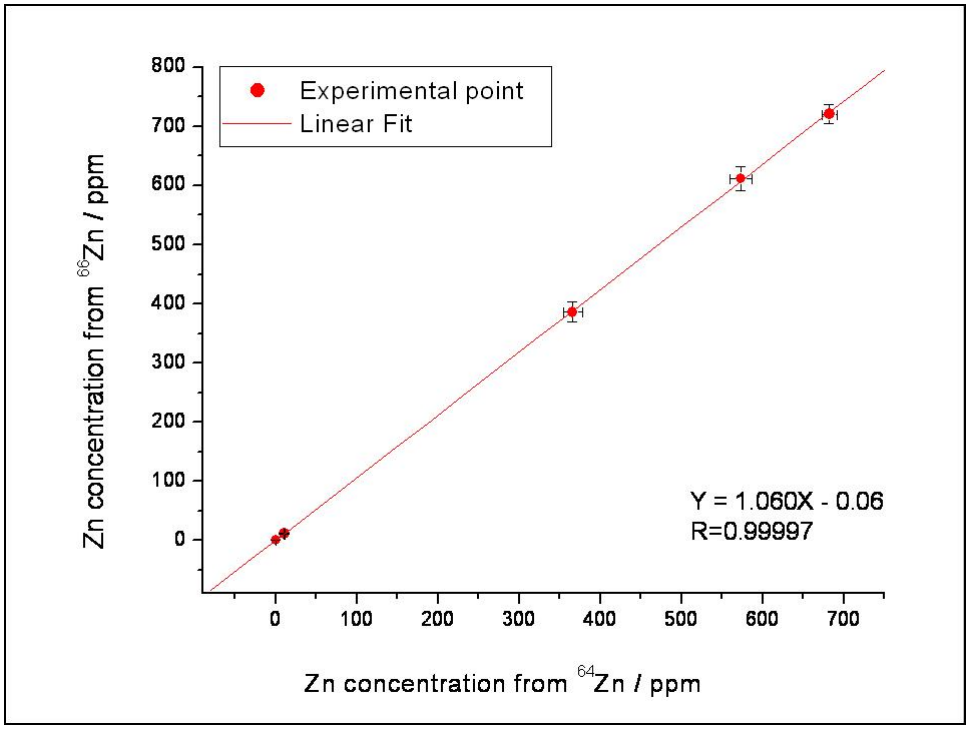

A-Figure 9: Correlation of the concentration of Zn in CRM samples using two different isotopes for the calculation.

MATERIAL: CERTIPURE® Standard calibration solution (Merck) at concentrations between 0 and 500 ppb, in HNO_3 2 %; internal standard ^{103}Rh 100 ppb.
ICP-MS:. 5 main runs averaged, 100 ms acquisition time for each element, with 5 sweeps per run.

Recovery of Certified Reference Material (CRM)

Five certificated reference materials (CRM[1]) of dry biological samples and sediments were dissolved as indicated for “solid samples” and measured by ICP-MS under the same conditions as the shells and calibrated with the external calibration curve. The concentration, recovery for the dry mass as percent of the given concentration is plotted in A-Figure 10 and A-Figure 11. The uncertainty was propagated from the concentration errors in the measurements and in the material.

[1] Commission of the European Communities- Community Bureau of Reference- Report EUR10997, EUR11850 and EUR8119.

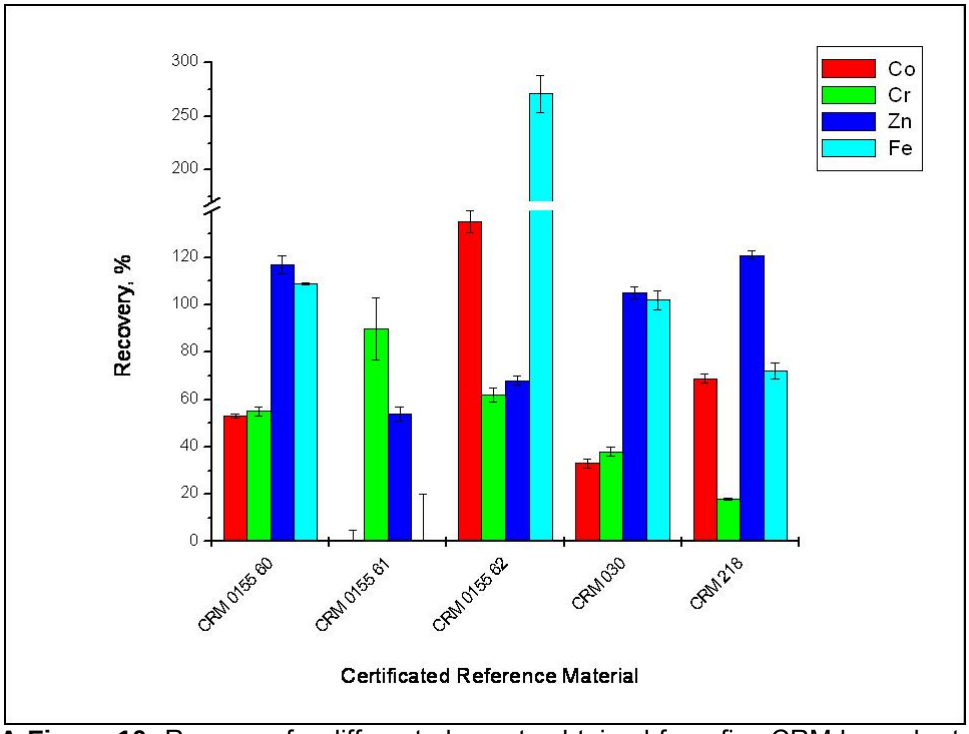

A-Figure 10: Recovery for different elements obtained from five CRM by a short irradiation.

MATERIAL: 100 mg of different CRM, treated as solid sample (see Chapter 2), internal standard ^{103}Rh 10 ppb.
ICP-MS PARAMETERS: 5 main runs averaged, 100 ms acquisition time for each element, with 5 sweeps per run.

As it can be observed from the latter and next figures for most elements measured the recovery was more or less about 50 %. This low recovery can be attributed to the sample preparation. In the case of shells, the matrix dissolves very well in each acid (i.e HCl : HNO_3) and only a very little portion of material (the insoluble organic matrix) remains insoluble. That was not the case for biological and sediment CRM matrices where a big amount of the initial sample was not dissolved with this method. Indeed, it for digestion of biological material much more strong processes are recommended in literature, microwave or sonically assisted digestions (Azouzi et. al, 2003).

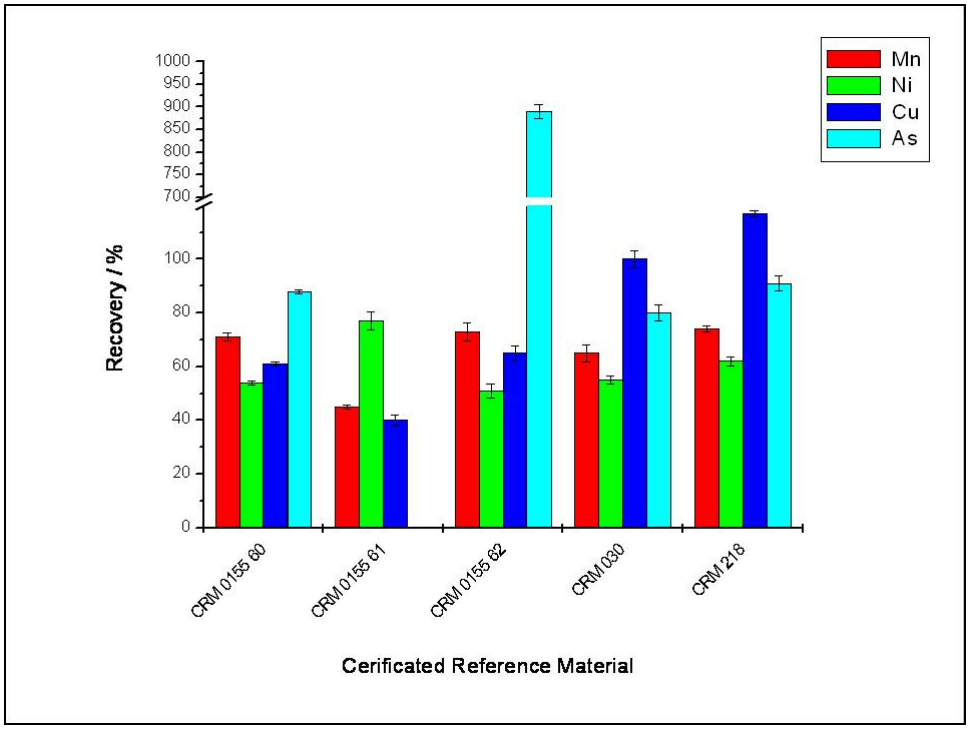

A-Figure 11: Recovery for different elements obtained from five CRM by a short and a long irradiation.

MATERIAL: 100 mg of different CRM, treated as solid sample (see Chapter 2), internal standard ^{103}Rh 10 ppb.
ICP-MS PARAMETERS: 5 main runs averaged, 100 ms acquisition time for each element, with 5 sweeps per run.

The concentration of iron and arsenic in CRM 015562 (*Olea europaea*) samples were found about much bigger than the certificated value. This extremely big deviation could be attributed to a contamination or unhomogenities in the sample preparation, or to interference in the measurement. Nevertheless this behaviour was not observed in the other samples.

AV.3 Comparison between both analytical techniques

INAA as well as ICP-MS were used as off-line techniques to determine trace elements in *cypraea* shells. The first one does not require any sample treatment and allows to measure trace as well as major elements together. The second method requires the dissolution of the sample and is only appropriate to measure trace and ultra trace elements. For INAA interferences caused by a high calcium enriched matrix can be overcome by optimizing the irradiation, decay and measurement times, to have the activity of ^{40}Ca as low as possible in comparison to the trace elements to be measure. For ICP-MS measurements, the presence

of this type of matrix creates not only isobaric interferences but also can damage the equipment if the concentration of the samples is not very diluted. This dilution of course diminishes the efficiency of detection for the trace elements which are in concentrations of five or six orders of magnitude lower than the major elements, with risk of contamination and loss of material in the preparation.

Interferences are also more problematic in ICP-MS as in INAA. The latter almost all interferences for the elements of interest can be calculated from other gamma emissions of the same interfering isotopes or sometimes can be avoided by optimization of the INAA parameters, as in the case of Na, optimizing the decay and irradiation times. In the case of ICP-MS, the best way to avoid the difficult isobaric interferences detection, measurement and calculation is to measure other isotopes of the same element, in case that the element is not mono-isotopic, and to prove the natural isotopic ratio between them.

The accuracy of both analyses, evaluated from the recovery of reference materials shows that for ICP-MS treated samples the recovery is around 60 %, and by INAA is around 100 %. The difference may be due to the fact that by INAA there is no sample pre-treatment. Nevertheless, from these results ICP-MS must not be sub-valuated as technique for trace element analysis in shells. It is to note that there is no commercially available shell material as CRM. Shell material dissolves very well in the solvents while the biological as well as the sediment CRM samples do not, and may require intense dissolution treatments as for example ultrasonic or microwave assisted digestion, which are not necessary for the shell material.

The values measured by INAA agree with the certificated values for CRM and SRM within ±15 % for almost all elements analyzed in concentrations bigger than 0.3 ppm. For concentrations lower than this value, the elements remain generally under the detection limit of the technique. For the ICP-MS measurements, the concentration limit is much more sensitive (i.e the calibration is made from 1 to 100 ppb), with a deviation lower as 5 % for SRM solutions. For CRM the deviation was generally bigger than 30 %, but this big dispersion was attributed to the preparation of the samples and not the measurement itself.
By ICP-MS highly dispersed data were obtained between different measurement days, and shift of the parameters were sometimes observed in long measurements, with the consequence of recalibration. These disadvantages were partially corrected by the use of an internal standard, which is not necessary in INAA.

As conclusion of the methodology analysis it was decided to use INAA as the main tool to quantify the main and trace elements of interest in *Cypraea* shell samples. Nevertheless the complication of the irradiations, the need of masses of approximately 150 mg and the practical impossibility to measure very large quantities of sample, makes ICP-MS a very useful and practical tool to evaluate all steps that have often been changed during the development of this research, such as determining the blanks of the extraction processes, the blanks of the different separation, the purification and concentration steps, or with the samples that are obtained in very low quantities, as for example the extracted proteins.

Appendix VI: Analysis and Comparison of HPLC and GE

AVI.1 Analysis of the HPLC-UV Technique

Limit of Detection for BSA

The detection limit of the coupled system HPLC-UV was studied with BSA, at different typical proteins absorptions: 220 nm, 254 nm and 280 nm. The first one has been found as the most sensitive wavelength to measure this protein. Standards of BSA in MilliQ water were prepared at different concentrations, between 10^{-2} μg/ml and 100 μg/ml. The protein content of the standards was verified with the Bradford test. The intensity of the maximum of the elution peak relative to the background level was plotted in A-Figure 12 against the concentration of the BSA in the sample.

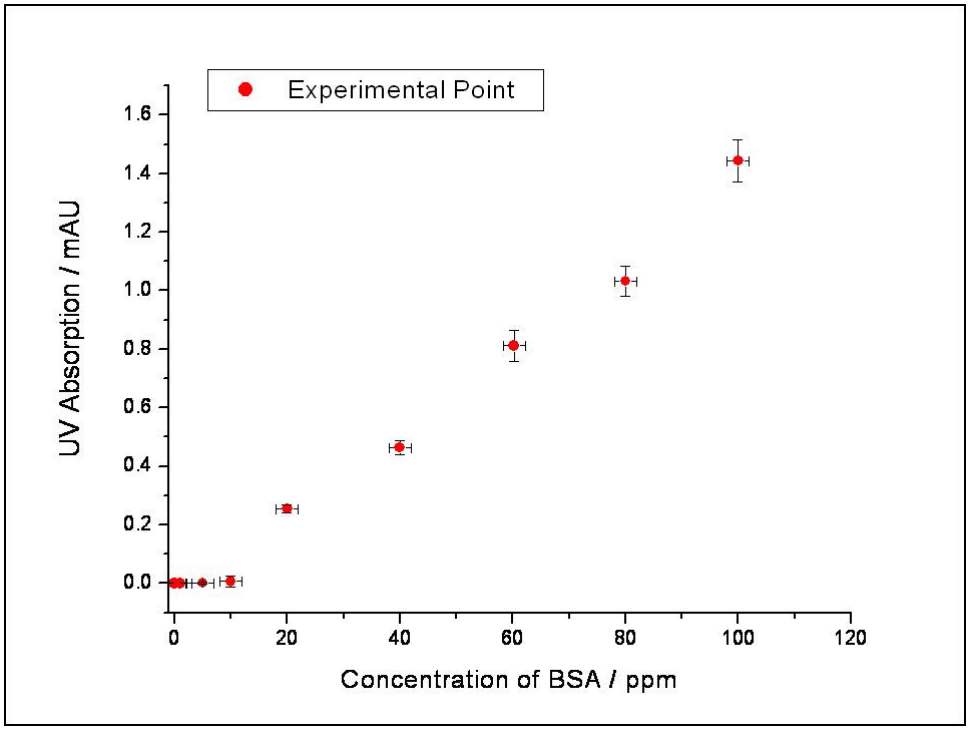

A-Figure 12: Detection limit for BSA with the BIOSEP column

HPLC UV: Column: *Biosep S2000*, Flux: 0.8 ml/min, Wavelength: 220 nm, Mobile Phase: Tris-HCl 20 mM, Injection Loop: 50 µl, Sample: BSA, Molar mass: 66kDa.

As showed in A-Figure 12, the detection limit found for BSA using the SEC column is around 20 µg/ml showing a linear relation to the concentration. This function is no longer linear for concentrations bigger than 1000 ppm (data not shown) and may indicate protein absorption on the column material, and non-linearity of the photometer.

Separation of a Standard Protein Mixture

The capacity to separate different proteins with the system HPLC using reverse phase or size exclusion techniques, by polarity or by size of the molecules respectively, was studied using a commercial protein cocktail mixture, Dalton®, at a concentration of 1mg/ml. From the seven proteins present in the cocktail, four peaks were separated with success by SEC with the *Biosep S 2000* column. The two first peaks, corresponding to 66kDa (a) and 45kDa (b) are only weakly observed.

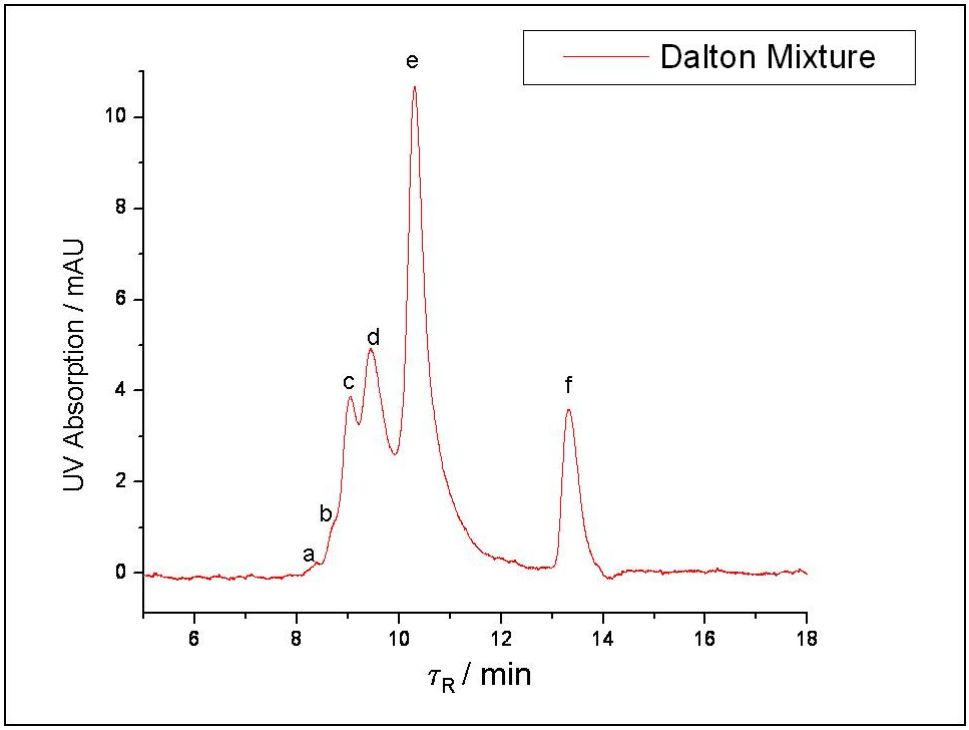

A-Figure 13: Absorption spectra at 220 nm of a mixture of proteins by SEC

HPLC UV: Column: *Biosep S2000*, Flux: 0.8 ml/min, Wavelength: 220 nm, Mobile Phase: Tris-HCl 20 mM, Injection Loop: 50 µl, Sample: Dalton cocktail mixture.

AVI.2 Analysis of the GE Technique

Limit of Detection for BSA

To evaluate the detection limit of both developing techniques used, BSA at different concentrations was prepared under reducing conditions and run as in the experimental method. The gel was developed using the *Coommasie blue* as well as the silver staining. Blank sample was MilliQ water.

As it can be observed by comparison of both gels (A-Figure 14), reduced BSA at a concentration 10ppm (250ng per spot) is good identified by *Coomasie Blue* staining. For the case of silver staining, the detection limit of reduced BSA is 1ppm (25 ng per spot). The apparition of the proteins coming from the very diluted (10ppm) standard in the silver stained gel but no in the *Coomasie Blue* stained one agrees once again with the previous result, showing low detection limit of this last technique, not only for BSA but also for other proteins.

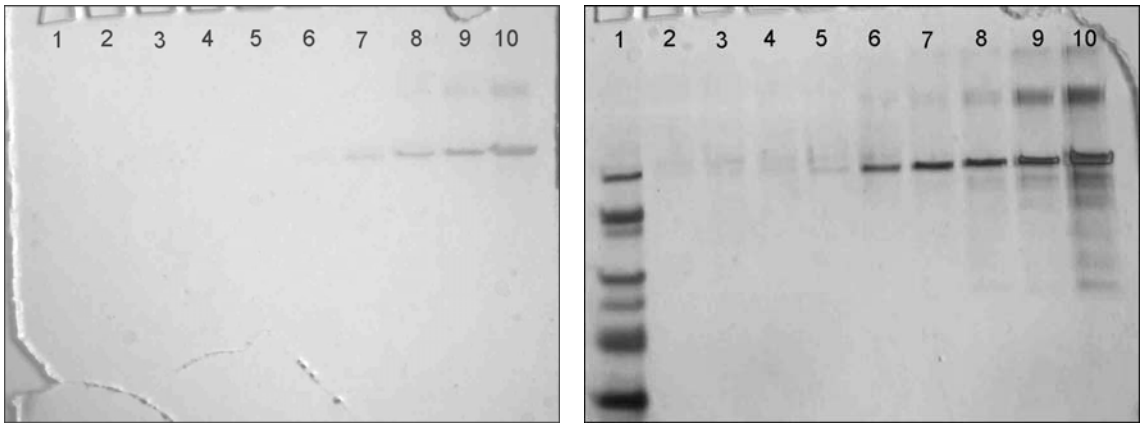

A-Figure 14: BSA Standard at different concentrations stained with *Coomasie Brillant Blue* (left) and with Silver staining (right). Line 1: Dalton® protein mixture in MilliQ water. Line 2: MilliQ water blank. Lines 3 to 10: BSA at concentrations of 0.1, 0.01, 1, 5, 10, 20, 40 and 100ppm respectively.

GE: Gel: Mops-TRIS-SDS 9%, Voltage: 200V, Current: 100 mA, Time: 40 min, Running Buffer: Mops-TRIS-SDS, Sample Buffer: Mops-TRIS-SDS, Reducing Agent: β-Mercaptoethanol, Sample: BSA and Dalton protein mix, Sample Quantity: 25 µl, Molar mass: 66kDa-14kDa.

Separation of a Standard Protein Mixture

To measure the protein separation achieved by GE under the conditions used, a DALTON® protein mixture cocktail from Sigma was prepared under reducing and non reducing conditions, and run as indicated in the experimental set up. The results are shown in the next figure. As already studied in the previous section, the gel in A-Figure 15 agrees with the fact that the silver staining is much more accurate as the *Coomasie Blue* for protein detection, inclusive for other proteins than BSA. In the case of *Coomasie Blue* only reduced proteins can be detected. However not all masses were stained. With the silver method all proteins were well stained, and this study shows that reduced proteins are clearly better separated than non reduced ones, highlighting the advantages of a reducing sample preparation. As conclusion, using the silver staining method on reduced samples, for the running conditions written in A-Figure 14, the separation and staining of the protein cocktail is well achieved.

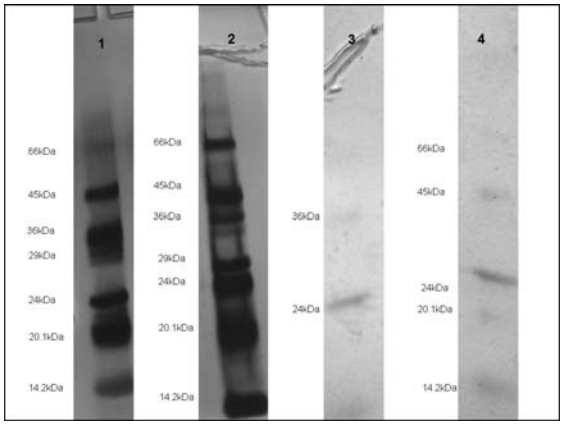

A-Figure 15: Standard protein mixture under reducing (2 and 4) and non reducing (1 and 3) conditions, stained with *silver staining* (1 and 2) and with *Coomasie Brillant Blue* (3 and 4). Same GE conditions as A-Figure 14.

AVI.3 Summary of Conditions

High Performance Liquid Chromatography and Gel Electrophoresis were chosen as separation techniques for the study of the shell organic matrix, in the range of 300kDa–70Da. The comparison of both techniques is comprised in A-Table 4:

Parameter	***HPLC (SE/RP)***	***Gel Electrophoresis***
Separation	Size / polarity	Size
Mass Range	300kDa-70Da	90kDa-70Da
Time per run	45min	35min
Additional requirements	no	Gel developing
Buffer	Tris-HCl 20mM	MOPS-Tris-SDS
Working pH	7.4	7
LD for BSA, ppm	20 ppm	1 ppm
Dalton Mixture 1mg/ml	4 peaks for 7 proteins	7 spots for 7 proteins

A-Table 4: Comparison of the two separation techniques used in this work.

Appendix VII: Interferences to the Bradford Test

AVII.1 The effect on the linearity

Standard samples of BSA were prepared in water as well as in AcH-buffer 15%. Four independent samples were measured at 595nm, and the result averaged. The calibration curve was fitted for both batch measurements (See A-Figure 16 and A-Figure 17).

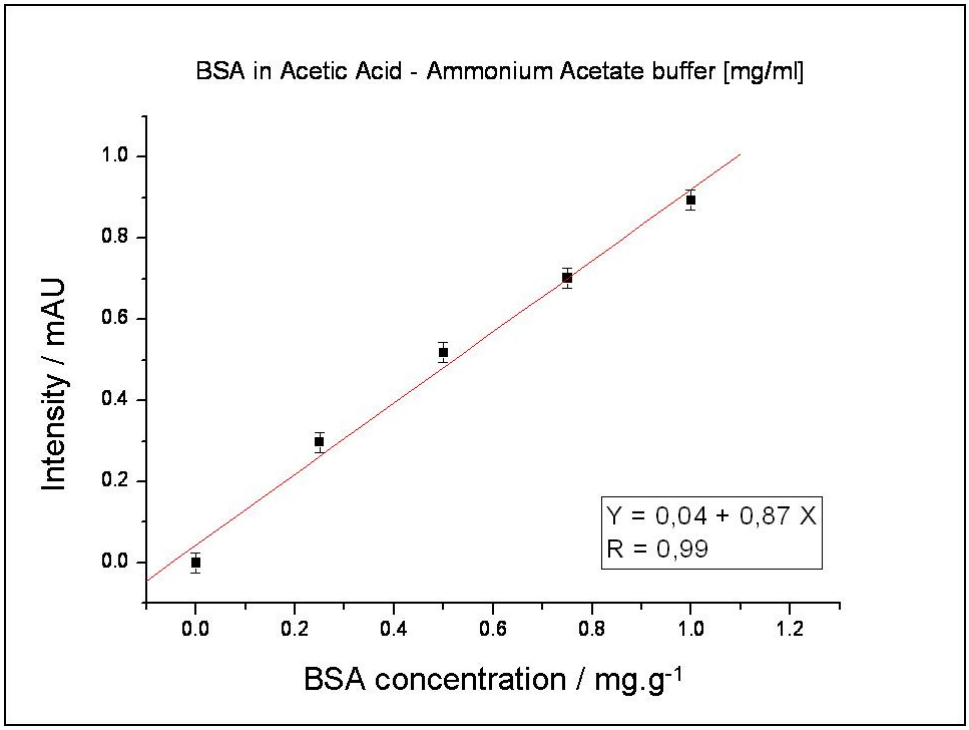

A-Figure 16: Bradford test linearity for a BSA sample prepared in AcH-buffer. Intensity at 595nm using as reference sample AcH-buffer 15%.

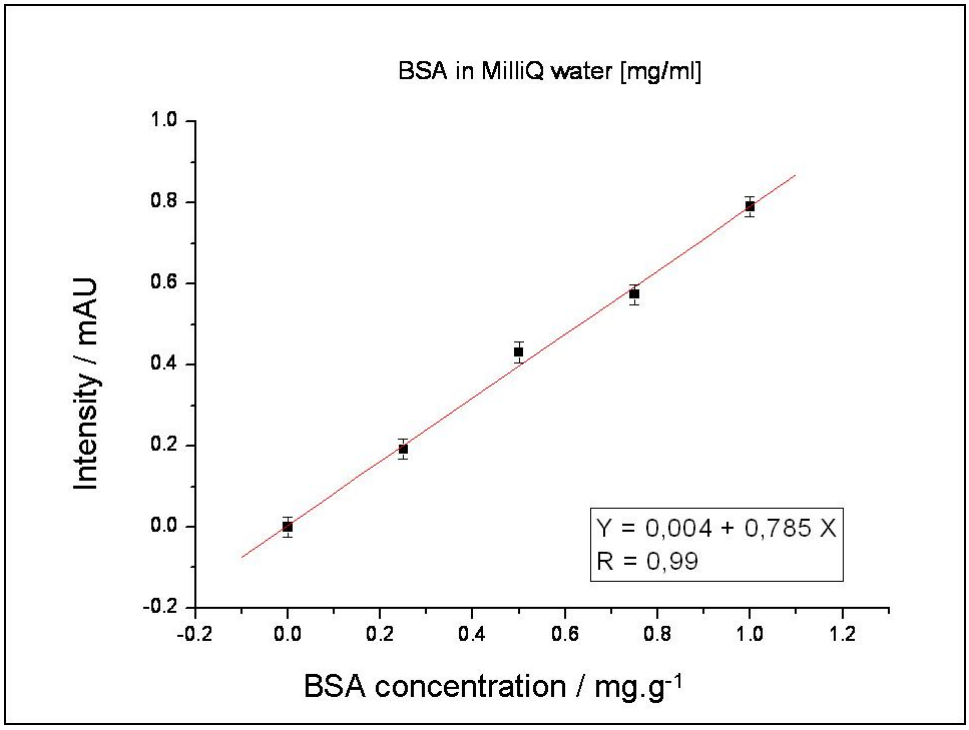

A-Figure 17: Bradford test linearity for a BSA sample prepared in MilliQ water. Intensity at 595nm using as reference sample MilliQ water.

As observed from both figures the effect of the buffer in which the sample is diluted does not affect the linearity of the methods (at these protein concentrations). Nevertheless the slope of the calibration curve is in this case larger for AcH-buffer than for water samples. The presence of not well removed acetic acid on one particular sample, will cause an interference on the intensity measured. The same was observed for example for HCl (data not shown), with the difference that in this case the slope is smaller than those obtained with water.

AVII.2 The effect on the absolute value

To study the effect of the concentration of the interfering substances on the test, different concentrated solutions of AcH-buffer, HCl, NaN_3 (used as antibiotic in the samples) and $CaCO_3$ were prepared. The samples were diluted in MilliQ water to obtain concentrations between 10% to 10^{-6} %, and the micro Bradford test applied (A-Figure 18). Three independent samples as well as three standard solutions were averaged. The error per sample, for the same sample (in/out + standard deviation) is <3%. The standard deviation of the three measurements remains <7%.

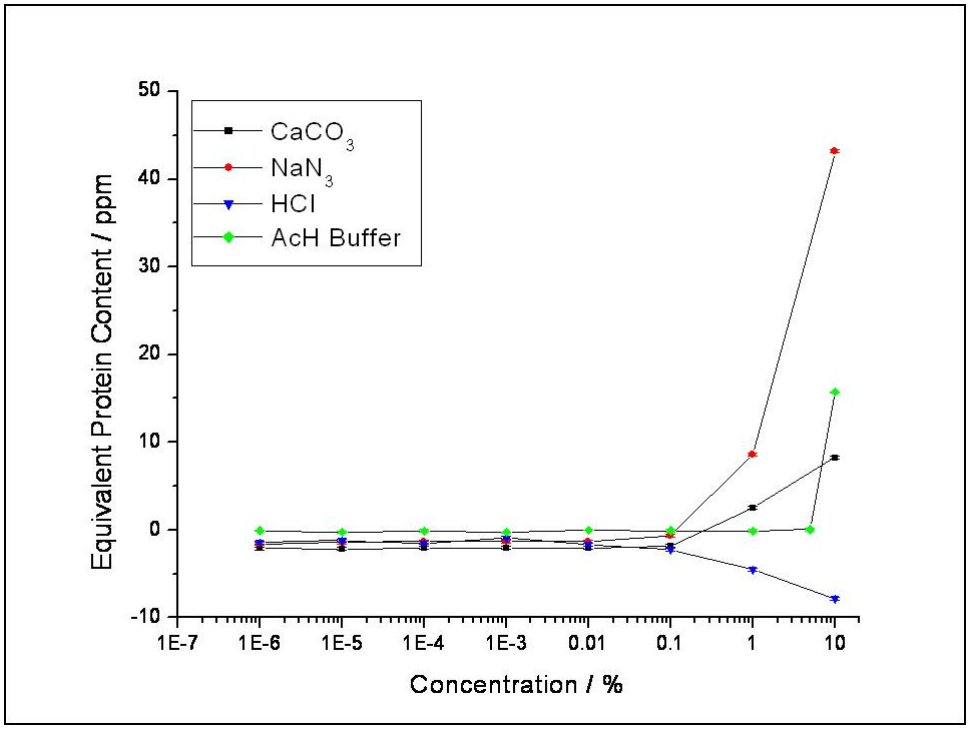

A-Figure 18: Equivalent protein content for different interfering substances. Error bars are smaller as the point. The chosen method was the micro Bradford test.

From the last graph is concluded that there is no interference for the Bradford Test if the interfering substance concentration remains lower than mg/ml.

AVII.3 Residual $CaCO_3$ – Effect of filtration and Centrifugation

The presence of not well demineralised calcium carbonate in the samples yields in an interference signal, as shown in A-Figure 18. Centrifugation and filtration were tested as preparation methods in order to get rid of the interferences. 1ml solution of $CaCO_3$ from concentrations between 5% and 0.01% (m/v) were centrifuged at 14000rpm for 10min or filtrated with 0.22μm MWCO syringe filters (Roth®). The Bradford test then did not more show any interference. No significant differences were found between both processes.

Appendix VIII: Bibliographic Analysis about the shell OM

Some years ago, as an answer to the actual science ways, an interdisciplinary alternative to pure biology, mineralogy and chemistry has found its place together in the “bio-mineralogy”. Scientists of all over the world have been trying to understand how the animal kingdom developes biogenic forms of minerals. Calcium Carbonate (CC) present in exoskelets of molluscs, snails, and corals, or Calcium Phosphate (CP) constitutional part of teeth and bones of mammals, are some examples in the big lists of the today studied bio minerals.

Not only the structural form in which these bio minerals are found in nature, but also how they are constructed have been of interest to the scientific community in the lasts years, and much information is being discovered. It is known that the mineral structure of the snail and mollusc shells is made with help of an organic matrix (OM). It was observed that the OM encloses each bundle of crystallites in a discrete sheath, binding them together to form the shell structure. So far, studies have reported that the organic matrix constitutes 0.01 to almost 10% of shell weight (Bedouet, 2001).

Biochemical analysis of the molluscan shell OM started a century ago with the studies of Bowerbank (1844) and Brøogly (1930). Gregoire (1972) compiled an exhaustive list of summarized results (Almeida, 1998). Nevertheless the composition of the OM in most biomineralized tissues in most of phyla remains partially unknown. To our knowledge there is only one study about the organic matrix in a *Cypraea* shell, where the crossed lamellar layer was studied in *Cypraea leviatan* in comparison with other gastropods and bivalves (Dauphin, 2000).

AVIII.1 State of the art

Some functions attributed to the organic matrix

Minerals of biological origin are surprisingly more stable, durable and strong as its abiotic partners. The only difference between them is the presence of an organic matrix developed

inside the crystallites. This association between the OM and the mineral is for example believed to be responsible of a 3000 times greater fracture toughness in comparison to the abiotic mineral aragonite (Weiner, 1986). Briefly explained, the organic matter creates defects in the perfect mineral lattice and enhances the fracture toughness by both absorbing, redistributing stress and deviating the propagation of cracks along the cleavage planes of calcium carbonate (Berman, 1990; Gao, 2003). More evidences of the durability and protective effect achieved through the OM are also found in the fact that not only rests of OM, but also original aragonite (notoriously unstable form of calcium carbonate) was found in Cretaceous mollusc's fossils (Clark, 1998).

These wonders are not only related to the material properties; also bio-mineralization and shell microstructure can be explained in terms of the OM. For instance Belcher (1996) and Weiss (2000) identified some components of the OM as responsible of calcification inhibition or promotion. Indeed it has been accepted that the formation, morphological development and crystallography of the bio-composite minerals are controlled by the intrinsic stereo chemical recognition of macromolecules (Choi, 2000). An interesting illustration is the in vitro crystallization under treatment with two matrix proteins of *Pinctada maxima,* that show the growth of platy aragonite layers highly similar to that found in mother pearl (Kono, 2000).

The composition of the organic matrix

The organic matrix, responsible of creating the mineral structure in which the animal soft body will be protected during its existence, is composed mainly of glycoproteins, acidic proteins, mucopolysacharides and β-chitin (Marxen, 1997; Marin, 2001; Dauphin, 2003; Wang, 2003; Wada, 1964; Gre´goire, 1972; Krampitz, 1976; Weiner, 1979; Samata, 1990). In molluscs it is secreted by the periostracal groove in the mantle border involving a quinone tanning of proteins (Meenakshi, 1969). Despite of common features like acidity or non-discrete apparent molecular weights, the organic matrices differ in sugar contents (Dauphin, 2002), sulfur species (Dauphin, 2003) and amino acid composition from microstructure to microstructure, among the phyla, in relation to the health state of the animals and to the characteristics of the environment.

The soluble and insoluble organic matrices

The OM is generally divided into water soluble (SOM) and water insoluble (IOM) matrix fractions (Balmain 1999; Bédouet 2001; Marxen 2003). The SOM fraction was extensively studied since the ´70s (Grégoire 1972), but not all components and their biochemical

implications are yet understood. The proteins belonging to the SOM fraction range from small to medium size, generally less than 70kDa (Bowen, 1996). They are generally (Weiner, 1979) acidic due to relatively high mole fractions ratios of aspartic acid. Weiner and Addadi (1991) proposed to divide the SOM from calcium carbonate bio-minerals as aspartic acid rich glycoproteins, glutamic acid – serine rich glycoproteins or polysaccharide rich. For example acidic carbohydrate rich proteoglycans, with continuous distribution of molecular weights, are known to be the Ca-binding proteins of the SOM in *Biomphalaria galabrata* shells (Marxen, 2000).

To date the water insoluble matrix, has been difficult to characterize. It was reported to be an aggregate of proteinaceous material with a significant component of polysaccharide. Complete hydrolysis followed by amino acid analysis showed a high content of glycine and alanine (30-60%), with high proportion of hydrophobic residues (Bedouet, 2001).

The amino acid sequence of the organic matrix

Recently, several genes encoding the matrix components have been isolated and their deduced amino acid sequences (See A-Table 5 for a comparison between different molluscs) have been clarified (Kono 1999). Aspartic acid, glutamic acid, serine and glycine are found as the main amino acid components (Almeida 1998). Halloran (1995) demostrated that the dominant amino acids of the SOM are aspartic acid, glutamic acid, glycine and serine/phosphoserine, and indicate the presence o domains of hydrophobic amino acids, polyphosphoserine and polyaspartic acid. He suggested the dominant amino acid sequence of the SOM to be chains of different number of Gly or Ser units. The IOM has shown to contain greater amounts of glycine, alanine and hydrophobic amino acids residues .

Author	***Matrix***	***Specimen***	***Asp***	***Gly***	***Ser***	***C-H***	***P-***
Dauphin, 2000	**SOM** Nacreous layer	*Pinctada fucata*	24%	9%	-	-	-
Dauphin, 2000	**SOM** Nacreous layer	*Pinctada martensi*	26%	11%	-	-	-
Samata, 1990	**SOM** Calcitic foliated layer	*Patinopecten*	27%	7%	-	-	-
Halloran, 1995	**SOM** whole shell	*Adamussim colbecki*	31%	18%	29%	1.5%	12.8%

A-Table 5: Amino acid main composition of different organic matrices. Asp=aspartic Acid, Gly=Glutamic Acid, Ser=Serine, C-H= Carbohydrates, P- =Phospates

The presence of Sulfur

In many works, the simple SEM/EDX or microprobe observation of transversal sections detected presence of S in the inter-prismatic walls and sometimes also in intra-prismatic material. Wada (1964) considered the speciation of sulfur in bio-crystals, recognizing the acidic mucopolysaccharide to be a sulfuric ester, probably chondroitin sulfate. Later he proposed that sulfated groups (as polysaccharides) play a major role as active sites and nucleation centers for the crystallization of bio-minerals (Wada 1980). Dauphin (2003) detected high amounts of sulfur in oyster shells of *Pina nobilis* (4500ppm) and *Pinctada maxima* (3100ppm), confirming through EXAFS analysis the presence of sulfated (SO_4) species, as sulfated sugars, and in lower quantities as amino acid species.

The presence of lipids and carbohydrates

Specific mineral associated lipids have been reported sometimes (Blumer, 1965), including fatty acids, cholesterol, phytadienes, ketones and in some cases n-alkanes (Cobabe, 1995).

AVIII.2 The Inter- and Intra-crystalline Organic Matrix

Electron microscopy studies of mollusk shells have clearly shown that the organic matrix wraps individual units such as prisms or nacreous tablets, and is the reason for that this matrix has been characterized as inter-crystalline. Besides this easily observed matrix, an intra-crystalline soluble matrix is present.

A schematic representation of both matrixes is in A-Figure 19. The schema shows how a mixture of organic material like proteins and sugars, bind inorganic elements to form crystals, in the case of the intra-crystal matrix and, to bind crystals between them in the case of the inter-crystal matrix. Inter- and intra-crystalline organic matrices control the orientation, morphology and polymorphous phases, and thus differ in composition between different structures.

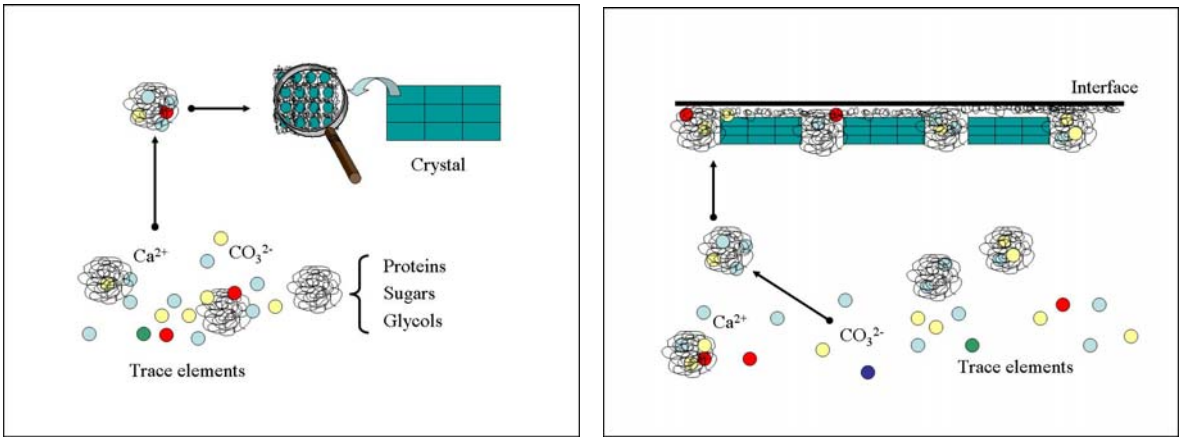

A-Figure 19: intra (left) and inter (right) crystalline matrices, in the case of a prismatic microstructure.

OM of the prismatic layers

The firsts studies about the prismatic organic matter intercalated in the mineral structure of the shells was done in pearl oysters. This fact is not surprising, not only because oysters (and specially pearl oysters) are important as economical resource, but also because their shell is a simple two layer composed structure, with an outer calcitic and an inner aragonitic layer. The prismatic units and their inter- and intra-prismatic organic material present the biggest size over the mussels, thus facilitating its extraction and further study. For example, the prisms present in *Pinna* and *Pinctada* oysters, shown to be the largest (50 to 100 μm) of the biomineralized prisms (Bowerbank, 1844), remarkable not only per size and form of the mineral crystal, but also because they are surrounded by a 1-8μm thick inter-crystalline organic matrix (Dauphin, 2003) that allows easy extractions and further characterization. In contrast, intra-prismatic matrices are not always present in oysters, as for example in the case of *Pinctada* (Dauphin, 2003).

Inter- and intra-prismatic organic matrices have also shown to differ in the sulphur species and amino acid contents between them. Indeed Nakahara found that the inter-prismatic walls of *Pinna* and *Atrina (Pteriomorpha, Pinnidae*) have lower acidic amino acid contents (aspartic and glutamic acids) and higher sulfated amino acid contents than the intra-prismatic organic matrix (Nakahara, 1980). In agreement with these data, Suzuki and Uozumi (1981) noticed that the inter-prismatic organic matrix is acidophilic, whereas the intra-prismatic organic matrix is basophilic.

The components extracted from the inter-prismatic matrix could be divided also in soluble and insoluble parts (Dauphin, 2002). SEM observations showed that complete decalcification

of the prismatic layer in *Pinna* and *Pinctada* mussels does not destroy the inter-prismatic organic wall Thus, suggesting that the main part of soluble organic matrices extracted from the calcitic layers comes from the intra-prismatic zone and not from the inter-prismatic one (Dauphin, 2003).

OM of the nacre sheets

The inter-lamellar organic sheets surrounding nacre units have shown under TEM analysis to be composed of a three layered structure: two electron dense outer layers enclosing an electron lucent layer (Nakahara, 1979). Chemically these layers have also been characterized as water insoluble and soluble, respectively.

OM of the Crossed Lamellar Layer

Differential thermal analyses of several Bivalvia shells show that the OM of the crossed lamellar layers differs from those of the prismatic layers (Kobayashi, 1973). The first reference found corresponds to Uozumi (1972) who described the third order lamellae surrounded by an organic matrix (conchyolin). Weiner (1977) has shown that the protein fraction of the soluble matrices of crossed lamellar layers of some mollusks have variable non-discrete molecular weights, in agreement with the results obtained from Dauphin (Dauphin, 2000b) for six different gastropods and bivalves, including the C*ypraea leviathan* specimen.

Appendix IX: Bibliographic Analysis of the Different Extraction Methods

As it was already said, OM is present in the shells at very low concentrations. Thus further organic analysis in the biomineral requires the separation of the inorganic part. This process, known as demineralization, implies the destruction of the calcium carbonate binding. In fact the demineralization can be achieved through acid attack or complexation of the Ca^{2+} ion with another reagent, as for example EDTA. However, the biggest problem of the demineralization step is the possible destruction of the proteins or interesting organic-metal bindings. For this reason the process must be done very carefully. A summarized list of different extraction processes found in literature is presented in at the in A-Table 1 and 2, at the end of this append.

AIX.1 The Extraction Solvent

The mildest extraction found in literature was made from nacre powder with water in a non decalcifying process (Mouries, 2001). The author explains that this type of treatment should not extract the intra-crystalline matrix strongly linked to the mineral, but also not the insoluble part of the inter-crystallite matrix. In addition to this soft process some cases are present where the chosen extraction medium is EDTA at different concentrations, in basic pH. Such processes are highly time consuming. In contrast the biggest group of scientists uses an acidic attack, with acetic acid or HCl at different concentrations and pH in the acidic range. The most careful extractions solubilize first the shell powder in water or acidic water (pH around 5) and add the acid drop wise slowly under continuously stirring.

AIX.2 The pH Treatment

About pH treatment of shell decalcification, a big variety of work has been found in literature. Generally, the value of pH taken for the extraction was between 4 and 8, and it coincides with the range in which proteins are not destroyed. Nevertheless there are some cases where very low pH was chosen, as for example in the investigations of Bowen (1996), who

decalcified shell nacre powder of different species to obtain with success the IOM, dropping 12HCL in water at a pH below 2. The difference between basic and acidic conditions was mentioned by Halloran, who studies the amino acid composition of the soluble and insoluble matrix of *Adamussium colbecki* demineralising the shell with acetic acid 2% (pH1.2) as well as with EDTA10% (pH 8). In this case acetic acid was chosen, because of the ease with which it could be removed from the proteins and the speed of demineralization, but no significant differences were observed in the total amino acid composition of the differently treated samples (Halloran, 1995).

From these experiences it can be concluded that the pH is not such a critical factor for the survival of the OM, or for the amino acid composition analysis. Nevertheless these works have not been dealing directly with speciation analysis. The fact that pH out of the range (4-8) may change the 3D conformation of the proteins, with the consequence that interesting metallorganic complexes may be lost, made us decide to respect the range pH 4-pH 7.5.

AIX.3 The Use of Preservatives

Working with high volumes of decalcified sample, especially when the pH has been adjusted to around 7, introduces the risk of bacteria and protease activity. Some authors decided to add 0.01% (m/v) of NaN_3 as antibiotic and 0.04% AESBF as protease inhibitor (Marxen, 2000; Kono 2000) during the demineralization process. In both cases the sample was then dialyzed exhaustively.

AIX.4 The Separation of Insoluble and Soluble Matrices

Once the sample has been demineralized, and the OM are in solution or suspension, the next step is to separate the water soluble and insoluble parts. In most cases present in literature, the separation was made by centrifugation at different speeds, and few authors have used filtration as a method. For purification and purification with pre-concentration, dialysis and ultracentrifugation-filtration against water, was the most elected methodology respectively. The further concentration of samples was almost always lyophylization.

AIX.5 The Solubilization of the IOM

Further study of the IOM for some experiences the sample should be in liquid phase, involving a solublilization process. Reports of partial solubilization in SDS 10% after heating at 100ºC (Bedouet 2001, Bowen 1995) or in NH_4OH (Samata 1999) are found in literature. Nevertheless the amount of IOM solubilized with success is always low, as for example in the case of Bedouet, who reports that only 0.05% of the IOM could be solubilized in this way.

Extraction Processes of the SOM

Author	***Material***	***First rinsed***	***Solvent***	***shell***	***Added***	***Separation***	***Purification SOM*** / ***Purification IOM***	***Concentration SOM*** / ***Extraction IOM***	***Recovery SOM*** / ***Recovery IOM***
Bedouet, 2001	Nacre *Pinctada maxima* *Haliotis tuberculata*	n.s.	200ml Acetic Acid 6.5M 3hs	20g (50-100μm)		14000g 5 min	Dialyzed water	Lyophilization	0.17% *Pinctada* 0.15% *Haliotis*
							Washing and centrifugation	Air dried	1.3% *Pinctada* 2% *Haliotis*
Halloran, 1995	*Adamussium colbecki*	Boiling 10 min 30% H2O2 Boiling 10min 50% NaClO	Acetic Acid 2% pH 1.8	In dialysis tubing 1kDa		20000 g 10 min 10ºC	Dialysis water	Lyophilization	0.298±0.17 %
							Resuspended in water	Lyophilization	0.196±0.143 %
Marxen, various	*Biophalaria glabrata*	6% NaClO	Suspended in 50ml 10-5N HCl drop HCl, pH>5, 4ºC	100g	0.01% NaN_3 + 0.04% AESBSF	16000g 20min	Dialysis water 6kDa Liofilized Redisolved in water Desalted in a p2 column	Lyophilization	0.70%
							Washed exhaustively	Lyophilization	0.76%
Mouries, 2001	Nacre *Pinctada Maxima*	n.s.	200ml Water	100gr		3500 rpm 30 min			1mg/ml
Kono, 2000	Nacre, Prismatic *Pinctada Maxima*	n.s.	EDTA.4Na 10%	n.s.	0.01% NaN_3	15000 g 20 min	Dialysis water	Lyophilization	SOM
Dauphin, various	*CLL, N, P* *Pina* n*obilis* *Pinctada maxima*, others	n.s.	Acetic Acid pH4	n.s.		21000g 15min	MilliQ Filtron 3kDa	Lyophilization	SOM
Cobabe, 1995	*Codackia* *Arca*	Sonicated 5sec DiChlorMethane/methanol 4:1	DCM/MeOH 4:1	n.s.		n.s.		Lyophilization	SOM
Marin 2001	Prismatic *Pina nobilis*	Diluted NaClO (0.2g/100ml) Several hours	Suspendend in 20ml water drop Acetic Acid 20% or 5% until pH 4 Overnight, 4ºC	Between 3 and 25g		5500g 15min	Filtered in Amicon 10kDa against water, 4ºC	concentrated to 4ml Amicon 10kDa, 4ºC	SOM

A-Table (A) : Review of different extraction techniques.

Extraction Processes of the SOM - continuation

Author	***Material***	***First rinsed***	***Solvent***	***shell***	***Added***	***Separation***	***Purification SOM*** / ***Purification IOM***	***Concentration SOM*** / ***Extraction IOM***	***Recovery SOM*** / ***Recovery IOM***
Choi, 2000	*Cassostreas Gigas*	NaOH 5%	10lt Acetic Acid 2% pH 1.8	50g Inside the dialysis membrane 12kDa		30000g 20 min	Dialized at 4ºC for 2 days	Lyophilization	SOM
Sarashina, 1998	Foliated layer *Patinopecten yessoensis*	10% NaClO 48hs	3lt EDTA 0.5M pH 8 72hs 4ºC	100g		Filter cheesecloth	Ultrafiltration agains water	Ultrafiltration to 50ml and Lyophilization	0.03%
Samata, 1999	Nacre *Pinctada fucata*	n.s.	EDTA-4Na 10% pH 7.6	n.s.		15000g 15min			IOM
Almeida, 1998	*Cassostreas Gigas*	NaOH 5%	Acetic Acid 10%	n.s.		n.s	Washing and centrifugation	Lyophilization	IOM
Balmain 1999	Nacre *Pinctada Maxima*	n.s.	1M Acetic Acid / ethanol pH 4	n.s.		n.s.	Washing with ethanol	Air dried	IOM
Balmain 1999	Nacre *Pinctada Maxima*	n.s.	EDTA 0.1M pH 7.4	n.s.		n.s.	Washing with buffered water pH 7.4	Air dried	IOM
Bowen, 1995	Nacre *Haliotis Conus Tridacna*	n.s.	50ml water drop HCl 12M pH <2	2g		Filter 0.45μm	Resuspended / filtered 5ml EDTA 0.25M pH 8 5ml Tris 0.01M pH 8.6 5ml water	Desiccator dried	1%

A-Table (A): Review of different extraction techniques.

Extraction Processes of the IOM

Author	*Material*	*Matrix*	*Solvent*	*Heating*	*Precipitation*	*Separation*	*Washing*	*Dried*	*Recovery*
Bedouet, 2001	Nacre of *Pinctada maxima* *Haliotis tuberculata*	Dried IOM	SDS 10% + 10%BME	10-40 min 50º to 100º	methanol/chloroform/water 4:1:3	14000g 10 min	Washing with methanol 14000g x10min	Air dried	0.045 % soluble in SDS/BME)
Bowen, 1995	Nacre Haliotis Conus Tridacna	-	SDS 10%	1h 100º	-	-	-	-	Solution for electrophoresis
Samata, 1999	-	-	Diluted alkali solution of NH4OH, pH 8.5	-	-	15000g 20min	-	-	-

A-Table (B): Review of different extraction techniques.

Appendix X: Experimental Study of the Different Extraction Steps

The extraction method developed was studied subdivided into five steps: powdering, demineralization, purification, pre-concentration and lyophylization. For all steps, two or more methods were tested and compared. Parameters to decide for the better process were in first place the final protein content achieved and the absence of organic as well as metallic contaminations. In second place the processes were compared by time and necessary experience, material and costs.

AX.1 Powdering Methods

The analysis and extraction of the organic matrix present in the bio-mineral of *Cypraea* snails requires the powdering of the shells. Two types of powder material were prepared, an average powder material as well as a layer separated material. Both types of samples are described in Chapter 2.

Blanks of the Powdering methods

Some authors observed different types of contaminations using different powdering methods. (Spex-certiprep, home page) reported for example a 200 times Co enrichment by powdering with a tungsten press. The trace elemental concentration found by ICP-MS for the *average material* in comparison to the *layer specific material* samples do not show alarming differences (that could be understand as a hint to contamination in the powdering process). In this case, due to the fact that the tungsten press is only used to fracture the material which in addition is protected in plastic bags, the results do not show such contaminations. To analyse the *average material* powdering method, three types of treatment were compared: (A) cut with a diamond saw, (B) fractured by a tungsten carbide press and (C) powdered with an agate mill. Five grams of each sample were then digested and aliquoted (See Chapter 2, section 2.7). Three samples of each treatment were measured by off line ICP-MS and averaged (A-Table 6). The standard deviation between the three samples is shown in the next table.

Element	*SD*
Cr^{50}, Cr^{53}	25%
Mn^{56}	21%
Fe^{57}	6%
Co^{59}	2%
Ni^{60}, Ni^{62}	6%
Cu^{63}, Cu^{65}	7%
Zn^{64}, Zn^{66}	4%
Cd^{111}, Cd^{114}	2%

A-Table 6: Standard Deviation of the concentrations found for different powdering treatments.

The trace elemental concentration found by ICP-MS for the different powdering treatments does not alarm contaminations with the studied elements. The deviation observed for Cr and Mn could be caused for differences or heterogeneity in the material (for example the piece treated by A comes from the top of one specimen, while the samples treated with B and C are an average of the complete shells of 10 to 12 animals).

For the *specific layer material* method, the samples treated with the diamond Milling cutter have shown by INAA a contamination with silver. This contamination was observed only at the beginning, in the firsts treated samples and not any more after. A possible origin of the Ag leakage could have been some sort of silver glue used to bind the diamonds to the cutter.

Comparison between the two powdering methods

In the case of the first method, the obtained powder is an average of the whole shell or shells milled. The method does not give layer separated samples but has the advantage of easily getting larger average samples (Compare the amounts obtained with both methods in A-Figure 3 of Chapter 2). Comparing to the fracturing and Milling method, this latter allows for preparation of samples according to specific properties like per colours or layers, etc. On the other hand, this method is very time consuming and requires technical experience.

Summary of Powdering Methods

	Average Material	***Layer Specific Material***
Method	1)Tungsten press 2) Agate mill	Diamond milling cutter
Type of powder	Shell average	Specific per layer
Quantity / 4hours work	200g shell	1g shell
Experience Requirement	low	high
Personal Requirement	15%	100%
Inorganic contamination	Not observed	Ag (at the beginning)

A-Table 7: Comparison of powdering parameters for the different methods.

AIX.2 Decalcification Methods

The demineralization of the samples requires the destruction of the crystal bindings between the cation Ca^{2+} and the anion $(CO_3)^{-2}$. This effect could be reached through a demineralization process, using for example an acid reaction or a complexation with an agent as EDTA. In this work, only acid attacks were performed using a slow titration.

Titration with a burette

A plastic capillary tip was mounted at the end of a glass burette of 50ml (See A-Figure 20). The burette was washed three times with MilliQ water after use, and once with the eluent. The flux was adjusted to around 20 drops per minute in the burette when the tip is in air, and then was directly put into the solution. Indeed the presence of the capillary in the solution avoids the formation of big drops. The system was mounted on a magnetic stirrer and placed inside an ice bath (See A-Figure 20).

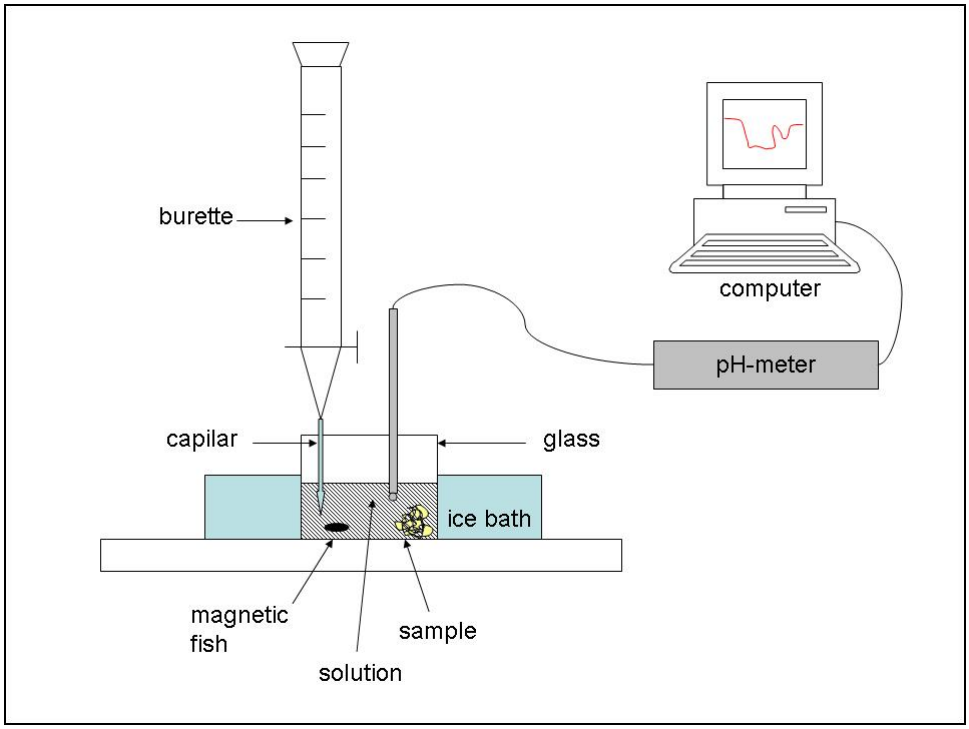

A-Figure 20: Experimental set up of the digestion**.**

The temperature and pH were registered with an online coupled pH-meter. Data acquisition was made with the program Achat®. The pH was controlled manually, adjusting the flux of acid to the sample. The pH was not let to go below 4, and the temperature was maintained between 4 ºC and 8 ºC during the evolution of the decalcification process.

AIX.3 Separation Methods

In case that the sample has particulate material which must be separated, one or two of the following process have been applied:

Decantation

The simplest process to be applied for separation of soluble and insoluble fractions is decantation. For this purpose the solution sediments about five minutes and the liquid is then transferred to another beaker slowly. This process has the advantage that big particulate material is easily extracted without introducing any contamination into the sample.

Filtration

Syringe filtration through a membrane of 0.22μm was used to separate big insoluble particles, in case that they can be discarded, because this system does not allow recovering of the separated material. Two types of filters have been checked, Rotilabo® P666-1 and Rotilabo® P664-1cellulose mix ester (Roth®).

Centrifugation

In this case, the samples were put in a correspondent centrifugation tube, closed, and centrifuged. If the sample must be re-suspended and centrifuged repeatedly, the re-dilution was made by shaking the closed vessel manually or with an automatic shaker for some seconds. The parameters of the different centrifuges used are described below (A-Table 8):

	Big	***Medium***	***Small***
Centrifuge	Heraus	Sigma	Eppendorf
Model	Megafuge 1.0	301	5417R
Temperature	room	room	4 -50ºC
Speed	4000 rpm	2000rpm	2000rpm
Vessel capacity	50ml	15ml	1.5ml
Places	12	16	32
Axis	Horizontal	Horizontal	Fixed 60º

A-Table 8: Centrifugation parameters for different sample amounts

Blanks of the separation methods

1ml MilliQ water samples were centrifuged (1hour, maximum revolution) in the 1 ml, the 15 ml and the 50 ml vessels. 5 ml MilliQ water were also filtered and recollected. The resultant blanks were measured for trace analysis composition and for organic contaminant presence by ICP-MS off line and HPLC-UV spectrometry, respectively.

The filtered and centrifuged water blanks compared with untreated water samples did not show any differences in the trace elements observed for the centrifugation or the filtration (data not shown). Nevertheless, the results obtained in the HPLC-UV spectra using the

Biosep S2000 column and measuring the absorption at 220 nm show clearly that the filters introduce a signal, not observed in the case of centrifuged blanks (See A-Figure 21).

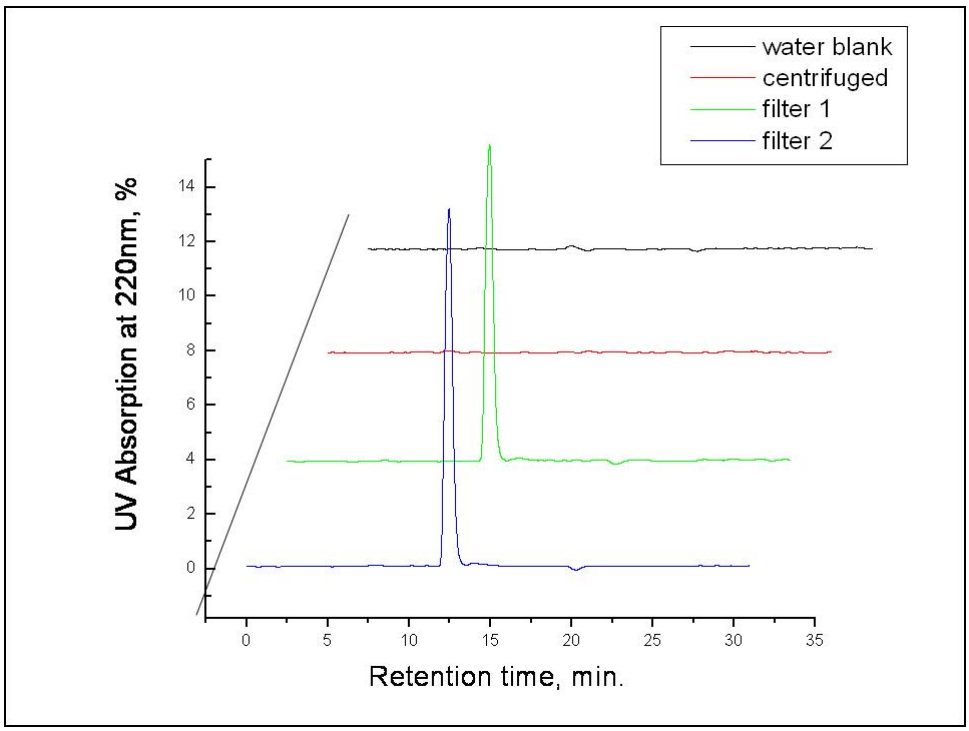

A-Figure 21: SE-HPLC-UV spectra of a MilliQ water sample, centrifuged and filtered with two different jeering filters.

MATERIAL: MilliQ water
CENTRIFUGATION: 1ml MilliQ water, at 10000rpm for 60min.
FILTRATION: 1ml MilliQ water filtered in (1) Rotilabo® P666.1 and (2) in Rotilabo® P664.1.
HPLC-UV: Column: *Biosep S2000*, Mobile Phase: 20mM TRIS-HCL pH7.4, Flux: 0.8ml/min, Wavelength: 220nm.

Comparison of the separation methods

Because of the organic contamination observed for the filtration system, only centrifugation and/or decantation were chosen as preparative separation method.

Summary of separation methods

	Decanting	*Filtration*	*Centrifugation*
Time required	15min	5min	15-90min
Parameter	Mass	Size	Mass
Temperature	room	room	4 -50ºC
Volume	1000ml	5ml	1.5, 15, 50ml
Organic contamination	no	yes	no
Inorganic contamination	no	no	no
Personal requirement	10%	100%	50%

A-Table 9: Comparison between different separation techniques.

AIX.4 Purification Methods

The purification and desalting of the matrices was done through dialysis and/or ultracentrifugation-filtration (UCF). In both cases, the sample is purified when the solution in which the sample is diluted, is changed to MilliQ water, in a diffusion process.

Dialysis

A dialysis process is based on the diffusion through a membrane of a more or less well determined mass cut off (MWCO). All elements that have a higher mass than the MWCO are retained inside the membrane bag and the rest is distributed in the buffer in which the membrane bag is immersed (See A-Figure 22). Once achieved the equilibrium between the solutions in both sides of the membrane, the diffusion is stop. Therefore the buffer must be changed continuously. The more often the buffer is changed and the larger the buffer volume, the better is the desalting achieved.

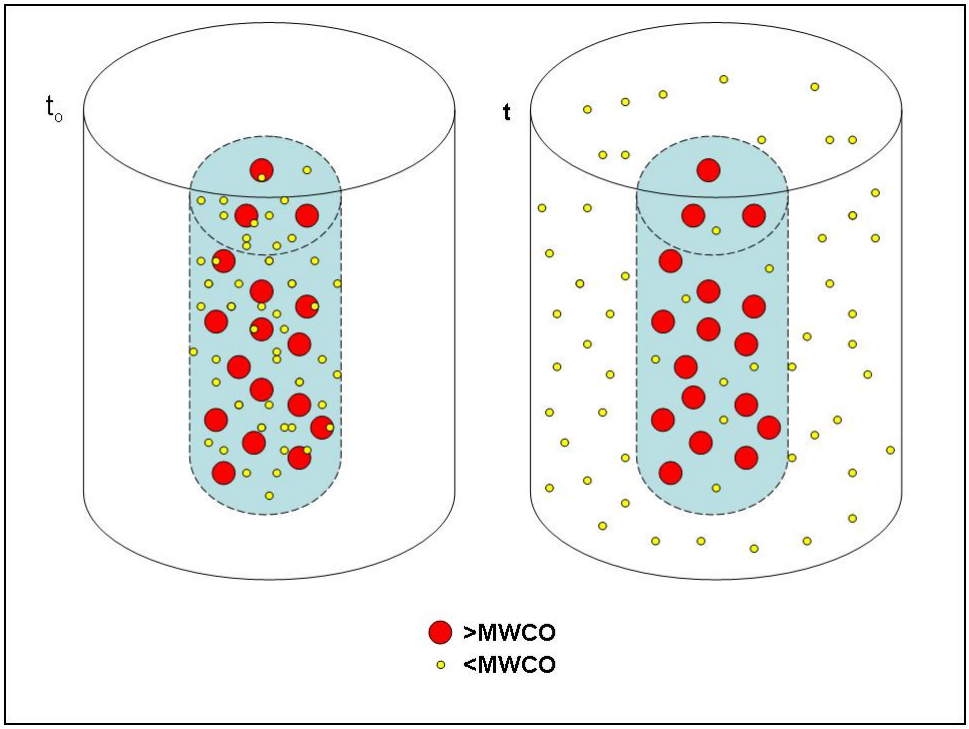

A-Figure 22: schematic representation of a dialysis process, showing molecules bigger and smaller than the membrane MWCO.

Materials

For the dialysis process regenerate cellulose dialysis membranes of Sigma® of mass weight cut off (MWCO) 3.5kDa, 5.8cm flat width. The membrane is delivered wet in NaN_3 0.01% and needs to be washed in MilliQ water for one hour to remove the components in which it is conserved.

Experimental Set up

The membrane was cut into pieces of about 10cm. 25ml of sample were put inside each bag, and closed with plastic clips. The bags were immersed in a 1L baker glass (See A-Figure 23) under continuous stirring and dialyzed for at least 2 days, changing the dialyzing water each 8 hours. If some material had precipitated in the bags, it was removed after by centrifugation (10 min at 4000 rpm).

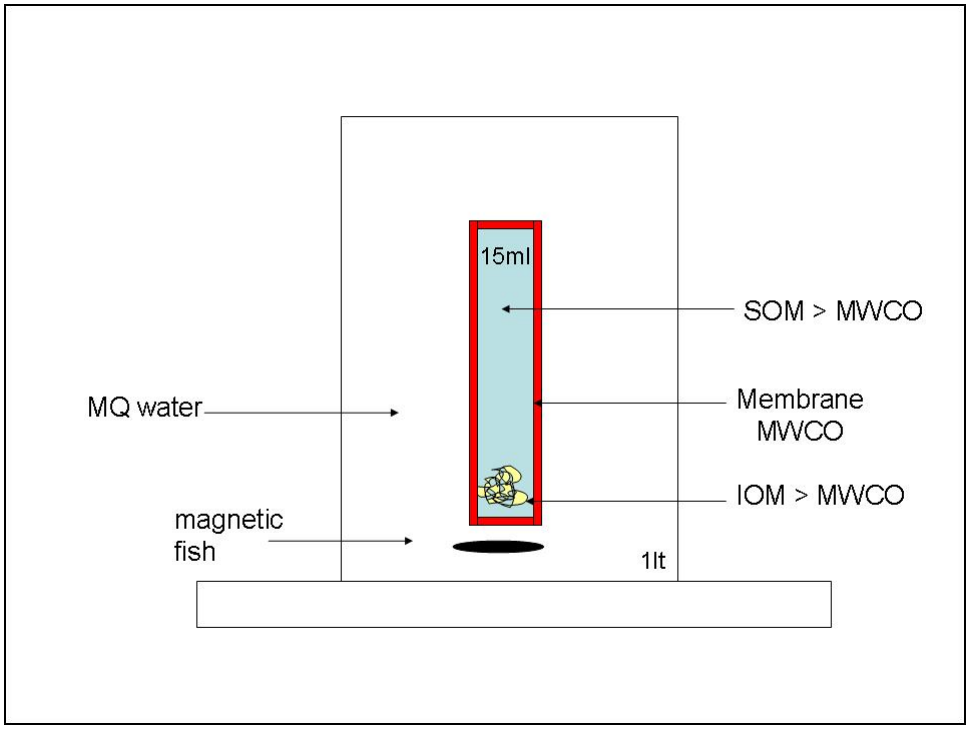

A-Figure 23: schematic representation of a dialysis set up.

Theoretical speed of desalting

The speed, in which a sample, diluted in a solvent A, can be desalted in MilliQ water using a dialysis membrane with a 3kDa MWCO, was calculated theoretically using a diffusion law. The equilibrium time was taken as 8 hours (Pierce, home page). The result is shown in A-Figure 24.

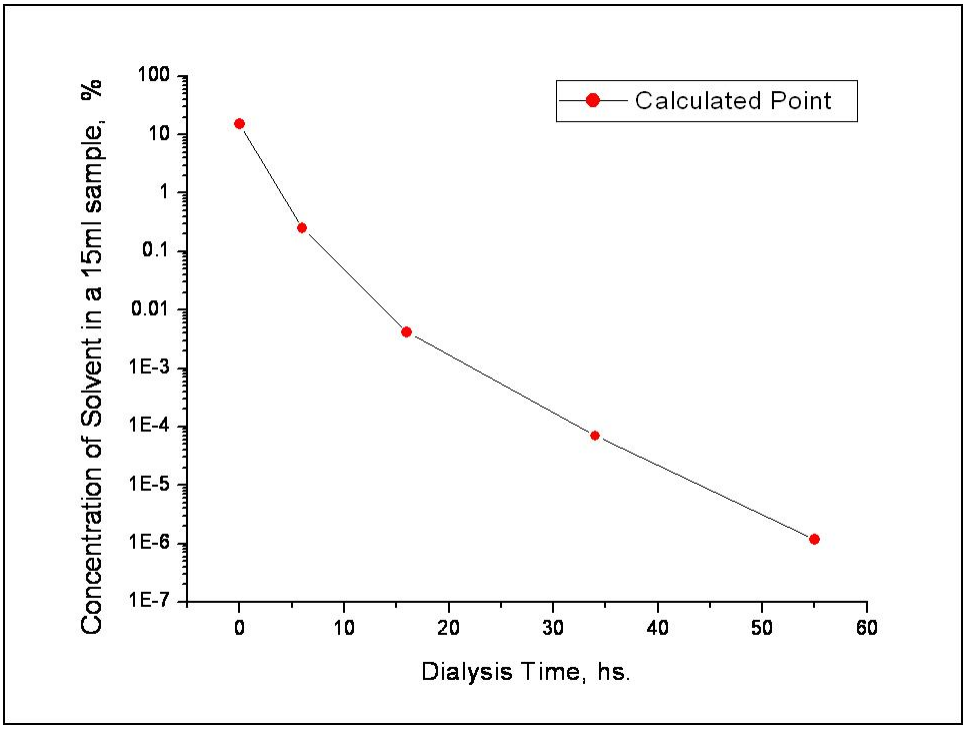

A-Figure 24: Theoretical dilutions curve of a solvent A (25ml) in MilliQ water (1000ml) by dialysis with SPECTRAPORE CE membranes (MWCO 3.5kDa). The constant of equilibrium was chosen as 8 hours.

From the curves analyzed in A-Figure 24, is concluded that, by a theoretical dialysis, good desalting results may be achieved. A sample diluted in a solvent with an initial concentration of 15%, needs three days dialysis, with changes each 8 hours, to be desalted down to 10^{-6}%. One of the drawbacks of this method is the small amounts of sample that can be dialyzed.

Blank Samples

25ml MilliQ water were dialyzed against 900ml MilliQ water as outside buffer. During two days, the water has been changed each eight hours. Each time 1ml was sampled for analysis, and conserved at -10ºC. All the samples were then analyzed by HPLC-UV together the same day, and the “day zero” blank was pure MilliQ water.

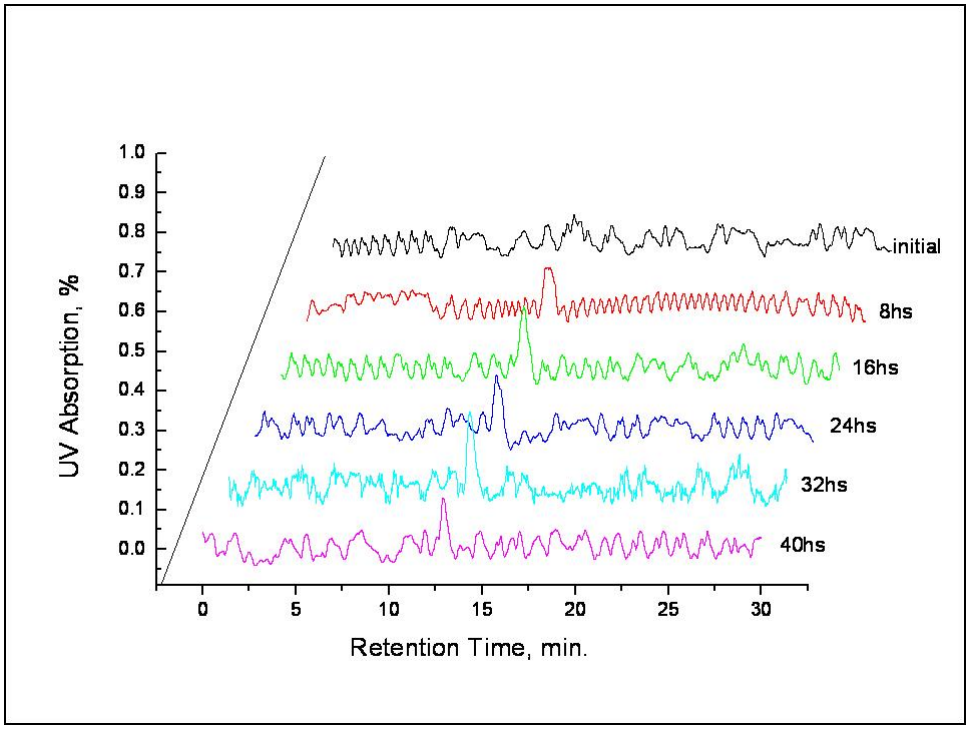

A-Figure 25: SE-HPLC-UV spectra of a MilliQ water standard dialyzed with SPECTRAPORE CE membranes (MWCO 3.5kDa) during three days.

MATERIAL: MilliQ water
DIALYSIS: SPECTRAPORE 3.5kDa dyalisis membrane. Dialyzing 25ml sample against 1lt MilliQ water, changing it three times per day.
HPLC-UV: Column: *Biosep S2000*, Mobile Phase: 20mM TRIS-HCL pH7.4, Flux: 0.8ml/min, Wavelength: 254nm.

Ultracentrifugation Filtration

The UCF process consists basically also in a diffusion process through a porous membrane. The main difference from the dialysis is that for this case the gradient vector is not the concentration difference, but the centrifugal force. For this reason the equilibrium is forced much more quickly as for the dialysis. In A-Figure 26 is shown a representation of the UCF process for a sample containing two types of molecules (bigger and smaller than the membrane pore).

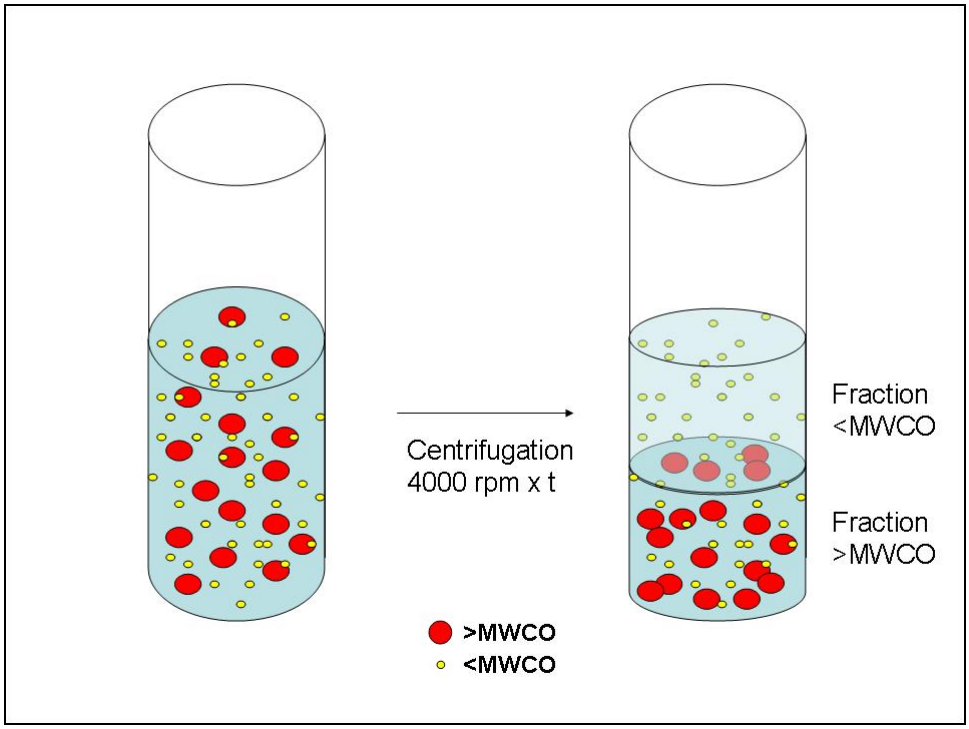

A-Figure 26: schematic representation of an UCF system.

After the centrifugation process, the big molecule fraction (>MWCO) is concentrated in volume, while the <MWCO fraction shows only small molecules. In this way, the fraction >MWCO was purified from the small molecules.

Materials

Ultracentrifugation-filtration tubes of Amicon® of regenerated cellulose membranes with a cut off of 3kDa and a volume of 15ml were tested. In this case the filters are delivered semi-dry, and the conservation reagent is NaN_3 0.01%. Both parts of the tubes were washed before use with MilliQ water. The membrane was not allowed to dry between the pre-washing process and the use.

Experimental Set up

In this case, 15ml samples were put inside the tubes, and centrifuged at 4000rpm for 90min. After that, the fraction <MWCO was discarded and the fraction >MWCO (concentrated approximately to 3-5ml) was filled up again to 15ml with MilliQ water (in the same UCF tube). The process was repeated at least six times (See A-Figure 27).

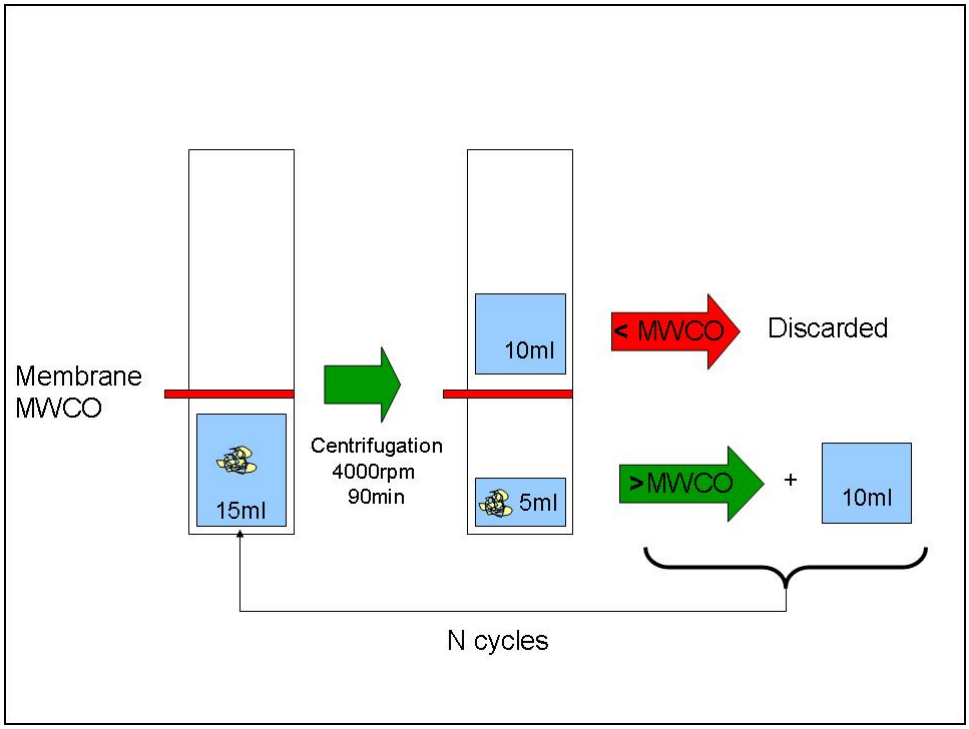

A-Figure 27: Schematic representation of an ultracentrifugation-filtration process.

Theoretical speed of desalting

In the case of the UCF process, the speed, in which a sample, diluted in a solvent A, can be desalted against MilliQ water can also be calculated theoretically using volume-to-concentration relations. The idealized hypothesis for the calculation is that smaller molecules (<MWCO) distribute normally in the whole volume of the sample. The volumes *V* obtained after centrifugation at 4000rpm for different centrifugation times were measured experimentally, the theoretical concentration achieved is observed in A-Figure 28.

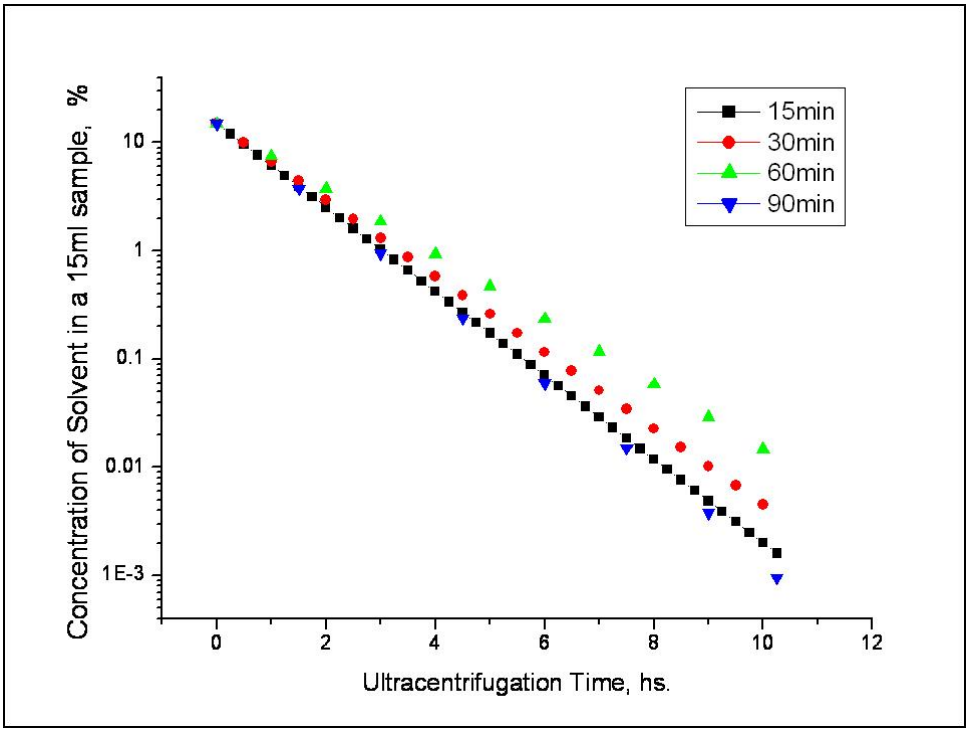

A-Figure 28: Theoretical desalting curves of a solute A (15ml) in MilliQ water (between 5ml and 10ml) by ultracentrifugation-filtration with CENTRIPREP AMICON YM 3 (MWCO 3kDa). The constants of dilution were measured experimentally.

From the analysis of the A-Figure 28 is observed that a good compromise between final time of the experience and personal requirement in the laboratory is to change the buffer eight times each 90min (total time: 10 hours). Nevertheless the concentration of the original solute in the samples remains over 10^{-3}%. The advantage of this process is the reproducibility of the samples through the volume control.

Blank Samples

Blank samples of 15ml MilliQ water were centrifuged in UCF tubes at 3000rpm for 90 minutes. After each cycle, the fraction <MWCO was sampled and frozen at -10ºC. MilliQ water was added to the >MWCO fraction to fill up to 15ml and the procedure repeated six times. The samples were analyzed together the same day by HPLC-UV and the results are shown below (A-Figure 29):

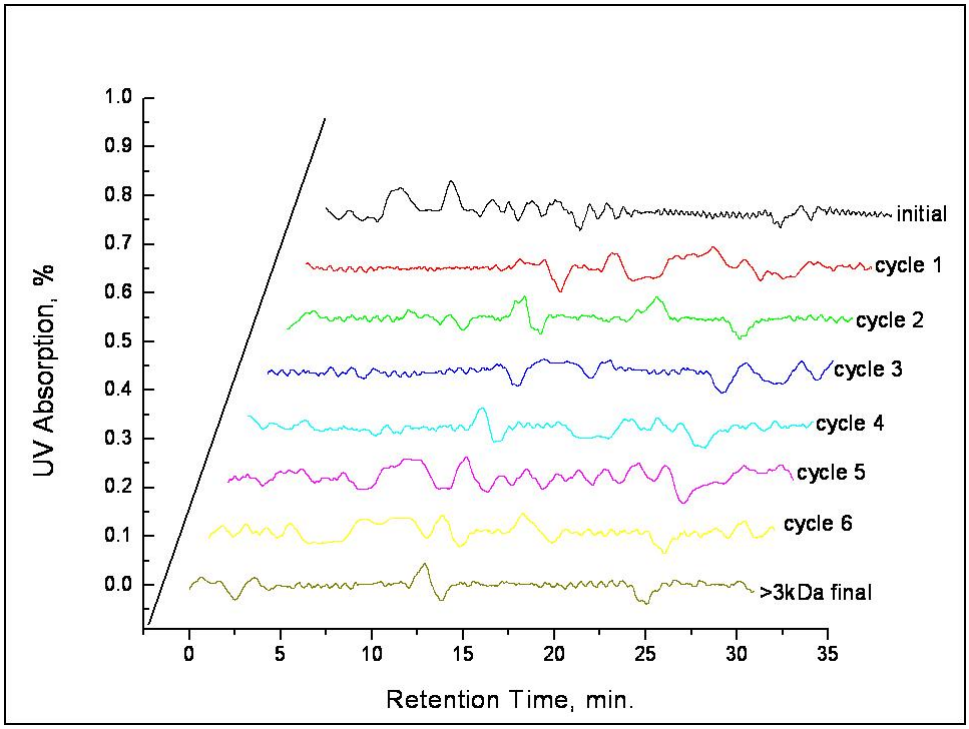

A-Figure 29: HPLC-UV detection of an ultracentrifuged MilliQ water blank sample.

MATERIAL: MilliQ water
UCF: ultracentrifugal filters Centriprep Amicon YM3 MWCO 3kDa, centrifuged 90 min - 3000rpm , in 6 cycles.
HPLC-UV: Column: BIOSEP S 2000, Mobile Phase: 20mM Tris-HCl pH 7.4, Flux: 0.8ml/min, Wavelength: 220nm

As it can be seen from A-Figure 29, the signal observed at 220nm for the UCF samples is only an about 0.5% noisy signal. No degradation of the UCF membrane or organic contamination is visible in the spectrum.

Comparison between the two desalting methods

The experiments done with the dialysis as well as with the UCF have shown that both methods can be used to desalt the samples. For final concentrations around 0.01% both methods are comparable, and the main difference lies in the time and personal requirement. UCF needs continuous attention, but ends in a very repetitive process. Another difference is the temperature of both processes. In UCF the temperature of the samples increases by centrifugation about 30ºC, contrary to the dialysis that is made at room temperature. A third difference is the concentration achieved for the sample. With dialysis there is no concentration, while for UCT there is an about 3x concentration.

Summary of purification methods

	Dialysis Membrane	***Ultracentrifugation Filter***
Material	25cm membrane	1 UCF tube
Initial Concentration	15%	15%
Initial Volume	20-25 ml	15 ml
Final Volume (> 3kDa)	20-25 ml	3 ml
Total Time	2 days	10 hours
Buffer Change Number	5	8
Buffer Quantity Needed	3l	150ml
Personal Requirement	10%	80%
Final Salt Concentration	10^{-6} %	10^{-3}%
Separation	good	good
Traced elements	no	no
Organic contamination	no	no

A-Table 10: Work, time and characteristic parameters to compare the two desalting methods tested to extract the SOM from the shell powder.

AIX.5 Pre-concentration Methods

The sample volumes obtained after the desalting process can vary between 25ml and 500ml. These volumes are to high to be treated and a pre-concentration process become essential. For that, two methods were tested. At first a rotatory evaporation concentration was used. The samples were treated in a thermal bath at 50ºC, under 40mbar atmosphere. This method has shown low repeatability of the results and loss of material in the concentration balloons. For thee reasons, another method was also checked concentration by UCF. Both processes are analyzed and compared as follows.

Rotatory Evaporator (Rotavapor)

For this concentration procedure a standard rotatory evaporator from Heilolph® model VV2000, with a diagonal condenser V1-51-311, was used coupled with a diaphragm vacuum pump and vacuum controller CVC24 of Vakuubrand®. The pressure achieved for aqueous solutions were 80-65mbar.

Experimental set up

The liquid sample, with a volume between 50 and 500ml is put into a glass balloon. The balloon was attached to the rotavapor equipment and submersed in a water bath at 50ºC. The vacuum pump was connected and the pressure allowed to go down to 65mbars. To achieve a concentration of 1/3 of the initial volume, the sample needs between 30 and 60 minutes. The personal requirement is full time during the process, to avoid the possibility of precipitation or sample drying. The concentration factor is determined from the balloon weight before and after the process.

Ultracentrifugation Filtration

For the pre-concentration with the UCF process, UCF filters YM3 (MWCO 3kDa) from AMICON® were used in a Heraus® centrifuge model Megafuge 1.0, operated at 4000rpm.

Experimental set up

This second process is no other than the same used for purification, with the difference that the >MWCO fractions were summed and centrifuged again successively, as shown in the next schema (A-Figure 30):

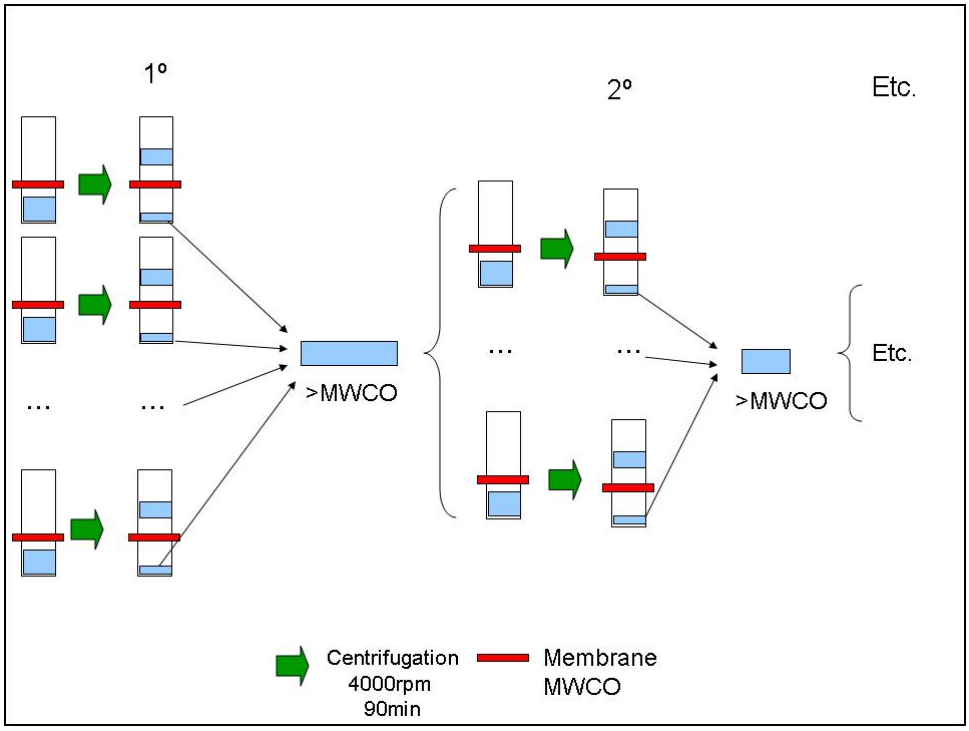

A-Figure 30: schematic representation of a pre-concentration process using ultracentrifugation-filtration.

The concentration factor can be easily calculated knowing the initial and final volume of the >MWCO fraction. The big advantages of this process are first that the concentration of the samples allows purification at the same time, avoiding the precipitation of material, as in the case of the rotavapor; in this way the method assures the conservation of the protein conformations. Second that the concentration achieved and final volumes are highly reproducible. Third that temperature and pressure are not changed drastically in the sample. Fourth that the surfaces the sample interacts with are smaller, avoiding loss of material on the walls. The disadvantage of this method is that the volume that could be processed is very low in comparison to the time required, and the cost per sample.

Comparison between the pre-concentration processes

Both processes are similar in time and personal requirements. The first observable difference is that a big amount of sample can be rotavapored, while the UCF allows only 15ml to be

concentrated in successive steps. Nevertheless this latter allows for the multi sample concentration, while in a rotavapor only one type of sample per time can be handled.

The main difference intrinsic to the two processes is that in a rotavapor proteins are subject to changes of pressure and temperature, which may affect the conformation of the proteins if not induces metallo-protein decomplexation too. In contrast in UCF, the samples are concentrated by a solvent displacement and no physical parameters other than the concentration are changed.

The excellent (>99%) repeatability of this latter process, the fact that it allows multiple sample treatment, and the low affection of the samples by physical changes, was enough to prefer it over the rotavapor for the pre-concentration processes.

Summary of pre-concentration methods

	Rotavapor Concentration	***Ultracentrifugation Filtration***
Initial Volume	20-25 ml	15 ml
Final Volume	7 ml	3 ml
Total Time	50 min	4.5 hours
Simultaneous Samples	1	12
Temperature	50ºC	room
Personal Requirement	100%	80%
Repeatability	75%	>99%

A-Table 11: Parameters to compare two concentration methods used to extract the SOM of the shell

AIX.6 Conservation Methods

Most of the proteins and peptides are known to be thermodynamically unstable. Increasing the temperature favors the displacement of the thermodynamic equilibrium and accelerates kinetic reactions. In liquid samples, the risk of bacterial and fungi growth and activity of protease enzymes is also favored at higher temperatures. To inhibit reactions that can

destroy or change the material, the samples, the standards and the blanks must be conserved. The used processes are described below.

Cooling and/or Freezing

The liquid samples and dry standards were put in a refrigerator at 10ºC, for short periods, or in the freezer at -4ºC, for conservation longer than a week.

Lyophylization

Purified and pre-concentrated samples were dried using a freeze dry process. For that the samples were frozen with liquid nitrogen, and put in the lyophylization chamber. For 50ml samples the lyophylization was achieved after 48hs. The matrix so obtained was conserved dry at -10ºC or in some cases the final product was rediluted in MilliQ water, aliquoted and conserved also at -4ºC.

Summary of Conservation Methods

	Refrigeration Cooling / Freezing	***Liofilization and Freezing***
Final Sample State	Liquid / Ice	Dry mass
Total Time	some hours	2 days
Simultaneous Samples	yes	yes
Temperature	10ºC / -4ºC	-74ºC
Personal Requirement	no	Very low
Repeatability	100%	100%
Conservation periods	Low to middle (weeks – months)	Middle to long (months – years)
Risks / disadvantages	Bacterial activity Protease activity	Loss of volatile compounds Loss of protein conformation

A-Table 12: parameters to compare two conservation methods used with the SOM extracts.

Appendix XI: Comparison of Two Different Extraction Processes

For the organic matrix extraction two types of solvent were tested. On one hand an acetic acid ammonium acetate buffer system (abbreviated AcH-buffer), with a constant pH around 4.75, and on the other hand a mild acid attack with HCl 15%. In this append, blanks of $CaCO_3$ treated with both techniques are tested for all the steps of the extraction process and compared.

AXI.1 Overview of both extraction processes

The extraction using a buffered system

A demineralization process was performed with p.a. AcH buffer (pH 4.75) in water solution. The advantage of this method is that the pH remains without drastic changes, around 5 during the process. There are two difficulties intrinsic to this solvent. On one hand the fact that the buffer system has many components makes difficult the theoretical idealization of the process. On the other hand, the presence of amino groups belonging to the buffer could interfere with the measurements of the protein content and identification, as for example with Bradford test and FTIR measurements which are sensible to amino-groups. A second difficulty of the AcH buffer system is to bring the final sample to a neutral pH. Because it is a buffered system, a large quantity of Na(OH) or Acetate must be added to move it from the buffer range.

The extraction using HCl

In the case of the demineralization using HCl, the system can not be buffered. Nevertheless the absence of ammonium groups avoids the possible interferences with further protein measurements. A second advantage is that this system, unlike buffered systems, can be easily approximated to pH 7 by neutralization with a base. Clearly the big disadvantage of this method is that the titration must be done very carefully, because the pH diminishes abruptly after the whole carbonate has reacted.

AXI.2 The System AcH-buffer

The concentration of the AcH-buffer vs. the volume of the sample

To find the most convenient concentration of the buffer solution in relation to the volume of the final sample, this experiment was carried out: one gram of shell sample was treated with different buffer concentrations, ranging from 0% (pure MilliQ water, pH 5.50) to 50% acetic acid buffer (pH 4.76). Higher concentrations were avoided to prevent the organic matrix damage and for difficulty of the further purification. The final volume was plotted (See A-Figure 31) against the concentration of the acid.

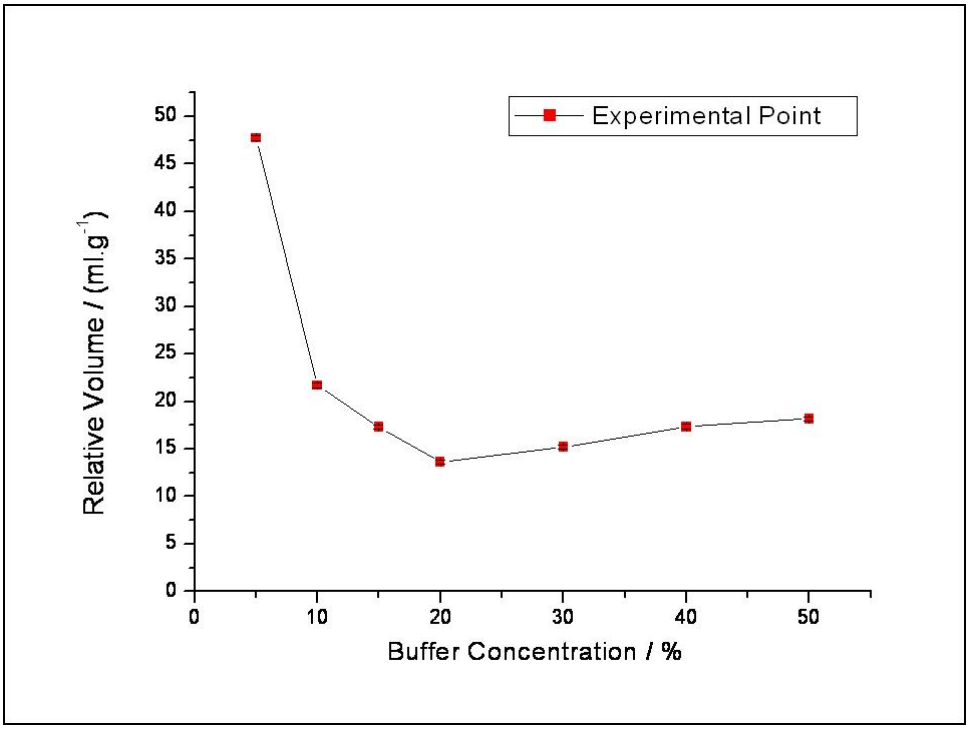

A-Figure 31: Demineralization of 1g of $CaCO_3$ with different concentrated AcH-Buffer. The graphic shows the Buffer concentration against the final volume of the sample. The error bars are smaller than the point.

Only water does not dissolve the sample completely, and the product obtained is a particulate suspended solution. To dissolve only one gram of sample at concentrations raging of 5% to 1% acetic buffer, from 50 to 200ml solvent are needed. The high dilution and therefore volumes need very long concentration processes. Comparing the volumes required to dissolve 1gr sample with buffer concentrations between 5% and 50%, the minimum

volume has been achieved with 20% buffer. The solution of AcH-buffer 15% was chosen to have less problems with the purification steps, since the volume obtained with concentrations between 15% and 50% did not differ substantially.

The pH behaviour

10ml MilliQ water were put inside a 50ml glass beaker, mounted in the titration apparatus under ice bath. The AcH-buffer was dropped until a pH 4.75 was reached. Ten grams of powdered $CaCO_3$ was suspended in the water solution and the mixture was well stirred for about two minutes. AcH-buffer 15% was dropped under continuously stirring until the whole carbonate had reacted. The results are plotted in A-Figure 32. As it can be seen from this graphic, the pH of the solution decreases slowly while the acid drops react with the mineral. When the complete decalcification is achieved, the system AcH-buffer reaches the equilibrium with a pH 5.4 and remains stable. Thanks to the buffer action, the pH of the solution remains during the whole decalcification over pH 5.

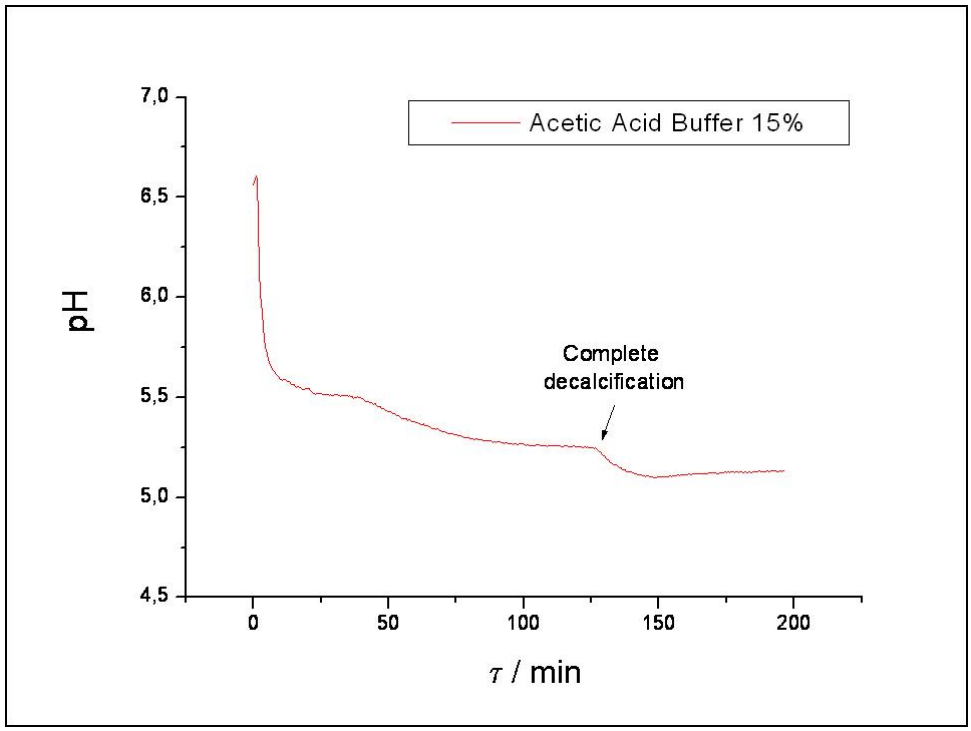

A-Figure 32: Time dependent pH found in the demineralization of 10g of $CaCO_3$ with AcH-buffer 15% (at 4 ºC). The arrow shows the point where the solid material is completely demineralized

The UV absorption

The absorption spectrum of acetic acid, ammonium acetate and AcH-buffer, of different procedence and purities, diluted at different concentrations were measured with the *lambda 2000* spectrometer. In each case 2ml sample were put in a SP glass cuvette, and measured between 190 and 300nm, against a MilliQ water reference. The absorption background was corrected measuring water against water. The speed of scanning was elected 120nm/min.

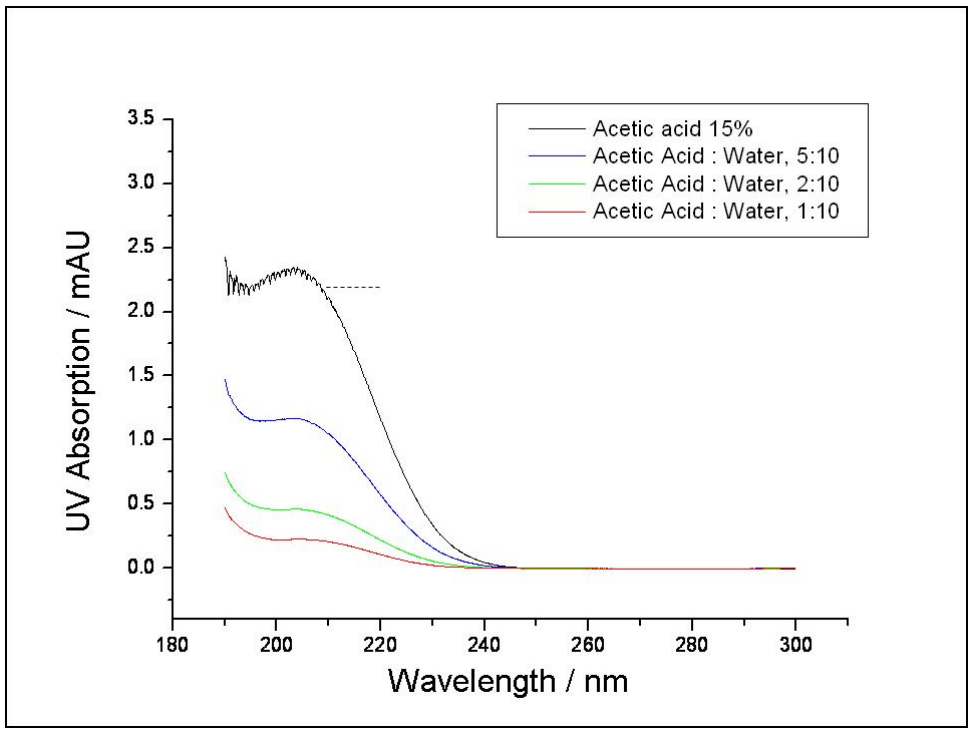

A-Figure 33: **UV absorption spectra of acetic acid in water at different concentrations.** Dashed line: saturation limit of the equipment.

MATERIAL: Acetic acid in milliQ water.
UV: Detection system: *Lamda2* spectrometer. Cuvettes: 3ml cuvettes SQ glass. Wavelength: 190-300nm. Scanning speed: 120nm/min. Reference: MilliQ water.

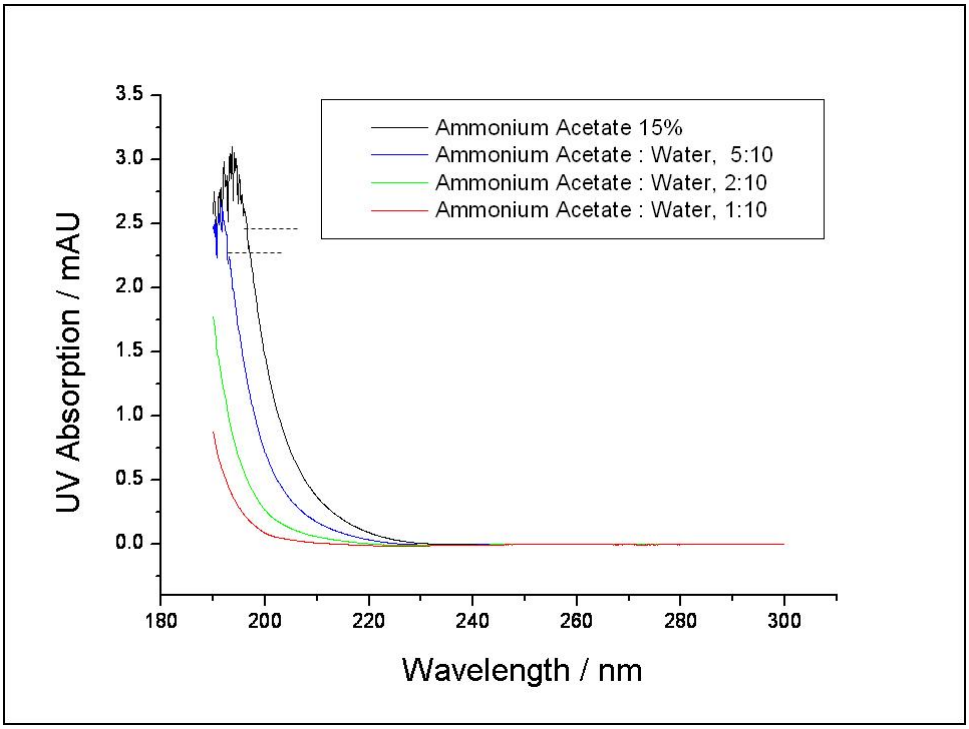

A-Figure 34: **UV absorption spectra of ammonium acetate in water at different concentrations**. Dashed line: saturation limit of the equipment.

MATERIAL: Ammonium acetate in milliQ water.
UV: Detection system: *Lamda2* spectrometer. Cuvettes: 3ml cuvettes SQ glass. Wavelength: 190-300nm. Scanning speed: 120nm/min. Reference: MilliQ water.

The analysis of the A-Figures 3 and 4 makes clear that the acetic acid has interference at low wavelengths, with an absorption maximum at 210nm. This effect was observed in high purity redistilled acid as well as p.a. acids, and may be an intrinsic signal of the acid. Acetate samples did not show this behavior. For AcH-buffer, the absorption spectrum is similar to that of the acetic acid. No interference is observed, for wavelengths ≥210nm, when the concentration of the AcH-buffer is around 10^{-6}%, with the detection limit of this technique.

From this analysis is concluded, first that the use of AcH-buffer for the demineralization implies that the sample must be very well purified after the solubilization, and second for all security to avoid interference signals it must be measured at wavelengths larger than 230nm.

The HPLC-UV analysis

The component solvents of the system AcH-buffer were analyzed by SEC, for concentrations between 15% and 10^{-4}%, detecting the UV absorption at 202nm (See A-Figure 35 to A-Figure 37).

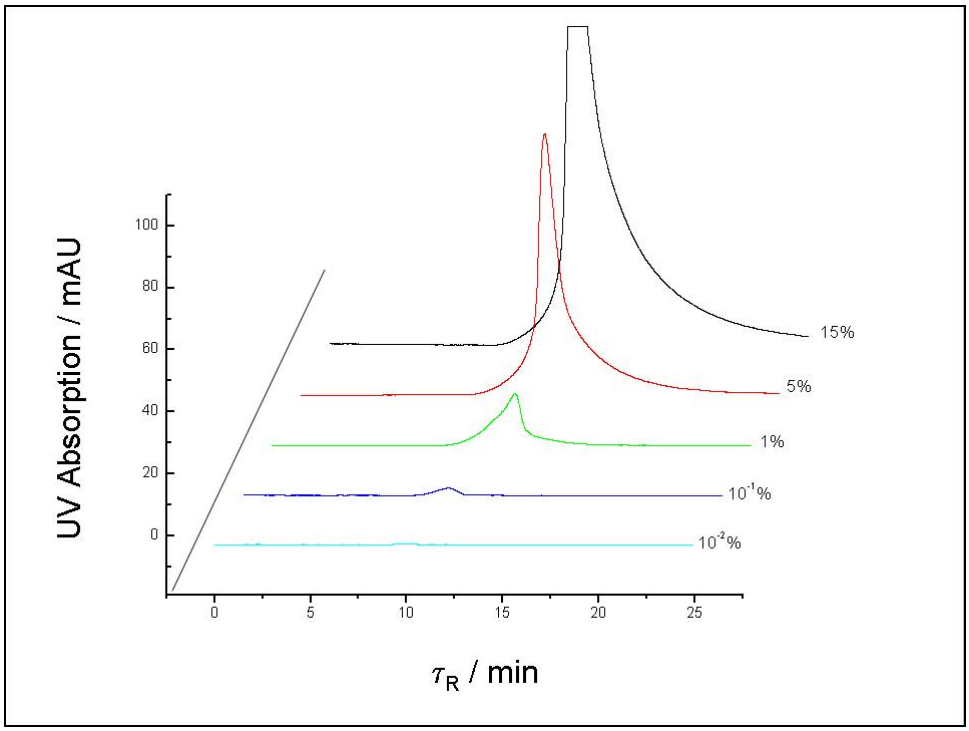

A-Figure 35: SE-HPLC-UV chromatogram showing ammonium acetate in water at different concentrations.

SE-HPLC-UV: Column: *Biosep S2000*. Mobile phase: MilliQ water. Flux: 0.8ml/min. Injection Volume: 100µl. Wavelength: 202nm

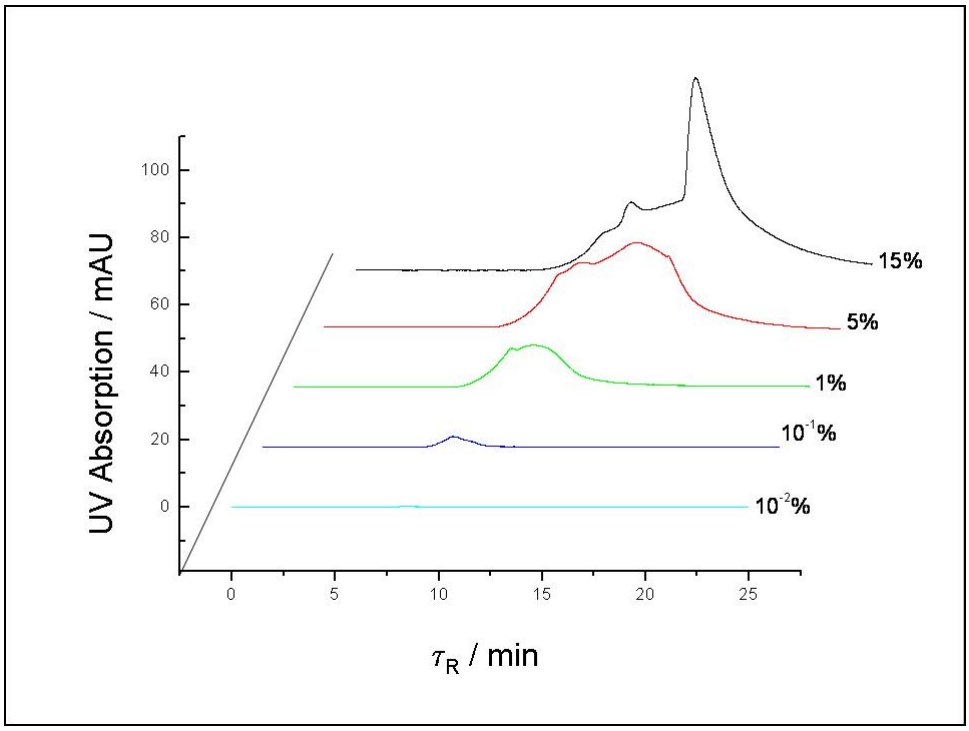

A-Figure 36: SE-HPLC-UV chromatogram showing acetic acid in water at different concentrations.

SE-HPLC-UV: Column: *Biosep S2000*. Mobile phase: MilliQ water. Flux: 0.8ml/min. Injection Volume: 100µl. Wavelength: 202nm

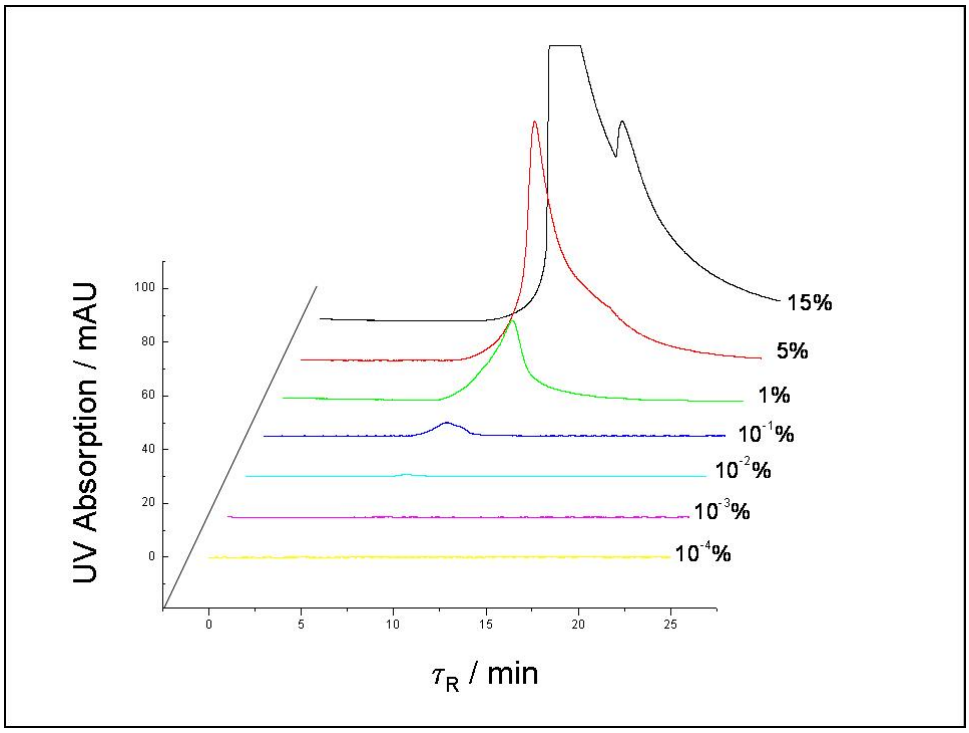

A-Figure 37: SE-HPLC-UV chromatogram showing AcH-buffer at different concentrations.

SE-HPLC-UV: Column: *Biosep S2000*. Mobile phase: MilliQ water. Flux: 0.8ml/min. Injection Volume: 100μl. Wavelength: 202nm

In this case, the wavelength 202nm was chosen to improve the detection of the solutes. The components of the acetic acid that could be observed as a peak in the UV analysis at 210nm (A-Figure 33) are separated in the *Biosep S2000* as two components that elute at 12 min and 15min approximately. From the analysis of the two components of the AcH-buffer, it is clear that the first of these peaks is present in the acetate solution and the other one in the acetic acid solution. They remain under the resolution of the instrument for concentrations under 10^{-3}%.

The Bradford Analysis

AcH-buffer samples, of concentrations from 15% to 10^{-6}% were measured by micro Bradford assay. The solvent has a positive interference that could be interpreted as protein presence. The results are shown in A-Figure 38. As a conclusion from the previous plot, AcH-buffer can be used without interferences for micro Bradford assays, when the buffer concentration is lower than 10^{-3}%.

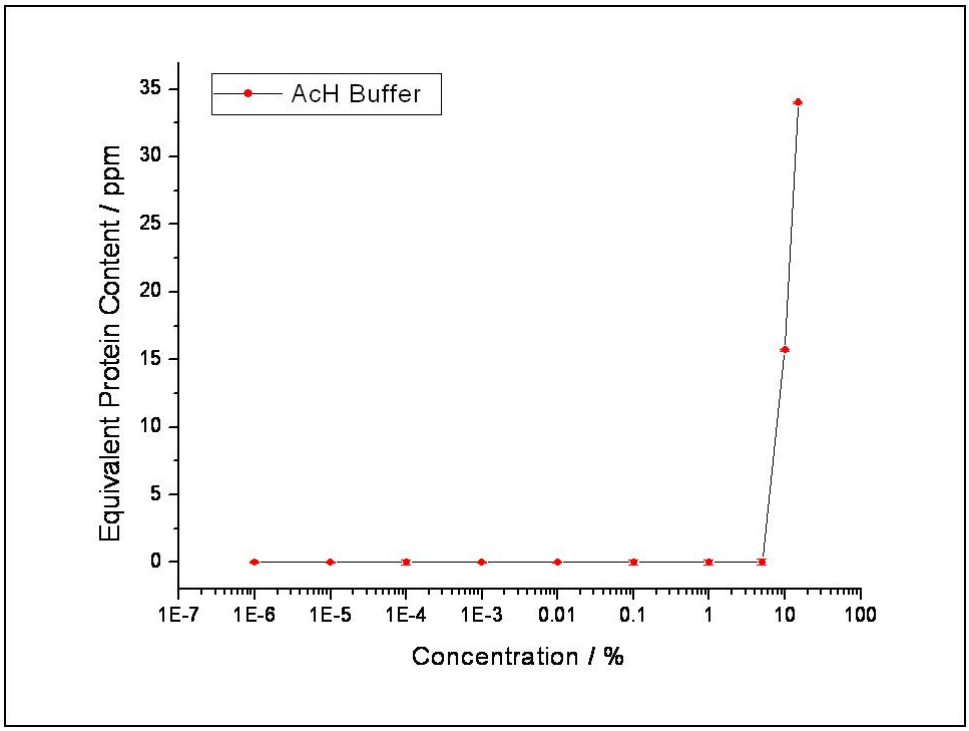

A-Figure 38: Bradford positive interference of the AcH-Buffer.

BRADFORD TEST: Method: micro analysis. Cuvettes: Semi-micro, 1.5ml, plastic. Wavelength: 595nm. Reference: MilliQ water Blank: Bradford of MilliQ water.

Purification by dialysis

A blank similar to that of real shell samples was developed demineralizing 10gr of $CaCO_3$ with 25ml AcH-buffer 15% as explained in “materials”. The mixture was dialyzed against MilliQ water, for two days, in a 3kDa membrane. The dialyzing water was changed each 8hs. Each change, the dialysis bag was opened and 1ml was sampled. The samples were analysed all together by HPLC-UV chromatography using the *Biosep S2000* column. The results are shown in A-Figure 39 and A-Figure 40.

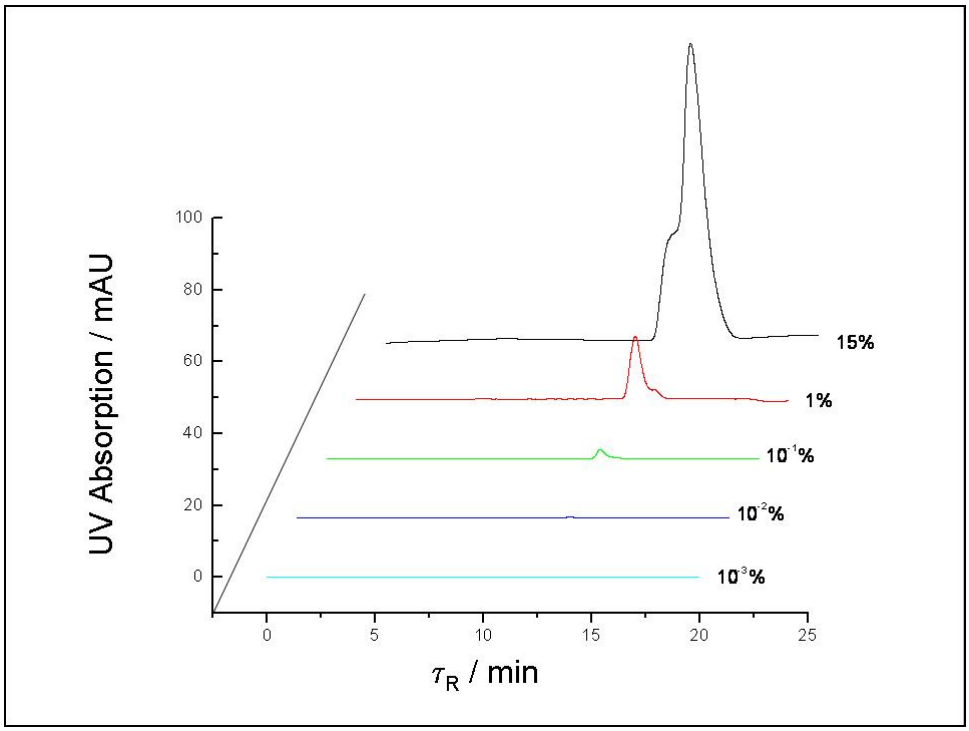

A-Figure 39: SE-HPLC--UV chromatogram showing the purification by dialysis of a $CaCO_3$ sample demineralized with AcH-buffer 15%.

MATERIAL: 10 g $CaCO_3$ demineralized with 25 ml AcH-buffer 15 %.
SEC: Column: *Biosep S2000*. Mobile phase: 20 mM Tris-HCl pH 7.4. Flux: 0.8 ml/min. Injection Volume: 100 µl. Wavelength: 220 nm.
DIALYSIS: 3 kDa MWCO Spectrapore 7 RC.regenerated cellulose, 25 ml sample against 500 ml MilliQ water. MilliQ water changed each 8 h

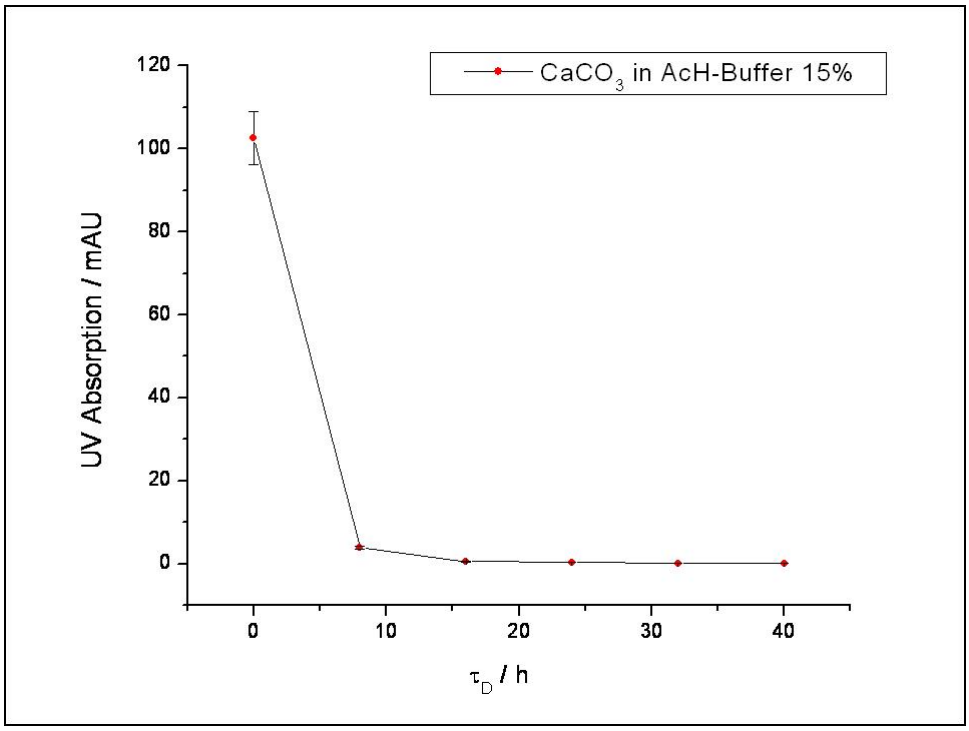

A-Figure 40: Maximum UV signal (around τ_R 13 min) from each chromatogram of **A-Figure 39**.

From the analysis of A-Figure 39 and A-Figure 40 is concluded that a $CaCO_3$ sample, demineralized with AcH-buffer 15%, measured at 220nm, shows a big UV absorption that may interfere with the protein detection. Nevertheless, under a dialysis process against MilliQ water, the sample absorption is lowered under the detection limit of the UV detector after three buffer changes.

This result could be also extended to shell samples, with the difference that these latter contain also organic matrix. The behavior of the dialysis membranes under demineralized $CaCO_3$ and protein presence was studied adding to the previous blank solution a mixture of BSA (66kDa), Citochrome C (12kDa), Cobalamine (1kDa) and Thiourea (77Da) in concentrations of 1mg/ml. The new mixture was dialyzed in the same process as the blanks. The results are shown in A-Figure 41. At the beginning of the dialysis, the citochrome and cobalamine samples are overlapped by the AcH-buffer peak. At the end of the dialysis only BSA and Citochrome are present. The acid and the proteins of smaller mass than the MWCO disappeared. It is to note that the concentration of both samples is lower than the initial one.

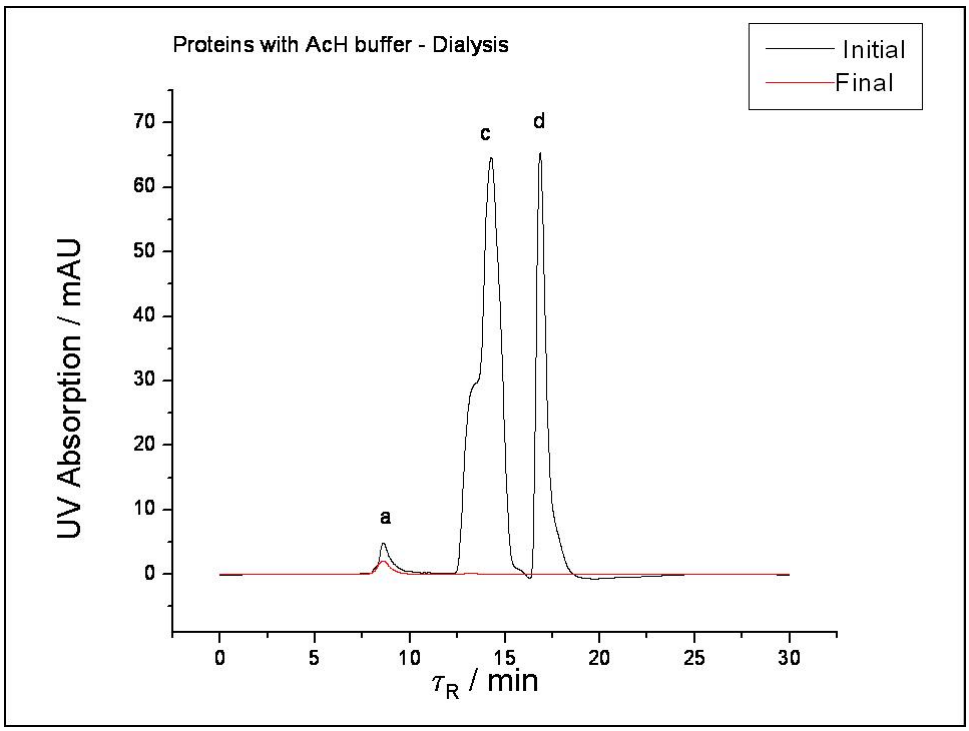

A-Figure 41: SE-HPLC-UV chromatogram showing the purification by dialysis of a protein mixture in $CaCO_3$ blank, demineralized with AcH-buffer 15 %.

MATERIAL: BSA (a), Citochrome C (b), Cobalamine (c) and Thiourea (d) at concentrations of 1mg/ml in a solution of $CaCO_3$ decarboxilated with AcH-buffer 15%. (Note: b is not observed because of the AcH interference).
UCF: 3000rpm × 90min, 6 cycles. The >3kDa fraction was refilled with MilliQ water.
SEC: Column: Biosep 2000. Mobile phase: Tris-HCl buffer pH 7.4. Flux: 0.8 ml/min. Injection Volumen: 50 μl. Wavelength: 220 nm.

Purification by UCF

The same blank used in the purification by dialysis (previous section) was purified by UCF. Samples with and without protein were filtrated in UCF tubes against MilliQ water, for six cycles of 90min each one. At the end of each cycle, the <3kDa fraction was collected and frozen. At the end of the six cycles, also the >3kDa was sampled. The samples were analyzed all together by HPLC-UV chromatography using the *Biosep S2000* column and Tris-HCL buffer pH 7.4 as mobile phase. The results for blanks with and without proteins are shown in A-Figure 44 and A-Figure 42 respectively.

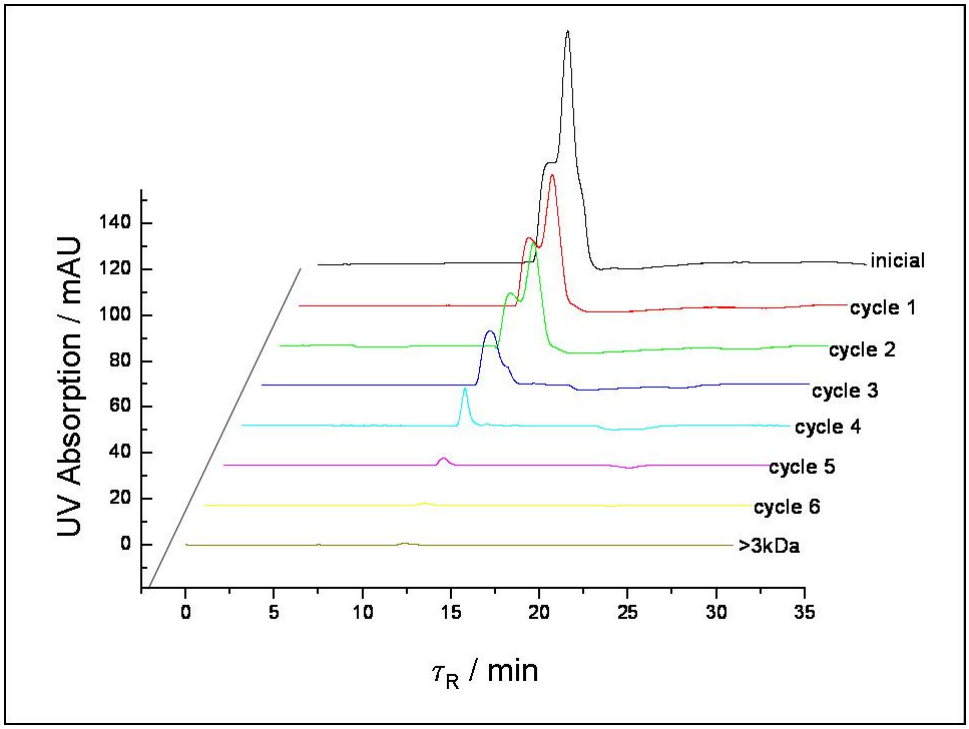

A-Figure 42: SE-HPLC-UV chromatogram showing the purification by UCF of a $CaCO_3$ blank demineralized with AcH-buffer 15 %.

MATERIAL: $CaCO_3$ decarboxilated with AcH-buffer 15 %.
UCF: 3000 rpm × 90 min, 6 cycles. The >3kDa fraction was refilled with MilliQ water.
SEC: Column: Biosep 2000. Mobile phase: Tris-HCl buffer pH 7.4. Flux: 0.8 ml/min. Injection Volumen: 50 µl. Wavelength: 220 nm.

As observed from A-Figure 42 and A-Figure 43 the purification of an AcH-buffer demineralized $CaCO_3$ blank by UCF by the sixth cycle is almost achieved. In the fraction >3kDa only a low trace of AcH-buffer is visible at this wavelength.

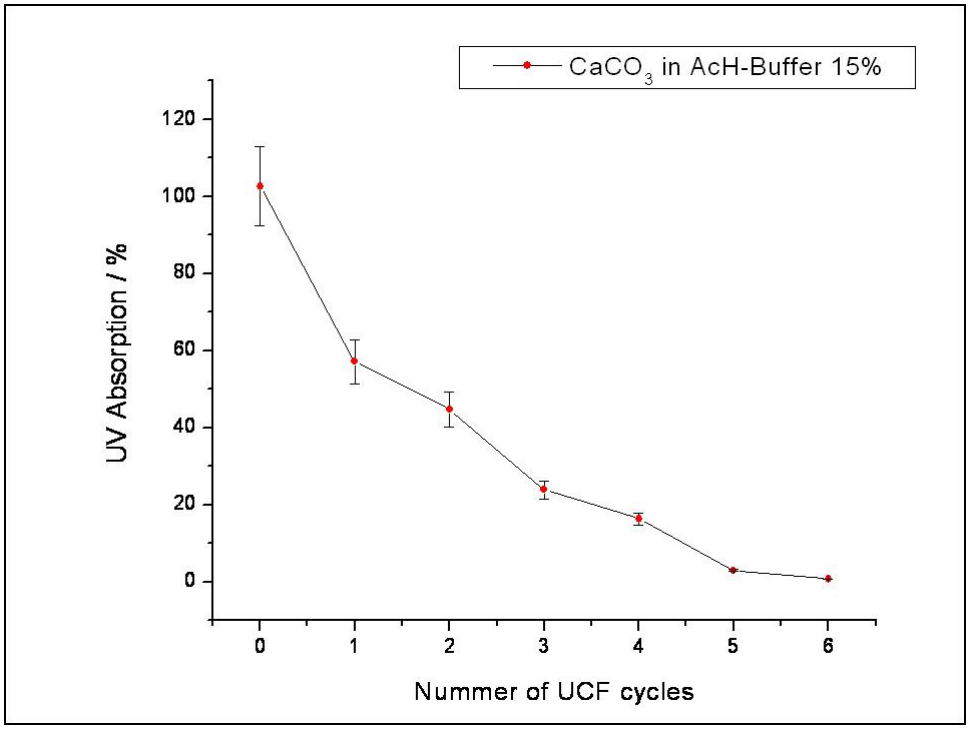

A-Figure 43: Maximum UV signal (around τ_R 13 min) from each chromatogram of A-Figure 42.

When proteins are added to a decarboxilated mixture of $CaCO_3$ with AcH-buffer, the presence of the solvent peaks interfere with the measurement. Clear is for example the case for Citochrome and Cobalamine, which appear at the beginning covered under the AcH-buffer peaks. After the six cycles of ultrafiltration with MilliQ water, BSA and Citochrome are found almost completely purified from buffer and small proteins. Signals of Thiourea and Cobalamine are very low. The big advantage of this method is that the proteins present in the fraction >3kDa are concentrated about 3 times of the initial value, as mentioned before.

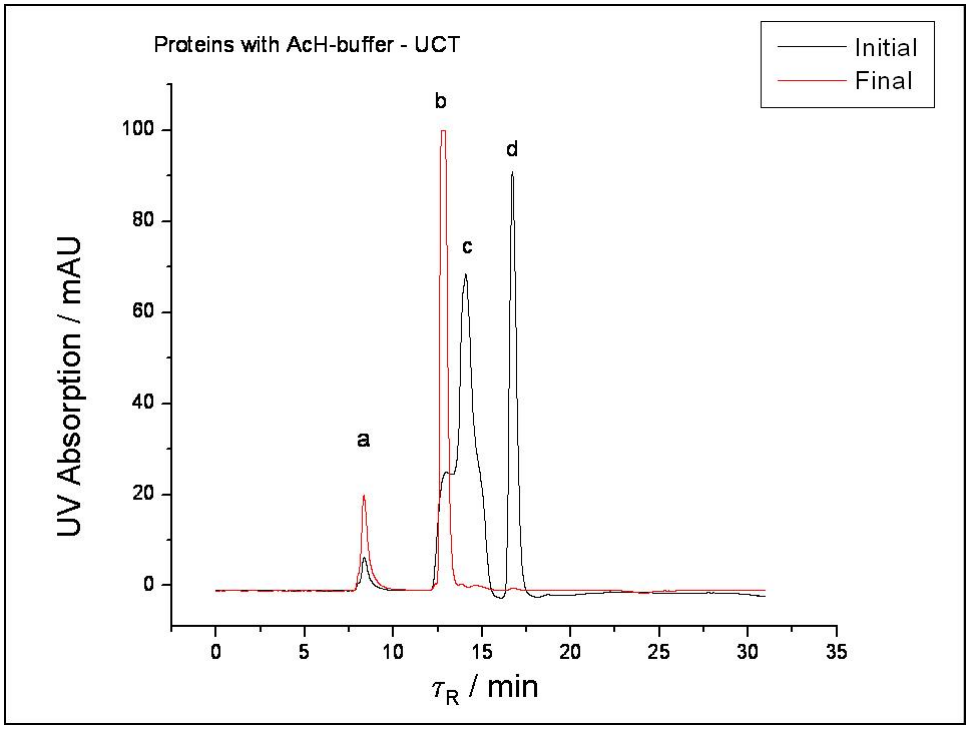

A-Figure 44: SE-HPCL-UV chromatogram showing the purification by UCF of a protein mixture in $CaCO_3$ blank demineralized with AcH-buffer 15 %.

MATERIAL: BSA (a), Citochrome C (b), Cobalamine (c) and Thiourea (d) at concentrations of 1mg/ml in a solution of $CaCO_3$ decarboxilated with AcH-buffer 15%.
UCF: 3000 rpm × 90 min, 6 cycles. The >3kDa fraction was refilled with MilliQ water, and the <3kDa fraction sampled and analyzed.
SEC: Column: *Biosep S2000*. Mobile phase: Tris-HCl buffer pH 7.4. Flux: 0.8 ml/min. Injection Volumen: 50 μl. Wavelength: 220 nm.

Overview for the system AcH-buffer

The conclusion of this experience is that the samples treated with AcH-buffer need at least 40 hours dialysis or six cycles of purification by UCF to eliminate completely the buffer. The second process is also good to concentrate the fraction of proteins bigger than the membrane cut off. BSA and Citochrome were concentrated about three times of the initial concentration. The fact that BSA and Citochrome did never appear in the <3kDa fraction, for both methods, demonstrates no big membrane damage for the system AcH-buffer.

AXI.3 System HCl-Water

Concentration of HCl vs. the volume of the sample

One gram shell can be dissolved with approximately 7 g of HCl 37 % in a quick reaction. Of course, as a strong acid, the pH of the solution if the HCL is 37% concentrated will at least affect the conformation of the proteins if not destruct them totally. A more convenient concentration of HCl was calculated from the theoretical quantity needed to neutralize 100 g of $CaCO_3$, from the relation of the molar masses: 166 ml of HCl 37 % must be diluted in a volume of water that allows a pH approximately around 4.

To achieve this there are two ways, one is to dilute the 166 ml in water with an initial concentration of 10^{-4}M. This is theoretically possible, but implies a huge volume for the 166 ml needed. A second possibility is to suspend the sample in enough water and add HCl in small drops (10-50 μl), so that the concentration of HCl for one drop of acid in the whole sample is around 10^{-5} M or 10^{-4} M, and wait that calcium carbonate neutralizes the acid, and the equilibrium is again reached to add the next drop. That was the method chosen. In this case, for 100 g $CaCO_3$, diluted in 100ml water, the pH is maintained successfully about 4 adding 50 μl drops of HCl, with a final volume of approximately 300 ml.

Sample quantity dependence

Unlike the buffered system, for the HCl extraction process there is a difference in how the acid affects the sample with the size of the sample. For this reason two procedures were implemented.

Small amount samples (1g)

In this case the sample volume, small in comparison with the volume of a drop of HCl, makes difficult the pH control. To avoid the protein destruction by low pH, 1gr of sample was diluted in 10ml HCl 10^{-5} N, and HCl 15 % was added in 5 μl steps with an automatic titrator, pumping directly into the solution. The pH was controlled during the process (pH>4). The process was done at 4 ºC.

Large amount samples (10 to 100g)

The mass of shell was diluted in an equal mass of HCl 10^{-5} N. HCl 15 % was dropped direct in the solution, at low fluxes. The pH and temperature were controlled during the whole process (pH>4, 4 ºC). Each time 200ml of solution were obtained, the sample was let to sediment. The soluble fraction was separated and brought to pH 7 with NaOH 1 M. NaN_3 0.01 % was added and the fraction was stored at 4 ºC. The rest (not yet demineralised fraction) was again diluted in HCl 10^{-5} N and the process repeated until all material was decalcified.

The pH behaviour

Controlling the pH of a $CaCO_3$-HCl solution in the correct manner so that it remains always above 4 is not easy. When the amount of $CaCO_3$ that has no yet reacted is very low, the process must be slow or the pH equilibrium is strongly affected (See A-Figure 45). Other trick to avoid this effect is to decant the semi demineralized sample, store the liquid, and restart the process with the rest of the $CaCO_3$.

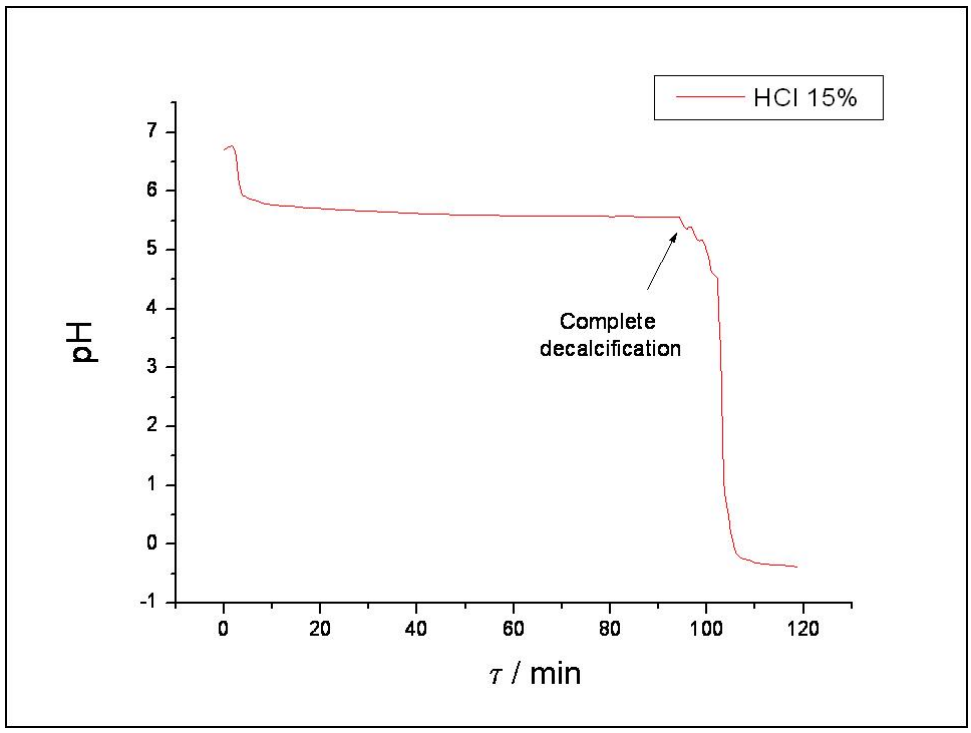

A-Figure 45: Time dependent pH found in the demineralization of 10g of $CaCO_3$ with HCl 15% (at 4 ºC). The arrow shows the point where the solid material is completely demineralized.

The UV absorption

The absorption spectrum of HCl diluted at different concentrations was measured with the *Lambda 2* spectrometer (A-Figure 46). In each case 2ml sample were put in a SQ quartz cuvette, and measured between 190 and 300nm, against a MilliQ water reference. The absorption background was corrected measuring water against water. The speed was 1nm/sec.

From the analysis of the A-Figure 46 is concluded, first that the HCl has a sharp UV edge, that shifts to <200nm wavelengths for concentrations $<10^{-2}$ %. Second, as direct consequence of the first observation, that the use of the system of HCl is better than the system AcH-buffer for measuring UV absorption without interferences in the 200-240nm range.

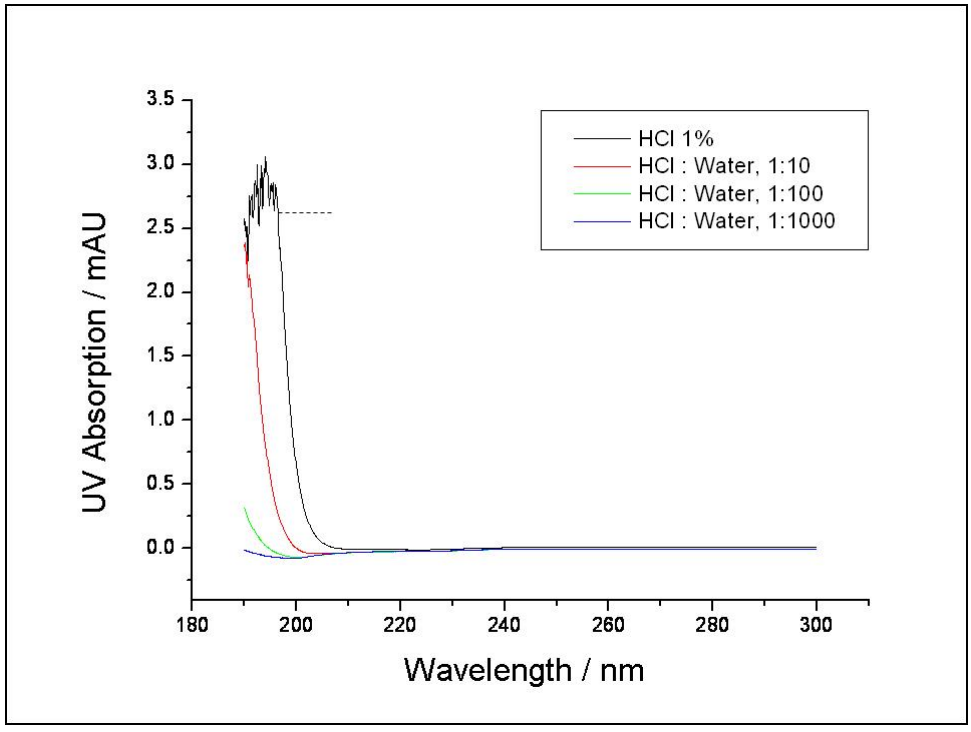

A-Figure 46: UV absorption spectra showing the behavior of the HCl solvents at different concentrations. Dashed line: saturation limit of the equipment.

MATERIAL: HCl in milliQ water.
UV: Detection system: *Lamda2* spectrometer, Cuvettes: 3ml cuvettes SQ glass, Wavelength: 190-300nm, Scanning speed: 1nm/sec, Reference: MilliQ water.

The HPLC-UV analysis

The HCl solvents were analyzed by SEC with the *Biosep S2000* column for concentrations between 15% and 10^{-6}%, detecting the absorption at 210 nm (See A-Figure 47). The components of the hydrochloric acid that could be observed as a peak in the UV analysis at 210 nm are separated in the *Biosep* as three components that elute at 8min, and 14min. At concentrations below 10-4% these peaks are lower than 0.25 mAU of the absorption range.

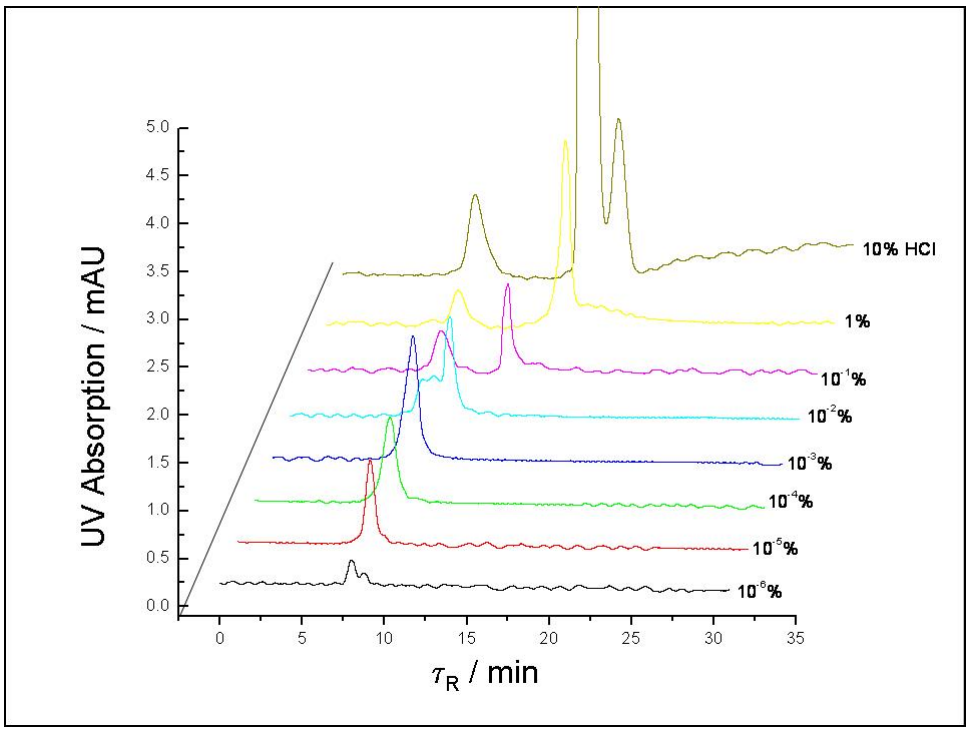

A-Figure 47: SE-HPCL-UV chromatogram showing HCl at different concentrations.

MATERIAL: HCl in milliQ water at concentrations: 15% to 10^{-4}%
SE-HPLC-UV: Column: *Biosep S2000*. Mobile Phase: MilliQ water. Flux: 0.8ml/min. Injection Volumen: 100µl. Wavelength: 210nm.

The Bradford Analysis

HCl samples, of concentrations from 10 % to 10^{-6} % were measured by micro Bradford assay. The solvent has a negative interference which could be misinterpreted as a lower protein content. The results are shown in A-Figure 48. From this graphic it is clear that the HCl has no more disturbing interferences for concentrations equal to 10^{-5}%, which is two orders of magnitude higher than with the AcH-buffer. It means that for Bradford analysis the sample must be very well purified.

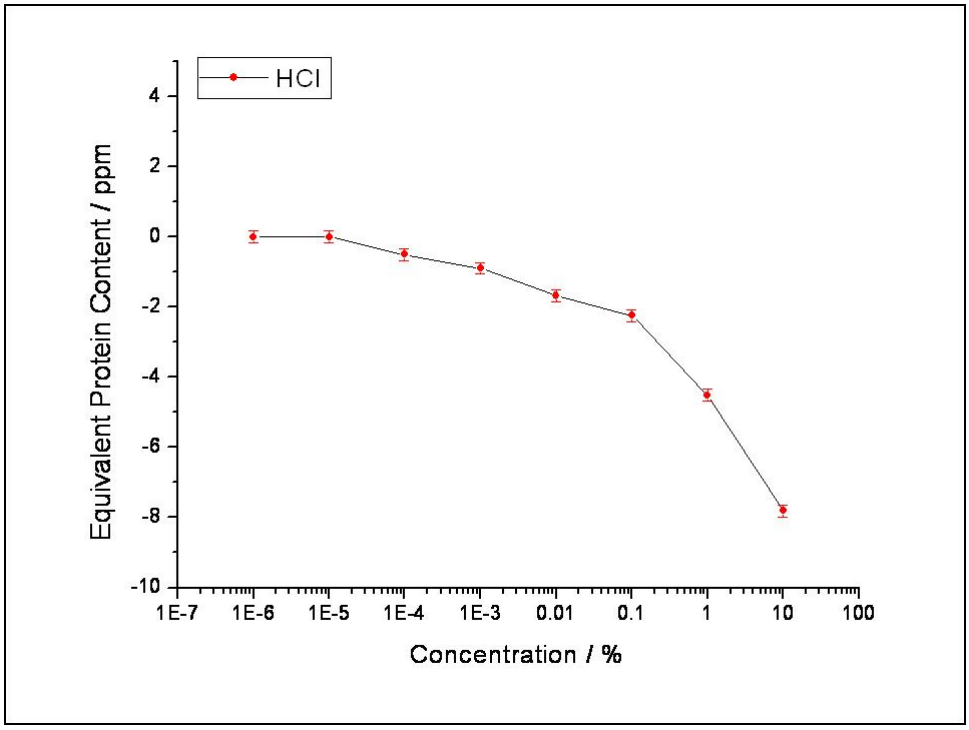

A-Figure 48: Bradford negative interference from the HCl.

MATERIAL: HCl 10% to 10^{-6}%
UV: Wavelength: 595nm. Method: Bradford micro analysis. Cuvettes: Semi-micro, 1.5ml, plastic.. Io Reference: MilliQ water. Blank: Bradford of MilliQ water

The purification by dialysis

A blank similar to that of real shell samples was developed demineralizing 10gr of $CaCO_3$ with HCl 15%. After the total reaction, the solution was neutralized with Na(OH) 1M. A mixture of BSA (66kDa), Citochrome (12kDa), Cobalamine (1kDa) and Thiourea (77Da) was added to the blank solution in concentrations of 1mg/ml. Samples with and without protein were dialyzed against MilliQ water, for two days, in a 3kDa membrane. The dialyzing water was changed each 8hs. Each, the dialysis bag was opened and 1ml was sampled and frozen. The samples were analyzed all together by HPLC-UV chromatography using the Biosep 2000 column and Tris-HCl buffer pH 7.4 as mobile phase. The results for blanks with and without proteins are shown in A-Figure 19 and 21 respectively.

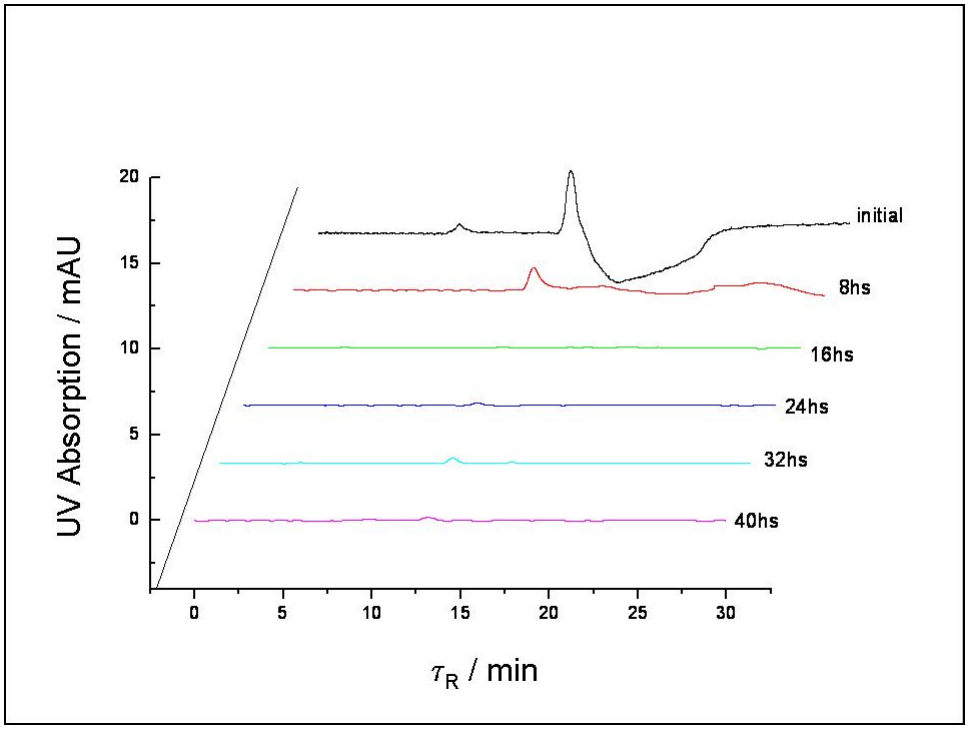

A-Figure 49: SE-HPLC-UV chromatogram showing the purification by dialysis of the $CaCO_3$ blank decarboxilated with HCl 15%.

MATERIAL: $CaCO_3$ decarboxilated with HCl 15%.
DIALYSIS: 3 kDa MWCO Spectrapore 7 RC.regenerated cellulose, 25 ml sample against 500 ml MilliQ water. MilliQ water changed each 8 h
SEC-UV: Column: Biosep 2000. Mobile phase: Tris-HCl buffer pH 7.4. Flux: 0.8ml/min. Injection Volumen: 50µl. Wavelength: 220nm.

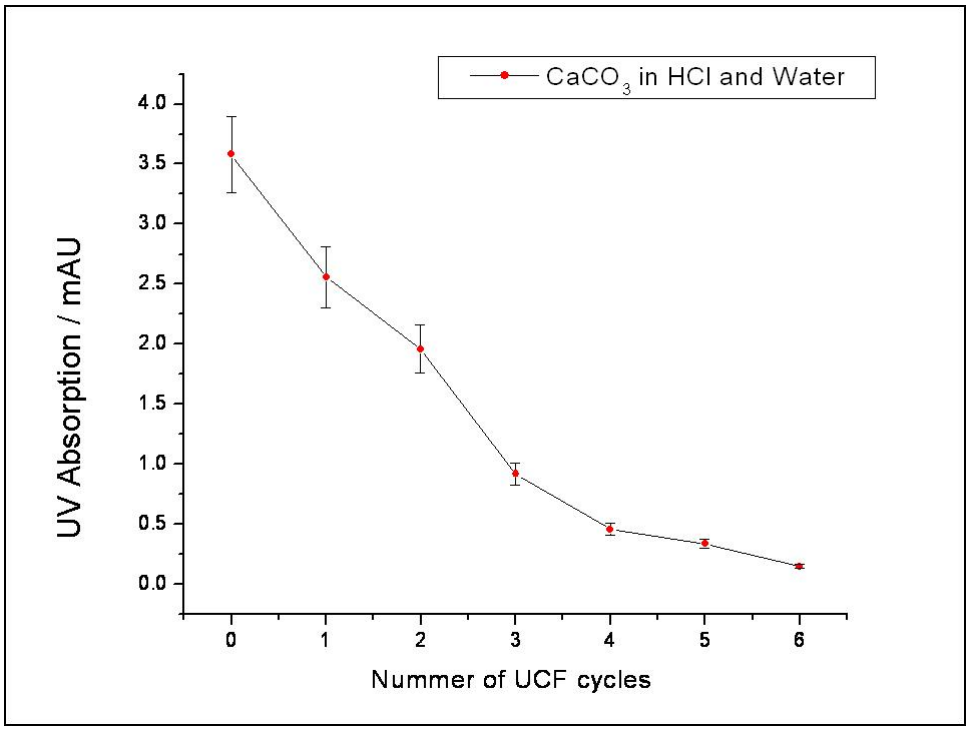

A-Figure 50: Elution profile by SEC. Maximal UV signal for each chromatogram of A-Figure 49.

As observed in A-Figure 50, the blank of $CaCO_3$ demineralized with the HCl, measured at 220nm, shows a very small UV absorption (lower than the 4%) at the beginning of the experiment. The purification with MilliQ water by dialysis is for the third cycle almost achieved.

When proteins (A-Figure 51) are added to a sample of HCl decarboxilated $CaCO_3$, the presence of the solvent peaks do not interfere with the measurement. After 40 hours of dialysis against MilliQ water, no more signals of small proteins are visible. The fraction >3kDa shows only the strong presence of BSA and Citochrome C, and traces of cobalamine.

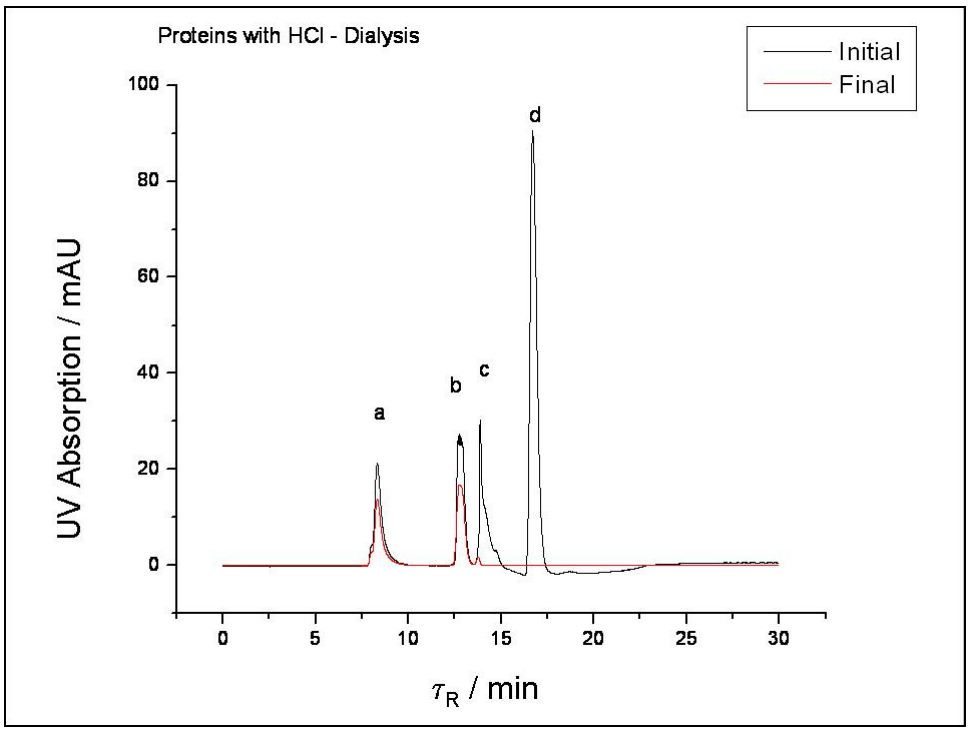

A-Figure 51: SE-HPLC-UV chromatogram showing the purification by dialysis of a protein mixture in $CaCO_3$ blank demineralization with HCl 15%.

MATERIAL: BSA (a), Citochrome (b) Cobalamine (c) and Thiourea (d) at concentrations of 1mg/ml in a solution of $CaCO_3$ decarboxilated with HCl 15 %.
DIALYSIS: Spectrapor 7 RC. MWCO 3.5 kDa.
SEC-UV: Column: Biosep 2000. Mobile Phase: Tris-HCl buffer pH 7.4. Flux: 0.8 ml/min. Injection Volumen: 50 µl. Wavelength: 220 nm.

The purification by UCF

The same blanks used for the purification by dialysis were purificated by UCF. Samples with and without protein were filtrated in UCF against MilliQ water, for six cycles. At the end of each cycle, the <3kDa fraction was collected and frozen. At the end of the six cycles, also the >3kDa was sampled. The samples were analyzed all together by HPLC-UV chromatography using the *Biosep S2000* column and Tris-HCL buffer pH 7.4 as mobile phase. The results for blanks with and without proteins are shown in A-Figure 52 and A-Figure 54 respectively.

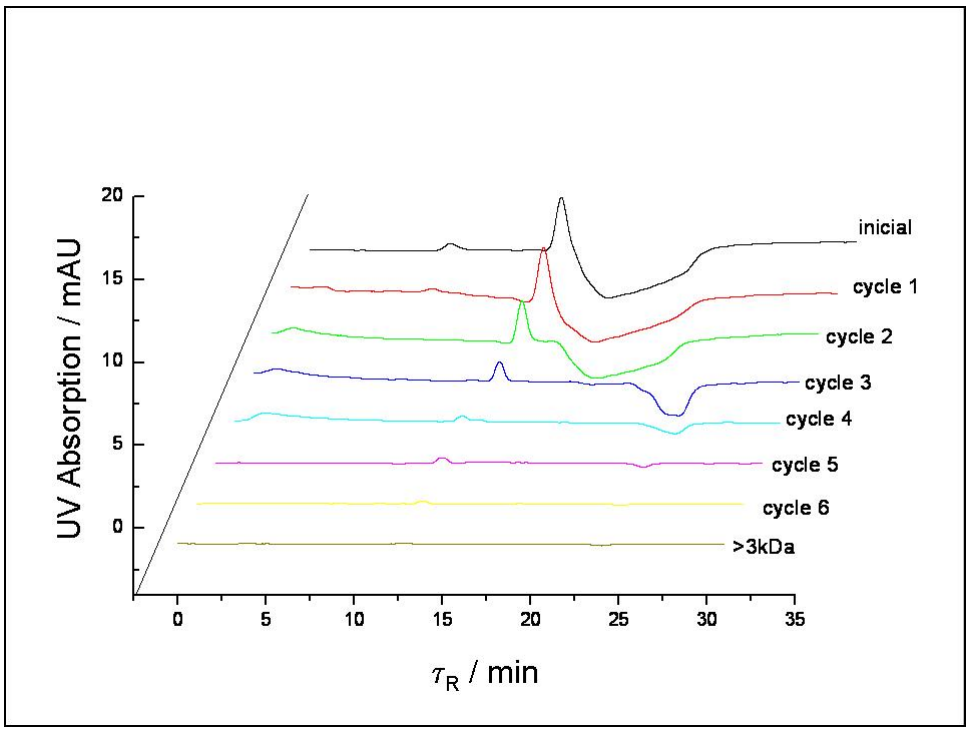

A-Figure 52: SE-HPLC-UV chromatogram showing the purification by UCF of the $CaCO_3$ blank demineralized with HCl 15%.

MATERIAL: $CaCO_3$ demineralized with HCl 15%.
UCF: 3000rpm × 90min, 6 cycles. The >3kDa fraction was refilled with MilliQ water.
SEC-UV: Column: *Biosep S2000*. Mobile Phase: Tris-HCl buffer pH 7.4. Flux: 0.8 ml/min. Injection Volumen: 50 μl. Wavelength: 220nm.

As observed in A-Figure 52 and A-Figure 53, the blank of $CaCO_3$ demineralized with the HCl, measured at 220nm, shows a very small UV absorption (lower than the 5%). The purification with MilliQ water by UCF is for the fifth cycle almost achieved.

When proteins (A-Figure 54) are added to a HCl demineralized $CaCO_3$ sample, after five cycles of UCF with milliQ water, no more signals of small proteins are visible. The fraction >3kDa shows only the presence of BSA and Citochrome C.

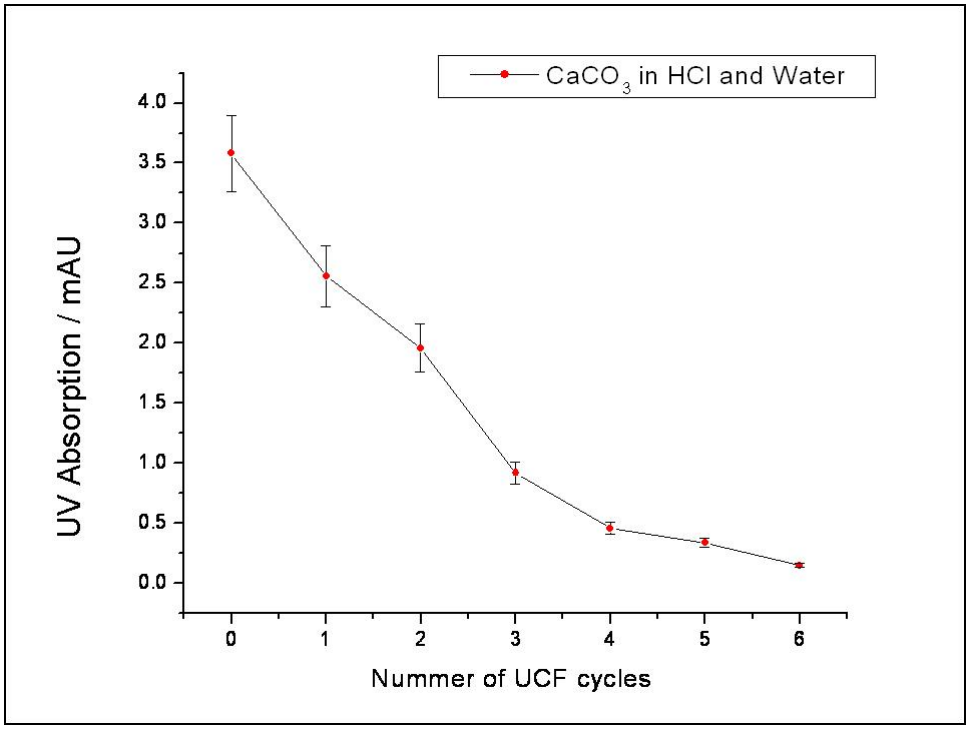

A-Figure 53: Maximum UV absorption (around τ_R 13min) from each chromatogram of A-Figure 52.

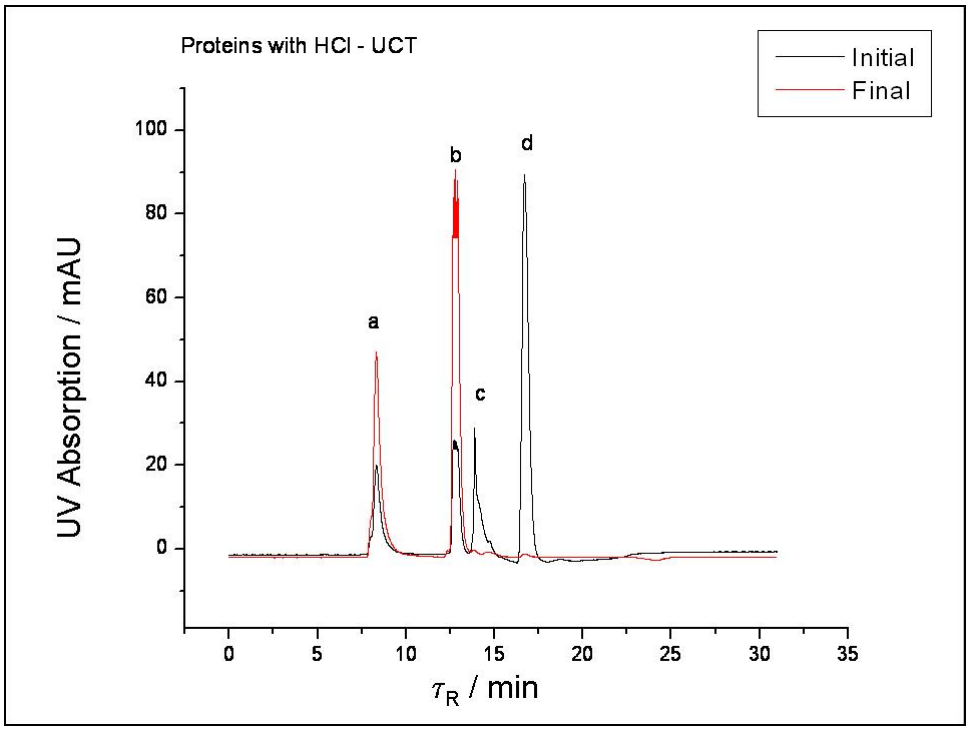

A-Figure 54: Purification of a protein mixture in CaCO3 blank decarboxilated with AcH-buffer 15% by UCF. Elution profile by SEC-UV.

MATERIAL: BSA (a), Citochrome C (b) Cobalamine (c) and Thiourea (d) at concentrations of 1mg/ml in a solution of $CaCO_3$ decarboxilated with HCl 15%.
UCF: 3000 rpm × 90 min, 6 cycles. The >3kDa fraction was refilled with milliQ water.
SEC-UV: Column: Biosep 2000. Mobile Phase: Tris-HCl buffer pH 7.4. Flux: 0.8ml/min. Injection Volume: 50µl. Wavelength: 220nm.

Summary for the system HCl

The conclusion of this experience is that the samples treated with HCL need at least four cycles with UCF or 16 h dialysis to be purified almost completely from the acid. The former process for the system HCl is also well suited to concentrate the fraction of proteins bigger than the membrane cut off. BSA and Citochrome C were concentrated about three times over the initial concentration, while by dialysis there were a loss of about 35 % of the sample.

AXI.4 Conclusion

Two extraction methods were evaluated. The extraction analysis using a buffered system of AcH-buffer, facilitates the posterior by INAA because it does not generate an important background for this technique. Nevertheless, the presence of the amino groups may interfere with the organic measurements, as for example the protein quantification. In addition, acetic acid as well as acetate, the components of the buffer, have a strong UV absorption interfering with HPLC/UV and UV measurements in the range of interest. For this reason, following the demineralization, the solution must be purified. Two methods of purification, dialysis and ultracentrifugation-filtration have been checked. At least 40h dialysis or six cycles of purification are needed to diminish the interfering signal to a background level.

In comparison to the buffered system, the HCl-water system has the disadvantage that the pH can change abruptly, destroying the shell proteins. Therefore the demineralization must be done very carefully. Nevertheless, the system HCl has many advantages over the buffered system. HCl has very low UV absorptions and because the HCl solution has no amino groups, does not interfere positively in protein quantification tests or FTIR analyses. In addition it needs only 16h of dialysis or four cycles of UCF to be purified almost completely.

Comparing the purification methods, both were applied satisfactorily to HCl and AcH-buffer systems. The UCF method has the big advantage that it increases the concentration of the samples in the range >MWCO, while the dialysis needs an extra concentration step. Nevertheless this last method is cheaper, requires less work and almost no attention, and allows preparing samples of very different volume (from 10ml to 500ml), maintaining the purification parameters constant between small and big samples. These three reasons made this method the choice for the purification.

Appendix XII: Evaluation of the Extraction Process with HCl 15% in *Cypreae tigris* Average Material

To evaluate the extraction process, only the “large amount” methodology was investigated because it permits to extract measurable quantities of organic matrix, even if some fraction is lost in the process. The “small amount” methodology was evaluated only for pH behaviour of the decalcification step.

A 50gr average material sample of *Cypraea tigris* powdered shells was demineralized with HCl 15%, purified by dialysis and ultracentrifugation filtration and concentrated by lyophilization. The components of the organic matrix extracted were separated using GE and SE-HPLC, and analyzed by protein content, UV absorption, molecular mass and trace elements content using diverse methods.

AXII.1 Decalcification

The pH and temperature of the solutions were measured using an *INOLAB*® pH-meter with a *WTW SenTix81* electrode. The equipment was calibrated before each measurement with pH 4.01 and a pH 6.58 calibrated solutions (Schott®) at room temperature. The equipment was coupled with an acquisition data program, *Achat-II*® version 2.0, where pH and temperature are registered on line against time. The pH value was acquired each 5sec.

Using the methodology described for “large” and “small” amounts of material, the pH was maintained effectively above 4 for average material shell samples. The complete decalcification in both cases was done between 4 and 8ºC and achieved after one hour and 20 minutes, for 50gr and 1gr samples respectively. It is to note that this latter must be done very carefully.

AXII.2 Pre-concentration

After pH control of the demineralization, the concentration step is the second difficult point of the organic matrix extraction in shell samples. A concentration step is generally not required for “small amount” samples. In this case the final volume (25ml to 35ml) can be dialyzed or lyophilized without problems. The “large amount” brings a final volume of around 500ml. This quantity is almost unworkable, for a laboratory directed to trace element investigations. Rotating evaporation and ultracentrifugation-filtration were tested as concentration methods. For the first one, the 500ml samples are ok and the material can easily be concentrated. Nevertheless during the process, the pH, the temperature and the pressure of the samples are drastically changed. In addition, the proteins were observed to stick to the glass parts, and then were very difficult to recover. The UCF applied as concentration method, could be used for “small amounts” samples. For this process, one UCF tube (15ml) is used for each 1gr sample (25ml), and the process is repeated twice or three times to achieve final volumes around 5ml. For the “big amount” (500ml) samples 12 tubes (maximum capacity of the centrifuge) were use simultaneously, in two or three centrifugation rounds, to achieve a final volume of 100ml. More concentration produces difficulties in the sample recovery, because organic matrix remains attached to the plastic walls and the membrane.

It was concluded from the research and comparison of both available methods, that the risk to loss or affect the proteins are too big. It was decided to avoid a pre-concentration step using bigger dialysis membranes. The SPECTRAPORE C7, of 5cm flat width, allows to process small as well as big amounts samples in the same way, and the final concentration is then achieved through lyophylization.

AXII.3 Purification

Ultracentrifugation-filtration and dialysis have shown to be excellent methods to purify the samples of the inorganic solvents and salts. The SOM obtained from the preparation of 50g of average material shell is shown in A-Figure 55. As can be observed from this plot, both methods give the same results after HPLC separation and protein quantification analysis, demonstrating that neither dialysis nor UCF produce organic contamination or losses of material. The only parameter that favors dialysis against the UCF, especially in case of the

"large amount" samples, is that this latter takes more time and work than the first method. To purify 500ml of solution by dialysis, using membranes of 5cm flat width, about 50cm membrane is used and 5 L MilliQ water are needed and changed each 8 hours, during two days. For the same solution quantity, using UCF tubes, about 30 UCF tubes of 15ml are needed. In addition the *Rotamac* centrifuge rotor (used in this work) allows only 12 tubes per time. The purification by UCF takes completely about 18hours, against the 2 days of dialysis, with almost not work needed. The final decision, made over these two reasons, was to use dialysis as purification step.

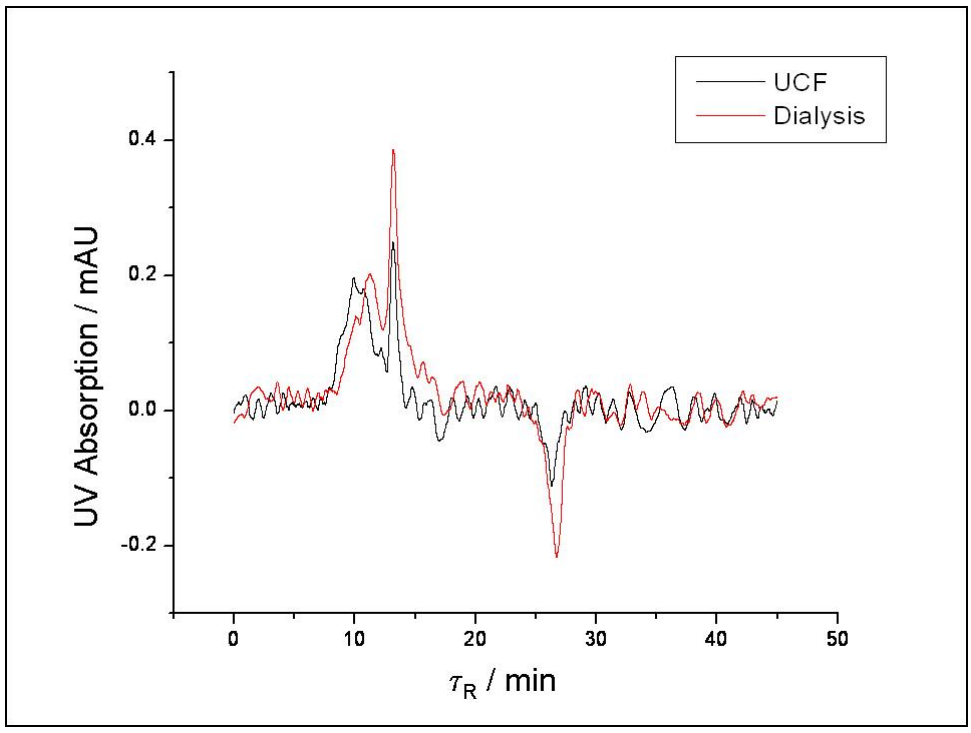

A-Figure 55: SE-HPLC-UV chromatogram showing the SOM extracted from *C. tigris* shells using dialysis or UCF as purification method.

MATERIAL: SOM extracted from 50g average material of *C. tigris* shells, decarboxiled with HCl 15%, rediluted in MilliQ Water.
UCF: 15ml 3kDa Amicon® UCF tubes, centrifuged at 3000rpm during 60min. Purification with MilliQ water in 6 cycles.
DIALYSIS: 500ml sample in 3kDa MWCO dialysis membrane Spectrapore7 against 5lt MilliQ water, changing buffer each 12h, during two days.
SEC: column: *Biosep S 2000*, Mobile Phase: 20mM Tris-HCL pH 7.4, flux: 0.8ml/min, wavelength: 220nm.

AXII.4 Conservation

After the dialysis, the samples have shown to suffer changes after a time (for example start to smell after a week). To avoid the use of antibiotics and antiproteases, the liquid material was divided in 45ml aliquots, frozen at -10ºC overnight and lyophilized at -15ºC, immediately after the dialysis. The whole process has taken about 48h. The final samples were conserved at -10ºC. These lyophilized samples have the advantage that they can be diluted as desired, achieving better concentrations than initially present after the dialysis. This methodology has shown to be very reproducible and does not affect the sample, as shown for a *C. tigris* periostracum sample, which SOM has been extracted running the "small amount" method. The chromatogram after dialysis and following the lyophylization (A-Figure 56) show the same structure, concentrated about one and a half times.

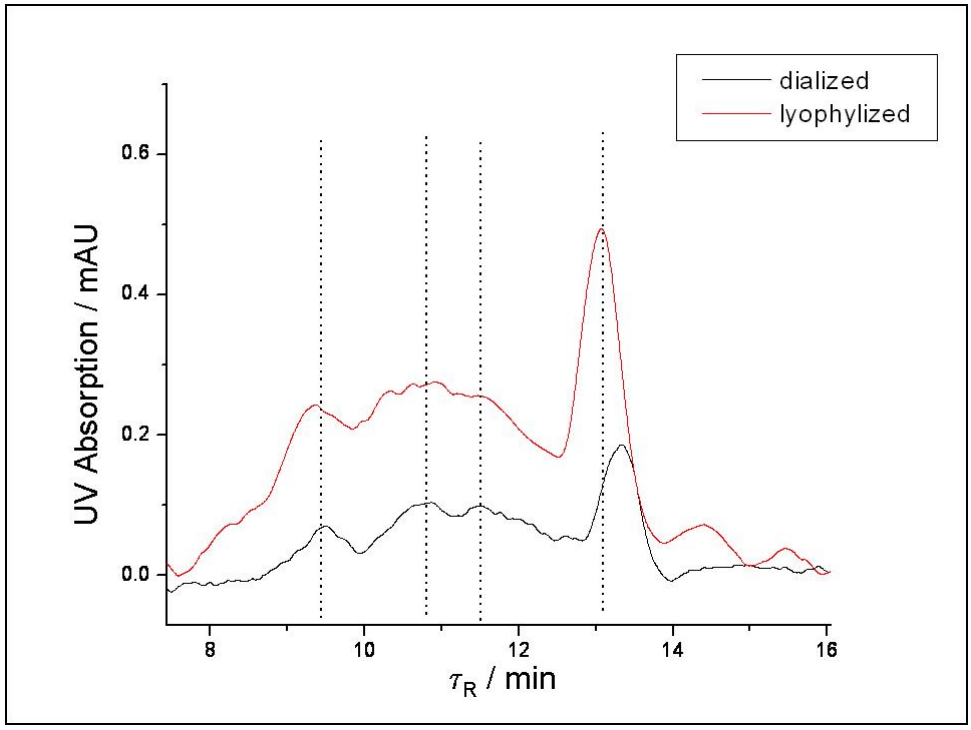

A-Figure 56: SE-HPLC-UV chromatogram showing the SOM extracted from *C. tigris* shells using dialysis as purification method.

MATERIAL: SOM extracted from 50g average material of *C. tigris* shells, decarboxiled with HCl 15%, rediluted in MilliQ Water.
DIALYSIS: 500ml sample in 3kDa MWCO dialysis membrane Spectrapore7® against 5lt MilliQ water, changing buffer each 12h, during two days.
LYOPHYLIZATION: 48hs, -14ºC.
SEC: column: *Biosep S 2000*, Mobile Phase: 20mM Tris-HCL pH 7.4, flux: 0.8ml/min, wavelength: 220nm.

AXII.5 Characterization of the SOM

UV Spectroscopy

The UV absorption spectrum of the SOM extracted from 50g average material of *Cypraea tigris* shells was measured, rediluted in MilliQ water, from 190 to 300nm, in QS quartz glass cuvettes. The reference used was MilliQ water and the running speed was 120nm/min. The results obtained for this measurement are shown below (A-Figure 57).

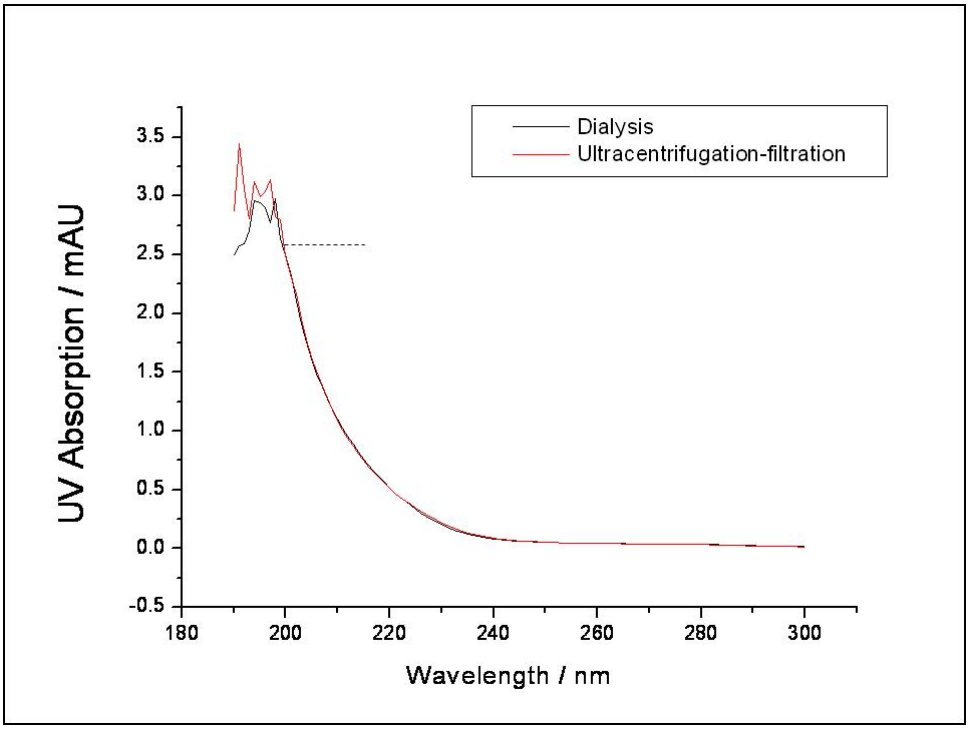

A-Figure 57: UV absorption spectra of the SOM extracted from *C. tigris*, using two different purification methods. Dashed line: saturation limit of the equipment.

MATERIAL: Material: SOM extracted from 50g powdered shell, with HC1 15% using the using the "large amount" extraction method. Solvent: MilliQ Water
UCF: 15 ml 3kDa Amicon® UCF tubes, centrifuged at 3000 rpm during 60min. Purification with MilliQ water in 6 cycles.
DIALYSIS: 500ml sample in 3 kDa MWCO dialysis membrane Spectrapore7 against 5lt MilliQ water, changing buffer each 12h, during two days.
UV PARAMETERS: Cuvette: 3 ml QS quartz glass, ØWindow: 3 mm, Reference: MilliQ water, speed: 120 nm/min, wavelength: 300-190 nm.

In this case, also the UV spectrum obtained by purification through ultracentrifugation-filtration was plotted (red). As it can be observed from A-Figure 57, both spectra are very

similar, in agreement with the conclusion that the purification is well achieved with dialysis as well as with the UCF method, and with the hypothesis that no contaminations or sample loss occurred; two independent different prepared samples give the same result. From both spectra, a big absorption is observed around 190-200nm and no signals at 254nm or 280nm (typical protein absorption wavelengths) are observed. Nevertheless, it does not mean that this sample has no proteins. As comparison also BSA was analyzed at different concentrations:

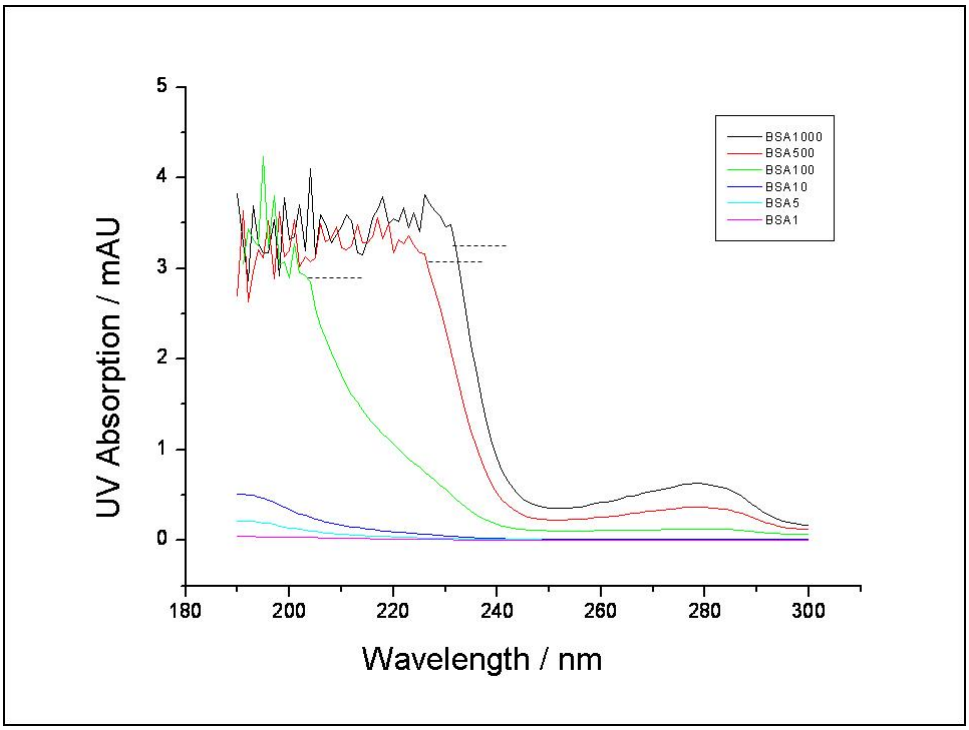

A-Figure 58: UV absorption spectrum of BSA at different concentrations.

MATERIAL: Material: BSA. Solvent: MilliQ Water
UV: Cuvette: 3ml QS quartz glass, ØWindow: 3mm, Reference Io: MilliQ water, speed: 120nm/min, wavelength: 300-190nm.

In this case, it is observed that the signal at 280nm is only visible for higher concentrated samples (500 and 1000ppm). Lower concentrations yield in a spectrum similar to that observed for the SOM samples (A-Figure 57).

Bradford tests

The total protein content was quantified by the Bradford Test, measuring the absorption at 595nm with a *Lambda 2* spectrometer, using the modified micro test. Averaging ten measurements, on the protein content for the SOM extracted from 50g of average material for *Cypraea tigris* shells, and recalculating this concentration to the concentration in the shell powder yields (19.7 ± 0.2) µg/g for the SOM purified by dialysis and (18.2 ± 0.2) for the SOM purified by ultracentrifugation filtration. Both results are equal within the error.

Ellmans tests

The presence of free sulfhydryl groups in the SOM was investigated using the colorimetric *Ellmans* tests. The standardization was made with cysteine in MilliQ water, at concentrations between 0 and 300ppm. The test was negative for all samples, independent of the purification method used.

Gel Electrophoresis

Gel Electrophoresis was used to separate the OM per mass, using MOPS tris-glycin gels, running with tris-glycin buffer, at 200V and 100mA for half an hour approximately. The standardization was made with the Dalton® cocktail mixture of proteins. Reducing and non reducing conditions were evaluated. More details about the GE methodology are found in Chapter 4 “Separation Methods”. The results are shown below (A-Figure 59):

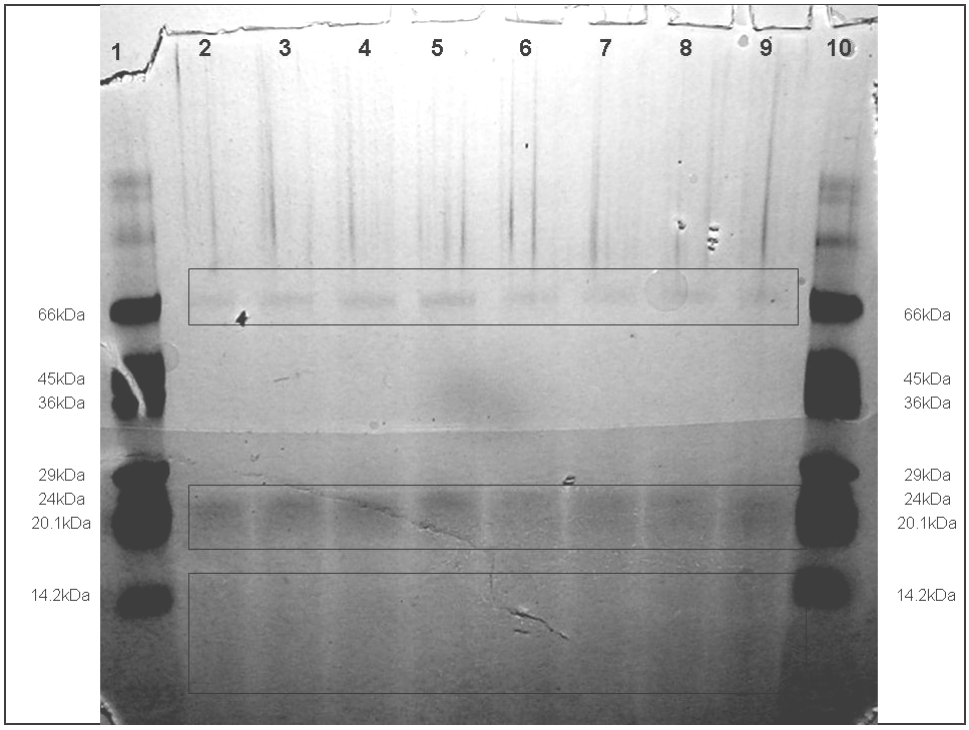

A-Figure 59: GE of the SOM. Lines 1 and 10, standards. Lines 2 to 9 SOM of different aliquots. 1-5 under reducing conditions, 6-10 under nonreducing conditions.

MATERIAL: Material: SOM extracted from 50g powdered shell, with HCL.
Solvent: MilliQ Water Reducing: with Mercaptoethanol at 70C during 1hour.
GEL PARAMETERS: Gel: MOPS tris-glycin 9%, Buffer: Mops-Tris-glycin,
Voltage: 200mV, Current: 100mA, Time: aprox. 40min.

As it can be seen from A-Figure 59, the SOM extracted from the average material shell powder, decalcified with HCl presents two continuous bands at masses of 25-20kDa and 14-7kDa. In addition, a clear spot is visible in the range of the 66kDa. The second conclusion of this analysis is that no differences are observed in the treatment with or without reducing agents.

The IOM extracted in SDS 10% produced no signal when run in the MOPS gels, under silver or *Coomasie Blue* staining. This effect may be an interference of the SDS used to dissolve the sample. Other gels or methodologies were not checked with this matrix.

HPLC-UV

Size exclusion and reverse phase chromatography coupled to an UV detector and/or an ESI-MS were used to separate and detect the components of the SOM extracted from 50g average material of *Cypraea tigris* shells. SEC column *Biosep S2000* from Phenomenex® was used to characterize the solution. In addition RP measurements were done with the

column were *Protonsil-C18-300* from Bischoff®. The absorption was detected at 205, 210, 220, 254, 270 and 280nm.

The results achieved for the SOM and the IOM from the SE chromatography are plotted in the next A-Figures. As it can be seen from A-Figure 60, the SOM signal here is very low (<1%), but the signal to noise ratio remains around 22.5. The analysis shows a not well separated chromatogram. Two main peaks or zones are clearly visible: the first is a bright signal that elutes between 8 and 12 minutes, which correspond to a masses in the range of 70-20kDa; the second one is a sharp peak for masses between 15-12kDa. The presence of the unresolved and bright peak hint to a continuous mass sample, in agreement with the data observed by GE. It is to note that the *Biosep S2000* column does separate the standard Dalton® (66-14kDa) in the same range of elution times. A negative signal is also observed for 27min, retention time that is already outside of the SEC range.

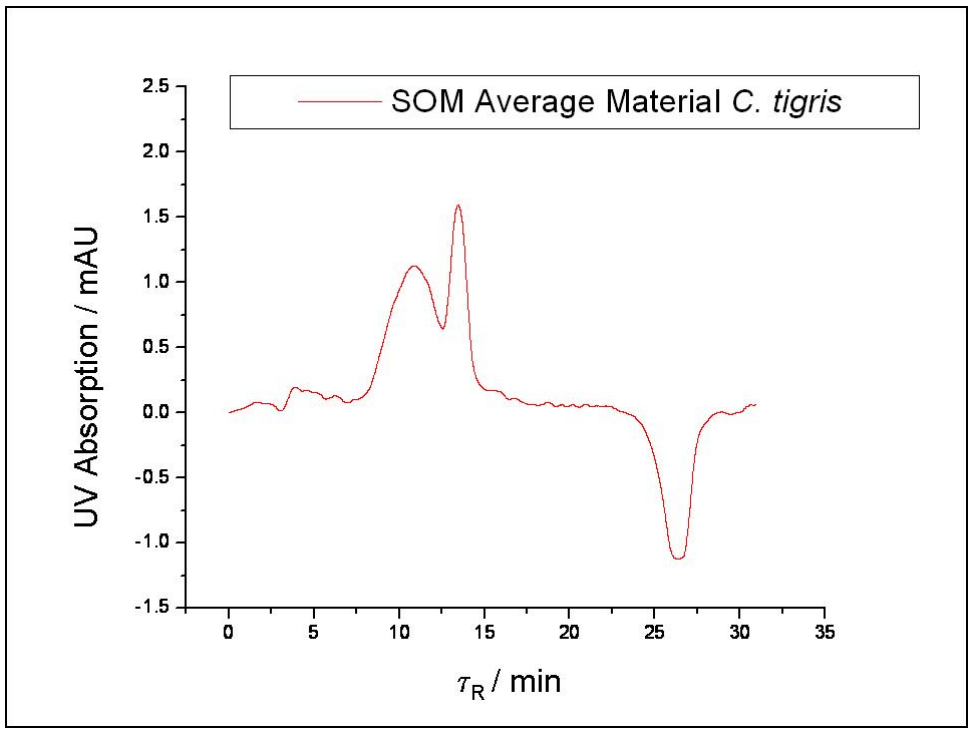

A-Figure 60: SE-HPLC-UV spectra of the SOM extracted from *C. tigris* shells.

MATERIAL: SOM extracted from 50g average material of *C. tigris* shells, demineralized with HCl 15%, purified by dialysis, lyophilized and re-suspended in MilliQ Water.
SEC: column: *Biosep S 2000*, Mobile Phase: 20mM Tris-HCL pH 7.4, flux: 0.8ml/min, wavelength: 220nm.

For the case of the IOM re-extracted in SDS, the chromatogram observed after SEC separation is plotted in A-Figure 61. In this case, after the subtraction of the SDS blank, the intensity is 25 times bigger than that observed for the SOM, with a signal to noise ratio bigger than 250. For this experiment it is to note that the main peaks corresponds also to the main peaks observed for SDS, with the difference that this latter one has a signal of about 3% of that of the IOM. That, in addition to the fact that the first peak elutes almost with the interstitial volume of the column, could mean that the observed peaks are only an artifact. With these results it is not possible to determine whether the peaks belong to large proteins or to large size micelles of IOM and SDS complexes.

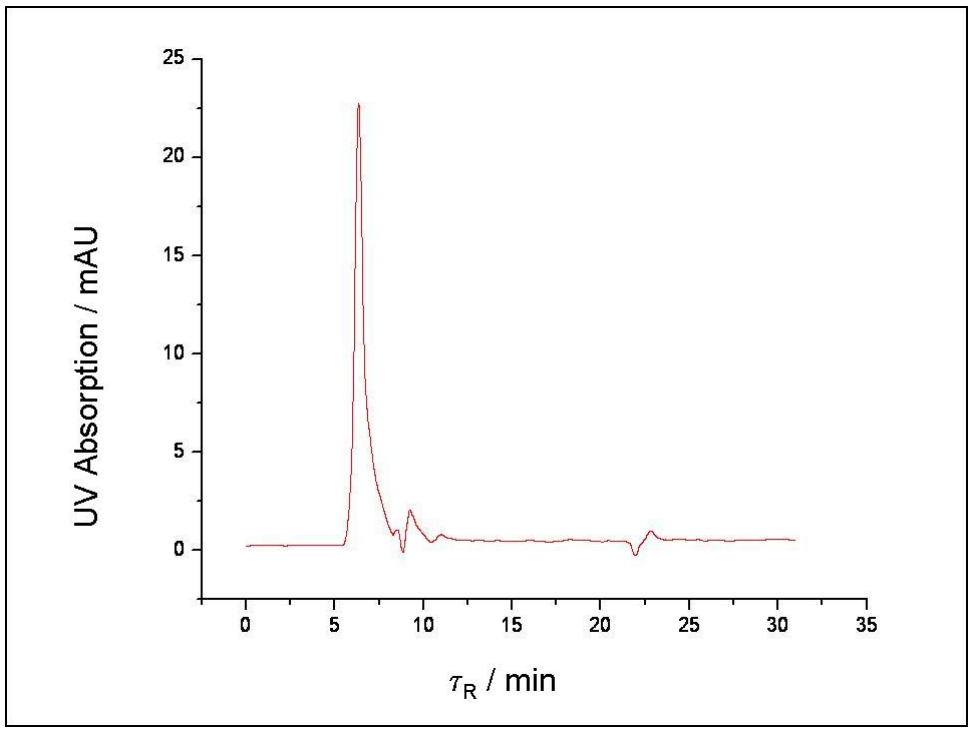

A-Figure 61: SE-HPLC-UV chromatogram of the IOM extracted from *C. tigris* shells.

MATERIAL: IOM extracted from 50g average material of *C. tigris* shells, demineralized with HCL, resuspended in SDS at 100ºC for one hour.
SEC: column: *Biosep S 2000*, Mobile Phase: 20mM Tris-HCL pH 7.4, flux: 0.8ml/min, wavelength: 220 nm. Blank spectra subtracted: SDS 10%.

AXII.6 Conclusion

The organic matrix extraction from 50gr average material of *Cypraea tigris* powdered shells with HCl 15% has been a successful. Soluble and insoluble organic matrices could be obtained and analyzed.

The demineralization using HCL 15% in MilliQ water has been optimized to maintain always a pH above 4 for the “big amount” as well as for the “small amount” samples. A step of pre-concentration by ultra-centrifugation-filtration was avoided using a 3kDa membrane of 5cm flat width, which allows a fill volume of about 9ml/cm, minimizing loss of sample or contamination. Lyophylization has shown to be the best method to concentrate and conserve the samples.

The SOM extracted accounts for about the 0.5% and the IOM for the 2% of the shell weight, although not all this material is *Coomasie blue* positive. Both matrices could be analyzed with HPLC and Gel electrophoresis. The matrices differ substantially. For the SOM, three main types of material were found by GE with blots that correlate with the masses of 66kDa, 25-20kDA and 14-7kDa. In SEC two bright peaks elute with the masses 70-20kDa and 15-12kDa respectively.

The IOM was analyzed after partial solubilization in SDS 10%. In this way the masses obtained correspond to 329kDa, 58kDa, 34kDa and 8.5kDa by HPLC. Nevertheless it could not be determined if these masses were real proteins or artifacts due to the extraction with a detergent. In addition, the extract could not be analyzed by GE with the MOPS gels. Because of the latter reasons, this matrix was not further studied.

Appendix XIII: Tables of Results

The absolute value of the trace elemental concentration found by INAA on powder shell samples is shown in Table 13 for *C. tigris*, in Table 14 for *C. talpa* and in Table 15 for *C. zebra*. The layers are indicated with the initial letters of the words: periostracum (P), coloured layer (C), striped layer (S), magenta layer (M) and white layer (W). The uncertainties are smaller than 15 %.

C. tigris		Trace Element / ppm					
		Co	Cr	Fe	Zn	Br	Mn
Layer	P	0.58	0.92	87.51	38.36	5.25	24.89
	C	0.22	0.61	83.05	19.40	2.12	11.97
	S	0.13	0.47	26.00	13.59	1.74	10.66
	M	0.02	0.39	36.48	2.36	1.31	3.46
	W	0.03	0.29	26.70	5.87	2.34	7.83

Table 13: Trace element concentrations found in *C. tigris* shells. Results obtained with INAA.

C. talpa		Trace Element / ppm					
		Co	Cr	Fe	Zn	Br	Mn
Layer	P	0.50	1.35	884.08	19.95	22.48	124.92
	C	0.15	1.48	420.06	74.44	0.84	353.88
	S	0.24	2.57	46.04	101.66	17.52	246.98
	W	0.16	0.30	26.30	8.41	2.89	70.40

Table 14 : Trace element concentrations of found in *C. talpa* shells. Results obtained with INAA.

C. zebra		Trace Element / ppm					
		Co	Cr	Fe	Zn	Br	Mn
Layer	P	0.06	0.50	99.70	26.28	7.50	23.24
	C	0.04	0.25	6.56	25.11	1.76	56.23
	S	0.03	0.81	11.00	14.69	1.11	47.97
	M	0.09	0.57	22.52	13.64	0.71	21.35
	W	0.23	0.55	13.50	16.17	0.55	10.55

Table 15: Trace element concentrations found in *C.zebra* shells. Results obtained with INAA.

The absolute value of the major elemental concentration found by INAA on powder shell samples is shown in, A-Table 17 and A-Table 18 for *C. tigris, C. talpa* and *C. zebra* respectively.

C. tigris		Major Element / ppm		
		Ca	Na	Sr
Layer	P	471917	4662	2904
	C	449529	5431	1671
	S	454119	5277	1309
	M	439286	5542	1384
	W	449805	5824	1501

A-Table 16: Major element concentrations found in *C.tigris* shells. Results obtained with INAA.

C. talpa		Major Element / ppm		
		Ca	Na	Sr
Layer	P	419229	4814	1650
	C	412794	5531	4085
	S	465479	5458	1469
	W	450567	5644	1283

A-Table 17: Major element concentrations found in *C.talpa* shells. Results obtained with INAA.

C. Zebra		Major Element / ppm		
		Ca	Na	Sr
Layer	P	424493	5090	3734
	C	414430	6173	2087
	S	444144	5805	1513
	M	426747	5372	1429
	W	451242	4875	1351

A-Table 18: Major element concentrations found in *C.zebra* shells. Results obtained with INAA.

The absolute value of the protein concentration found by the Bradford test on powder shell samples is shown in A-Table 19, A-Table 20 and A-Table 21 for *C. tigris, C. talpa* and *C. zebra* respectively. The uncertainty given is absolute.

Cypraea tigris		Protein Content / ppm	
		X	ΔX
Layer	P	285.7	0.9
	C	37.2	0.5
	S	4.5	0.4
	M	6.9	0.2
	W	7.9	0.6

A-Table 19: Protein Content found by Bradford test in *C. tigris* shells.

Cypraea talpa		Protein Content / ppm	
		X	ΔX
Layer	P	426	3
	C	1	2
	S	1	2
	W	2	1

A-Table 20: Protein Content found by Bradford test in *C. talpa* shells.

Cypraea zebra		Protein Content / ppm	
		X	ΔX
Layer	P	342	2
	C	90.0	0.8
	S	5.0	0.6
	M	8	1
	W	11.3	0.4

A-Table 21: Protein Content found by Bradford test in *C. zebra* shells.

Appendix XIV: Data of Some Standards Used

Protein	*Mass*
Albumin, Bovine	66kDa
Albumin, egg	45 kDa
Glyceraldehyde	36 kDa
C. Anhydrase	29 kDa
Trypsinogen	24 kDa
Trypsin Inhibitor	20.1 kDa
α-Lactalbumin	14.2 kDa

Table 22: Mass of the proteins included in the Dalton® protein mixture.

Type of matrix	Name	Material	Certified Elements	Indicated Elements
Plant leaves	CRM 0155 60 CRM 0155 61 CRM 0155 62	Lagarosiphon Platidhypnidium Olea Europaea	Cd, Cu, Hg, Mn, Pb, Zn.	Ag, Al, As, Au, B, Br Ca, Ce, Cl, Co, Cr, Cs, Eu, F, Fe, K, La, Mg, Mo, N, Na, Ni, P, Rb, S, Sb, Sc, Si, Se, Sn, Ta, Ti, Tl, Tb, U, V, W. .
Cereal	CRM 191	Lyophilized brown bread	Cd, Pb, Se, Cu, Zn, Fe, Mn	Ag, Ca, Cl, Cr, Hg, Mg, Na, P, K, Se.
Sediments	CRM 277	Estuarine Sediment	As, Cd, Cr, Cu, Hg, Ni, Pb, Sc, Se, Zn.	Ag, Al, Ba, Be, Br, Ca, Ce, Co, Cs, Eu, Fe, Ga, K, La, Mg, Mn, Mo, Na, P, Rb, Sb, Si, Sn, Sr, Ti, Th, U, V.

Table 23: Elements certified in the CRM used for INAA.

Appendix V: List of Solvents

Solvent	*Origin*
MilliQ water	MilliPore System
HPLC water	Bischoff
HPLC Acetonintril	Fischer Scientific
HPLC Methanol	Fischer Scientific
SDS 0.5% in MilliQ water	Fluka
NaN_3 0.05% in MilliQ water	Sigma
Tris-HCL pH 7.4	Sigma
Acetic Acid p.a.	Fischer Scientific
HCl 30% ultra pure	Sigma
HNO_3 ultra pure	Sigma
Mercaptoethanol	Sigma

Table 24: Solvents used in this research.

Curriculum Vitae

Dr. rer. nat.
Nuclear Engineer
Analía Leticia Soldati Valente

Address: Richard Schirrmann 14
App 602 B
55122 - Mainz
Germany

Email: morasoldati@yahoo.com.ar

Name: Analía Leticia Soldati Valente
Date of Birth: 17th march 1978
Place of Birth: Buenos Aires
Civil Status: single
Nationality: Argentinian

EDUCATION

- ***PhD.,*** Johannes Gutenberg University. Mainz, Germany.
  August 2003 - March 2006.

- ***Nuclear Engineer*****,** Instituto Balseiro. Centro Atómico Bariloche.
  Universidad Nacional de Cuyo.
  San Carlos de Bariloche, Argentine.
  August 1998 - June 2002

- ***Basic Engineering Cycle***, Universidad Nacional del Comahue.
  San Carlos de Bariloche, Argentine.
  January 1996 - June 1998.

- ***Bachiller Perito Mercantil***, Instituto Germano Argentino Primo Capraro.
  San Carlos de Bariloche, Argentine.
  March 1990 - December 1995.

LANGUAGE KNOWLEDGE

- Spanish: mother language
- English: speak fluently, understand, write and read
- German: speak fluently, understand, write and read.
- Portuguese: understand and read reasonably good.

ACADEMIC EXPERIENCE

- PhD thesis at the Johannes Gutenberg University, under the supervision of Prof. Dr. Wolfram Baumann. Title of the Research: ***„Metals and their bindings in periostracum of Cypraedae shells“***. Grant from the program “Trace analysis of elemental species: Develepment of methods and applications”, since August 2003.

- Engineering thesis at the Neutron Activation Analysis Laboratory, RA6-CAB-CNEA under the supervision of the doctors María Arribere and Sergio Ribeiro Guevara. Title of the research: „***Implementation and evaluation of a chemical extraction process and a nuclear measurement method of methylmercury in a biological matrix (low concentrations*)“**: Grant from CNEA. January 2001- July 2002.

WORK EXPERIENCE

- Participation as engineer in the research project ***“Measurement of impedance of in-vitro cell cultures”*** at the Biotechnology and Cavitation Laboratory-CAB-CNEA. July 2002-October 2002.

STAGES

- Institute for Nuclear Chemistry, Johannes Gutenberg University. Mainz, Germany. Nine months. October 2002 – August 2003.

- Neutron Activation Analysis Laboratory, RA6-CAB, CNEA. San Carlos de Bariloche, Argentine. Eighteen months January 2001- July 2002.

- Nuclear Centre Atucha I. Two weeks. September 2000.

- Neuwerck Gymnasium, Student International Exchange Program with Germany. Mönchengladbach, Germany. Three months. January 1995 – March 1995.

TECHNIQUES

- **Trace elements analysis:** INAA, ICP-MS, LA-ICP-MS, SEM-EDX, Microprobe.
- **Spectroscopy techniques:** Gamma and Alfa Stpectroscopy, Raman Spectroscopy, FTIR, XPS, Absorption and Fluorescence Spectroscopy, X-ray Difraction.
- **Microspcopy techniques:** Field Emision Scanning Electron Microscopy, Laser Scanning Confocal Microscopy, Light Microscopy.
- **Protein separation and characterization techniques**: Size exclusion and Reverse Phase High Performance Liquid Chromatography, with UV/Vis, ICP-MS detectors, Gel Electrophoresis.
- **Proteomics**: Metal-Protein complexes. Protein extraction. Protein cuantification and characterization.
- **Hipheneted techniques:** HPLC-ICP-MS, GC-ICP-MS, HPLC-ESI-MS, GE-LA-ICP-MS.

- **Laboratory work:** Used to work in nuclear chemistry, microbiology, analytical chemistry , and spectrometry laboratories. Clean rooms.
- **Sample handling:** Biological probes, cell cultures, soils, sediments. Handling of pre/post irradiation samples. Clean procedures to measure trace elements in ppm and ppb levels.

CONGRESSES ASSISTED

- IV Workshop on Elemental Speciation, Mainz, Germany. 29/30 Sep. 2005
- NAMLS08, Rio de Janeiro, Brasil. 17/22 April 2005.
- CANAS05, Freiberg, Germany. 6/10 Mar. 2005.
- III Workshop on Elemental Speciation, Mainz, Germany. 5/6 Nov. 2004.
- Euroanalysis XII , Salamanca, Spain. Sept. 2004.
- II Workshop on Elemental Speciation, Mainz, Germany. 6/7 Nov. 2003.
- I Workshop on Elemental Speciation, Mainz, Germany. 17/18 Oct. 2002

ORAL PRESENTATIONS

- ***Ist Mangan an die Protein- oder an die Mineralphase von Cypraea-Schneckengehäusen gebunden?*** Oral Presentation at the "IV Workshop für Elementspeziation" 29/30 Nov. 2005.
- ***Speziation in Biomineralien am Beispiel von Schneckengehäusen***. Oral Presentation at GRK II Seminar „Elementspeziation" auf der Ebernburg. 4/5 Nov.2004.
- ***Especiación de Metales en Conchas de Caracol.*** Invited Oral Presentation under the Bilateral Colaboration between Uni Mainz – Uni Valencia with the Analytical Chemistry Group of Prof. De la Guardia, Universidad de Valencia, Spain. Sept. 2004.
- ***Metals and their bindings in Periostracum of Cypraedae shells: Last Advances***. Oral Presentation at GRK II Doktorandenseminar „Elementspeziation". 23 June 2004.
- ***Metals and their binding in Periostracum of Cypraea talpa and Cypraea zebra shells*** . Oral Presentation at GRK I Doktorandenseminar „Elementspeziation". 6/7 Nov.2003.
- ***Methilmercury Traces Determination in Biological Matrix by INAA.*** Invited Oral Presentation at the Divulgation Seminar of the Institut für Kernchemie. Universität Mainz, Feb. 2003.

LIST OF PUBLICATIONS

- ***Determination of Trace Elemental Species in Periostracum of Cypraea Shells.*** Dissertation zur Erlangung des Grades "Doktor der Naturwissenschaften". Soldati A., University Johannes Gutenberg, Mainz, Germany. March 2006.
- ***Cypraea tigris shells: Determination of trace elements and their relation to proteins with INAA help.*** Soldati A.L, Nascimento-Jähnke S.K., Vicente Vilas V., Baumann W.; Poster Presentation at NAMLS08, Rio de Janeiro, Brazil. 17/22 April 2005. Abstract Book, page 125.
- ***Speciation of metals in medicinal plants under different stress condition by HPLC-ICP-MS.*** Nascimento-Jähnke S.K., Soldati A.L., Vicente Vilas V., Baumann W.; Poster Presentation at NAMLS08, Rio de Janeiro, Brazil. 17/22 April 2005. Abstract Book, page 100.
- ***Trace elemental determination of teas used for shaman from Amazon area by neutron activation analysis.*** Nascimento-Jähnke S.K., Soldati A.L., Vicente Vilas V., Baumann W.; Poster Presentation at NAMLS08, Rio de Janeiro, Brazil. 17/22 April 2005. Abstract Book, page 99.
- ***Determination of metals in medicinal plants and soil from Amazon area by INAA and ICP-MS.*** Nascimento-Jähnke S.K., Soldati A.L., Vicente Vilas V., Baumann W.; Poster Presentation at NAMLS08, Rio de Janeiro, Brazil. 17/22 April 2005. Abstract Book, page 101.
- ***Trace element determination of metals in wine yards and wine leaves from middle Rhine Valley by INAA.*** Sound I., Soldati A.L, Vicente Vilas V., Baumann W.; Poster Presentation at NAMLS08, Rio de Janeiro, Brazil. 17/22 April 2005. Abstract Book, page 134.
- ***Trace Elemental Determination of Teas used for Shaman from Amazon Area by HPLC-ICP-MS.*** Nascimento-Jähnke S., Soldati A. L., Vicente Vilas Víctor, Sound I., Baumann W.; Poster Presentation at CANAS05, Germany. 6/10 march 2005.
- ***Trace Elemental Determination After Separation From a High Calcium Containing Biological Matrix.*** Soldati A.L, Nascimento-Jähnke S.K., Vicente Vilas V., Baumann W.; Poster Presentation at CANAS05, Freiberg, Germany. 6/10 March 2005.
- ***What can we learn from Cypraea species with respect to anti-adhesion protection of ship bodies? : Surface properties and metal content.*** Soldati A.L., Vicente Vilas V., Nascimento-Jähnke S.K., Baumann W.; Poster Presentation at IAK Universität Mainz, Germany. 01 Jan. 2005.
- ***Metallic trace element determination in bio-minerals. Chemical extraction and quantification***. Soldati A.L., Vicente Vilas V., Nascimento-Jähnke S.K., Baumann W.; Poster Presentation at IAK Universität Mainz, Germany. 26 Nov. 2004.
- ***Complexation of metals with organic compounds in brazilian medicinal plants.*** Nascimento-Jähnke S.K., Sound I., Soldati A.L., Vicente Vilas V., Baumann, W.; Poster Presentation at IV Scientific Meeting of the Spanish Society of Chromatography and Related Techniques. USP-CU. SECyT. Madrid 2004.

- ***Trace Metallic trace element determination in bio-minerals. Chemical extraction and quantification.*** Soldati A.L., Vicente Vilas V., Nascimento-Jähnke S.K., Baumann W.; Poster Presentation at Euroanalysis XIII, Salamanca, Spain. Sept. 2004.
- ***Determination of Organic Mercury in Biological Samples by Chemical Extraction Coupled with INAA.*** Soldati, Arribere, Ribeiro Guevara. Poster Presentation at 3.Mainzer Symposium über Spurenanalytik. Universität Mainz. Nov. 2003.
- ***Determination of Methylmercury Traces in Biological Matrix: Chemical Extraction and Nuclear Quantification with the Neutron Activation Analysis Technique.*** Soldati**,** A.L. Instituto Balseiro, Universidad Nacional de Cuyo, Centro Atómico Bariloche (Argentina). Comision Nacional de Energía Atómica, San Carlos de Bariloche, Argentina. Depto. de Ingenieria Nuclear e Investigación Aplicada. INIS-AR-V--069 {INISARV069}, 2002 127 p. Reference Number 33037919, Issue 3335.